



Swansea University  
Prifysgol Abertawe



Swansea University E-Theses

---

## Computational modelling of hysteresis and damage in reinforced concrete bridge columns subject to seismic loading.

Benamer, Mohamed R. Omar

How to cite:

---

Benamer, Mohamed R. Omar (2013) *Computational modelling of hysteresis and damage in reinforced concrete bridge columns subject to seismic loading.*. thesis, Swansea University.  
<http://cronfa.swan.ac.uk/Record/cronfa42309>

Use policy:

---

This item is brought to you by Swansea University. Any person downloading material is agreeing to abide by the terms of the repository licence: copies of full text items may be used or reproduced in any format or medium, without prior permission for personal research or study, educational or non-commercial purposes only. The copyright for any work remains with the original author unless otherwise specified. The full-text must not be sold in any format or medium without the formal permission of the copyright holder. Permission for multiple reproductions should be obtained from the original author.

Authors are personally responsible for adhering to copyright and publisher restrictions when uploading content to the repository.

Please link to the metadata record in the Swansea University repository, Cronfa (link given in the citation reference above.)

<http://www.swansea.ac.uk/library/researchsupport/ris-support/>

CIVIL AND COMPUTATIONAL ENGINEERING CENTRE  
SWANSEA UNIVERSITY



Swansea University  
Prifysgol Abertawe

COMPUTATIONAL MODELLING OF HYSTERESIS  
AND DAMAGE IN REINFORCED CONCRETE BRIDGE  
COLUMNS SUBJECT TO SEISMIC LOADING

MOHAMED R. OMAR M BENAMER  
474825

SEPTEMBER 2013

DISSERTATION SUBMITTED TO SWANSEA UNIVERSITY IN  
FULFILMENT OF THE REQUIREMENTS FOR THE DEGREE OF  
DOCTOR OF PHILOSOPHY IN CIVIL ENGINEERING

ProQuest Number: 10798017

All rights reserved

INFORMATION TO ALL USERS

The quality of this reproduction is dependent upon the quality of the copy submitted.

In the unlikely event that the author did not send a complete manuscript and there are missing pages, these will be noted. Also, if material had to be removed, a note will indicate the deletion.



ProQuest 10798017

Published by ProQuest LLC (2018). Copyright of the Dissertation is held by the Author.

All rights reserved.

This work is protected against unauthorized copying under Title 17, United States Code  
Microform Edition © ProQuest LLC.

ProQuest LLC.  
789 East Eisenhower Parkway  
P.O. Box 1346  
Ann Arbor, MI 48106 – 1346





## ABSTRACT

Box-girder bridges supported by single reinforced concrete (RC) columns are expected to sustain seismic shocks with minor structural damages in seismically active regions where transportation is substantially required for rescuing and evacuating tasks. Such viaducts are vulnerable to damage when they are subjected to strong ground motions and acceleration pulse records, especially when responding in a flexural mode or having relatively low core confinement.

Using a nonlinear dynamic solver that applies the fibre element method, global and local damage curves are computed based on the dissipated energy under hysteretic curves and based on constitutive curves, respectively. The RC bridge with seismic isolation bearing is used as an alternative system to control the damage, and modelled using linkage elements between the substructure and super structure. It was found that seismic isolation can be controlled to dissipate partial seismic energy so that the RC column gains the least possible minor damage.

Using a MatLab program, a fibre element nonlinear model was built using a simplified iterative process and simplified constitutive relations. The number of fibres and elements under the dynamic loading was found to be affecting the final results of the analysis.

Using crack growth modelling based on fracture mechanics, the combined discrete element/finite element explicit-Elfen code was applied to investigate the crack growth in 3D dynamically loaded RC columns. Despite its excessive computational cost and time, this code provides reliable information about local damage in the RC column core.

Earthquake records with the pulse acceleration phenomenon have a severe damage potential on the structure. The difference in damage intensities was detected by crack growth modelling for the same problem using different loading rates. Critically stressed zones can be investigated independently by using the relative response technique, in which responses from the numerically analysed structure are re-used as applied loads onto a small-scale crack model for the critical member.

Two general conclusions can be obtained; bridges with single RC columns designed by the demand/capacity criterion could suffer severe damage and possible collapse when subjected to strong ground motions. Secondly; hysteresis-based methods provide a global damage evaluation based on strength and ductility only regardless of the damage growth inside the concrete core and the buckling of bars, which could lead to progressive collapse.

## Declaration

This work has not previously been accepted in substance for any degree and is not being concurrently submitted in candidature for any other degree.

Signed ..... (candidate)

Date ..... 17-09-2013 .....

## Statement 1

This thesis is the result of my own investigations, except where otherwise stated.

Other sources are acknowledged by footnotes giving explicit references. A bibliography is appended.

Signed ... (candidate)

Date ..... 17-09-2013 .....

## Statement 2

I hereby give consent for my thesis, if accepted, to be available for photocopying and for inter-library loan, and for the title and summary to be made available to outside organisations.

Signed ..... (candidate)

Date ..... 17-09-2013 .....

# TABLE OF CONTENTS

Abstract	i
Declaration and statements	ii
Table of Contents	iii
Acknowledgements	iv
Publications and Contributions	v
List of Figures	vi
List of Tables	ix
Notations	x
Abbreviations	xiii
Chapter 1 Introduction	1
Chapter 2 Literature Preview	13
Chapter 3 Basic Theory of Earthquake Analysis of Structures	68
Chapter 4 Fibre Element Method for Dynamic Nonlinear Problems	105
Chapter 5 Nonlinear Numerical Analysis and Damage Assessment	136
Chapter 6 Combined DE/FE Nonlinear Analysis	184
Chapter 7 Effect of Loading Rates on the Fracture of RC Columns/ Multi-Scale Analysis 230	230
Chapter 8 Conclusions, Recommendations and Future Work	253
Appendix A	-1-
Appendix B	-15-
Appendix C	-17-
Appendix D	-19-

# ACKNOWLEDGEMENTS

To my parents, my wife and members of my family, for their continuous support and encouragement.

Special thanks to my supervisor Prof. Yuntian Feng, for his assistance and effort in answering my questions throughout my research period in the Civil and Computational Engineering Centre in Swansea University.

To all those who offered assistance without expectation of a return, their assistance made an important support for this work, I give my thanks to:

Junichi Sakai, Dr. Eng., Public Works Research Institute, 1-6 Minamihara, Tsukuba, Ibaraki, 305-8516, Japan, for providing me with the input data of strong motion accelerations recorded near Tsugaru Bridge during the 1983 Nihonkai Chubu in Japan.

The technical support team of the Seismostruct software company in Italy, for offering technical information concerning the software, and providing me with the configuration of long-history record files.

Jun Kato, Rockfield Company, Swansea, U.K., for providing his consultation about the fracture mechanism in the Explicit-Elfen code.

Erick I. Saavedra Flores, Civil Engineering Department, School of Engineering, University of Santiago in Chile, for explaining important concepts in concrete confinement.

Freddy E. Piña Burgos, Assistant Professor, Department of civil engineering, University of Santiago in Chile, for explaining about the topic of Performance-based seismic assessment.

Abbas Moustafa, Associate Professor, Department of Civil Engineering, Faculty of Engineering, Minia University, Minia 61111, Egypt, for explaining the separation of energy curves.

Reed Helgens Associate executive director, Consortium of Universities for Research in Earthquake Engineering (CUREE), and Stephen A. Mahin, Structural Engineering, Mechanics and Materials, University of California, Berkeley, for providing me with near fault earthquake records.

My colleagues in Swansea University; Dr. Zainorizuan Bin Mohd Jaini, for his explanation about the Explicit-Elfen code, and Dr. Bruce Jones, for offering an access to use his pc system.

The IT Team, College of Engineering, Room 42, Talbot Building, Swansea University, for their computer technical support.

Student Advisor's office in Swansea University, for supporting my legal stay in the UK.

The Libyan Ministry of Higher Education and their Libyan Cultural Affairs office in London, for sponsoring my tuition fees and living expenses in the UK.

## PUBLISHEMENTS & CONTRIBUTIONS

1. 9th International Conference on Earthquake Resistant Engineering Structures, 8-10 July 2013, A Coruña, Spain. <http://www.wessex.ac.uk/13-conferences/eres-2013.html>.  
*'Seismic Response of Damage and Energy Dissipation in Reinforced Concrete Bridge Columns'*.  
M. O. Benamer, Y. Feng, Civil and Computational Engineering Centre, Swansea University.
2. The Young Engineers Conference, 4<sup>th</sup> July 2013, Newcastle University, UK. SECED - Society for Earthquake and Civil Engineering Dynamics.  
<http://conferences.ncl.ac.uk/seced2013/aboutseced2013/>  
*'Seismic Reliability of Reinforced Concrete Bridge Columns Based on Global Damage Approach (with and without seismic isolation)'*.  
M. O. Benamer, Y. Feng, Civil and Computational Engineering Centre, Swansea University.
3. 4<sup>th</sup> International Conference on Computational Methods in Structural Dynamics and Earthquake Engineering. Kos Island, Greece, 12–14 June 2013. <http://compdyn2013.org/>  
*'Seismic Reliability of Reinforced Concrete Bridge Columns Based on Damage Approaches'*.  
M. O. Benamer, Y. Feng, Civil and Computational Engineering Centre, Swansea University.
4. The Third International Conference on Computational Modeling of Fracture and Failure of Materials and Structures (CFRAC 2013), 5-7 June, Prague, Czech Republic.  
<http://www.cimne.com/iacm/main.htm>.  
*'Fracture in Reinforced Concrete Bridge Columns Under Seismic Loading'*.  
M. O. Benamer, Y. Feng, Civil and Computational Engineering Centre, Swansea University.
5. A Review Of Suggested Updates For Eurocode 8, by Edmund Booth, consultant and Ziggy Lubkowski, Arup, 24<sup>th</sup> April, 2013. SECED facebook page:  
<https://www.facebook.com/groups/261864180545298/?fref=ts>  
*'A Criticism on the Eurocode8, part 2: Seismic Design on Bridges'* (workshop notes).  
M. O. Benamer, Civil and Computational Engineering Centre, Swansea University.
6. International Conference on Computational Mechanics (CM13), 25-27 March 2013, Durham, UK. <http://www.dur.ac.uk/cm13.conference/>  
*'Seismic Assessment in Reinforced Concrete Bridge Columns Based on Local and Global Damage Approaches'*.  
M. O. Benamer, Y. Feng, Civil and Computational Engineering Centre, Swansea University.
7. International Conference on Computational Mechanics (CM13), 25-27 March 2013, Durham, UK. <http://www.dur.ac.uk/cm13.conference/>  
*'Multi-scale Seismic Analysis of Reinforced Concrete Beam-Column Joints'*.  
M. O. Benamer, Civil and Computational Engineering Centre, Swansea University, Benghazi University, Libya.
8. The 20th UK Conference of the Association for Computational Mechanics in Engineering. 27 – 28th March 2012, the University of Manchester, Manchester.  
<http://www.acmeuk.org/meeting.html>  
*'Energy-Based Seismic Assessment For Reinforced Concrete Bridge Columns With Fixed Connections And Isolated Bearings'*.  
M. O. Benamer, Y. Feng, Civil and Computational Engineering Centre, Swansea University.
9. The 19th UK Conference of the Association for Computational Mechanics in Engineering, 5-6 April 2010, Heriot-Watt University, Edinburgh  
*'Damage-Based Fracture Analysis For The Evaluation Of Seismic Performance Of RC Bridge Columns'*.  
M. O. Benamer, Y. Feng, Civil and Computational Engineering Centre, Swansea University.

# LIST OF FIGURES

Figure 1.1: Damage of concrete and bar buckling .....	3
Figure 1.2 Levels of reliability [3] .....	4
Figure 1.3 Flexural top deck of the freeway collapsed due to the 1989 Loma Prieta earthquake accounting for a large fraction of the fatalities, even though the epicentral distance is about 100 km...5	
Figure 1.4 Flexural and shear modes of failure .....	5
Figure 1.5 Destruction of plastic hinge zones [5] .....	8
Figure 2.1.a Capacity/Demand spectra [13], Figure 2.1.b Estimated damage at performance point....	19
Figure 2.2 Comparison of the design energy spectrum and those relevant to most significant strong ground motion records: Imperial Valley College, (Imperial Valley, 1979), Kobe JMA (Kobe, 1995), Sylmar Parking Lot, Newhall, Rinaldi, and SCS (Northridge, 1994). Soil S2. $D_f < 5$ km. $6.5 \leq M \leq 7.1$ . $\mu = 4$ . [24]. .....	22
Figure 2.3 Inelastic design spectrum, dissipated energy spectrum, and required deformation.....	22
capacity spectrum, for design ductility $\mu = 5$ and design ground motion specified .....	22
by 1g; 85 cm/s and 44 cm. [15]. .....	22
Figure 2.4 Variation of damage curves [29], Figure 2.5 Variation of crack width curves [29].....	24
Figure 2.6 Limits of structure performance in a load-deflection relationship [44].....	29
Figure 2.7 Evolution of the damage indices during the numerical simulation [45].....	30
Figure 2.8 Final damage portraits of RC columns [46] .....	32
Figure 2.9 Analysed RC columns with aspect ratios from 3 to 10, and analytical model with unbonded strands at the column centre [47]. .....	34
Figure 2.10 Dynamic response of columns with aspect ratio =6, subjected to Lexington Dam record [47].....	35
Figure 2.11 Set-up of RC specimen and the resulting damage [49] .....	36
Figure 2.12 Reversely proportional relationship between axial and lateral forces for cantilever-type RC structures under dynamic loading [49]. .....	37
Figure 2.13 Cross section of all specimens and PRC-UJ specimen [51] .....	38
Figure 2.14 Damages in specimens at plastic hinge zones [51].....	39
Figure 2.15 Damaged volume element [52]                      Figure 2.16 Closing and re-opening criteria [52] .....	42
Figure 2.17a) Lumped plasticity model of a beam-column element. b) Generalized stresses. c) Generalized deformations. [54].....	42
Figure 2.18 Bridge pier as cantilever beam with forces at plastic hinge section $x_3$ [55] .....	45
Figure 2.19 Hysteretic models [24].....	46
Figure 2.20 Analytical modelling for a shaking table specimen [58] .....	47
Figure 2.21 Shear spring using limit state material model [58].....	48
Figure 2.22 Models with different end springs and corresponding drift responses [58].....	48
Figure 2.23 Elastic column with the concentrated hinges at the ends [58] .....	49
Figure 2.24 Axial strain vs. rotation of an RC beam failing in shear after flexural yielding [61]. .....	50
Figure 2.25 Proposed model for analyzing the longitudinal axial strain in the plastic hinge region of RC beams [61]. .....	51
Figure 2.26 Idealization of the smeared crack model .....	52
Figure 2.27 Crack controlled by the discontinuity interfaces in a 'dog bone' test, with coarse and fine meshes [64]. .....	55
Figure 2.28 Controlled discretized section in fibre element modelling [69].....	56
Figure 2.29 Configuration of Lattice elements for a RC column [71].....	56

Figure 3.1	Stress change in a 2D plane of a cube element.....	70
Figure 3.2	Propagation of stress waves in an elastic medium; Longitudinal and Transversal waves...	76
Figure 3.3	Stresses on a cube element. ....	77
Figure 3.4	Force diagram for the moving ground and for the equivalent stationary base .....	86
Figure 3.5	Rotational motion diagram .....	87
Figure 3.6	First response stages of force-deformation curve: actual and elastoplastic idealization ...	89
Figure 3.7	An elastoplastic system and its corresponding linear system .....	90
Figure 3.8	The reduction factor and the ductility factor, a) $R_y \equiv \mu$ , b) $R_y \ll \mu$ . [14] .....	94
Figure 3.9	Elastic and Inelastic Design Spectra for ground motion record $u_g(t)$ with $u_{go} = 1g$ , $u_{go} = 48\text{ins}$ and $u_{go} = 36\text{ in}$ ; $\mu = 1, 2$ and $8$ ; $\zeta = 5\%$ . [10].....	96
Figure 3.10	Comparison of base shear coefficients from elastic design spectrum and International Building Code [10] .....	97
Figure 3.11	Flow chart of ductility-based seismic design for elastoplastic systems.....	98
Figure 3.12	Types of fracture modes .....	99
Figure 3.13	Central crack in an infinite plate due to a remote load $\sigma$ .....	99
Figure 3.14	Energy Balance between Stable and Instable Crack Propagation [21].....	101
Figure 4.1.a)	Two-dimensional fibre element. b) Fibre section of the element.....	111
Figure 4.2	Diagram of incremental axial strain of the $k^{\text{th}}$ fibre.....	112
Figure 4.3.a and 4.3.b	Idealized re-loading paths [3].....	114
Figure 4.4	Envelope curves of concrete stress-strain model [3] .....	115
Figure 4.5	Flow Chart for non-linear dynamic solver using the Finite Fibre Elements.....	121
Figure 4.6.a)	RC column cross section, b) Column structure .....	122
Figure 4.7	Modelling components of RC members by fibre elements [5].....	123
Figure 4.8	Artificial ground acceleration record.....	124
Figures 4.9.a and 4.9.b	Constitutive models used by the SeismoStruct for concrete and steel, respectively .....	125
Figure 4.10	Base-shear/displacement hysteresis curve .....	126
Figure 4.11	Base-moment/rotation hysteresis curve.....	126
Figure 4.12	Base shear forces by SeismoStruct and code analyses. ....	127
Figure 4.13	Relative displacements by SeismoStruct and code analyses. ....	127
Figure 4.14 and 4.15	Constitutive curves for concrete and steel end fibres in the first element in both SeismoStruct and code analyses .....	128
Figure 4.16	A comparison of displacement responses.....	130
Figure 4.17	Lateral displacements of all elements. Figure 4.18 Resisting forces for all elements ....	132
Figures 4.19 and 4.20	Axial strains and axial stresses of all fibres at PH element, respectively.....	132
Figure 4.21	Hysteresis with $EGt$ *-term = 0 Figure 4.22 Elastic Hysteresis with $EGt$ *-term.....	133
Figure 5.1 a)	Properties of specimen, b) Published results [1] c) Hysteresis by the SeismoStruct.....	139
Figure 5.2	400%-Scaled ground accelerations in the x, y and z directions.....	141
Figure 5.3.a)	Shaking table specimen b) x & y-Displacement responses at the c.g. of the structure .	141
Figure 5.4.a	Seismostruct fibre model Figure 5.4.b x-Displacement responses at the c.g. of the ..	141
	structure, modelled by Seismostruct. ....	141
Figure 5.4.c	y-Displacement responses at the c.g. of the .....	141
	structure, modelled by Seismostruct. ....	141
Figure 5.5 a)	Full energy absorption b) Full energy recovery c) Partial energy recovery with residuals d) Degradation of stiffness and strength in successive loops.....	146
Figure 5.6	Damage as corresponding to the dissipating energy before recovery, on one side of the hysteresis [8].....	148
Figure 5.7	Designed RC bridge column [9].....	149





Figures 6.20, 6.21, 6.22, 6.23 and 6.24 Fracture in concrete and axial forces in the reinforcement bars at 0.1, 0.2, 0.3 0.4 And 0.5 seconds, respectively. ....	221
Figure 6.25 Axial tensile & compressive forces (N) on longitudinal bars at plastic hinge zone. ....	222
Figure 6.26 Buckling of some bars causing instability at 626.3MPa of bar tensile stresses.....	223
Figure 6.27 Confinement of stirrups reaching only 4.5% of ultimate steel tensile stress. ....	223
Figure 6.28 Base-shear versus displacement curves of collapse under different failure criteria ....	225
Figure 6.29 & 6.30 Fracture state indicator and axial plastic Y-strains under 1.62MN lateral load..	226
Figure 7.1 Strain rate associated with different types of loading [2] .....	232
Figure 7.2 Softening slope as a function of strain rate [1] .....	232
Figure 7.3 Different fundamental periods for different structures .....	234
Figure 7.4 Displacement in RC bridge columns      Figure 7.5 Loading rates.....	236
Figures 7.6, 7.7 and 7.8 Stress-strain curves at 1.414 g/s, 1.88 g/s and 2.801 g/s loading rates.....	237
Figure 7.9 Different Rates of Applied Forces at Top of Structure.....	239
Figure 7.10 Load-Deflection curves by different analyses for the structure under Loma Prieta ....	240
Figures 7.11, 7.12, 7.13 and 7.14 Concrete fracture and steel tensile forces due to applied loads of 0.821, 1.208, 1.619 and 2.03 MN, respectively, for longer duration case (A).....	242
Figures: 7.15, 7.16, 7.17 and 7.18 Concrete fracture and steel tensile forces due to applied loads of 0.821, 1.208, 1.619 and 2.03 MN, respectively, for shorter duration case (B) .....	242
Figure 7.19 Flow-chart of the Relative Response Method .....	246
Figure 7.20 Large-scale non-linear analysis of RC frame structure subject to Lexington Dam .....	246
Figure 7.21 Small-scale FE model.....	247
Figure 7.22 Displacement relative responses of joints J3(n313) & J1(n311), used as applied loads relative to the stationary joint J2(n312) .....	248
Figure 7.23 half-member configurations of small-scale modelling .....	249
Figure 7.24 Displacement of column members relative to the stationary joint J2, showing cracks and reinforcement bars forces.....	250
Figure 7.25 Crack growth and the fracture state indicator in stationary joint J2 .....	250
Figure 8.1 Earthquake intensities in Libya from 1907 to 2005, magnitudes from 2.6 to 7.1 [10].....	263

## LIST OF TABLES

Table 1.1 Types of RC box-girder bridges .....	7
Table 2.1 Description of bridge damage states (taken from HAZUS 97) [26] .....	25
Table 2.2 Summary of Damage Indices DI and corresponding Limit States LS for concrete columns and seismic isolation bearings [26,35,36,38,39,40,41].....	27
Table 2.3 Summary of excitations, responses and damages for the three column types under shaking table tests [46].....	32
Table 2.4 Near-field earthquake strong ground motions used for dynamic analysis [47]. ....	34
Table 2.5 Description of specimens and damages under strong ground motion tests [51].....	39
Table 5.1 Capacity limits for R/C column [9]. ....	151
Table 5.2 Max & Min responses for the R/C column with aspect ratios 3,6 and 10, under 10 different strong motion seismic records [9].....	157
Table 5.3 Peak displacements and damage events in the x-direction [2].....	159
Table 5.4 Damage states at different dissipating energy rates .....	164
Table 6.1 Mechanical properties of concrete and useful relations.....	189
Table 6.2 Fracture Analysis Responses of The RC Column Structure Under Loma Prieta .....	219
Table 7.1 Responses of RC column under long and short duration applied lateral loads.....	241

# NOTATIONS

## Notes:

1- Notations with (normal face) are scalar quantities, notations with (*italic bold face*) are local vectors or matrices, and notations with (**bold face**) are global vectors or matrices.

2- Notations from chapter 2 are not included in this list since they vary as they follow different published papers and text books.

$a$  and  $b$  constants at Newmark's method

$A_k$  cross section area of the k-th fibre

$A$  peak pseudo acceleration of the structure at its top level.

$c, c_\theta$  damping factor of an element, rotational damping, respectively.

$\bar{c}$  wave speed

$c_u$  shear strength, or cohesion, of the material

$d$  displacement

$d_D, d_C$  displacement demand and capacity, respectively.

$d_R$  residual displacement

$d_y, d_p$  yield and plastic displacements, respectively.

$d_u$  ultimate lateral displacement of the column

$d_i, D_i$  local and global damage indices, respectively.

$D$  diameter of RC column

$D_{mono}, D_{iso}$  damage in monolithic (non-isolated) and isolated structures, respectively.

$e$  rate of change of volume

$E_{d,i}$  dissipating energy at cycle (i)

$E_{d,n}$  total dissipating energy for all cycles (n)

$E$  elastic modulus

$E_k$  elastic modulus of the k-th fibre

$E_i$  elastic modulus of the k-th fibre at time-step  $i$

$E_{conc}$  elastic modulus of concrete

$E_{steel}$  elastic modulus of steel

$EA_t^*, EG_t^*, EI_t^*$  parameters of the stiffness matrix of the fibre element

$E_D$  damping energy

$E_I$  the energy input to the structure

$E_K$  kinetic energy

$E_S$  strain energy

$E_Y$  yielding energy, or yield dissipated energy

$E_{Absorbed}$  absorbed energy

$E_{Dissipated}$  dissipated energy

$E_{Recoverd}$  recoverd energy

$E_n^d, E_{nn}^d$  degraded elastic modulus for failure and rotated failure planes  $n$  &  $nn$ , respectively.

$f_o$  computed natural frequency for a multi-span footbridge structure

$f_I, f_D, f_S$  mass inertia, damping force and restoring force or base-shear force, respectively.

$f_S(u, \dot{u})$  elastic and yield resisting force in an inelastic system.

$(f_s)_i$  resisting elastic force for a linearly elastic system at time-step  $i$ .

$(\mathbf{f}_s)_i$  resisting elastic force vector at time-step  $i$

$(\Delta f_s)_i$  incremental restoring forces at time-step  $i$

$(\Delta \mathbf{f}_s)_i$  global incremental restoring forces vector at time-step  $i$

$\Delta \mathbf{f}$  incremental nodal forces and moments of the fibre element

$(f_s(u, \dot{u}))_i$  resisting force for an inelastic system at time-step  $i$ .

$f_{s_o}$  initial restoring forces

$f_y$  yield strength of the global structural system, also the flexural capacity of the structure

$\bar{f}_y$  normalized yield strength of the system.

$f_t$  tensile strength of material

$F_c$  also  $f'_c$  concrete axial strength

$F_y$  steel axial strength

$F$  and  $Q$  yield surface and plastic potential surface, respectively.

$F_1, F_2, F_3$  3 different forces of linkage-elements

$G$  energy release rate per unit *new* crack area  
 $G_f$  fracture energy  
 $h$  column height  
 $i$  time-step  
 $k, k_t, k_\theta$  stiffness, tangential stiffness and rotational stiffness.  
 $\hat{k}$  grand stiffness  
 $(k_i)_s$  secant stiffness at time-step  $i$   
 $(k_i)_t$  tangential stiffness at time-step  $i$   
 $(\hat{k}_i)_t$  grand tangential stiffness at time-step  $i$   
 $\mathbf{k}$  local stiffness matrix  
 $\mathbf{k}_i$  global stiffness matrix at time-step  $i$   
 $\hat{\mathbf{k}}_i$  global grand stiffness matrix at time-step  $i$   
 $\hat{\mathbf{k}}_i^r$  reduced global grand stiffness matrix at time-step  $i$   
 $K$  stiffness coefficient of seismic isolation bearing SIB  
 $K1, K2$  pre-yield and post-yield stiffness coefficients of SIB, respectively.  
 $\mathbf{l}, \mathbf{1}$  local and global influence vectors equal 0's and  $\pm 1$ 's according to the DOF of the structure.  
 $l$  characteristic length of smallest element.  
 $L$  length of element  
 $L_p$  plastic hinge of length measured from the column base  
 $m$  mass of an element  
 $\mathbf{m}, \mathbf{m}$  local and global mass matrices, respectively.  
 $M_1, M_2, M_3$  3 different moments of the linkage-element  
 $M_i, M_D, M_S$  inertia moment, damping moment and restoring moment or base-moment, respectively.  
 $M_{b_o}$  peak base moment  
 $\Delta M$  incremental moment force at middle of fibre element  
 $\Delta M_j$  incremental moment force at joint  $j$  of fibre element  
 $\Delta N$  incremental axial force at middle of fibre element  
 $\Delta N_j$  incremental axial force at joint  $j$  of fibre element  
 $p_i$  applied force at time-step  $i$ .  
 $\Delta p_i$  load increment at time-step  $i$ .  
 $\Delta \hat{\mathbf{p}}_i, \Delta \hat{\mathbf{p}}_i$  local and global grand load increments at time-step  $i$ , respectively.  
 $p_o$  initial restoring force  
 $P_{eff}$  external effective force.  
 $\mathbf{p}(t)_{eff}, \mathbf{p}(t)_{eff}$  local and global effective loads, respectively.  
 $q_n(t)$  modal coordinate, also known as generalized displacement.  
 $\mathbf{q}, \dot{\mathbf{q}}, \ddot{\mathbf{q}}$  global generalized displacement, velocity and acceleration.  
 $\Delta Q_j$  incremental shear force at joint  $j$  of fibre element  
 $r$  hardening ratio, or ratio of the post-yield to pre-yield, also  $\kappa_{py}$  and  $K2/K1$   
 $R_d, R_s$  residual deformation, residual stresses, respectively.  
 $R_y$  yield strength reduction factor  
 $T_n$  natural period of the structure  
 $t_i$  time at time-step  $i$   
 $\Delta t$  constant time interval  
 $\Delta t_i$  time interval at time-step  $i$ , also constant.  
 $u_i, \dot{u}_i, \ddot{u}_i$  displacement, velocity and acceleration at time-step  $i$ , respectively.  
 $\Delta u_i, \Delta \dot{u}_i, \Delta \ddot{u}_i$  displacement, velocity and acceleration increments at time-step  $i$ , respectively.  
 $\dot{u}_o, \ddot{u}_o$  initial velocity and acceleration, respectively.  
 $\mathbf{u}, \dot{\mathbf{u}}, \ddot{\mathbf{u}}$  local displacement, velocity and acceleration, respectively.  
 $\ddot{u}_g, \ddot{u}_{g_o}$  ground acceleration, peak ground acceleration.  
 $u_j(t)$  displacement response at node  $j$   
 $u^t$  total displacement  
 $u$  relative structural motion displacement  
 $u_g$  rigid ground motion displacement  
 $u_o, \dot{u}_o, \ddot{u}_o^t$  peak displacement, velocity and acceleration responses of structure's top, respectively.  
 $u_m, u_y$  maximum inelastic displacement, yield displacement, respectively.  
 $U_a$  change in elastic strain energy (energy drop).

$U_\gamma$  tensile surface energy change  
 $U_o$  total energy of specimen + its loading system, *before* the crack is introduced, (constant)  
 $\Delta u_i$  global displacement increment at time-step  $i$ .  
 $\Delta u$  incremental nodal responses (displacements and rotations) of the fibre element  
 $\Delta u_j$  incremental nodal vertical displacement at joint  $j$  of fibre element  
 $\Delta v_j$  incremental nodal lateral displacement at joint  $j$  of fibre element  
 $V_{b_o}$  peak base shear  
 $V_o$  initial volume  
 $\Delta V$  volume change  
 $w$  damage parameter  
 $W$  weight of superstructure  
 $y_k$  distance from the element centroid to the  $k^{\text{th}}$  fibre

$\beta$  and  $\gamma$  constants for Newmark method

$\gamma_e$  surface energy per unit area, or surface tension

$\Gamma$  nodal participation factor.

$\varepsilon_n, \varepsilon_{nn}$  strain in the failure and rotated failure planes  $n$  and  $nn$ , respectively.

$\varepsilon_x, \varepsilon_y, \varepsilon_z$  strains in the  $i$ -direction.

$\Delta \varepsilon_k$  axial strain increment at  $k^{\text{th}}$  fibre

$\Delta \varepsilon_a$  incremental axial strain at the centroid of the element

$\Delta \varepsilon_c$  incremental axial concrete strain

$\Delta \varepsilon_v, \Delta \varepsilon_q$  incremental volumetric and deviatoric strains, respectively.

$\Delta t_{cr}$  critical time-step.

$\zeta$  time between time  $t_i$  and  $t_{i+1}$ , also damping ratio (chapter 3)

$\theta$  column curvature, also scalar parameter (chapter 3)

$\theta_p$  plastic curvature capacity

$\Delta \theta_j$  incremental nodal rotation at joint  $j$  of fibre element

$\Delta \phi$  incremental curvature of the element

$\kappa_{py}$  ratio of the post-yield stiffness to the initial stiffness, also  $r$  and  $K2/K1$ .

$\mu$  ductility factor

$\mu_d, \mu_{Demand}$  ductility demand

$\mu_u, \mu_{Capacity}$  ultimate ductility (capacity)

$\nu$  Poisson's ratio

$\xi$  damping coefficient

$\rho$  material density

$\rho_l$  longitudinal reinforcement ratio

$\sigma_k$  axial stress of the  $k$ -th fibre element

$\sigma_{allowable}$  allowable stress

$\sigma_{ult}$  ultimate axial compressive stress of concrete (ultimate strength)

$\sigma_T$  also  $\sigma_t$  tensile strength

$\sigma_i$  principal stress invariant  $i$ , ( $\sigma_{1,2,3}$ )

$\sigma_n, \sigma_{nn}$  stress in the failure and rotated failure planes  $n$  and  $nn$ , respectively.

$\sigma_d$  deviatoric stress

$\sigma_m, \bar{\sigma}$  mean stress and second deviator stress invariant

$\varphi$  angle of dilation

$\phi$  angle of friction

$\Phi_{jn}$  modal shape  $n$  at node  $j$

$\Phi$  global modal shape

$\omega_n$  natural angular frequency.

$\Omega$  spectral matrix

# ABBREVIATIONS

AR	Aspect Ratio
BDSI	Bi-Directional Seismic Isolation
c.g.	centre of gravity
Caltrans	California Transportations Department
DE/FEM	Discrete Element/Finite Element Method
DB	Displacement-based formulation
DOF	Degree Of Freedom
FBPH	Force-Based formulation with Plastic Hinge
FEM	Finite Element Method
FE	Fibre Elements
FPS	Friction Pendulum Systems (seismic isolation)
IM	Intensity Measure
JRA	Japanese Road Association
LRB	Lead Rubber Bearings
MDOF	Multiple Degree Of Freedom
PH	Plastic Hinge
PRSI	Partially Restrained Seismic Isolation
PGA	Peak Ground Acceleration
PVA	Peak Ground Velocity
PVA	Peak Ground Velocity
PVD	Peak Ground Displacement
PBSE	Performance-Based Seismic Engineering
PBSD	Performance-Based Seismic Design
RC	Reinforced Concrete
SDC	Seismic Design Criterion
SDOF	Single Degree Of Freedom
SIB	Seismic Isolation Bearings, also Base Seismic Isolation Bearings
SSI	soil-structure interaction

# Chapter 1

---

## Introduction

---

### Contents

1.0 INTRODUCTION .....	2
1.1 PERFORMANCE-BASED SEISMIC ENGINEERING.....	2
1.2 LEVELS OF RELIABILITY .....	3
1.3 DAMAGE RISKS.....	4
1.3.1 Levels of Vulnerability to Damage .....	4
1.3.1.1 Peak Response to Strong Ground Motion .....	5
1.3.1.2 Failure Mode in Single Columns.....	5
1.3.1.3 Confinement and Ductility .....	6
1.3.1.4 Long Duration Pulse.....	8
1.4 OBJECTIVES & METHODOLOGY OF THE CURRENT PROJECT .....	8
1.5 OUTLINES OF THE THESIS.....	10
1.6 REFERENCES .....	12

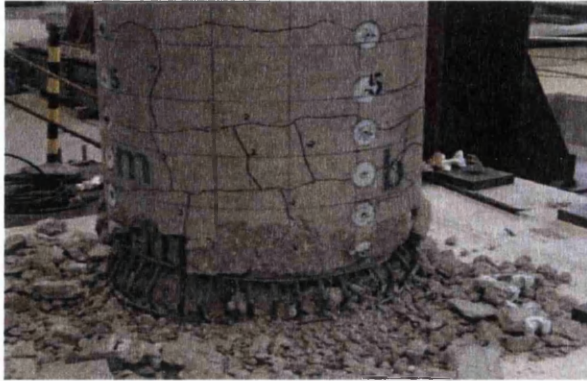
# 1.0 INTRODUCTION

## 1.1 PERFORMANCE-BASED SEISMIC ENGINEERING

The principle of Performance-Based Seismic Design (PBSD) has played a vital role in Earthquake Engineering. Its significance is to assure that the constructed buildings will resist the effects of earthquake ground motions of different severities within acceptable limiting levels of damage. This implies that the seismically loaded structure will not be damaged beyond certain limit states [1]. In general, Performance-Based Seismic Engineering (PBSE) has a broad concept which includes the evaluation of damage in structural members, non-structural facilities and also floor contents. In terms of structural members, PBSE is concerned with all aspects of the building process, such as the design criteria, selection of a structural system, layout proportions, detailing of the structural members, construction quality control and long-term maintenance. However, the majority of research work in this concern is associated with determining the different levels of reliability that a building can act under specified levels of excitations [1].

Damage in the designed members is highly significant in Performance-Based Seismic Engineering. However, many reinforced concrete (RC) bridge columns are seismically designed according to the Demand/Capacity principle of Seismic Design Criteria (SDC), which assumes the functionality of this principle as far as the structural strength and ductility is greater than the seismic demand. This research is questioning the validity of this assumption in RC bridge columns under strong ground motion and other conditions. It is a general concept in Eurocode 8 and also other codes that 'the bridge should retain its structural integrity and adequate residual resistance after the seismic event' [2]. However, there are structural parts in the RC bridges that are susceptible to damage by their contribution to energy dissipation during the seismic event, but the structure should still sustain emergency traffic [2]. Therefore, one of the design principles in bridge engineering is to allow local minor damages in the bridge columns, considering the initiation of plastic hinge (PH) zones. The concept of a plastic hinge in the design methodology presumes the loss of the concrete cover only, known as spalling, and the initiation of non-linear straining of the longitudinal bars along the PH zone. However, this may not be the case during severe earthquakes, where, severe local damage may destroy the concrete core of the column section, and could lead to a total collapse of the structure, especially when the longitudinal reinforcement bars are

severely deformed or buckled, as shown in Figure 1.1. The main goal of this research is to investigate the damaged plastic hinges at the core of RC bridge columns when subjected to earthquake loading.



**Figure 1.1: Damage of concrete and bar buckling**

## **1.2 LEVELS OF RELIABILITY**

There are different scale levels for a structure that could be investigated and assessed in order to determine the levels of dissipated energy. These scale levels are: the material, the section, the member and the global scale of the structure. In order for a structure to resist an earthquake strike without failing its required serviceability, performance and safety requirements, all of these scale levels should be reliable during and after the earthquake incident. The terms for the levels of reliability [3], are expressed in the following diagram in Figure 1.2. Material reliability is often measured by the constitutive relationship, yield strength and ultimate strength. Section is tested by its ductility, and the member's reliability is dependent on its hysteretic behaviour. At a global scale, the whole structure is accounted for resisting seismic loading as its flexural and shear performance is acceptable.

Researches targeted the seismic failure process from different levels of reliability for several structures, but none of them can be dominant and the output energy can dissipate through any one of those levels, therefore, it is a matter of a case-study investigation that should be carried out individually in order to realise the less reliable level that may cause the severe damage.



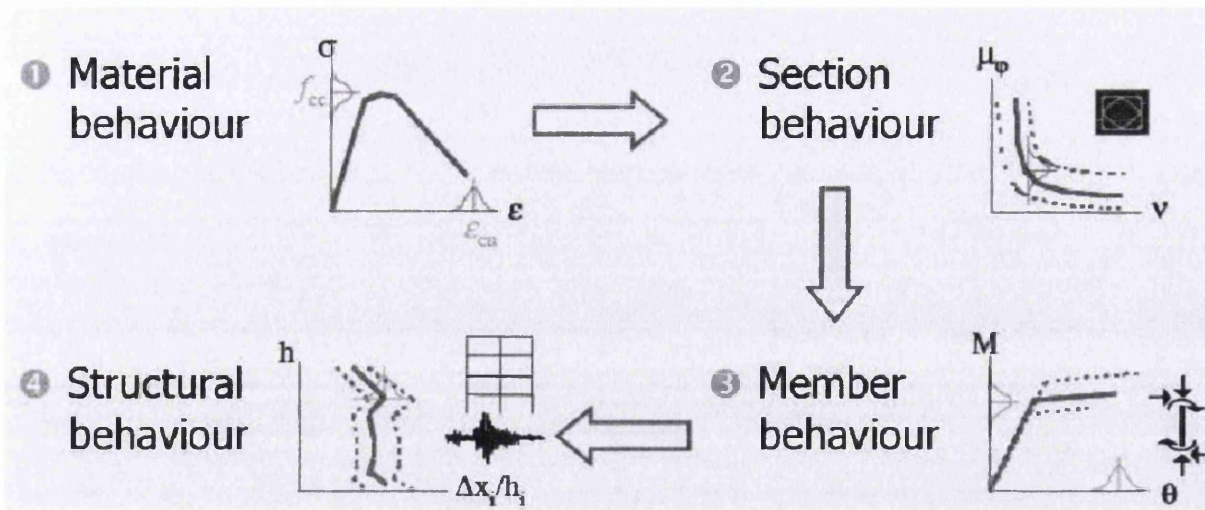


Figure 1.2 Levels of reliability [3]

This research is concerned about one of the most important levels of reliability, which is the level of member's behaviour, in which the reliability of reinforced concrete RC bridge column is tested under seismic loading, knowing that the RC column member is seismically designed according to the Demand/Capacity principle of Seismic Design Criteria (SDC).

### 1.3 DAMAGE RISKS

In addition to local damage of the member and global damage of the structure, two other important issues are also crucial to PBS design for RC bridge columns, and should be taken into consideration; the residual displacement after an earthquake, and the structure's displacement exceeding the allowable lateral displacement stated by building codes. These two issues, if not considered, can also reduce the seismic performance of the structure, even in case of low damage levels. However, these issues are not within the scope of this work.

#### 1.3.1 Levels of Vulnerability to Damage

Vulnerability to damage in this particular problem of the RC bridge column is increasing according to several factors, such as loading intensity, failure mode, direction of loading, confinement, ductility, rate of loading and others. This structure becomes more vulnerable to damage when levels of vulnerability to damage are not controlled. This can be briefly explained in the following sections.

### 1.3.1.1 Peak Response to Strong Ground Motion

The magnitude of the Peak Ground Acceleration (PGA) in strong ground motion is the major cause of damage severity in RC bridge columns, as larger loads cause greater deflections. Therefore, the level of vulnerability to severe damage is high as PGA's are high. Other seismic parameters are also effective, such as the type of soil and distance from the seismic fault, which could promote the structural response to a higher damage extent. The damage of the Loma Prieta earthquake is severe at the part of the bridge settled in soft soil, as shown in Figure 1.3.

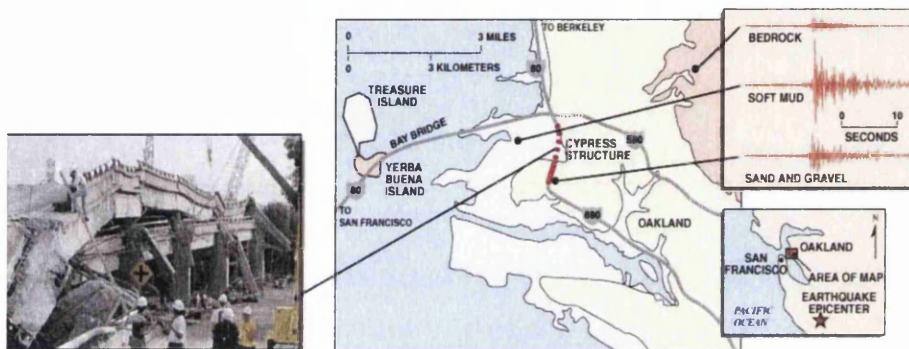


Figure 1.3 Flexural top deck of the freeway collapsed due to the 1989 Loma Prieta earthquake accounting for a large fraction of the fatalities, even though the epicentral distance is about 100 km.

### 1.3.1.2 Failure Mode in Single Columns

Deflecting in the longitudinal direction of bridges supported on single columns is more likely to function in the shear mode of failure, since the upper end is connected to a highly rigid viaduct structure. However, deflecting in the transverse direction of the bridge is more likely to act in the flexural mode of failure as can be seen in Figure 1.4.

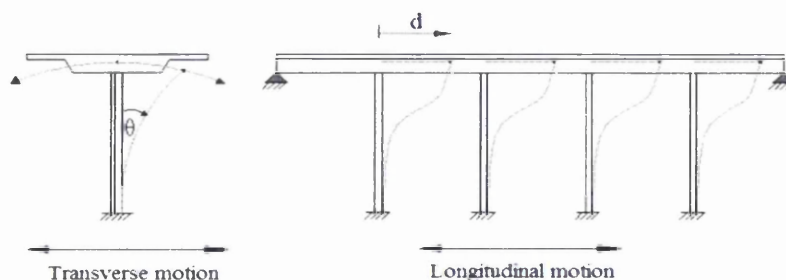


Figure 1.4 Flexural and shear modes of failure

Failure of single-column structure is fully dependant on the performance of the RC single column. In case of deflecting in the transversal direction, the flexural mode of failure increases the column's vulnerability to damage since that flexure is restricted to one member only. In contrast to bridges, other structures with multiple columns, such as multi-floor framed buildings, have their flexural failure mode performed by applying the axial tensile stresses on some columns and compressive stresses on others. In such case, damage is less vulnerable to become critically grown in one member only. For a wider view on common RC box-girder bridges on single and multiple piers, Table 1.1 summarizes the types of RC box-girder bridges on single and multiple columns [4]. It is a fact that many viaduct structures are supported by single piers which take less traffic space and are architecturally suitable to both single-cell and multiple-cell box-girder viaducts.

### **1.3.1.3 Confinement and Ductility**

The main purpose of confinement of RC columns is to initiate inward transverse stresses on the column core. Such stresses have a significant role in strengthening the concrete section especially at the critical zones of plastic hinges. One of the important methods for initiating confinement is the transverse reinforcement stirrups or hoops. They can produce inward ring stresses around the concrete column core to counteract the concrete outward strains due to axial forces of the structure dead load. If the dead load is relatively low, as in the case of single-cell box-girder bridges, low confinement is produced, and thus, the column is more vulnerable to damage under lateral motion. This is one of the main reasons that such structures could initiate crack growth inside the column core quite easily. Ductility of the structure is significantly compromised by the crack growth inside the column core, since the longitudinal reinforcement bars would be extremely exposed and could severely deform or buckle, leading to total collapse.




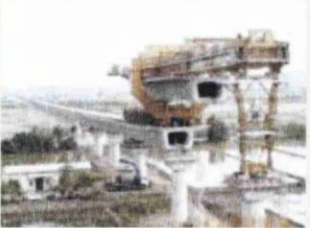

Type	Cast	Type Of Pre-Stressing (Pre-Tensioning/Post-Tensioning)	Connection To Piers		Construction Method	Supporting Piers
<b>In-Situ Multi-Cell Box-Girder Decks</b>	<i>In-Situ</i>	Pre-Tensioned (Span-By-Span Pre-Stressing)	Continuous, By Cantilevering & Pre-Tensioning		Span-By-Span Erection (Span + Short Cantilever)	Single Or Multiple RC Columns 
		Or Post-Tensioned Tendons			Or <i>In-Situ</i> Balanced Cantilever + <i>In-Situ</i> Cantilevers Using <i>Form Travellers</i> + <i>In-Situ</i> Mid-span	Single RC Columns 
<b>In-Situ Single-Cell Box-Girder Decks</b>						
<b>Precast Segmental Box Girder Decks</b>	Precast	Post-Tensioned Tendons	Continuous, By Pre-Tensioning	With Mortar Joints	Span-By-Span Erection Or	Single RC Columns 
				Or With Match-Cast Joints (Epoxy Or Dry Joints)	Balanced Cantilever Erection Or Progressive Placing Erection	
<b>Precast Full-Length Box-Girder Decks</b>	Precast	Pre-tensioned	Simply-Supported on Bearings (Rubber < 50m Span, Mechanical > 50m Span)		Lifting, Rolling, & Positioning Units	Single RC Columns 
			Continuous		Precast Balanced Cantilevers + Lifting & Positioning Middle Units	
<b>Incrementally-Launched box-girder decks</b>	<i>In-Situ</i>	Post-Tensioned Tendons	Continuous, By Arch Effect (Vertical Shear Action)		Balanced Cantilever Erection	RC Wall 

Table 1.1 Types of RC box-girder bridges



### 1.3.1.4 Long Duration Pulse

In relevance to damage, several earthquake records show that relatively long duration impulses with low frequency have the potential to cause further damage, more than those records having similar PGA's but with relatively short duration impulses and higher frequency. The phenomenon of long duration and low frequency is known as the Acceleration Pulse [5], which causes higher ground velocity and larger ground movement. This increases the seismic hazard, causing a more extensive response by the structure in terms of lateral displacement and damage of the column base.



Figure 1.5 Destruction of plastic hinge zones [5]

## 1.4 OBJECTIVES & METHODOLOGY OF THE CURRENT PROJECT

The levels of vulnerability to damage in RC bridge columns such as intensity of seismic loading, failure mode, direction of loading, confinement, ductility and rate of loading could lead to severe damage if they are not controlled. Designing RC columns according to the seismic design criterion of balanced demand and capacity of column ductility is not sufficient to attain plastic hinges with minor damages, especially when many levels of vulnerability are not controlled. The main goal of this research is to investigate the damaged plastic hinges at the core and cover of the RC bridge columns when subject to earthquake loading.

Seismic analytical models based on beam-column elements are used to perform non-linear dynamic analyses, to predict the plastic behaviour at pre-failure stages and strength degradation at post-failure stages. But they are not capable of predicting the local crack

growth and its effects on adjacent zones. Therefore, fracture analysis is significantly important to simulate the local damage in a small-scale model in order to have a more reliable understanding of such problems under any level of vulnerability. However, it is important to know that the damage growth mechanism in quasi-brittle 3D continuum under dynamic loading is still a complex subject in Mechanics of Materials [6].

Two major approaches have been followed with this aspect, the first approach is using the Fibre Element Method to perform a non-linear dynamic analysis, and to determine the global damage by using the energy-based method. In addition, this analytical model is used to approximate the local damage in the cover and core of the RC column section, by using a stress-based method. The second is a small-scale approach in which the Discrete Element/Finite Element Method (DE/FEM) is used to determine the local damage in the elements for only a short duration of the seismic history record. Despite its excessive computation time and capacity, the DE/FEM model provides significant information about the local damage state in the RC column core, which enhances understanding of the seismic performance of the structural member under any level of vulnerability.

When several levels of vulnerability compile together in one structure, it is very important to think of other alternatives of structural systems that are more capable to resist the seismic loading. It is not logically successful to adopt the same structural system for different cases of loading, failure modes, confinements and rates of loading. Two important tasks should be considered in this respect:

1. Adopting structural alternatives for single RC columns supporting single or multi-cell box-girder bridges, such as Seismic Isolation Bearings SIB's, carbon fibre reinforced polymers CFRP [5], steel confinement jackets [6], pre-stressed (post-tensioned) columns and buckling-resistant braces BRB. Such systems are specially designed to plastically control the damage in the RC columns and dissipate the seismic energy during the extreme seismic event in the safest manner. Other alternatives such as seismic-energy dissipation braces [7] are utilised to maintain the main frame members to remain perfectly elastic during the earthquake event, and allow secondary members to deflect plastically with minimal damage.
2. Adopting small-scale fracture analyses to investigate thoroughly the structural damage, and introduce a more reliable design for the RC single columns

supporting box-girder bridges. Typical designs with seismic design criterion SDC based on the Demand/Capacity principle must be verified for the functionality and non-disruption of the assumed ductility of the structure. Fracture analysis should also be utilised to verify the workability of RC columns enhanced with one of the aforementioned structural damage-controlled devices such as SIB's, CFRP's and BRB's.

## **1.5 OUTLINE OF THE THESIS**

Chapter 2 is concerned with a literature preview for the topics related to this research in general, and the publications of some of the subjects discussed in the chapters of this research. Chapter 2 reviews topics on seismic performance, seismic spectra, damage indices and fragility measures. It also focused on important shaking table tests that are significantly used in this research, and addresses a variety of numerical tests that were introduced by researchers to simulated RC columns under seismic loading.

Chapter 3 is concerned with an explanation of the theoretical basis upon which many of the topics of this research have been discussed and numerically analysed. The main topics in this research include Equilibrium of Forces in the Elastic Medium, Equation of Motion for the Dynamic Body, Failure and Non-linear behaviour of Isotropic Materials, topics in Earthquake Engineering, Fracture and other selected dynamic topics.

Chapter 4 is concerned with applying the Fibre Element Method in a computational algorithm by using the MatLab program, to solve non-linear dynamic problems, and investigating some of the parameters that influence the validity of the code when compared with the results of one of the Fibre Element software packages; the SeismoStruct [10].

Chapter 5 applies the SeismoStruct software to solve a case study that was analysed and investigated in several important technical report publications in the field of RC reinforcement concrete bridge columns under strong ground motion earthquakes. In this chapter, more investigations are conducted about energy-based damage, stress-based damage and the global and local damage indices. There are more investigations about energy dissipation, and its correspondence to the damage potential. In addition to discussing the importance of applying the seismic isolation bearings as one of the major devices to dissipate

the seismic energy and mitigate the damage potential in the RC bridge columns when subjected to strong ground motion.

Chapter 6 is dedicated to the application of the combined Discrete Element/Finite Element Method to solve the same proposed problem by using the Explicit-Elfen algorithm that's developed in Swansea University, and has been applied in various fracture analyses. In this chapter, the proposed problem of RC bridge column is set up, and the theoretical basis for failure criterion, fracture model, pre-failure, post-failure and post-fracture for concrete as a quasi-brittle material is explained, in addition to the elasto-plastic behaviour of the steel reinforcement bars. Difficulties that have been encountered and the computational problems concerning the time-steps, time of computational analysis and initiation of cracks are also discussed.

The local damage can be determined in the column's cover and core at every time-step, and the mode of failure is monitored in the concrete and steel reinforcement bars. Important conclusions were obtained in terms of disruption of the assumed ductility in RC bridge columns when subjected to levels of damage vulnerability.

In chapter 7, two different topics are presented; the effect of loading rate on the performance of RC bridge columns, and the multi-scale analysis in RC structures. In the first topic, fracture analyses are conducted to investigate the effect of different loading rates on the RC damage. The second topic is presenting a technique for analysing a small-scale model from a larger-scale model in order to conduct the fracture analysis for a beam-column joint selected out of a global RC frame structure.

Chapter 8 concludes the major achievements from this research, in addition to important recommendations and practical suggestions for the design of single-RC columns supporting single and multi-cell box-girder bridges. Additionally, specified points of criticism on the Eurocode8 are documented, in relation to the topic of this research. Finally, a proposed future work that links between research and practice is suggested, with possible applications on the field of motorway bridges in seismically active regions in Libya.



## 1.6 REFERENCES

- [1] R. D. Bertero, V. V. Bertero. Performance-based seismic engineering: the need for a reliable conceptual comprehensive approach. *Earthquake Engineering Structural Dynamics*, 2002; 31:627-652 .
- [2] European Committee for Standardisation. Eurocode 8: Design Provisions for Earthquake Resistance of Structures, Part 2: Seismic Design of Bridges. ENV1998-2, CEN, 1998.
- [3] Lecture Notes on Levels of Reliability.
- [4] P. Mondorf. *Concrete Bridges*. London ; New York: Taylor & Francis, 2006.
- [5] J.P.Singh. Characterization of ground motion for severity and damage potential. <http://nisee.berkeley.edu/lessons/singh.html>.
- [6] S. Chao, C. Loh. Inelastic response analysis of reinforced concrete structures using modified force analogy method. *Earthquake Engineering and Structural Dynamics*: 36:1659–1683. 2007.
- [7] A. A. Abdelrahman, S.H. Rizkalla. Deflection Control of Concrete Beams Pretensioned by CFRP Reinforcement. *Journal of Composites for Construction*, 1999, Vol. 3, No 2, pp. 55-62.
- [8] H. IL. Jeong, J. Sakai, S. A. Mahin, Shaking Table Tests and Numerical Investigation of Self-Centring Reinforced Concrete Bridge Columns. Pacific Earthquake Engineering Research Centre, PEER Report 2008/06, University of California, Berkeley.
- [9] T. Takeuchi. Japanese Demand for High Seismic Performance and Energy Efficiency, *SECED Newsletter* Vol. 23 No.4 August 2012.
- [10] Bibliography of SeismoStruct Earthquake engineering Software, SeismoStruct v5.2.2 Official release of 22/08/2011.

# Chapter 2

---

## Literature Preview

---

### Contents

2.0	INTRODUCTION .....	15
2.1	EARTHQUAKE ENGINEERING AND STRUCTURAL DYNAMICS .....	17
2.1.1	Historical Background on PBSE.....	17
2.2	ENGINEERING APPROACHES IN EARTHQUAKE PROBLEMS.....	18
2.2.1	The Displacement-Based Approach .....	18
2.2.1.1	The capacity-demand spectrum .....	19
2.2.2	Energy-Based Approach .....	20
2.2.3	Combination of Displacement-Based and Energy-Based Approaches.....	22
2.2.4	Damage and Performance-Based Seismic Design PBSB .....	23
2.2.5	Damage-Based Approach .....	23
2.3	SEISMIC DAMAGE & DAMAGE INDICES.....	25
2.3.1	Definition of the Damage State.....	25
2.3.2	Assessment of the Seismic Damage .....	25
2.3.3	Typical Damage Indices .....	27
2.3.3.1	The damage index of Mergos & Kappos .....	28
2.3.3.2	Other Damage Indices.....	28
2.3.4	Performance Limits in Damaged Members .....	29
2.3.5	Fragility curves .....	30

2.4 SHAKING TABLE TESTS FOR SEISMICALLY DESIGNED RC BRIDGE COLUMNS.....	31
2.4.1 Nishida and Unjoh [46].....	32
2.4.2 Sakai and Mahin [47].....	33
2.4.3 Sakai and Unjoh [49].....	35
2.4.4 Jeong, Sakai and Mahin [51] .....	38
2.5 NUMERICAL MODELS .....	40
2.5.1 Numerical Modelling using the Damage Theory.....	40
2.5.1.1 Continuum Damage Model (CDM), Calayir and Karaton [52].....	40
2.5.1.2 Lumped Damage Model, Alarcon E. et al. [54].....	42
2.5.1.3 Continuum Damage Model under Force Equilibrium Mechanics for Bridge Piers, S. Oller, A. Barbat [55].....	44
2.5.2 Numerical Models based on Empirical Models.....	46
2.5.2.1 Beam-Column Non-linear Element Modelling Supplemented with Empirical Drift Capacity Models. Yavari, Elwood and Wu. [58].....	47
2.5.2.2 Strain-Curvature Empirical Model. Lee and Watanabe [61].....	49
2.5.3 FEM Numerical Modelling based on Smeared and Discrete Approaches .....	51
2.5.3.1 The Smeared Cracking Model .....	51
2.5.3.2 The Discrete Cracking Model.....	52
2.5.3.3 Fracture Mechanics Modelling .....	53
2.5.4 Fibre Elements and Lattice Elements Numerical Models.....	55
2.5.5 Numerical Models Conjugated with Seismic Evaluation Approaches and Performance-Based Concepts for Bridges.....	57
2.5.5.1 Numerical models using the Ambient Vibration Technique .....	57
2.5.5.2 Numerical models using the System Identification (SI) Methodology .....	58
2.5.5.3 Energy Concentration and Critical Earthquake Loading .....	59
2.5.5.4 Software Packages of Dynamic Solvers .....	60
2.6 REFERENCES .....	60

## 2.0 INTRODUCTION

Earthquake effects have been a growing interest in the recent years for many structural engineers in both structural analysis and design. In addition to regular moving loads of vehicles and self-weights, reinforced concrete bridges have taken a wide portion of research in their liability to resist severe lateral loads due to wind forces, flood waves and earthquake strikes. Bridges serve as vital links that are required to be functional after an earthquake to provide access to hospitals, fire stations and a variety of other important services. A bridge failure data base website by Cambridge university [1] lists over 380 bridge failure cases which occurred over the world between 1800 and 2009, documenting the reason of failure attributed to natural hazards (such as earthquakes, wind storms, soil failure and floods), overloading, design error, human error, and others. Over 230 bridge failure occurred between 1970 and 2009 [1].

On the seismic issue, many research efforts focused on investigating the ductility and integrity of the bridges' supports; namely, piers and supporting columns. Such supports were very much tested for their seismic resistance together with their foundations, soil-structure interactions and bearings carrying the bridge deck. The research efforts were conducted on both the experimental and analytical models which are supported by theory and mathematical background, in addition to field observations on site for damage assessment after the earthquake event.

Earthquakes have affected bridge structures as they are excited by seismic loads laterally (or transversally), longitudinally and vertically. Responses of bridges differ according to the structural configuration, material, bridge type and seismic site. For example, girder-type bridges with single frames, multi-spans, transversal column lay-outs or single piers respond differently when subjected to an earthquake.

In this work, focus will be directed towards investigating the behaviour of reinforced concrete (RC) single columns supporting box-girder bridges when subjected to earthquakes. Single and multi-cell box-girder viaducts are widely used in the construction field with various forms and methods of structural layouts as in accordance to the type and size of the designed bridge. The considered box-girder in this research belongs to the (In situ single-cell box girder) family of bridges.

In this type, a bridge deck is constructed span by span and cast in place using different construction methods and according to different structural formulations. In situ single-cell

box girders could span from 40 to 270 meters [2], and are most likely to be excited by ground motions at any direction of the seismic action. However, such girders with prescribed constant depths could span up to 70 meters only. Single-cell box girders with struts supporting side cantilevers of the girder deck have been successfully used in several projects in the UK and worldwide [2].

The structural design for bridges is based on the limit state conditions stated in several Codes of Practice for RC bridge design. The limit state given in the (BSi) is the permissible deflection and crack of a RC section [3]. This has been articulated for dead load and moving load cases which are imposed on the bridge, in addition to the seismic-equivalent lateral loads which is statically imposed on the piers. However, vertical seismic effect on building structures has not been included into practice except under special conditions [4]. Moreover, vertical seismic vibrations are to be considered when the ground acceleration is greater than 0.6g [5]. Quite relatively few researchers have discussed the nature and damaging effect of the seismic vertical component on the reinforced concrete bridge decks. The Eurocode8 considers its effect if the structure is located within 5km of a seismo-tectonic fault or in a highly classified seismic zone [5]. Some researchers assumed that 2/3 of the lateral seismic load could be equivalent to the vertical seismic component [5], however, this estimation does not necessarily reflect a general condition of the seismic nature [4].

The BS5400 (BS code for bridge design) excludes any dynamic effects on bridges apart from the impact effect due to highway loadings [3]. According to the BS5400, only footbridges are to be dynamically analysed since they are excited by  $0.50\sqrt{f_o}$ , where  $f_o$  is the computed natural frequency for a multi-span footbridge structure [3].

These comments, clearly, underestimate the effect of ground motions on bridges and particularly the combined lateral and vertical seismic components on bridges, therefore, neglecting its corresponding contribution in structural response, especially when evaluating the damage effect. In fact, incidents of considerable post earthquake structural damages can be attributed to the vertical components of the ground motion, especially for bridges with footings based on soft soils, such as the bridge collapse during the Luma Peirta earthquake in 1989, where those segments of the bridge erected on soft soils were severely damaged. Due to the effect of combined horizontal and vertical ground motion, other cases occurred in 1994 in Northridge, Hyogo-Ken Nanbu earthquake in Japan in 1995, Chi-Chi earthquake in Taiwan in 1999 and Bhuj earthquake in Gujarat in India in 2001 [6].

## 2.1 EARTHQUAKE ENGINEERING AND STRUCTURAL DYNAMICS

Earthquake Engineering is the scientific field concerned with protecting society, the natural and man-made environment from earthquakes by reducing the seismic risk to socio-economically acceptable levels [7]. In general, it is concerned with the study of structural behaviour in response to seismic excitations. One of the main objectives of earthquake engineering is ‘to design, construct and maintain structures to perform at earthquake exposure up to the expectations and in compliance with building codes’[8]. In other words, the structure should be properly designed so as to withstand the seismic loading effects with an acceptable level of damage.

In general, Earthquake Engineering is thoroughly related to major topics in Structural Dynamics Engineering, which covers all loaded structures that respond in a fairly faster frequency  $\Omega$ , (or less faster by a limit), than their natural frequencies  $\omega_n$ ; i.e  $0.25 < \frac{\Omega}{\omega_n} < 10$ . In more precise terms, structures behaviour is dominantly dynamic when they are unable to respond, i.e. to deflect, as quickly to the time-dependent loading, thus they vibrate, and their maximum response  $u^{max}$  would be different from peak response under a static loading  $u^{stat}$  of the same magnitude; i.e., their Dynamic Factor would either be larger or less than unity, or  $D_f = \frac{u^{max}}{u^{stat}} \neq 1.0$ .

In the following sections, some of the main topics in Earthquake Engineering and Structural Dynamics are reviewed from selected published research papers. Some of these topics are directly related to the subject of this research, and others are indirectly relevant to it. Before this it is useful to have a historical background on the topic of Performance-Based Seismic Engineering (PBSE), which is related to many topics in Earthquake Engineering.

### 2.1.1 Historical Background on PBSE

Before 1990 the US International Building Code had adopted a force-based concept for design, which focused on strengthening members’ sections to take extra load, but it did not consider the overall behaviour of the structure [9]. Buildings with such design strategy have shown poor performance during earthquake incidents.

From 1990 to date, the Eurocode8 has laid a new base for the so called capacity-design strategy which has adopted deformation-based and energy-based approaches to reach a seismic design [9]. The philosophy of the capacity design is to dissipate energy throughout the building itself. For a portal frame structure, a strong-column/weak-beam design strategy would be adopted to let the inelastic energy dissipate throughout plastic hinges, which initiate on those weak beams. For different types of structures the plastic hinges would have different positions on the structure [9].

The plastic hinges, or damaged spots, are the means through which most inelastic energy is dissipated, and act as 'hysteretic damping devices' that would bring the structure to some balanced energy state and force equilibrium. It would control the failure of a structure to the minimum extent in order to increase Life Safety measures.

This strategy has changed after the 1994's North Bridge earthquake and 1995's Kobe earthquake [9]. Both earthquakes caused a huge loss in the economy and tremendous costs, people started to think about preserving a structure's serviceability as much as life safety. This brought up what is known as Performance-based strategy which focuses on limiting the expected damage in the design to maintain the structure's serviceability after the earthquake incident [10]. Serviceability and reparability of the assessed structures are very much related to the state of damage that the structure has incurred.

This leads to the field of evaluation of damage in RC structures, which requires knowledge about fracture mechanism and simulation of crack growth as the structure is subjected to the seismic excitement. In addition, Performance-based design requires experience in designing the RC structural members so as to control the position and magnitude of the expected damage of plastic hinges [10].

## **2.2 ENGINEERING APPROACHES IN EARTHQUAKE PROBLEMS**

### **2.2.1 The Displacement-Based Approach**

One of the most popular methods that has been used in earthquake engineering practice and research is the displacement-based approach, which is based on constructing the Pseudo Velocity-Acceleration-Displacement (V-A-D) Elastic Response Spectra, which assign the peak motion parameters for the target earthquake. The Pseudo V-A-D Inelastic Response Spectra are then found from the elastic spectra either by the equal-energy principle or the

equal-displacement principle, using the strength reduction-ductility-period ( $R-\mu-T$ ) relationship [11].

### 2.2.1.1 The capacity-demand spectrum

The Applied Technology Council (ATC) published the ATC-40 [12], for the PBSE for existing RC buildings, which constructs the displacement-capacity curve through running the so-called Push-over test analysis, in which the (whole structure) is tested to its ultimate ductile capacity under static loading for the purpose of evaluation. Then, both demand and capacity curves are plotted together in a pseudo acceleration/pseudo displacement graph, Figure 2.1, in order to determine the so-called (Performance Point) [13], at which the structure is evaluated as seismically balanced [13]. The seismic Capacity-Demand ratio ( $C/D$ ) is used as an explicit expression to check the structure performance near collapse, thus if  $C/D < 1.0$ , the bridge is regarded safe, with acceptable damage effects. Then, damage can be estimated according to the displacement of the performance point, as shown in Figure 2.1.b, which should indicate a relatively low damage index.

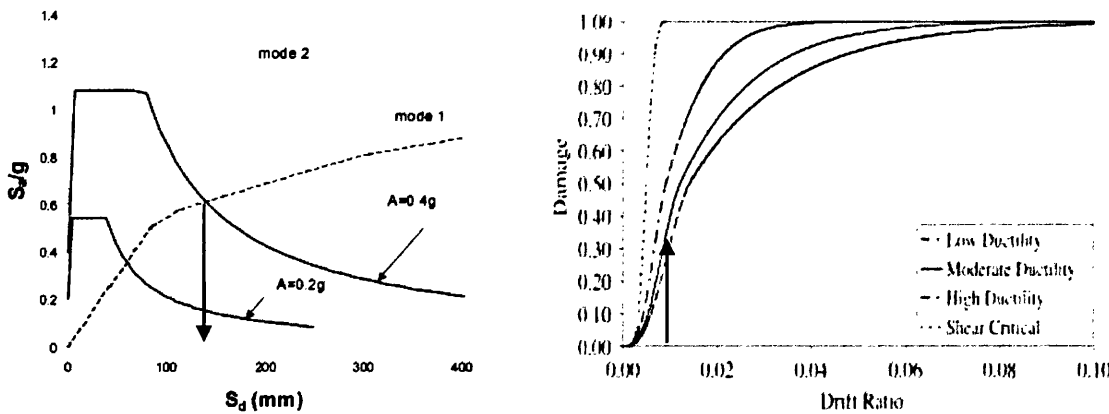


Figure 2.1.a Capacity/Demand spectra [13]. Figure 2.1.b Estimated damage at performance point

Sung et al [14] argued that conventional seismic evaluation methods for existing bridges have drawbacks and are not reliable, since they adopt a simplified strength-based linear procedure to estimate the non-linear demand of the earthquake. Moreover, they consider a single structural performance only (one ground motion intensity) to determine the demand [14]. On the other hand, R. Riddell and E. Jaime [15] argued that the performance-based design need not to be specified through a set of ground motions of different intensities, but through one design motion with performance controlled by the selected design parameters (strength or ductility) and deformation capacity supplied.



## 2.2.2 Energy-Based Approach

The design concept of conventional maximum value-based seismic design method is based on the monotonic loading condition, which does not take into consideration the cumulative damage caused by the seismic excitation with hysteretic characteristics [16]. However, this will lead to unexpected damage in structures for earthquake load even slightly larger than the design load of maximum value [16]. The direct displacement-based design method is a maximum value-based seismic design method but it indirectly accounts for the energy dissipation due to inelastic deformation, therefore many researchers made a lot of effort in the field of energy-based seismic engineering [16]. The main design parameter in energy-based seismic design methods is the hysteretic energy response of a structure. The hysteretic energy is a 'counter weight' for the earthquake induced damage, and therefore, the design procedure will take into account all possible accumulated damage effects. The concept of energy was first induced in seismic design by Housner [17], five decades later researchers started to pay attention to this concept! Riddell and Garcia [16] introduced a method for constructing the energy demand spectrum based on 52 earthquake records, and deduced that damage occurs not only due to maximum ductility attained but also due to the hysteretic energy dissipated by the structure. Leger and Dussault [18] investigated the effect of viscous damping on energy dissipation of structures, Akbas et al. [19] developed a procedure to dissipate energy by accumulative plastic response, assuming linear distribution of dissipated energy along the height of the building. Leelataviwat [20] used the concept of energy balance to develop an energy-based seismic design method. Using the balance energy concept Dasgupta [21] obtained a base shear force for a buckling-restrained braced frame (BRBF) that's significantly smaller than that obtained by the displacement-based design approach. Kim et al. [22] also used the energy balance concept for a BRBF by having the hysteretic energy demand equal to the energy dissipated by the buckling-restrained braces. H. Choi and J. Kim [16] proposed a seismic design procedure for BRBF structures using hysteretic energy spectra and accumulated ductility spectra, assuming frame members to remain elastic during the earthquake loading event, whilst BRB members sustain all seismic input energy and dissipate it independently. This was also performed by the energy balance concept but with using a different scheme to compute the hysteretic energy [16]. H. Choi and J. Kim used 20 earthquake records to construct the spectra for SDOF structures and verify this design procedure [16].

Bojorquez et al. stated that even though there is no agreement on the way that energy demands should be accounted for, all experimental and analytical studies indicate that structures can be protected from the effect of plastic demands by limiting their maximum deformation demand to be significantly smaller than the ultimate deformation capacity [23]. Accounting for cumulative plastic deformation demands can be achieved through the use of one of the following [23]:

- Damage indices; which are capable of considering the cumulative plastic deformation demands, or
- Dissipated hysteretic energy spectra.

Bojorquez et al. proposed a reliability-based seismic evaluation procedure for the seismic design of steel structures, taking into account the reliability and cumulative deformation demands through the use of normalized dissipated hysteretic energy spectra [10].

Recent studies have advised the use of energy concepts as an alternative way to the traditional design strategies for the identification of both seismic demands imposed by the earthquakes and structural capacities that meet with such demands [24]. Decanini and Mollaioli [24] stated that the energy balance formulation is much more effective in concept than the force equilibrium equation since it provides explicit control of balance over the input and dissipated energy. The considered energy is the inelastic input energy, which is the sum of the hysteretic energy and the damping energy, since the accumulation of kinetic and strain energy rates is zero [11]. Hysteretic energy spectrum is more comprehensive than other spectra, and is best correlated with damage [24], therefore, Decanini and Mollaioli [24] suggested a method to estimate seismic demands of hysteretic energy (dissipated energy) from the knowledge of both the elastic and inelastic input energy spectra. They also confirmed that damage depends on both ductility and energy dissipation, but the sensitivity of the input energy towards ductility and energy dissipation depends on the intensity of the ground motion [24]. They constructed a design hysteretic energy spectrum envelope, Figure 2.2, relevant to the hysteretic model of the most significant strong ground motion records. Such a design envelope can be used to estimate any seismic demand on a certain structure [24]. Decanini and Mollaioli [24] found that the hysteretic energy to the input energy ratio is also varying along the period range, and is relevant to 3 major parameters; soil type, distance from the seismic fault and displacement-ductility ratio.

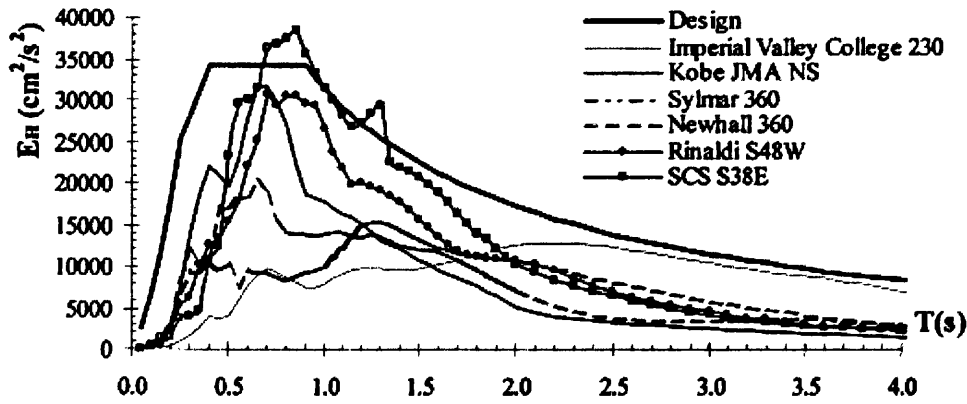


Figure 2.2 Comparison of the design energy spectrum and those relevant to most significant strong ground motion records: Imperial Valley College, (Imperial Valley, 1979), Kobe JMA (Kobe, 1995), Sylmar Parking Lot, Newhall, Rinaldi, and SCS (Northridge, 1994). Soil S2.  $D_f < 5$  km.  $6.5 \leq M \leq 7.1$ .  $\mu = 4$ . [24].

### 2.2.3 Combination of Displacement-Based and Energy-Based Approaches

The inelastic spectrum can be combined with energy-dissipation spectrum to account for damage related to the hysteretic behaviour. Estimates can be made of ultimate deformation capacity of the structure required to meet a given performance level when subjected to a given design earthquake [15]. This was derived using the Park and Ang damage indicator by Riddell and Garcia [15] and simplified to be plotted as in Figure 2.3.

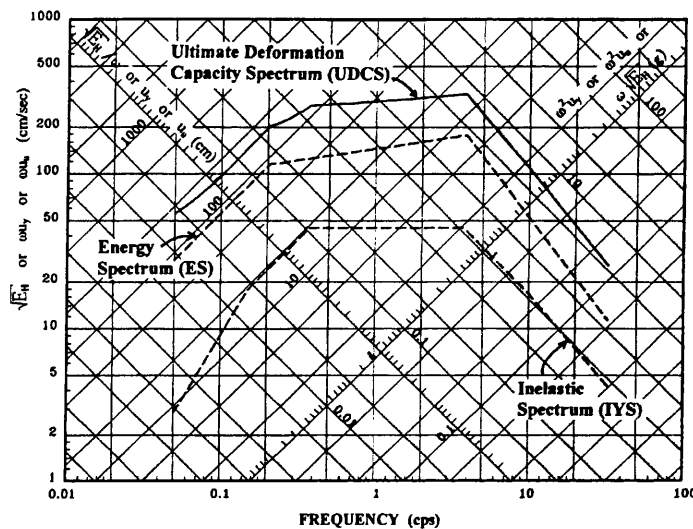


Figure 2.3 Inelastic design spectrum, dissipated energy spectrum, and required deformation capacity spectrum, for design ductility  $\mu = 5$  and design ground motion specified by 1g; 85 cm/s and 44 cm. [15].

## **2.2.4 Damage and Performance-Based Seismic Design PBSD**

R. Riddell and J.E. Garcia in 2001 [15] expected that damage assessment will become a central issue in the years to come, since the seismic codes emphasis has been towards strength of a structure to resist the base shear forces and base moments only, and no accurate verification of the seismic performance for the designed structure had ever been made [15]. The performance-based seismic design is used to ensure that specific damage-based criteria are met [25]. A performance objective represents a specific risk, stated in terms of the desired structural behaviour (or damage state) to be associated with a specific level of earthquake demand (or seismic hazard) [15].

In concern with bridges, Sung et al [14] stated in 2009 that conventional seismic evaluation of existing bridges show inaccurate and unreliable information since they use a strength-based concept to indirectly estimate the non-linear behaviour of structures. A seismic performance-based design of a structure implies that the seismic capacity of a structural response should meet the seismic demand of that structure under the target ground motion excitations. However, when a shortage of seismic capacity exists, certain damage would occur corresponding to that shortage. It is the damage index that expresses the shortage of efficiency in the structure, or it is the fragility index that describes the probability of exceeding the damage state [26]. The severity of damage is related to the amount of energy dissipated during the inelastic stage, and in RC structures concrete starts to sustain the damaging process much earlier before the steel reinforcement tends to yield [27]. Therefore, as fracture is very much related to the hysteretic energy and maximum ductility, fracture energy could be released in some critical members during minor damage stages of the structure [27].

There seems to be an agreement (between researchers) on the fact that the earthquake damage occurs not only due to maximum deformation (or max ductility) attained, but it is associated with the hysteretic energy dissipated by the structure as well [15].

## **2.2.5 Damage-Based Approach**

Most studies in fragility analysis on bridges use column ductility as the primary damage measure [26]. But other effective damage indicators are based on energy dissipation, and one of the best-known local damage indices is the one proposed by Park and Ang [28], which

defines a linear relationship between the displacement and a damage index, yet it involves the ductility and rate of dissipative energy [29]. Another approach was by Hwang et al [30] who used the capacity-demand ratio of the bridge columns to develop fragility curves.

As a qualitative descriptive approach, the HAZUS 97 is a technical manual used for estimating the structure loss in bridges due to lateral earthquake movements, and it determines the damage states as they vary between no damage -to- complete damage state [31]. An extension to the HAZUS table was created by Dutta [32]. HAZUS was used in an analytical study on typical bridges [26], in which damage states were classified in terms of ductility measures and displacement-based domains.

One of the recent researches was by Erduran and Yakut [29] in 2006 who developed displacement-based damage functions for the components of RC moment-resisting frames. They developed damage index curves for different ductility and PGA levels and crack width-rotation curves for different displacement levels [29], as shown in Figures 2.4 and 2.5. The variety in relationships between damage parameters indicated the complexity of damage evaluation in RC structures under seismic load and thus different formulae have been obtained for different RC members (columns, beams and walls) independently. Other parameters such as the structure's period also affects the damage. During a severe load with a long-period structure, the hysteretic energy increases and the maximum deformation could become close to the ultimate deformation value, affecting the damage index significantly [15].

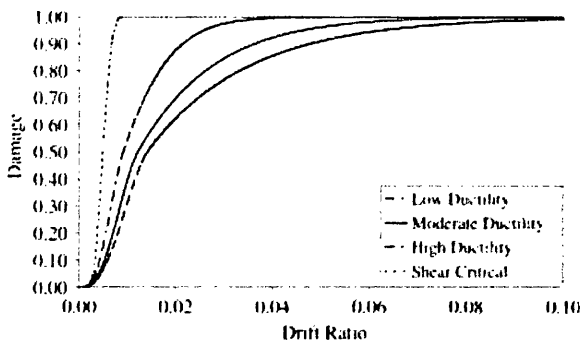


Figure 2.4 Variation of damage curves [29].

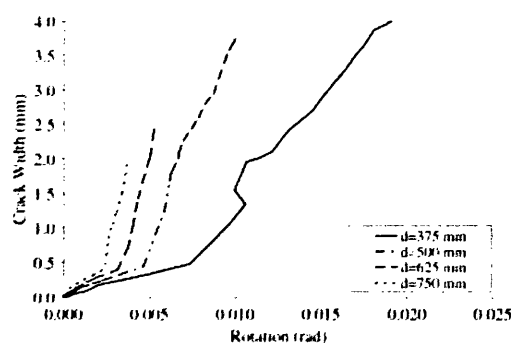


Figure 2.5 Variation of crack width curves [29]

Important notes on damage-based inelastic spectra by Basu and Gupta [33] stated that it is essential for the seismic design practice to incorporate a measure of cumulative damage in the inelastic spectra to provide information about forces and maximum inelastic deformation, in addition to the magnitude of associated damage. They summarized others' work based on the damage criterion such as Fajfar [34] who proposed equivalent ductility factors based on

damage and used them for constructing the inelastic spectra. Decanini and Mollaioli [24] stated that recent seismic destructive events showed that values of ductility higher than 4 implicate unacceptable damage levels. On the other hand, several authors do not agree about how earthquake input energy is sensitive to ductility [24].

## 2.3 SEISMIC DAMAGE & DAMAGE INDICES

### 2.3.1 Definition of the Damage State

Pier columns are most critical components in conventional highway bridges with continuous deck and monolithic abutments, a number of studies have developed the criteria for their damage index and corresponding limit states based on the damage status or loss of load-carrying capacity [35]. Different damage indices are based on different measurers such as curvature ductility, displacement ductility and residual displacements. HAZUS [36] defined 4 damage states, shown in Table 2.1 as slight, moderate, extensive and collapse damages. This definition is commonly adopted by many researchers.

Damage states	Description
No damage (N)	No damage to a bridge
Slight/minor damage (S)	Minor cracking and spalling to the abutment, cracks in shear keys at abutments, minor spalling and cracks at hinges, minor spalling at the column (damage requires no more than cosmetic repair) or minor cracking to the deck
Moderate damage (M)	Any column experiencing moderate cracking and spalling (column structurally still sound), any connection having cracked shear keys or bent bolts, or moderate settlement of the approach
Extensive damage (E)	Any column degrading without collapse (column structurally unsafe), any connection losing some bearing support, or major settlement of the approach
Complete damage (C)	Any column collapsing and connection losing all bearing support, which may lead to imminent deck collapse

Table 2.1 Description of bridge damage states (taken from HAZUS 97) [26]

### 2.3.2 Assessment of the Seismic Damage

Performance-based design needs to have a reliable assessment of the seismic damage potential since the cost of construction or rehabilitation of existing structures depends on the assessment of the seismic damage [37]. Excessive costs for new construction could result if

the expected intensity of the earthquake is greatly overestimated, severe damage and loss of life may occur if the intensity is seriously underestimated [37]. Therefore, “a reliable definition of seismic intensity has to relate to the effect of damage on structural behaviour in order to assess the potential seismic hazard and to classify the seismic input”[40]. E Cosenza and G Manfredi divided the damage Indices into 3 types [37]:

**1. Damage measures based on ground motion parameters**

This type is based on data from earthquake records alone with no structural response data involved. The peak parameters, which are PGA, PGV and PGD, are used to formulate the earthquake’s destructiveness that are called ‘Integral Parameters’ which are the basis for measures such as the Arias Intensity and the Saragoni Factor [26]. Integral parameters are the root mean square RMS of acceleration, velocity or displacement value for  $x(t)$  in the following definition of an integral parameter formula:

$$RMSX = \left[ \frac{1}{t_E} \int_0^{t_E} x^2(t) dt \right]^{1/2} \quad (2.1)$$

where  $t_E$  is the total duration of the earthquake record, which is very influential on the level of structural damage. “Records with large acceleration and spectral values produce slight damage if the duration is short (e.g. the Ancona earthquake in 1972), whereas records with low acceleration and long duration can be very destructive (e.g. the Mexico earthquake in 1985)” [37]. The integral parameters are effective for measuring the energy content of a seismic event, and for including the seismic duration. Other damage measures do not associate the seismic duration in their formulations.

**2. Damage measures based on Linear response:**

These are simply the maximum elastic pseudo-acceleration, pseudo-velocity and displacement determined for destructive earthquakes. Elastic spectral representation can be assumed as a basic measure of the earthquake’s potential. Other parameters based on these values are also used as measures for destructive earthquakes.

**3. Damage measures based on Non-Linear response:**

The damage potential in an in-elastic system depends on two parameters:

- 1) The inelastic pseudo-acceleration, or simply the plastic acceleration, which represents the strength demand of the ground motion on an inelastic system. The plastic acceleration represents the behaviour of the structure independent of the dissipated energy.

- 2) The hysteretic energy that represents the cyclic collapse in an in-elastic structure that shows a cumulative damage. The energy dissipation is due to the plastic cycles in the structural response. In order for the structure to dissipate the total amount of hysteretic energy, the structure has to develop a number of plastic cycles to reach the maximum ductility, or maximum plastic displacement.

### 2.3.3 Typical Damage Indices

Typical damage states for concrete columns and bearings are shown in Table 2.2, with their corresponding damage index criteria available in the literature [36]. In this table the damage is captured an based on either curvature ductility, displacement ductility, loss of load-carrying capacity, drift ratio, displacement or shear strain. This description of damage states given by HAZUS97 and other sources [26,35,36,38,39,40,41] provides one of the important qualitative damage definitions for loaded RC columns. The definition of the damage states are usually based on recommendations of previous studies and results from experimental tests, but engineering judgement should also be used when determining the damage states, as they vary depending on type, age and condition of the bridge [26].

Bridge component	DI	Slight (DS = 1)	Moderate (DS = 2)	Extensive (DS = 3)	Collapse (DS = 4)
Column	A Physical phenomenon	Cracking and spalling	Moderate cracking and spalling	Degradation without collapse	Failure leading to collapse
	B Section ductility $\mu_k$	$\mu_k > 1$	$\mu_k > 2$	$\mu_k > 4$	$\mu_k > 7$
	C Displacement ductility $\mu_d$	$\mu_d > \mu_{first-yield}$ (1.0)	$\mu_d > \mu_{yield}$ (1.20)	$\mu_d > \mu_{cc=0.002}$ (1.76)	$\mu_d > \mu_{max}$ (4.76)
	D $\gamma = (\mu_d + \beta\mu_h)/\mu_u$	$\gamma > 0.14$	$\gamma > 0.40$	$\gamma > 0.60$	$\gamma > 1.0$
	E Load carrying capacity loss $\beta_h, \beta_v$	$\beta_h > 0\%$	$\beta_h > 2\%$	$\beta_h > 5\%$	$\beta_h > 20\%$
		$\beta_v > 5\%$	$\beta_v > 10\%$	$\beta_v > 25\%$	$\beta_v > 50\%$
Bearing	F Drift ratio $\theta$	$\theta > 0.007$	$\theta > 0.015$	$\theta > 0.025$	$\theta > 0.050$
	B Displacement $\delta$	$\delta > 0$ mm	$\delta > 50$ mm	$\delta > 100$ mm	$\delta > 150$ mm
	G Shear strain $\gamma$	$\gamma > 100\%$	$\gamma > 150\%$	$\gamma > 200\%$	$\gamma > 250\%$

**Table 2.2 Summary of Damage Indices DI and corresponding Limit States LS for concrete columns and seismic isolation bearings [26,35,36,38,39,40,41]**

The Damage Indices for columns are: Physical phenomenon, Curvature ductility  $\mu_k$ , Displacement ductility  $\mu_d$ , Shear strain  $\gamma = (\mu_d + \beta\mu_h)/\mu_u$ , horizontal and vertical Load Carrying Capacity Losses  $\beta_h, \beta_v$  and Drift ratio  $\theta$ . The Damage States corresponding to each of these Indices are defined according to the following limits: Slight(DS=1), Moderate(DS=2), Extensive(DS=3) and Collapse(DS=4). It is obvious that these damage indices depend mainly on the response of the structural member regardless of other seismic factors such as the hysteretic energy and duration of the earthquake record. They can also



differ in estimating the damage intensity, since each one records a different aspect of the structure's response for different modes of failure, such as either shear or flexural modes of failure.

### 2.3.3.1 The damage index of Mergos & Kappos

Mergos & Kappos [42] introduces a more specific Damage Index for damage assessment of RC columns, which combines both curvature and shear distortion. They consider that an RC member may fail either in flexure mode, in shear mode or in both. Hence, the total damage occurs when an RC member reaches flexure capacity or shear deformation capacity. This is represented by:

$$D_{tot} = 1 - \left(1 - \frac{\varphi_{max}}{\varphi_u}\right)^a \left(1 - \frac{\gamma_{max}}{\gamma_u}\right)^b \quad (2.2)$$

Where,  $\varphi_u$  is the curvature capacity and  $\gamma_u$  is the shear distortion (strain) capacity. The variables a & b depend on the variation of  $D_{tot}$ , and are taken as 2/3 [42]. However, this index is valid only in conjunction with methods that utilises moment-curvature and shear-strain hysteretic relationships for the calculation of element flexibility matrix [42]. This index is not appropriate when the shear-flexure interaction is disregarded [42].

### 2.3.3.2 Other Damage Indices

The following 3 Damage Indices share common response descriptors, and are produced by an inelastic SDOF structure subjected to ground motion loading [43]. They are based on:

- (parameters from monotonic loading analysis): ultimate displacement  $x_u$ , ultimate ductility  $\mu_u$ , yield displacement  $x_y$  and yield strength  $f_y$ , which are independent of the loading history.
- (parameters from ground motion loading analysis): maximum displacement  $x_{max}$  and maximum ductility  $\mu_{max}$ , which depend on the loading history.

These 3 Damage Indices are namely [43];

1. Powell & Allahabadi (1988) proposed the Damage Index based on ultimate ductility,

$$DI_\mu = \frac{x_{max} - x_y}{x_u - x_y} = \frac{\mu_{max} - 1}{\mu_u - 1} \quad (2.3)$$

2. Cosenza et al. (1993) and Fajfar (1992) [34] proposed a damage index based on the structure hysteresis energy  $E_H$  as follows:

$$DI_H = \frac{E_H / f_y x_y}{\mu_u - 1} \quad (2.4)$$

$DI_\mu$  does not include the effect of hysteretic energy, and  $DI_H$  does not include the effect of repeated cyclic loading.

3. Park and co-workers (1985) developed a simple damage index based on experimental data. The Park & Ang index is:

$$DI_{PA} = \frac{x_{max}}{x_u} + \beta \frac{E_H}{f_y x_y} = \frac{\mu_{max}}{\mu_u} + \beta \frac{E_H}{f_y x_y \mu_u} \quad (2.5)$$

$\beta$  is a positive constant that weighs the effect of cyclic loading on structural damage, and is extracted from experimental data. The damage is measured on the basis of the remainder of unity left from this demand-capacity ratio.

Park & Ang damage index does not take into account the effect of plastic cycles, but rather considers the dissipated energy under a monotonic-type loading [18], while computations of the analytical damage consider non-linear hardening, softening and unloading behaviour, giving a more accurate definition for the damage.

### 2.3.4 Performance Limits in Damaged Members

In comparison with the previously mentioned description of damages, the state of structural damage based on Park & Ang damage index  $DI$  is defined in a more practical classification, associating the reparability of the structure after damage as [45]:

- (a) repairable,  $DI < 0.40$ ,
- (b) beyond repair,  $0.4 < DI < 1.0$ , and
- (c) a state of total collapse,  $DI > 1.0$ .

El-Attar and Ghobarah [44] introduced another classification of the damage index based on the load-deflection relation in a monotonic loading analysis such as a force-drift relationship, as shown in Figure 2.6. The performance of a structure is defined in terms of damage states as a structure with no damage, minor damage, repairable damage un-repairable damage and progressive collapse.

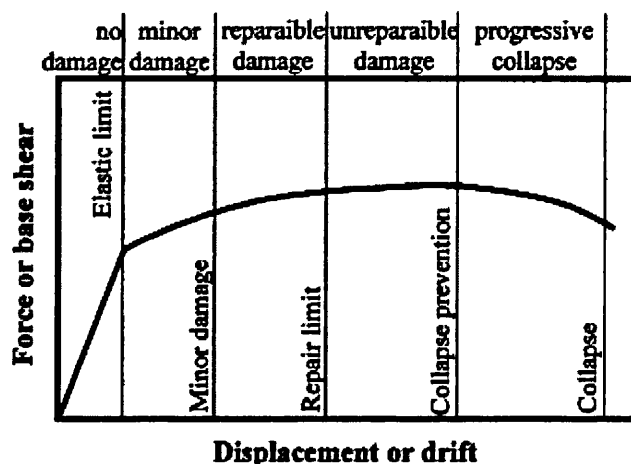


Figure 2.6 Limits of structure performance in a load-deflection relationship [44]

Enrique Alarcon and a group of researchers [45] developed a numerical model for RC members associated with fracture theory. The model provides the answer for the following important question concerning the use of damage indices; For a given set of damage values, how safely can the damaged structure be used, and to what extent it is repairable.

Enrique Alarcon and a group of researchers [45] used the Griffith criterion for the energy release rate of a member with damaged hinges to construct a model that simulates the stiffness degradation of the member under cyclic loading, and allows to characterise the elastic and collapse prevention limits by knowing the cracking, yielding and ultimate moments of the member's cross section. Such prevention limits correspond to the required damaging values [45]. Together with the Damage Index DI the proposed model is also capable of predicting a Reparability Index RI, as shown in Figure 2.7. From the plot of the two indices, all damages prior to the intersection point of the two curves are theoretically repairable, and all points past to the intersection point are un-repairable.

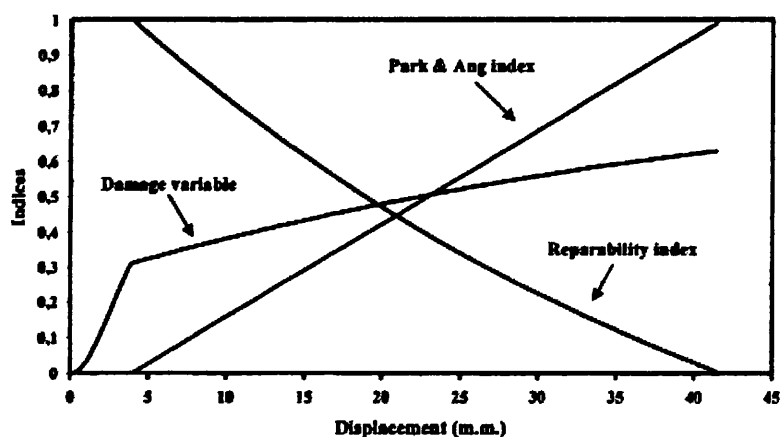


Figure 2.7 Evolution of the damage indices during the numerical simulation [45]

### 2.3.5 Fragility curves

“Fragility curves describe the probability of a structure being damaged beyond a specific damage state for various levels of ground shaking”[26]. This means that when a structure is most probable to exceed its damage state to a higher damage state, it is highly fragile. Such a measure is as useful as the damage index since it describes the damage state qualitatively as a damage state classification. Fragility curves are independent from damage indices in the way that a high fragility curve for a structure can describe the high probability to exceed the damage state for a high or low damage index, i.e. a highly fragile curve may be used to

describe an element with a slight or minor damage state, while a low fragile curve may be used to describe an element with an extensive damage state [26].

Fragility curves are also useful to compare between different bridge components (columns, fixed bearings, expansion bearings, deck, etc.) along different PGA's, showing which component is more vulnerable at a certain PGA, and also comparing between different bridge systems. E. Choi et.al. [26] have developed fragility curves for 4 types of bridges in Central & Southern US, subjected to PGA's from 0.1g to 0.7g in the longitudinal direction, and were analysed analytically using the DRAIN-2DX fibre element software. It was concluded that the bridges run from least vulnerable to most vulnerable in the PGA intensity scale as follows: pre-cast multi-span continuous, steel girder multi-span continuous, pre-cast multi-span simply supported and steel girder multi-span simply supported [26]. This indicates that multi-span simply supported bridges with steel girders are most likely to exceed their damage states at low PGA's in this comparison, while multi-span continuously supported pre-cast bridges are less likely to exceed their damage states at low PGA's in this comparison [26]. Fragility curves can also be developed based on empirical data, i.e. reported bridge damage data from past earthquakes and they are used for economic loss estimation as well as a basis for assigning retrofit prioritization [26].

## **2.4 SHAKING TABLE TESTS FOR SEISMICALLY DESIGNED RC BRIDGE COLUMNS**

Results from both model simulation and experimental work verify the validity and reliability of the analytical hypothesis for the proposed engineering problem. In RC bridge structures under seismic loading, shaking table tests are conducted for either down-scaled bridge RC models or full-scale RC structural members [29].

In this section, the work of 4 important published shaking table experiments and numerical models for RC piers is reviewed in detail, with important concluding remarks documented for the benefit of this PhD research study. These published papers and technical reports are, in a sense, related with some conclusions based on previous work, therefore for clarity; they are reviewed herein according to their publishing dates.

## 2.4.1 Nishida and Unjoh [46]

Nishida and Unjoh [46] conducted a series of shaking table tests for three types of cross sections, circular (600 mm in diameter), square (600 × 600 mm) and rectangular (450 × 800 mm), under a near field ground motion, and then conducted dynamic analyses to investigate the effect of bilateral loading. The specimens were excited by the JR Takatori Station record documented during the 1995 Hyogoken Nanbu Earthquake, which was used as the source of input waveform [46].

The excitations, responses and damages for the three columns are summarised in the following Table 2.3, and the final damages can be seen in Figure 2.8.

Specimen section	PGA, x-direction	Max lateral displacement x-direction	PGA, y-direction	Max lateral displacement y-direction	damage
Squared section	0.642g	0.120m	0.666g	0.200m	Peeling of cover and all 48 bars and few hoops buckled.
Circular section	80% of 0.642g	0.100m	80% of 0.666g	0.150m	Peeling of cover and 15 out of 48 bars buckled.
Rectangular section	90% of 0.642g	0.081m	90% of 0.666g	0.159m	Peeling of cover with severe damage and 12 out of 48 bars buckled. 30% of stiffness deterioration.

Table 2.3 Summary of excitations, responses and damages for the three column types under shaking table tests [46].

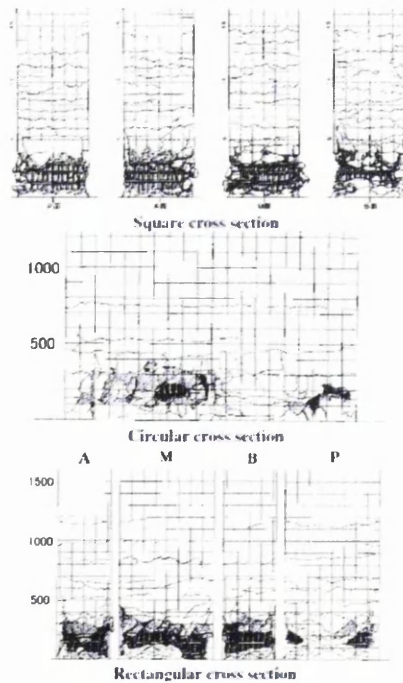


Figure 2.8 Final damage portraits of RC columns [46]

## 2.4.2 Sakai and Mahin [47]

Due to the lack of ductility capacity of bridge columns, the 1995 Hyogo-ken Nanbu, Japan, earthquake caused destructive damage to many bridges in that area [47]. Many bridges lost their functionality because of permanent deformation, although some bridges did not collapse in the earthquake [47]. ‘More than 100 reinforced concrete bridge columns experienced a tilt angle of more than 1 degree (1.75% drift) and these columns had to be removed and new columns built because of the difficulty of setting the superstructure back to the original alignments and levels’ [47, 48]. Many researchers realised the need to mitigate the residual displacements of bridges to ensure serviceability after the earthquake [47].

Sakai and Mahin [47] conducted a numerical investigation for a circular RC bridge column as part of a research project to develop a new method that mitigates post earthquake residual displacements. Sakai and Mahin [47] introduced a numerical model based on fibre elements, cracked stiffness elements and rigid elements to investigate the behaviour of RC 1.83 m-diameter columns whose aspect ratios are in the range from 3 to 10, as illustrated in Figure 2.9, and designed in accordance with the Seismic Design Criteria (SDC) of the California Department of Transportation (Caltrans) (2001). The residual displacements are computed according to the Japanese specification, with the ductility demand and the ultimate ductility, which are based on the demand/capacity balance of ductility. The residual displacements computed using the ductility demands are larger than 1% drift, which is the allowable residual displacement, according to the Japan Road Association JRA [47]. ‘If design criteria of limiting residual displacements were used, the target ductility demand commonly used in the U.S. by (CALTRANS) design practice would have to be substantially reduced, with corresponding impacts on strength, stiffness, and cost’ [47].

The analytical model is applied to determine the residual displacements for more than 250 RC column models with various configurations of ‘self-centring’ methods, which resulted in an 85% reduction of the quasi-static residual displacement [47]. ‘Self-centring’ or ‘re-centring’ systems are RC bridge columns with an unbounded, prestressing strand placed at the centre of the cross section, as shown in Figure 2.9, to reduce the residual displacements of the bridge structure after an earthquake event. Sakai and Mahin [47] applied 10 earthquake records of strong ground motions, listed in Table 2.4, to investigate the column behaviour under the dynamic loading.

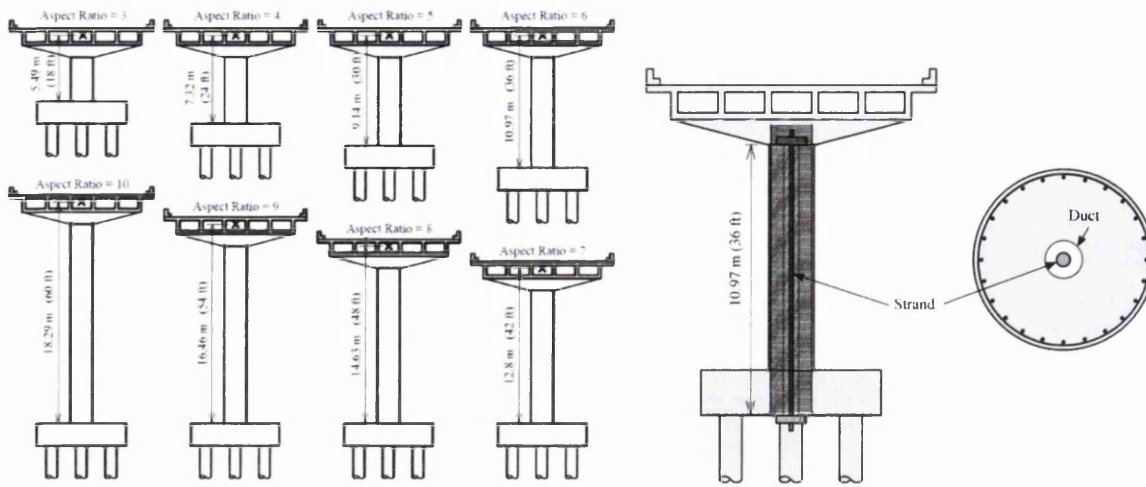


Figure 2.9 Analyzed RC columns with aspect ratios from 3 to 10, and analytical model with unbonded strands at the column centre [47].

Record	Earthquake	Magnitude	Epicentral Distance	PGA (m/sec <sup>2</sup> )	
				Normal	Parallel
Tabas	Tabas, Iran, 1978	7.4	1.2 km	8.83	9.59
Los Gatos	Loma Prieta, USA, 1989	7.0	3.5 km	7.04	4.49
Lexington Dam	Loma Prieta, USA, 1989	7.0	6.3 km	6.73	3.63
Petrolia	Cape Mendocino, USA, 1992	7.1	8.5 km	6.26	6.42
Erzincan	Erzincan, Turkey, 1992	6.7	2.0 km	4.24	4.48
Landers	Landers, USA, 1992	7.3	1.1 km	7.00	7.84
Rinaldi	Northridge, USA, 1994	6.7	7.5 km	8.73	3.81
Olive View	Northridge, USA, 1994	6.7	6.4 km	7.18	5.84
JMA Kobe	Hyogo-ken Nanbu, Japan, 1995	6.9	3.4 km	10.67	5.64
Takatori	Hyogo-ken Nanbu, Japan, 1995	6.9	4.3 km	7.71	4.16

Table 2.4 Near-field earthquake strong ground motions used for dynamic analysis [47].

Many researchers have studied analytically and experimentally such effect for various structural systems, using a series of shaking table tests and analytical studies to identify the key design variables and evaluate the effect of different ground motions and different column configurations for self-centring systems [51]. The results of the previous studies by Sakai and Mahin [47] demonstrated the basic viability and feasibility of self-centering columns for bridges. They also found that the local unbonding of the mild reinforcement increases the fatigue life of the column by reducing the possibility of developed peak strains [47].

In their numerical investigation, Sakai and Mahin [47] found that confinement of the concrete core by further increasing the amount of spiral reinforcement or providing steel jacketing provided more resistance to mitigate the possible crushing of the concrete core [47].

In respect to the loss of stiffness associated with the unbonding mild reinforcement in the plastic hinge region, Sakai and Mahin [47] suggested that increasing the area of the post-tensioning strand can compensate such small loss in stiffness.

Figure 2.10 shows the dynamic responses of 4 RC columns with aspect ratio of 6 and with different configurations of self-centring compared with normal RC column, subjected to Lexington Dam earthquake record [47]. The response shows a significant reduction of the residual displacements in the self-centred RC columns compared with the normal RC column.

Sakai and Mahin [47] studied the behaviour of self-centring in terms of the amount of post-tensioning applied in the column, since more compression forces due to the post-tensioning can increase the self-centring but it can also cause earlier failure in the confined section.

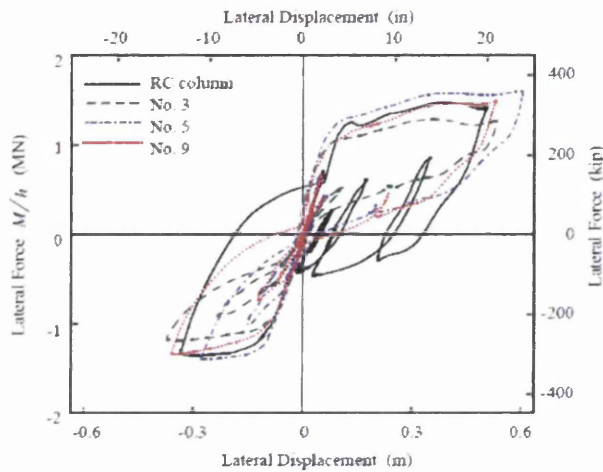


Figure 2.10 Dynamic response of columns with aspect ratio =6, subjected to Lexington Dam record [47].

### 2.4.3 Sakai and Unjoh [49]

Many researchers conducted a series of shaking table tests for RC bridge columns, subjected to static, quasi-static and dynamic unidirectional, bilateral and multidirectional loading conditions [46,47,48,50]. However, research on multidirectional dynamic loading on RC bridge columns is still limited due to the limitation of capacity of research facilities [49]. Although conducted tests provided valuable findings in seismic design concerning the multidirectional dynamic loading effects, most columns were tested under conditions of near field ground motion excitations, which usually have few dominant pulses, but no experimental investigations have been conducted under the repetition of strong pulses of ground motion until it was first performed by Sakai and Unjoh [49].



Advanced and reliable design procedures are still needed to evaluate seismic performance for RC bridge columns under multidirectional loading of the ground motion since the research in this area is still limited [49]. Further analyses are still needed for various ground motions, and reinforced concrete columns with various natural period and flexural strength [49].

Sakai and Unjoh [49] investigated the dynamic response of  $1/4$ -scaled circular RC bridge column specimen under multidirectional strong repetitive pulsating ground motion.

The selection of such ground motion was aimed to produce a target response of 0.17 m ( $\pm 10\%$ ), which was the maximum displacement obtained by the test of Nisida and Unjoh [46].

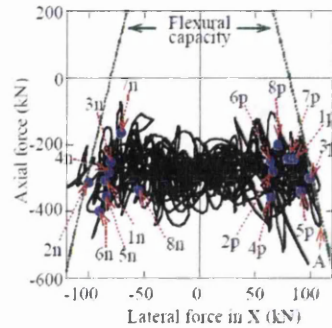
Out of 10 ground motion records with repetitions of strong pulses, the record on the ground surface near the Tsugaru Bridge during the 1983 Nihonkai Chubu earthquake, Japan was selected and scaled up by 400% for the required input, so that similar maximum displacement is obtained for a  $1/4$ -scaled specimen. The PGA's for the x, y and z directions after being scaled up were  $11.12 \text{ m/s}^2$ ,  $9.52 \text{ m/s}^2$  and  $8.2 \text{ m/s}^2$ , respectively, and the maximum lateral displacements were 0.192m in the x-direction before rebar fracture, and reached approximately 0.18m in the y-direction after rebar fracture. The specimen was subjected to severe cover spillings, rebars buckling and fracturing. In fact, 22 of 40 longitudinal reinforcing bars were fractured, which occurred mostly at the x-faces, and the core concrete was completely crushed at the bottom of the column, nevertheless, the specimen did not lose its stability [49]. Figure 2.11 shows the damaged RC column base at the beginning and end of the shaking table test.



Figure 2.11 Set-up of RC specimen and the resulting damage [49]

Sakai and Unjoh [49] spoke about a phenomenon in the relationship between lateral and axial forces, which are supposed to be proportionally related to the cantilever-type structures. They found that the response lateral force is not significantly affected by the fluctuation of the axial

force for cantilever-type structures, as can be seen from Figure 2.12, in which the lateral forces increase as the axial forces decrease. They attributed this phenomenon to the difference in natural frequencies in the two directions. The predominant natural period in the vertical direction (0.08 seconds) is 25% of that in the horizontal direction (0.3 seconds), and thus the lateral and axial forces barely reached their maximum values simultaneously [49].



**Figure 2.12** Reversely proportional relationship between axial and lateral forces for cantilever-type RC structures under dynamic loading [49].

### Concluding Remarks:

The resulting responses of this test were considered as one of the main inspirations for this PhD research work, since it showed very clearly by experimental evidence the vulnerability of a bridge RC single column, (typically designed based on a current seismic design code of Japan [49]), as it is subjected to multidirectional strong ground motion. It also showed the lack of reliable seismic performance when several levels of vulnerability are combined in one case.

The final results of this experiment, as stated by the authors are; “22 out of 40 longitudinal reinforcing bars were fractured, which occurred mostly at the x-faces, and the concrete core was completely crushed at the bottom of the column”, These findings are significantly important for this PhD research study, since it is focused on investigating the fracturing behaviour in the concrete core for seismically designed RC columns under strong ground motion excitements. What signifies the importance of investigating this problem is that most analytical models that determine the overall load-deflection relationship of similar problems do not in fact have the capability to compute the core damage under such a dynamic multi-directional loading. It should be noted that cracks due to dynamic multi-directional loading in a RC body are too complex to be simulated by FE formulations, and is still not finally achieved by researchers.

Mr Junichi Sakai provided this PhD work with the input data files for the ground motion records of Tsugaru Bridge 1983 earthquake of Nihonkai Chubu in Japan. The x, y and z ground acceleration records were used to obtain analytical results for the RC column structure which was modelled by using the (Seismostruct) non-linear dynamic solver.

#### 2.4.4 Jeong, Sakai and Mahin [51]

Jeong, Sakai and Mahin [51] conducted a series of shaking table tests to assess the ability of partially prestressed RC columns with unbonded post-tensioning tendons to reduce residual displacements resulting under strong earthquake ground motions. This work was conducted ‘to study the effect of debonding of the mild reinforcing bars in the area of the expected plastic hinge, to study the effect of incorporating steel jacketing, combined with local unbonding of the mild reinforcement, and to investigate the effect of magnitude on the prestressing force’ [51].

This work tested four RC bridge columns  $\frac{1}{4}$ -scaled specimens to conduct shaking table tests under strong ground motions. The four RC columns are all with unbonded prestressing tendons provided in the column centre. The second and third specimens PRC-U and PRCU2 had their longitudinal reinforcement bars debonded in the expected plastic hinge region, with some difference in the pre-stressing forces in the two cases. Bars are debonded by having them coated with wax and covered with a plastic sheath, to increase the fatigue life of the column. The last specimen PRC-UJ, shown in Figure 2.13, is also provided with debonded bars in addition to steel plate jackets incorporated at the expected plastic hinge zone [51].

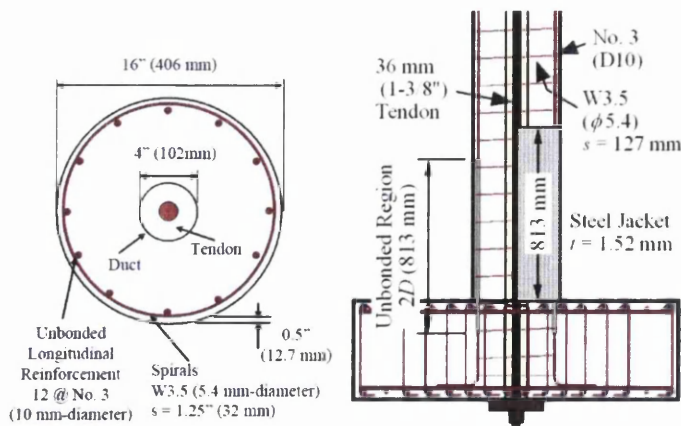


Figure 2.13 Cross section of all specimens and PRC-UJ specimen [51]



Confinement of the concrete core by further increasing the amount of spiral reinforcement or providing steel jacketing can improve the behaviour of the RC column. Moreover, steel jacketing can also prevent spalling in the column cover during the inelastic response [51].

Jeong, Sakai and Mahin [51] concluded that ‘as might be expected, the use of a higher pre-stressing force decreased the maximum displacements and residual displacements when subjected to the design and maximum level tests, but the damage to specimen PRC-U2 was more severe than to specimen PRCU, due to the effect of the higher pre-stressing force.’

Sakai and Mahin [47] studied the behaviour of self-centring in terms of the amount of post-tensioning applied in the column, since that more compression forces due to the post-tensioning can increase the self-centring but it can also cause earlier failure in the confined section. A summary of the seismic responses and damages are illustrated in both Table 2.5 and Figure 2.14.

specimen	Description of specimen provisions	Strong ground motion PGA	Max lateral displacement (m)	damage
PRC-2	Central post-tensioning tendons.	0.641g	0.2677	Developing cracks with 3 buckled bars
PRC-U	Central post-tensioning tendons with bars debonded at PH zone.	0.654g	0.2788	Developing cracks with 2 buckled bars
PRC-U2	Central post-tensioning tendons highly prestressed, with bars debonded at PH	0.618g	0.2512	Developing cracks with 6 buckled bars and 1 spiral fracture
PRC-UJ	Central post-tensioning tendons with bars debonded and steel jacket at PH zone.	0.650g	0.2445	Developing cracks with buckled steel jacket

Table 2.5 Description of specimens and damages under strong ground motion tests [51]



Figure 2.14 Damages in specimens at plastic hinge zones [51]

## **Concluding Remarks:**

Such post-tensioning provisions enhanced the RC columns with very strong elastic potential to reduce the possible residual displacements that occur in traditional RC bridge columns when subjected to seismic loading. Due to this elastic ability, less plastic deformations are produced since the prestressed section is forced to apply less ductile capacity. However, the deformation is still plastic and the column drift still causes significant plastic damage in the plastic hinge zone, as was shown in Figure 2.14, and also described in Table 2.5. Even though such damages were considered a spalling type of damage that hits the cover only, with bar buckling [51], it is not known how much crack growth could have damaged the column core in reality.

Having a reduced residual displacement with a severely damaged section is still not an ideal performance for seismic resistant structures. As a matter of fact, a reduced residual displacement is significantly important to ensure serviceability and preserve the bridge's functionality after an earthquake event [48], but the column must also be removed and replaced with a new one because of the high risk of possible core damage, consequently lost strength after being severely damaged and unreliability to resist another possible seismic strike.

## **2.5 NUMERICAL MODELS**

### **2.5.1 Numerical Modelling using the Damage Theory**

#### **2.5.1.1 Continuum Damage Model (CDM), Calayir and Karaton [52]**

The philosophy of this model is based on the Smeared Crack Approach (SCA), since it is based on determining the changes in the constitutive laws governing the cracking material without refinement of the mesh [52]. The constitutive laws of the CMD are based on the formation of the damage value  $d$ , which is based on Lemaitre's elastoplastic damage theory [3]:

$$\sigma^* = \frac{1}{1-d} \sigma \quad (2.6)$$

Where,  $\sigma^*$  and  $\sigma$  are the stresses after and before damage respectively. Lemaitre's principle for damage is based on determining the reduction in the net area of the loaded surface due to the distributed micro-cracks in the material volume [53].

If the stress directions are fixed as in the initial crack inclination, a zigzag propagation of the crack profiles in the mesh will cause severe stress locking [52]. Therefore, an improved Smearred Crack Approach (SCA), called the co-axial Rotation Crack Model (CRCM) is used in this model to alleviate the stress locking in the (SCA) [52].

In a 2D case for plain concrete, two damage parameters  $d_1$  and  $d_2$  are associated with the effective stress vector  $\{\sigma^*\}$  after damage and with Cauchy stress vector  $\{\sigma\}$  before damage, which makes the model orthotropic since there are two net area values  $A_1^*$  and  $A_2^*$  for the two perpendicular surfaces of the concrete infinitesimal element, as shown in Figure 2.15 [52]. Similarly; the constitutive matrices for the material after damage  $[D^*]$  and before damage  $[D]$  are related by the damage matrix  $[\Psi^*]$  as follows:

$$[D^*] = [\Psi^*]^{-1} [D] [\Psi^*]^{-T} \quad (2.7)$$

$$[D^*] = \begin{bmatrix} \frac{E_o(1-d_1)^2}{1-\nu} & \frac{E_o\nu(1-d_1)(1-d_2)}{1-\nu^2} & 0 \\ \frac{E_o\nu(1-d_1)(1-d_2)}{1-\nu^2} & \frac{E_o(1-d_1)^2}{1-\nu^2} & 0 \\ 0 & 0 & \frac{2G(1-d_1)^2(1-d_2)^2}{(1-d_1)^2+(1-d_2)^2} \end{bmatrix} \quad (2.8)$$

Where  $[D^*]$  is a function of the updated initial modulus of elasticity  $E_o$ , Poisson's ratio  $\nu$ , shear modulus  $G$  and damage values  $d_1$  and  $d_2$ , which are related to the net area values  $A_1^*$  and  $A_2^*$  and initial area  $A$ . Assuming that the damage occurs due to the tensile stresses only, the damage initiation is determined according to the tensile strength, with softening strains starting from post-failure until complete drop of the stress.

In implementation of the finite element modelling, the material constitutive matrix  $[D^*]$  after damage is updated in each integration point according to the status of damage. The stiffness matrix of the element is also updated using the updated  $[D^*]$  [52]. As shown in Figure 2.16, unloading and reloading are conducted by updating the unloading-reloading modulus of elasticity  $E_n$  as:

$$E_n = E_o \frac{(1-d_p)^2}{(1-\lambda)} \quad (2.9)$$

Where  $d_p$  is a damage parameter  $d_p$  which is related to the recoverable and inelastic strains, and  $\lambda$  is an experiment constant.

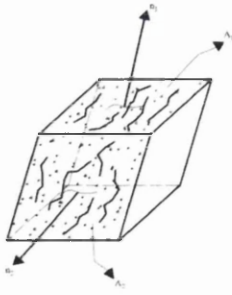


Figure 2.15 Damaged volume element [52]

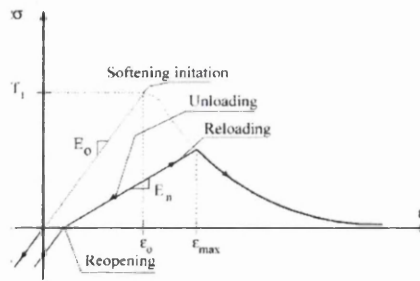


Figure 2.16 Closing and re-opening criteria [52]

### 2.5.1.2 Lumped Damage Model, Alarcon E. et al. [54]

Alarcon E. et al. [54] stated that Continuum Damage Mechanics are less suitable for the analysis of solids such as frames. Therefore, Alarcon E. et al. proposed a Continuum Damage Model (CMD) based on the combination of fracture and damage mechanics with the concept of plastic hinge, using a branch of Fracture mechanics called Lumped Damage Mechanics, where a family of models that combine damage and fracture mechanics with the concept of plastic hinges [54].

The main idea in this model is to use the damage variable in order to characterise the loss of stiffness and strength of RC members. In this model, a beam-column element is assumed to remain elastic, with two plastic hinges at the two element ends, as seen in Figure 2.17.

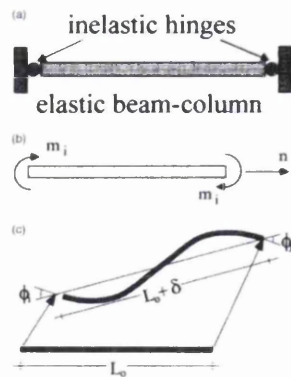


Figure 2.17a) Lumped plasticity model of a beam-column element. b) Generalized stresses. c) Generalized deformations. [54]

The constitutive relationship between the generalized stresses  $M = (m_i, m_j, n)$  and generalized strains  $\Phi = (\phi_i, \phi_j, \delta)$  can be expressed as a function of the damage parameters and plastic rotations as follows:

$$M = S(D)\{\Phi - \Phi^p\} \quad (2.9)$$

Where,  $\Phi^p = (\phi_i^p, \phi_j^p, 0)$  and  $\{\Phi - \Phi^p\}$  is the generalized elastic strains since the beam-column element should remain elastic in the analysis. The stiffness matrix  $S(D)$  is defined as:

$$\frac{1}{4-(1-d_i)(1-d_j)} \frac{EI}{L} \begin{bmatrix} 12(1-d_i) & 6(1-d_i)(1-d_j) & 0 \\ 6(1-d_i)(1-d_j) & 12(1-d_j) & 0 \\ 0 & 0 & 4-(1-d_i)(1-d_j) \frac{A}{I} \end{bmatrix} \quad (2.10)$$

If damage parameters  $d_i = d_j = 0$ , then the stiffness matrix takes its familiar form for the

beam-column element as: 
$$\begin{bmatrix} \frac{4EI}{L} & \frac{2EI}{L} & 0 \\ \frac{2EI}{L} & \frac{4EI}{L} & 0 \\ 0 & 0 & \frac{EA}{L} \end{bmatrix}$$

To solve for the rotations in the term of generalized strains, the damage variables  $d_i$  and  $d_j$  must be computed first. In this stage, the Damage Fracture Mechanics is combined with concept of plastic hinges, by using the Griffith criterion in a damaged hinge. The damage evolution in hinge  $i$  can be described using the Griffith criterion for the hinge  $G_i$  and the crack resistance of the hinge  $R(d_i)$  as:

$$G_i = R(d_i) \quad (2.11.a)$$

Or, 
$$\frac{m_i^2 L}{6EI(1-d_i)^2} = G_{cr i} + q_i \frac{\log(1-d_i)}{1-d_i} \quad (2.11.b)$$

For a given ultimate moment;  $m_{u_i}$ , the Griffith criterion is determined as:

$$\frac{m_{u_i}^2 L}{6EI(1-d_{u_i})^2} = G_{cr i} + q_i \frac{\log(1-d_{u_i})}{1-d_{u_i}} \quad (2.12.a)$$

and recovers as; 
$$2G_{cr i}(1-d_{u_i}) + q_i \log(1-d_{u_i}) + q_i = 0 \quad (2.12.b)$$

where,  $d_{u_i}$  is solved.

For a given plastic moment  $m_{p_i}$ , the Griffith criterion is determined as:

$$\frac{m_{p_i}^2 L}{6EI(1-d_{p_i})^2} = G_{cr i} + q_i \frac{\log(1-d_{p_i})}{1-d_{p_i}} \quad (2.13.a)$$

and recovers as; 
$$\frac{m_{p_i}}{1-d_{p_i}} - m_{y_i} = 0 \quad (2.13.b)$$

where,  $d_{p_i}$  is solved.

These parameters;  $d_{u_i}$  and  $d_{p_i}$  can be computed if the cracking, yielding and ultimate moments of the member's cross-section are known. These damage values represent those limits even in the case of hysteretic loadings with cyclic energy dissipation [54].



### 2.5.1.3 Continuum Damage Model under Force Equilibrium Mechanics for Bridge Piers, S. Oller, A. Barbat [55]

The proposed model is based on evaluating the local damage at given points in the structure, by means of local constitutive models which describe the accumulating damage due to the micro-structural damages [55, 56]. The global damage is also evaluated as a scalar depending on damage parameters that characterise the dynamic response of the whole system [55, 57].

The seismic damage is first evaluated at local level, which describes the state of the material after degradation by some damage index at the targeted cross section. Then, damage is evaluated at a cross sectional level based on adequate averages of the obtained local damage indices.

From continuum damage mechanics, the local damage is determined based on the isotropic damage constitutive law, where the model is based on two major criteria, firstly; the material degradation evaluated at structural points at the local level, secondly; the consequently reduced moment of inertia and cross section area of the bridge pier after the damage. The global damage evaluation is based on this reduction of the pier properties [55].

The following points explain in brief the numerical model:

1. During the non-linear process a residual force  $\Delta F_i^R$  exists since the elastic modulus and moment of inertia are changing, and the undamped lumped mass equation of motion for each pier is written as:

$$m_i a_i + F_i^{in} - \Delta F_i^R = 0 \quad (2.14)$$

where,  $m_i$  and  $a_i$  are the top girder and pier mass in the  $i$ th DOF and  $a_i$  is their acceleration.  $F_i^{in}$  is the internal cross-section resisting force.

2. The solution for this equation requires the iterative process using the non-linear Newmark's method, and the force equilibrium condition for this equation is achieved by eliminating the un-balanced residual force  $\Delta F_i^R$  at each time of the process, using the Newton-Raphson process. Indirectly, this process also eliminates the residual bending moment  $\Delta M = M^0 - M^{in}$ , which is the difference between the maximum elastic external moment (demand), and the pier internal strength moment after damage (capacity).
3. The changes in the pier stiffness and changes in the internal cross-section force  $F_i^{in}$  depends on the damage level reached at each point in the pier. This damage level is

evaluated by the continuum damage model criterion, which is based on the damage constitutive equation:

$$f(x_1, x_2, x_3) = 1 - d(x_1, x_2, x_3) = \frac{\tau^{max}}{\tau} e^{a(1 - \frac{\tau}{\tau^{max}})} \quad (2.15)$$

where,  $f(x_1, x_2, x_3)$  is the local damaged internal variable,  $d(x_1, x_2, x_3)$  is the damage index,  $\tau$  and  $\tau^{max}$  are the current and maximum tension strength at each point of the solid, with  $0 \leq \tau^{max} \leq \tau$  in the damaging case.

4. For each step of the non-linear analysis the properties of the system are updated for the damaged cross sectional area  $A(x_3)$ , for the first moment  $m_i(x_3)$ , for the second moment of inertia  $I_{ii}(x_3)$  and for the Product of Inertia  $I_{ij}(x_3)$  with respect to the principal axes  $(x_i, x_j)$ , at the base section  $x_3$  as follows:

$$\begin{aligned} A(x_3) &= \int_A f(x_1, x_2, x_3). dA \\ m_i(x_3) &= \int_A f(x_1, x_2, x_3). x_j. dA \\ I_{ii}(x_3) &= \int_A f(x_1, x_2, x_3). x_j^2. dA \\ I_{ij}(x_3) &= \int_A f(x_1, x_2, x_3). (x_i, x_j). dA \end{aligned} \quad (2.16)$$

Noting that the principal inertia axes  $(x_i, x_j)$  do change their position after damage, consequently the product of inertia would not be zero.

5. The incremental generalized strains are obtained according to the updated properties and the residual generalised stress.
6. The generalized internal stress is obtained based on the new section properties, and the Residual forces are the difference between the elastic generalized initial stress and the generalized internal stress.

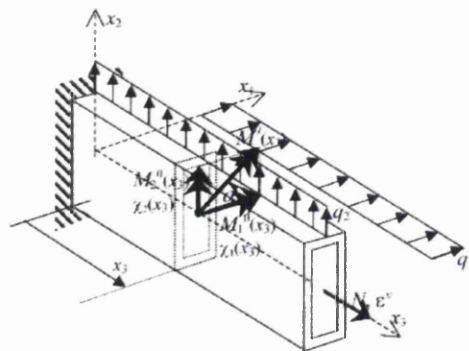


Figure 2.18 Bridge pier as cantilever beam with forces at plastic hinge section  $x_3$  [55]

### Concluding Remark:

This work is significantly important due to the practicality and simplicity of the proposed modelling method, and is very encouraging for similar and extended future work, since it was

partially funded and supported by European governments. The authors [55] made their acknowledgements to:

1. The European Commission, Environmental program RTD Project ENV4-CT-97-0574 “Advanced Methods for Assessing the Seismic Vulnerability of Bridges (VAB)”, the Global Change and Ecosystems program integrated project GOCE-CT-2003-505448 “Risk Mitigation for Earthquakes and Landslides (LESSLOSS)”,
2. The Spanish Government (Ministerio de Educacio’n y Ciencia), the project of REN2002-03365/RIES “Development and application of advanced approaches for the evaluation of the seismic vulnerability and risk of structures (EVASIS)”, the project of BIA2003-08700-C03-02 “Numerical simulation of the seismic behaviour of structures with energy dissipation devices”, and
3. The Spanish Government (Ministerio de Fomento) “Numerical simulation methodology for the reinforced concrete behaviour structures reinforced with composite materials”.

### 2.5.2 Numerical Models based on Empirical Models

To simulate the nonlinear behaviour under dynamic loading, numerical models are provided with built-in hysteretic models which were obtained from the hysteretic model test of load-deformation representation for a SDOF structure, such as Clough, Takeda, Slip, or Pinching and Degrading models [24]. As shown in Figure 2.19. These models are capable of representing the energy dissipation behaviour in the dynamically loaded RC member. However, they are not widely used anymore except for cases when representing special mechanisms in the structure such as slippage of bars and isolation bearings.

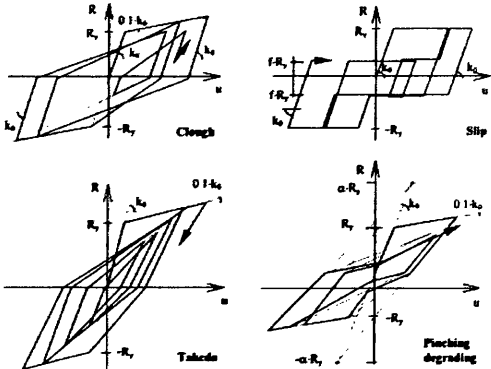


Figure 2.19 Hysteretic models [24]

**2.5.2.1 Beam-Column Non-linear Element Modelling Supplemented with Empirical Drift Capacity Models.** Yavari, Elwood and Wu. [58]

This model simulates previous work of shaking table tests performed on four RC frame columns by C. Wu [59]. The model employs force-based nonlinear beam-column elements, using the OpenSEES framework developed by the Pacific Earthquake Engineering Research Centre [60], which is an open modelling system available for international use, and mainly developed for earthquake engineering simulations. This model was used to simulate two different modelled approaches to investigate 4 RC frame columns resisting earthquake loading. The two fully ductile RC columns and two so called non-ductile RC columns differ in the modelling of the element ends in which zero-length slip springs simulate the ductile columns and the shear, axial and slip springs simulate the non-ductile columns. As shown in Figure 2.20, the model consists of a series of elements, nodes and springs, having each column consisting of a single force-based nonlinear beam-column element with five integration points and two zero-length elements located at the top and bottom of the beam-column element [58].

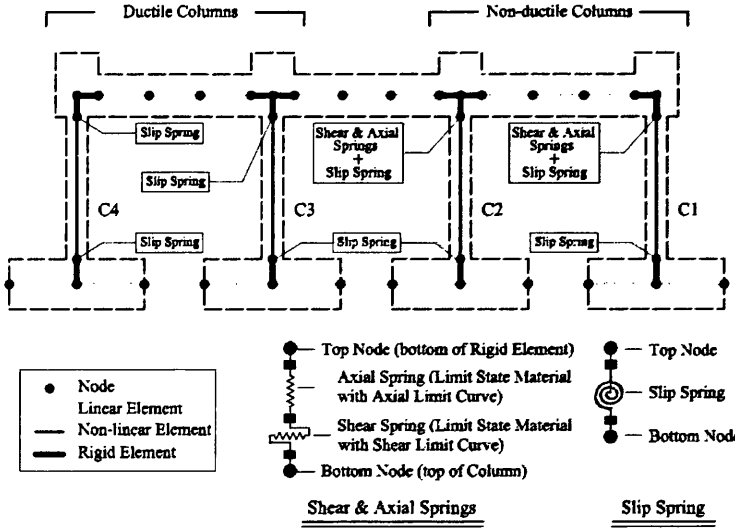


Figure 2.20 Analytical modelling for a shaking table specimen [58]

The four force-based nonlinear beam-column elements are provided with zero-length spring modelling ends. They are described as follows:  
 Non-ductile RC columns are supplemented with an empirical drift capacity model whose behaviour is defined by an empirical (Limit State) material model for shear and axial failure. The shear spring captures the behaviour of strength degradation and increases the shear

deformation as shown in Figure 2.21. Axial strength spring accounts for the axial failure. Both springs controlling the post-failure response for the element resulting from the strength degradation [59]. Slip springs are also provided to account for the possible slippage of reinforcement bars from the concrete.

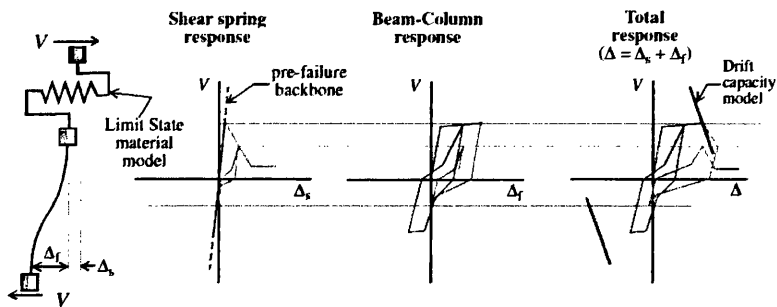


Figure 2.21 Shear spring using limit state material model [58]

Ductile RC columns provided with Slip springs only have been analysed. Other models with different end springs, shown in Figure 2.22, have also been performed in a parametric-like study to investigate the effects of such different modelling provisions.

For the purposes of this study, a ‘ductile’ column is defined by a ductile detailing common in current seismic building codes, while ‘nonductile’ column details are used before the introduction of ductile detailing requirements [58]. A column defined as ‘nonductile’ may display a moderately ductile response followed by a relatively brittle failure [58].

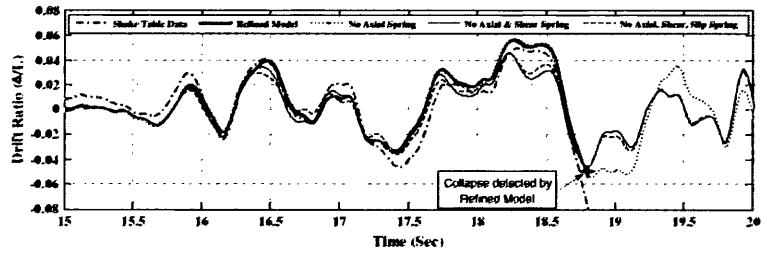
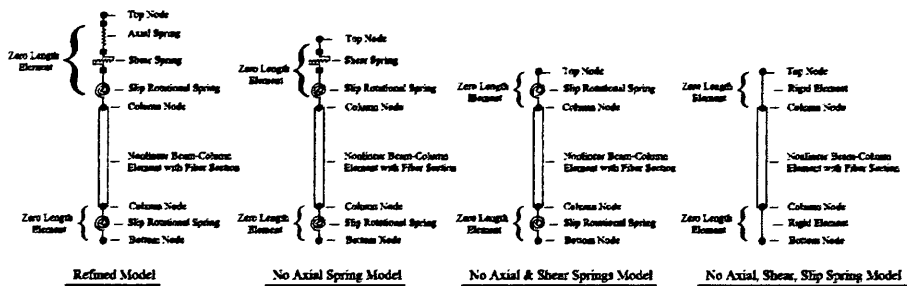


Figure 2.22 Models with different end springs and corresponding drift responses [58]

### Simplified non-degrading models using elastic elements:

RC columns are also simulated by simplified methods that use non-degrading models which are commonly used by many nonlinear analysis software packages in engineering practice. Elastic column elements with concentrated rotational springs are used to simulate simplified non-degrading models such as rigid-perfectly-plastic, and sudden degrading models such as the ASCE/SEI 41-06 model [11]. Figure 2.23 shows the elastic column with the concentrated hinges at the ends. The plastic moment capacity for the rotational plastic moment  $M_p$  is determined based on moment-curvature analysis using material constitutive models. For the considered frame in this study, S. Yavari et al. [58] concluded that nonlinear dynamic analyses using the ASCE/SEI 41-06 backbone model significantly overestimated the drift demands for the structure, and should therefore be revised, while a simple non-degrading concentrated plasticity model provided a good estimate of the drift demands but only for non-severe degradation of the lateral load resistance [58].

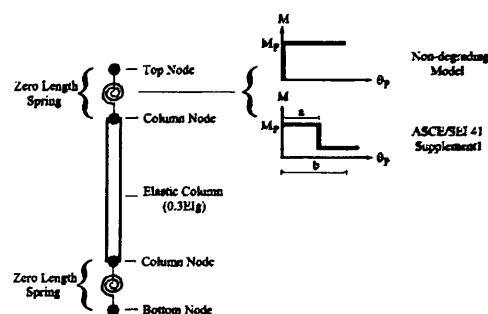


Figure 2.23 Elastic column with the concentrated hinges at the ends [58]

### Concluding Remark:

S. Yavari, K. Elwood and C. Wu. [58] concluded that the simple non-degrading concentrated plasticity model provided a good estimate of the drift demands but only for non-severe degradation of the lateral load resistance. This is a significantly important conclusion from researchers, such as C. Wu and K. Elwood [58 and 59], who worked in both modelling types; experimental and analytical, with their publications in the recent date of October 2008.

### 2.5.2.2 Strain-Curvature Empirical Model. Lee and Watanabe [61]

This model is based on documenting the experimental observations and sectional analysis of the rotational response and the axial strains in the plastic hinge region of a RC column being subjected to reversed cyclic lateral loading.

The longitudinal axial strains in the plastic hinge region are related to the rotation of the member as shown in Figure 2.24.

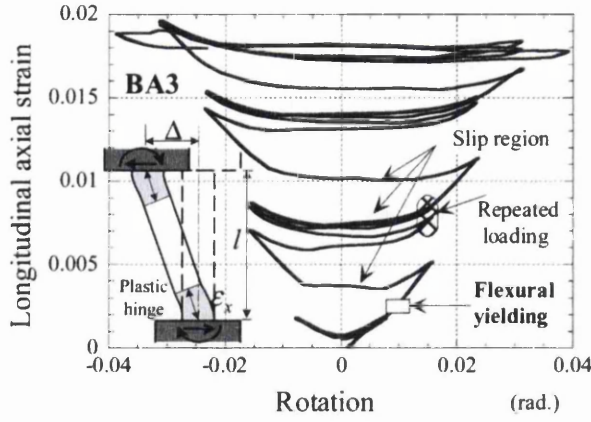


Figure 2.24 Axial strain vs. rotation of an RC beam failing in shear after flexural yielding [61].

This proposed strain–rotation relationship consists of four paths with different computations:  
 Path 1: Pre-flexural yielding or unloading region; in which the longitudinal axial strain,  $\varepsilon_x$ , at the centre of the beam's cross-section in the plastic hinge region. The cumulative axial strains  $\varepsilon_{x1}$  as given in path 1 are calculated as:

$$\varepsilon_{x1} = (1 - F)\varepsilon_{xf} \quad (2.17.a)$$

$$\varepsilon_{xf} = \frac{\frac{h}{2} - k_d}{d - k_d} \quad (2.17.b)$$

Where,  $F$  is the number of unloading cycles beyond flexural yielding,  $\varepsilon_{xf}$  is the axial strain at flexural yielding,  $k_d$  is the neutral axis depth corresponding to the flexural yielding,  $h$  and  $d$  are the overall and effective depths of the section respectively.

Path 2: Post-flexural yielding region; the longitudinal axial strain, in the plastic hinge region increases rapidly as the rotation increases beyond flexural yielding. The cumulative axial strains  $\varepsilon_{x2}$  as given in path 2 are calculated as:

$$\varepsilon_{x2} = \frac{(R_{pmp} + R_{pmn}) j_d}{2l_h} \quad (2.18)$$

Where,  $R_{pmp}$  and  $R_{pmn}$  are the positive and negative plastic rotations, respectively.  $j_d$  is the moment arm distance between the steel bars,  $l_h$  is the length of the plastic hinge region.

Path 3: Slip region; the change in the axial strain is negligible.

Path 4: Repeated loading region; the increase in the magnitude of axial strain is inversely proportional to the number of reloading cycles  $N_j$ . The member is loaded cyclically to the same rotation magnitude  $R_m$ . Based on experimental observations, the cumulative axial strains  $\varepsilon_{x4}$  as given in path 4 are calculated as:

$$\varepsilon_{x4} = \sum_{i=1}^m \sum_{j=1}^n \left( \frac{R_m j_d}{2l_h} \right)^{0.85} \frac{1}{4} N_j \quad (1 \leq N_j \leq 5) \quad (2.19)$$

The axial strains of paths from 1 to 4 are summed up to obtain the final cumulative value. The 4 paths locations in the strain vs. rotation diagram are shown in Figure 2.25.

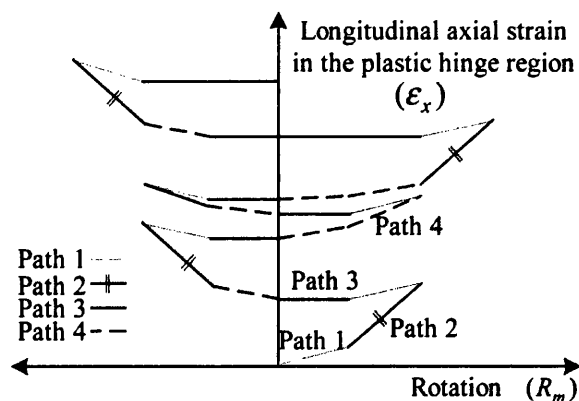


Figure 2.25 Proposed model for analyzing the longitudinal axial strain in the plastic hinge region of RC beams [61].

### 2.5.3 FEM Numerical Modelling based on Smeared and Discrete Approaches

The gradual growth of micro-cracking is gradually formed as the loaded concrete material exceeding its tensile strength limit. The internal tensile stresses during post-failure reduce due to gradual reduction of cohesive characteristics of the material. It is assumed that formation of visible cracking in the concrete is a brittle process, and it occurs once the internal resistance of the tensile stresses drop to zero. The concrete material is generally modelled by a Linear Elastic Fracture relationship using a tensile cracking criterion, such as the maximum stress criterion or the maximum strain criterion [62]. In general, there are three different approaches for crack modelling in the analytical studies of concrete structures using the FEM. They are: 1) Smeared Cracking modelling, 2) Discrete Cracking modelling and 3) Fracture Mechanics modelling. The selection of modelling type depends on the purpose of the analysis; smeared crack models, for example, are most suited if overall load-deflection outputs are desired. If the study of local behaviour is desired, then discrete cracking model is the best choice.

#### 2.5.3.1 The Smeared Cracking Model

In this approach, the cracked concrete is assumed to remain a continuum, and cracks are 'smeared out' in a continuous fashion, by representing an infinite number of parallel fissures across the cracked concrete element [62]. The onset of cracking introduces an orthotropic



plane, as shown in Figure 2.26, with new constitutive relationships governed by the tangent stiffness matrix, which is defined as:

$$[\bar{C}_t] = \begin{bmatrix} 0 & 0 & 0 \\ 0 & E & 0 \\ 0 & 0 & \beta G \end{bmatrix} \quad (2.20)$$

Where,  $E$  and  $G$  are the elastic modulus and shear modulus, respectively.  $\beta$  is a constant that depends on the integrity of the material to resist shear after cracking and under compressive stressing. In many applications,  $\beta = 0$  is assumed when cracks are open, i.e. during the tensile stresses, and  $\beta = 1$  is assumed when cracks are closed due to compressive stresses, implying perfect healing, or known as ‘aggregate interlocking’, for a closed crack with compressive strains across the closing cracks pattern. As  $\beta$  approaches 1, shear strength is reserved between the cracked concretes.

Moreover, smeared cracking models can allow for strength degradation in the crack direction for reinforced concrete materials [62].

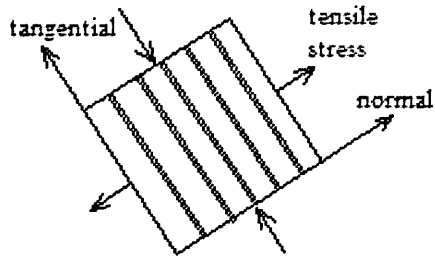


Figure 2.26 Idealization of the smeared crack model

### 2.5.3.2 The Discrete Cracking Model

The discrete modelling is based on explicit displacement disconnection at nodal points of the adjoining elements or across the element domain, depending on where the assumed cracking line takes place in a FE mesh. In either way, new nodes are constructed leading to a change in topology of the mesh as a crack is formed. In order to preserve the shear strength between the cracked elements when the cracks close under compressive stress unloading process, special ‘linkage elements’ are modelled to simulate the ‘aggregate interlocking’ process that controls the behaviour of the crack as it slides. The stiffness of these linkage elements decreases as the crack opens, and thus interlock forces decrease in large cracks [62].

### **2.5.3.3 Fracture Mechanics Modelling**

There are special fracturing situations that needed special modelling criteria using the basis of Fracture mechanics. Fracture due to twisting, shearing, compression and crushing require special modelling criteria, and special fracturing associating matters such as bond and dowel effects in RC material, crack width and stress concentration at crack tips are also specially treated in terms of modelling according to the point of interest of the research.

#### **2.5.3.3.1 Discrete tensile and compressive fracture in quasi-brittle materials, Klerck et al. [63]**

The aim of this model is to predict the fracturing development in rocks in a deep level mine [63]. The rock fails in a mechanism similar to that of a conventional uniaxial compression test, extension test and triaxial test at the stop face, excavation face and inside confined regions ahead of the mining face, respectively [63]. The proposed model uses such similarities to predict the fracturing developments according to the required region of the excavation. This is performed by employing a FEM application enhanced by Discrete Elements to simulate such conventional tests, and be able to define similar fracture developments on site accordingly.

The combined finite-discrete element DE/finite element FE under the Explicit-Elfen code, was used to perform the required modelling, but with a modified algorithm so that elements are possibly fractured under compressive stresses as well as typically fractured under tensile stresses. The DE/FE Explicit-Elfen code is based on the Mohr-Coulomb failure criterion for the non-linear definition of stresses.

There are two possibilities in crack modelling in the Elfen code; fixed and rotating crack modelling. In the rotating crack model, the crack direction and damage occur in the direction of the current principal stresses, while in the fixed crack model, the plastic strain accumulates across a pre-defined plane [63].

#### **2.5.3.3.2 Developments in the discrete approach**

As previously stated, Smeared Modelling and Discrete Modelling are the two main categories for numerical modelling of fracture. The former has the advantage of solving the problem within a continuum setting, while the discrete approach introduces the fracture in a straightforward manner in terms of displacement discontinuities (or jumps) and tractions, rather than in terms of stresses and strains [64]. However, in the smeared modelling approach

numerical difficulties could appear as strain localization occurs, requiring regularization of the continuum model to overcome this problem [64].

In recent years researchers have introduced several improvements to the classical formulations of the FEM in the field of discrete approach to solve fracture problems.

Since fracture problems are mainly based on the accuracy of stresses developed by the elements, accuracy of stress values should drive the discrete algorithm to inaccurate results.

In this aspect, classical finite elements have only one approximation of the stress over the element domain, which is a major disadvantage in the classical finite elements [65], especially when they are used to simulate cracks. Therefore, a hybrid element has been proposed, and there is a wide acceptance that hybrid formulations are the most accurate types for the finite elements [65]. In a hybrid element two fields are utilised; one field is assumed to approximate stresses over the element bulk domain, while the second one is assumed to approximate displacements over the boundaries. Another modification has been used to the Hybrid element which is the Trefftz function to produce the so called Hybrid-Trefftz element [65]. Trefftz elements use designated Trefftz functions to approximate the stresses in the element domain to satisfy the linear momentum balance equation, giving a much higher order formulation than those used by the classical finite elements [65]. A Hybrid-Trefftz element is successfully advantageous in crack modelling since that stresses in the element field and tractions in the cohesive element are fully independent, and no inconsistency may occur [65]. In this way all oscillations in the tractions that can occur on the cohesive surfaces are removed when solving non-linear equations [65].

As heterogeneous material concrete constituents are aggregates and the cement matrix, and the cracking occurs between these two different materials. Therefore, the crack path is designated to be controlled by the heterogeneities of the material, i.e. depending on the distribution of the aggregate bulks, as shown in Figure 2.27. To simulate such a continuum with designated discontinuities the so called interface concept was applied by many researchers [65]. The initial development for the interface elements was initially to model joints that simulate discontinuities inside rock bulks, but are now widely used to model fracture of quasi-brittle materials, such as concrete [66]. There are two basic types of interface elements: continuous interface elements, which are integrated over the crack face, and nodal interface elements which can be considered to be discrete spring elements [67].

G. Edwards et al. [65] implemented discrete cracks that are restricted to element boundaries using interface elements, using 10-noded tetrahedrons for the bulk, and 6-noded tetrahedrons as interface elements. The continuum is assumed to be elastic with geometrically nonlinear

hybrid-Trefftz stress elements, containing cohesive cracks restricted to element interfaces [64].

This topic is beyond the scope of this research, but has been reviewed for the benefit of a wider view.

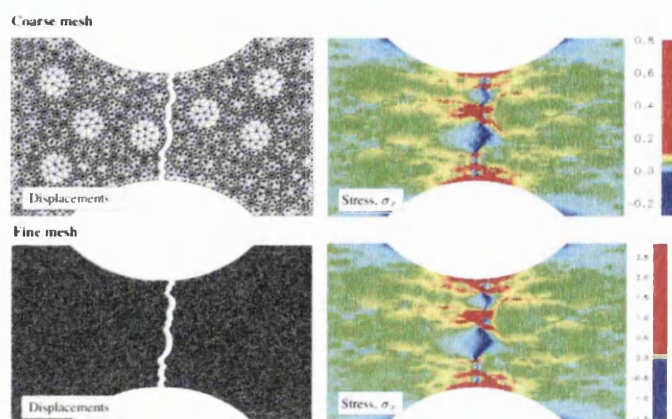


Figure 2.27 Crack controlled by the discontinuity interfaces in a 'dog bone' test, with coarse and fine meshes [64].

### Concluding Remarks:

The aforementioned topic is very recent, and the simulation of crack growth in quasi-brittle heterogeneous materials such as concrete is still under research, as well as the simulation of crack growth of concrete with embedded reinforcement bars. The complexity of the topic of fracture using discrete elements encouraged many researchers to apply various techniques, but it is a common fact in modelling that more accuracy in the performance of parameters approximations is usually conjugated with less a comprehensive approach for the problem. On the other side, approaches with less depth and more assumptions produce less accuracy but can handle more comprehensive problems, such as global RC structures under dynamic loading.

## 2.5.4 Fibre Elements and Lattice Elements Numerical Models

In the midway between FE models with 3D tetrahedral elements and bar-element models with Beam-Column 2D elements, the 2D Fibre elements and 2D Lattice elements have been employed in the numerical modelling to investigate the non-linear behaviour in skeleton (frame) structures. A member section is discretized into fibre elements which function in the fibres axial straining as a group and are controlled by constitutive linear and non-linear behaviour of the material to be assigned for each fibre, as shown in Figure 2.28. The fibres

configuration of the member geometry is very attractive to build longitudinal bars, post-tensioned strands and polymer tubes as fibres [68, 69], in addition to the concrete bulk, to simulate axial flexural forces and deformations for all materials. However, shear forces are obtained from the coupling effect of the stiffness matrix of the element. A drawback of the technique of fibre modelling is the lack of simulating the transverse reinforcements which formulate the confinement effect in structural members. As a substitute, fibres in the concrete core are upgraded according to theoretical basis to some nominal compressive strength as a result of the confinement of transverse hooks.

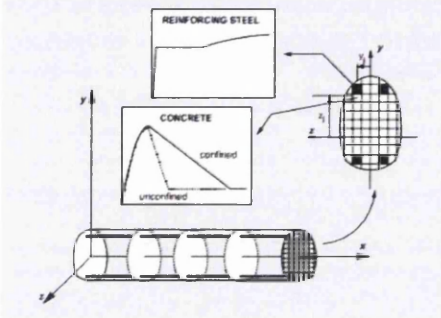


Figure 2.28 Controlled discretized section in fibre element modelling [69]

In contrast to the fibre element models, lattice element models are capable of predicting the shear failure at any section of the analysed member [70]. However, they have a major disadvantage in terms of processing time of the analysis due to the very large number of applied freedoms [71]. This is obvious as they incorporate different elements for different functions. As shown in Figure 2.29, the concrete region consists of flexural compression and tension members, diagonal compression and tension members, and global arch members. Longitudinal and transverse reinforcement bars are modelled by vertical and horizontal members, respectively. The 2D lattice elements model can be extended into a 3D model to incorporate multi-directional loading [71], but with larger number of freedoms and longer time of analysis, and consequently, the lattice element model is not popular.

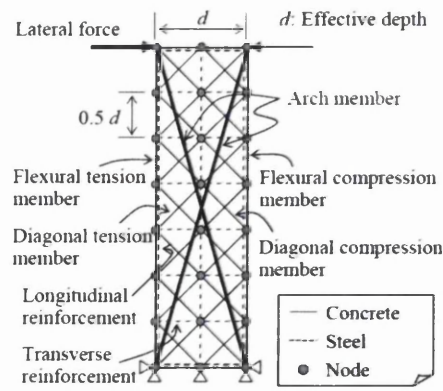


Figure 2.29 Configuration of Lattice elements for a RC column [71]

## **2.5.5 Numerical Models Conjugated with Seismic Evaluation Approaches and Performance-Based Concepts for Bridges**

Using an equivalent SDOF system for an idealized RC wall system, T. N. Tjhin et al. [72] used a theoretical approach based on the seismic spectra for different performance levels of the structure. They estimated the displacement of a RC ductile structure at yield, based on information from the Yield Point Spectra. Different performance levels of the RC wall are used to express the plastic hinge rotations and corresponding roof drifts.

T. H. Kim et al. [73] used a FEM computer program to model pre-cast RC segmental bridge columns, representing the interaction between the concrete and tendons using interface elements. The concrete elements design is based on the tension and compression stiffening modelling, in addition to the shear transfer modelling.

To improve the seismic performance of RC walls, K. Antoniadis et al. [74] evaluated the hysteretic response RC walls strengthened with Fibre-Reinforced Polymer (FRP), using numerical methods and verified by experimental tests. However, it was concluded that the overall seismic performance of the FRP walls was not better than that of the original walls, and further research is still needed in this field.

Y. Sung et al. [75] proposed a seismic evaluation method for existing bridges based on presenting the relationship between various structural performances and the actual PGA's of several earthquake records. Such a relationship is used to obtain a universal perspective on seismic evaluation of bridges. They proposed a simplified method to obtain the plastic hinge point PHP by the interpolation between the working load and ultimate load, which are obtained by using the SAP2000 software analysis for RC bridge framed columns [75].

### **2.5.5.1 Numerical models using the Ambient Vibration Technique**

The ambient vibration technique provides the engineer with mainly the natural frequencies of vibration and the corresponding deformed shapes for each excited mode of the existing bridge spans [76]. These dynamic characteristics are then used to match with those from the computational model of the bridge spans i.e. the bridge is remodelled by trial-and-error in order to make it respond dynamically as similar to the existing structure [76]. This is in contrast to the so-called 'blind analysis' in which only the input data is provided. At that stage time-history analysis can be obtained from computer analysis for any targeted ground motion to predict reliable results [76]. This procedure is mainly used for seismic evaluations

such as performance-based seismic evaluation, and several study cases using the ambient vibration process can be found in the literature, such as in [13] and [77].

### **2.5.5.2 Numerical models using the System Identification (SI) Methodology**

M. Chaudhary et al. [78] used an Identification Methodology known as System Identification (SI) to identify the system parameters. Many parameters were obtained by the help of a comparison process with seismic records obtained from bridge sensors previously mounted on Yama-age' bridge in Japan [78]. The main parameter obtained is the acceleration which is idealised according to some theoretical basis, based on the dynamic characteristics of frequencies, damping ratios and effective mode participation factors. The system parameters are then computed, which are; the column flexural stiffness, horizontal foundation stiffness, rocking foundation stiffness, abutment backfill stiffness, RC columns stiffness, rubber bearing stiffness, rubber damping ratio and coefficient of friction of side stoppers. Such parameters are then used to build the bridge model for the purpose of performance evaluation.

S. Chao, C. Loh [79] developed a Modified Force-Analogy Method (MFAM) to simulate the non-linear response of a RC structure, using beam-column elements with three different plastic mechanisms for the moment and shear force hinges. S. Chao, C. Loh [79] claimed that 'currently (stated in 2007), no theoretical or empirical equations can determine the internal force versus plastic deformation relationship accurately based on an element design'. They stated that even by using detailed finite element method complex degradation and pinching phenomenon of RC members cannot be estimated accurately, and further study is needed to establish the relationship between model parameters and the design properties, with the help of sophisticated System Identification (SI) techniques [79].

S.J. Li et al. [80] also utilized the System Identification technique to model non-linear hysteresis systems with slip action, which are considered complex and contain a large number of parameters. They proposed a three-stage iterative procedure to build the model. Modelling based on the SI methodology has a theoretical and practical interest over the years, and has also been used in the field of Structural Health Monitoring (SHM) and Structural Control [80].

### 2.5.5.3 Energy Concentration and Critical Earthquake Loading

The unsteady nature of ground motions causes non-stationary excitations, which results in severe pulses of the acceleration. An acceleration pulse is a phenomenon in earthquake records that has low-frequency and long-period pulses of acceleration which holds in a large potential to damage on the structure severely [81].

There is a significant effect of deterioration on structures due to the time-varying frequency content of the ground motion [82]. To prove that acceleration pulses are so damaging, Hancock and Bommer [83] investigated the increase in structure's period responses together with the progressive damage during the acceleration pulses. They showed that the records with strong accelerations and longer periods are the most damaging records.

Sasani and Bertero [84] carried out a review on structural responses under such acceleration pulses, also known as severe pulses, to investigate their damaging effect. Severe pulses imply that ground motions having their energy concentrated in time and frequency are producing much more structural damage than that with evenly distributed energy [85]. Cao and Friswell introduced a quantitative representation of the energy distribution of an earthquake record. This representation is known as the characteristic PGA or (CPGA) [85], which is based on a few components of a record with periods close to the structural fundamental period. Such components dominate the structural response and reflect the concentration of record energy in frequencies around the fundamental period [85].

Having a similar concern, Abbas [86] approaches the earthquake problem by deriving the critical earthquake loads as design inputs for inelastic structures. Using Fourier series, the earthquake acceleration is modulated by an envelope function which maximizes the inelastic responses according to predefined constraints [86]. To construct the critical seismic inputs, these constraints are based on the energy, PGA, PGV, PGD, upper bound Fourier amplitude spectra (UBFAS) and lower bound Fourier amplitude spectra (LBFAS) [86]. The problem is then formulated as determining the optimization variables such that maximizing the Park & Ang damage index subjected to those defined constraints [86]. This formulation was developed for SDOF and then developed for a MDOF structure; where a global index for the structure is defined in terms of a weighed function of the damage indexes for the individual structural members [86, 87]. In general the applied method can be used by the structural engineer to prescribe critical earthquake loads that could produce the worst scenario of damage at the structure under seismic loading [87].



Abbas comments on the unsteady nature of ground motions by saying “The occurrence of earthquake ground motions involves a high level of uncertainty. In fact, each earthquake brings out new surprises and teaches us new lessons” [87].

#### **2.5.5.4 Software Packages of Dynamic Solvers**

The NISEE Software Library CDROM is a collection of 116 research software codes which are available with their manuals through (The Earthquake Engineering Online Archive). The NISEE is the National Information Service for Earthquake Engineering, which is a production of the Pacific Earthquake Engineering Research (PEER) Centre, based in the university of California, Berkeley. Software such as OpenSees is an open-source software framework for earthquake analysis of structures developed by PEER researchers. The open-source nature of the framework enables researchers and engineers to add and share enhancements to the material and element models easily.

Similar to the SeismoStruct dynamic solver, which is used in this PhD research, but with more graphics capabilities, the Drain-3DX software package can give more information about the current damage states, such as yield, spalling and crushing. Other packages such as SAP(fibre-hinge element), ANSR(beam-column element with plastic hinge), PC-ANSR(fibre-hinge element) and OpenSees(force-based beam-column element) are earthquake engineering facilities that produce numerical solutions for the large scale problem, and are also capable of solving RC bridge structures under dynamic excitements.

The variety of models depends on reliability of simulation of the internal behaviour of quasi-brittle material and reinforced concrete structures under dynamic, quasi-static or static loadings. Selection of the model type depends on the desired output of the analysis and the context of the problem and its environment, restrictions of the geometry and availability of input data and material properties. It also depends on the degree of approximation required for the assumptions of the governing equations and their formulations. However, some formulations are powerful and robust for particular problems but they are not necessarily suitable for others.

## **2.6 REFERENCES**

[1] Bridge Forum, A forum for the dissemination of bridge engineering research, Bridge Failure Database, University of Cambridge, <http://www.bridgeforum.org/dir/collapse/year/>.

- [2] N.R. Hewson. Prestressed Concrete Bridges: Design and Construction. London: Thomas Telford, 2003.
- [3] L.A. Clark. Concrete Bridge Design To BS5400. Construction Press, 1983.
- [4] CALTRANS (2006), Seismic Design Criteria (Version 1.3), California Department of Transportation, Sacramento, California.
- [5] F. Legeron, M. N. Sheikh. Bridge support elastic reactions under vertical earthquake ground motion. *Engineering Structures* 31 (2009) 2317-2326.
- [6] R. DesRoches, S. Muthukumar. Implications of seismic pounding on the longitudinal response of multi-span bridges - an analytical perspective. *Earthquake engineering and engineering vibration*, 1671-3664(2004)01-0057-09
- [7] Y. Bozorgnia, V.V. Bertero. *Earthquake Engineering: From Engineering Seismology to Performance-Based Engineering*. 2004, CRC Press.
- [8] G.V. Berg. *Seismic Design Codes and Procedures*. 1983, EERI.
- [9] C. Taylor. *Earthquake engineering*. ICE Earthquake Seminar, University of Bristol, March 2010.
- [10] R.D. Bertero, V.V. Bertero. Performance-based seismic engineering: the need for a reliable conceptual comprehensive approach. *Earthquake Engineering and Structural Dynamics* 2002; 31:627-652.
- [11] A. K. Chopra, *Dynamics of Structures. Theory and Applications to Earthquake Engineering*, 3ed edition, Pearson Prentice Hall 2007.
- [12] ATC-40 (1996), *Seismic Evaluation and Retrofit of Concrete Building*, Applied Technology Council, California.
- [13] A. A. Shama , J. B. Mander, S. S. Chen, A. J. Aref. Ambient vibration and seismic evaluation of a cantilever truss Bridge, *Engineering Structures* 23 (2001) 1281–1292.
- [14] Y. Sung, W. Liao, W. P. Yen. Performance-based concept on seismic evaluation of existing bridges, *Earthq Eng & Eng Vib* (2009) 8:127-135 DOI: 10.1007/s11803-009-8151-3
- [15] R. Riddell, J. E. Garcia. Hysteretic energy spectrum and damage control *Earthquake Engineering and Structural Dynamics* 2001;30(12):1791–816.
- [16] H. Choi, J. Kim, Energy-based seismic design of buckling-restrained braced frames using hysteretic energy spectrum, *Engineering Structures* 28 (2006) 304–311.
- [17] K.R. Estes, J.C. Anderson. Hysteretic energy demands in multistory buildings. Seventh US national conference on earthquake engineering.2002.

- [18] P. Leger, S. Dussault. Seismic-energy dissipation in MDOF structures. *Journal of Structural Engineering*, ASCE 1992;118(5):1251–69.
- [19] B. Akbas, J. Shen, H. Hao. Energy approach in performance-based seismic design of steel moment resisting frames for basic safety objective. *The Structural Design of Tall Buildings* 2001;10(3):193–217.
- [20] S. Leelataviwat, S.C. Goel, B. Stojadinovi'c. Energy-based seismic design of structures using yield mechanism and target drift. *Journal of Structural Engineering*, ASCE 2002;128(8):1046–54.
- [21] P. Dasgupta, S.C. Goel, G. Parra-Montesinos, T.C. Tsai. Performance-based seismic design and behavior of a composite buckling restrained braced frame. In: 13th world conference on earthquake engineering. 2004.
- [22] J. Kim, H. Choi, L. Chung. Energy-based seismic design of structures with buckling-restrained braces. *Steel and Composite Structures* 2004;4(6):639–706.
- [23] E. Bojorquez, S.E. Ruiz, A. Teran-Gilmore. Reliability-based evaluation of steel structures using energy concepts. *Engineering Structures*. Volume 30, Issue 6, June 2008, Pages 1745-1759.
- [24] L. D. Decanini, F. Mollaioli. An energy-based methodology for the assessment of seismic demand, *Soil Dynamics and Earthquake Engineering* 21 (2001) 113-137.
- [25] R. Riddell, J.E. Garcia, E. Garces. Inelastic deformation response of SDOF systems subjected to earthquakes, *Earthquake Engineering and structural Dynamics*. 2002; 31:515-538.
- [26] E. Choi, R. DesRoches, B. Nielson. Seismic fragility of typical bridges in moderate seismic zones, *Engineering Structures* 26 (2004) 187–199.
- [27] J. Faleiro, S. Oller, A.H. Barbat, Plastic–damage seismic model for reinforced concrete frames, *Computers and Structures* 86 (2008) 581–597.
- [28] Y. J. Park, A. Ang. Mechanistic seismic damage model for reinforced concrete. *Journal of Structural Engineering*, ASCE1985;111(4) or (3) :722–39.
- [29] E. Erduran, A. Yakut. Component damage functions for reinforced concrete frame structures, *Engineering Structures* 29 (2007) 2242–2253.
- [30] H. Hwang, J.B. Jernigan, Y. Lin. Evaluation of seismic damage to Memphis bridges and highway systems. *Journal of Bridge Engineering*, ASCE 2000;5(4):322–30.

- [31] HAZUS, Earthquake loss estimation methodology. Technical Manual, National Institute of Building for the Federal Emergency Management Agency FEMA, Washington (DC), 1997.
- [32] A. Dutta. On energy based seismic analysis and design of highway bridges. Ph.D. Dissertation, Department of Civil, Structural and Environmental Engineering, State University of New York, Buffalo (NY), 1999.
- [33] B. Basu, V. K. GUPTA. A note on the damaged-based inelastic spectra. Earthquake engineering and structural dynamics. VOL. 25,421-433 (1996).
- [34] P. Fajfar. Equivalent ductility factors, taking into account low cyclic fatigue. Earthquake Eng. Struct. Dyn.,(1992) 21, 837–848.
- [35] J. Zhang, Y. Huo. Evaluating effectiveness and optimum design of isolation devices for highway bridges using the fragility function method. Engineering Structures 31 (2009) 1648-1660.
- [36] Federal Emergency Management Agency. Multi-hazard loss estimation methodology. Earthquake model. HAZUS99 User's Manual. Washington (DC); 1999.
- [37] E Cosenza, G Manfredi. Damage indices and damage measures. Prog. Struct. Engng Mater. 2000; 2: 50–59
- [38] H. Hwang, J.B. Liu, Y. Chiu. Seismic fragility analysis of highway bridges. MAEC report: project MAEC RR-4. Urbana: Mid-America Earthquake Centre; 2001.
- [39] K. R. Karim, F. Yamazaki. Effect of earthquake ground motions on fragility curves of highway bridge piers based on numerical simulation. Earthquake Eng Struct. Dyn. 2001;30:1839-56.
- [40] K. R. Mackie, B. Stojadinovic. Fragility curves for reinforced concrete highway overpass bridges. In: Proceedings of 13th world conference on earthquake engineering. Paper No. 1553. 2004.
- [41] J. Yi, S. Kim, S. Koshiyama. PDF interpolation technique for seismic fragility analysis of bridges. Eng Struct 2007;29:1312-22.
- [42] P. E. Mergos, A. J. Kappos, Seismic Damage Analysis Including In-elastic Shear-flexure Interaction,2009.
- [43] A. Mustafa. Damage-Based Design Earthquake Loads for SDOF Inelastic Structures. Journal of Structural Engineering. March 2011.
- [44] M. El-Attar, A. Ghobarah. Performance based evaluation of reinforced concrete buildings. Eur Earthquake Eng. 1998;12(2):22–9.

- [45] E. Alarcon, A. Recuero, R. Perera, C. Lopez, J. P. Gutierrez, A. De Diego, R. Picon, J. Florez-Lopez. A reparability index for reinforced concrete members based on fracture mechanics, *Engineering Structures*, 23 (2001) 687–697.
- [46] H. Nishida, S. Unjoh. Dynamic Response Characteristic of Reinforced Concrete Column Subjected to Bilateral Earthquake Ground Motions. Proc. of 13th World Conference on Earthquake Engineering, Vancouver, Canada, 2004, CD-ROM No. 576.
- [47] J. Sakai, S. Mahin. Analytical Investigations of New Methods for Reducing Residual Displacements of Reinforced Concrete Bridge Columns. PEER Report 2004/02, Pacific Earthquake Engineering Research Center, College of Engineering, University of California, Berkeley. September 2004.
- [48] K. Kawashima. Seismic design and retrofit of bridges. Proc. of 12th World Conference on Earthquake Engineering, 2000, CD-ROM No. 2828. New Zealand Society for Earthquake Engineering, Auckland, New Zealand.
- [49] J. Sakai, S. Unjoh. Earthquake simulation test of circular reinforced concrete bridge column under multidirectional seismic excitation. *Earthquake Engineering & Engineering Vibration* 1671-3664(2006)01-0103-08.
- [50] S. Mahin, M. Hachem . Bi-directional Seismic Response of Reinforced Concrete Bridges. International Workshop on Mitigation of Seismic Effects on Transportation Structures, 1999:13-24.
- [51] H. Jeong, J. Sakai, S. Mahin. Shaking Table Tests and Numerical Investigation of Self-Centering Reinforced Concrete Bridge Columns. PEER Report 2008/06, Pacific Earthquake Engineering Research Centre, College of Engineering, University of California, Berkeley. September 2008.
- [52] Calayir Y, Karaton M. A continuum damage concrete model for earthquake analysis of concrete gravity dam–reservoir systems. *Soil Dynamics and Earthquake Engineering* 25 (2005) 857–869.
- [53] Neto EA S, Peri'c D, Owen D. *Computational Methods for Plasticity Theory & Applications*, John Wiley and Sons, Ltd, Publication, 2008.
- [54] Alarcon E, Recuero A, Perera R, Lopez C, Gutierrez J, De Diego A, Picon R, Florez-Lopez J. A reparability index for reinforced concrete members based on fracture mechanics, *Engineering Structures*, 23 (2001) 687–697.
- [55] S. Oller, A. Barbat. Moment–curvature damage model for bridges subjected to seismic loads. *Computer Methods in Applied Mechanics and Engineering*, 195 (2006) 4490–4511.

- [56] Zienkiewicz O, Taylor R. The Finite Element Method, vols. 1 and 2, fourth ed., McGraw-Hill, 1988.
- [57] S. Arman, M. Grigoriu, Markov model for local and global damage indexes in seismic analysis, NCEER-94-0003, National Centre for Earthquake Engineering Research, 1994.
- [58] S. Yavari, K. Elwood, C. Wu. Collapse of a nonductile concrete frame: Evaluation of analytical models. *Earthquake Engineering and Structural Dynamics*. 2009; 38:225–241
- [59] C. Wu, W. Kuo, Y. Yang, S. Hwang, K. Elwood, C. Loh, J. Moehle. Collapse of a nonductile concrete frame: Shaking table tests. *Earthquake Engineering and Structural Dynamics*. 2009; 38:205–224.
- [60] OpenSEES. Open System for Earthquake Engineering Simulation. Pacific Earthquake Engineering Research Centre, University of California, 2005. Available from: <http://www.opensees.berkeley.edu>.
- [61] J.Y. Lee, F. Watanabe. Predicting the longitudinal axial strain in the plastic hinge regions of reinforced concrete beams subjected to reversed cyclic loading. *Engineering Structures* 25 (2003) 927–939.
- [62] W. F. Chen, A. F. Saleeb. *Constitutive Equations for Engineering Materials*. John Wiley & Sons. Inc.1982.
- [63] P.A. Klerck, E.J. Sellers, D.R.J. Owen. Discrete fracture in quasi-brittle materials under compressive and tensile stress states. *Computational Methods in Applied Mechanics and Engineering*. 193 (2004) 3035-3056.
- [64] L. Kaczmarczyk, C. J. Pearce. A corotational hybrid-Trefftz stress formulation for modelling cohesive cracks. *Comput. Methods Appl. Mech. Engrg*. 198 (2009) 1298-1310.
- [65] G. Edwards, L. Kaczmarczyk, C. J. Pearce. 3D Discrete Cohesive Crack Propagation in Heterogeneous Materials Using Hybrid-Trefftz Finite Elements. International Conference on Computational Mechanics (CM13) 25-27 March 2013, Durham, UK
- [66] J. A. Teixeira de Freitas, J. P. Moitinho de Almeida, E. M. B. Ribeiro Pereira, Non-conventional formulations for the finite element method, *Computational Mechanics* 23 (5-6) (1999) 488–501.
- [67] J. C. J. Schellekens, R. de Borst, The application of interface elements and enriched or rate-dependent continua to micro-mechanical analyses of fracture in composites, *Computational Mechanics* 14 (1) (1994) 68–83.

- [68] Z. Zhu, I. Ahmad, A. Mirmiran. Fiber element modeling for seismic performance of bridge columns made of concrete-filled FRP tubes. *Engineering Structures* 28 (2006) 2023–2035.
- [69] F. Taucer, E. Spacone, F. Filippou. A fibre beam-column element for seismic response analysis of EC structures. Earthquake Engineering Research Centre. Repor No. UCB/EERC-91/17, 1991.
- [70] J. Niwa, I. Choi, T. Tanabe. Analytical study for shear resisting mechanism using lattice model. *Concrete library of JSCE*, 26, 95-109. 1995.
- [71] T. Miki, J. Niwa. Nonlinear analysis of RC structural members using 3D lattice model. *Journal of advanced concrete technology*, Vol. 2, No. 3; 343-358, Oct. 2004.
- [72] T. N. Tjhin, M. A. Aschheim, J.W. Wallace. Yield displacement-based seismic design of RC wall buildings. *Engineering Structures* 29 (2007) 2946–2959.
- [73] T.-H. Kim, H.-M. Lee, Y.-J. Kim, H.M. Shin. Performance assessment of precast concrete segmental bridge columns with a shear resistant connecting structure. *Engineering Structures* 32 (2010) 1292-1303.
- [74] K. Antoniadis, T. Salonikios, A. J. Kappos. Evaluation of hysteretic response and strength of repaired R/C walls strengthened with FRPs. *Engineering Structures* 29 (2007) 2158–2171.
- [75] Y. Sung, W. Liao, W. Yen. Performance-based concept on seismic evaluation of existing bridges. *Earthquake Engineering & Engineering Vibration* (2009) 8:127-135.
- [76] M. Tsai, S. Wu, K. Chang, G. C. Lee. Shaking table tests of a scaled bridge model with rolling-type seismic isolation bearings, *Engineering Structures* 29 (2007) 694–702.
- [77] W. Ren, W. Zatar, I. E. Harik. Ambient vibration-based seismic evaluation of a continuous girder bridge, *Engineering Structures* 26 (2004) 631–640.
- [78] M. Chaudhary, M. Abe, Y. Fujino. Performance evaluation of base-isolated Yama-age' bridge with high damping rubber bearings using recorded seismic data. *Engineering Structures*, 23 (2001) 902–910.
- [79] S. Chao, C. Loh. Inelastic response analysis of reinforced concrete structures using modified force analogy method. *Earthquake Engineering and Structural Dynamics*: 36:1659–1683. 2007.
- [80] S.J. Li, H. Yu, Y. Suzuki. Identification of non-linear hysteretic systems with slip. *Computers and Structures*, 82 (2004) 157-165.

- [81] J. P. Singh. Characterization of ground motion for severity and damage potential. JP Singh & Associates, Richmond, California.1995.<http://nisee.berkeley.edu/lessons/singh.html>.
- [82] C-H. Yeh, Y. K. Wen. Modeling of nonstationary ground motion and analysis of inelastic structural response. *Struct Saf* 1990;8:281–98.
- [83] J. Hancock, J. J. Bommer. The influence of phase and duration on earthquake damage in degrading structures. In: *Proceedings of the thirteenth world conference on earthquake engineering*, Vancouver, Canada, paper no. 1990; 2004.
- [84] M. Sasani, V. V. Bertero. Importance of severe pulse-type ground motions in performance-based engineering: historical and critical review. In: *Proceedings of the 12th WCEE*, Auckland, New Zealand, paper no. 1302; 2000.
- [85] H. Cao, M.I. Friswell. The effect of energy concentration of earthquake ground motions on the nonlinear response of RC structures. *Soil Dynamics and Earthquake Engineering*, 29 (2009) 292– 299
- [86] Abbas Moustafa. Damage-based design earthquake loads for single degree of freedom inelastic structures. *Journal of structural engineering*, DIO: 10.1061/(ASCE)ST.1943-541X .0000074. March 2011.
- [87] Abbas Moustafa .Critical earthquake load inputs for multi-degree-of-freedom inelastic Structures. *Journal of Sound and Vibration* 325 (2009) 532–544.



# Chapter 3

---

## Basic Theory of Earthquake Analysis of Structures

---

### Contents

- 3.0 INTRODUCTION ..... 70
- 3.1 DIFFERENTIAL EQUATIONS FOR EQUILIBRIUM OF STATIC FORCES IN ISOTROPIC ELASTIC MEDIUM..... 70
  - 3.1.1 Solving the Elastic Body Problem ..... 73
- 3.2 DIFFERENTIAL EQUATIONS FOR EQUILIBRIUM OF DYNAMIC FORCES IN ISOTROPIC ELASTIC MEDIUM..... 73
  - 3.2.1 The Propagation of Waves of Distortion in the Elastic Medium ..... 74
  - 3.2.2 The Propagation of Waves of Dilation in the Elastic Medium ..... 74
  - 3.2.3 Longitudinal and Transversal Propagation of Stress Waves..... 75
  - 3.2.4 The Propagation of Waves in Isotropic Elastic structures ..... 76
- 3.3 THE EQUATION OF MOTION FOR THE DYNAMIC BODY (a different approach)76
- 3.4 FAILURE AND NON-LINEAR BEHAVIOUR IN THE ISOTROPIC MATERIALS 80
- 3.5 SOLVING THE EQUATION OF MOTION FOR NON-PERIODIC RESPONSES OF MDOF STRUCTURES SUBJECT TO EARTHQUAKE LOADING..... 80
  - 3.5.1 Applying the Modal Superposition Method for Solving a Non-Periodic Response of MDOF Structures Subject to Earthquake Loading ..... 81
    - 3.5.1.1 Applying the concept of modal expansion of MDOF responses..... 81
    - 3.5.1.2 Decomposition of the MDOF equation of motion into independent uncoupled equations..... 82
    - 3.5.1.3 Solving for the harmonic responses for all modes ..... 83
    - 3.5.1.4 Superposition of the expanded SDOF equations..... 84

3.5.2	Applying the Direct Integration Method, by using Newmark's Method with Implicit Integration, for Solving a Non-Periodic Response of MDOF Structures Subject to Earthquake Loading .....	84
3.6	TOPICS IN EARTHQUAKE ENGINEERING .....	85
3.6.1	Equation of Motion of a SDOF Structural System .....	85
3.6.2	Rotational Motion .....	87
3.6.3	Ductility: the Capacity and Demand .....	88
3.6.4	Yield Strength and Ductility Relation .....	89
3.6.5	The Equation of Motion for an Elastic System .....	91
3.6.6	Equation of Motion for an Inelastic System.....	92
3.6.7	Ductility Factor $\mu$ and Yield Strength Reduction Factor $R_y$ .....	93
3.6.8	Base Shear Coefficients and Ductility .....	95
3.6.9	Procedures for Strength-based Seismic Design .....	95
3.6.10	Procedures for Ductility-based Seismic Design.....	96
3.7	FRACTURE.....	99
3.7.1	The Energy Balance Approach .....	99
3.7.2	A Crack Growth .....	101
3.8	REFERENCES .....	103

### 3.0 INTRODUCTION

The proposed problem of this research is associated with several important engineering topics, which need to be explained before representing the research work. The problem is associated with equilibrium of dynamic forces in the isotropic elastic medium, failure and non-linearity in the isotropic materials, solving the equation of motion of MDOF structures subject to non-periodic earthquake loading, topics in Earthquake Engineering and topics in Fracture.

### 3.1 DIFFERENTIAL EQUATIONS FOR EQUILIBRIUM OF STATIC FORCES IN ISOTROPIC ELASTIC MEDIUM

Considering a cube element with stress change between each two parallel planes, as shown in Figure 3.1, the stresses in an infinitesimal element in a body can be represented in a cube element with a stress differential  $\partial\sigma_i$  along the change in dimension  $\partial x_i$ .

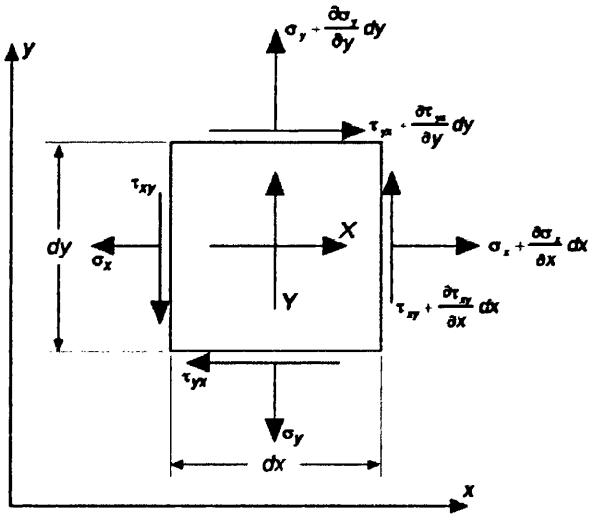


Figure 3.1 Stress change in a 2D plane of a cube element

The equilibrium is between the internal forces, stress multiplied by area, and the external forces, body forces multiplied by the volume. The equilibrium equation for 2 planes only is:

$$[(\sigma_x)_1 - (\sigma_x)_2] * \delta_y \delta_z + [(\tau_{yx})_3 - (\tau_{yx})_4] * \delta_x \delta_z + [(\tau_{zx})_5 - (\tau_{zx})_6] * \delta_x \delta_y + X * \delta_x \delta_y \delta_z = 0 \quad (3.1.a)$$

where,  $(\sigma_x)_1 - (\sigma_x)_2$  is the normal stress change between 2 parallel planes,  $\delta_y \delta_z$  is the change in area,  $(\tau_{xy})_3 - (\tau_{xy})_4$  is the shear stress change between 2 parallel planes, X is the

body force and  $\delta_x \delta_y \delta_z$  is the volume change. Body forces are forces per unit volume such as gravitational and mass inertia forces. The equilibrium equations for the other 4 planes are as follows [1]:

$$\left[ (\sigma_y)_3 - (\sigma_y)_4 \right] * \delta_x \delta_z + \left[ (\tau_{xy})_1 - (\tau_{xy})_2 \right] * \delta_y \delta_z + \left[ (\tau_{zy})_5 - (\tau_{zy})_6 \right] * \delta_x \delta_y + Y * \delta_x \delta_y \delta_z = 0 \quad (3.1.b)$$

$$\left[ (\sigma_z)_5 - (\sigma_z)_6 \right] * \delta_x \delta_y + \left[ (\tau_{yz})_3 - (\tau_{yz})_4 \right] * \delta_x \delta_z + \left[ (\tau_{xz})_1 - (\tau_{xz})_2 \right] * \delta_y \delta_z + Z * \delta_x \delta_y \delta_z = 0 \quad (3.1.c)$$

Shrinking the cube element into an infinitesimal cube element, and taking the limit for all of the faces:

$$\begin{aligned} \frac{\partial \sigma_x}{\partial x} + \frac{\partial \tau_{yx}}{\partial y} + \frac{\partial \tau_{zx}}{\partial z} + X &= 0 \\ \frac{\partial \sigma_y}{\partial y} + \frac{\partial \tau_{xy}}{\partial x} + \frac{\partial \tau_{zy}}{\partial z} + Y &= 0 \\ \frac{\partial \sigma_z}{\partial z} + \frac{\partial \tau_{xz}}{\partial x} + \frac{\partial \tau_{yz}}{\partial y} + Z &= 0 \end{aligned} \quad (3.2)$$

This is the *Equation of Equilibrium*, which *must* be satisfied at all points throughout the volume of the body in order to maintain equilibrium [2]. However, in case of dynamic loading problems, other body forces should be added to this equation to maintain equilibrium. From Continuum Mechanics, by substituting the following definition of normal strain components;

$$\varepsilon_x = \frac{\partial u}{\partial x}, \varepsilon_y = \frac{\partial v}{\partial y} \text{ and } \varepsilon_z = \frac{\partial w}{\partial z} \quad (3.3)$$

into the definition of stress components;

$$\sigma_x = \lambda e + 2 G \varepsilon_x, \sigma_y = \lambda e + 2 G \varepsilon_y \text{ and } \sigma_z = \lambda e + 2 G \varepsilon_z \quad (3.4)$$

the normal stress components are obtained as:

$$\begin{aligned} \sigma_x &= \lambda e + 2 G \frac{\partial u}{\partial x} \\ \sigma_y &= \lambda e + 2 G \frac{\partial v}{\partial y} \\ \sigma_z &= \lambda e + 2 G \frac{\partial w}{\partial z} \end{aligned} \quad (3.5)$$

where, u, v and w are the displacements at x, y and z directions, respectively.  $e = \varepsilon_x + \varepsilon_y + \varepsilon_z$  is the unit volume expansion,  $\lambda = \frac{\nu E}{(1+\nu)(1-2\nu)}$ ,  $\nu$  is the Poisson's ratio,  $E$  is the elastic modulus and  $G$  is the shear modulus,  $G = \frac{E}{2(1+\nu)}$ .

Similarly, shear strain components are defined as:

$$\gamma_{xy} = \frac{\partial u}{\partial y} + \frac{\partial v}{\partial x}, \quad \gamma_{yz} = \frac{\partial v}{\partial z} + \frac{\partial w}{\partial y} \quad \text{and} \quad \gamma_{zx} = \frac{\partial w}{\partial x} + \frac{\partial u}{\partial z} \quad (3.6)$$

By substituting the shear strain components into the following definition of shear stress components;

$$\gamma_{xy} = \frac{1}{G} \tau_{xy}, \quad \gamma_{yz} = \frac{1}{G} \tau_{yz} \quad \text{and} \quad \gamma_{zx} = \frac{1}{G} \tau_{zx} \quad (3.7)$$

the shear stress components are obtained as:

$$\begin{aligned} \tau_{xy} &= G \left( \frac{\partial u}{\partial y} + \frac{\partial v}{\partial x} \right) \\ \tau_{yz} &= G \left( \frac{\partial v}{\partial z} + \frac{\partial w}{\partial y} \right) \\ \tau_{zx} &= G \left( \frac{\partial w}{\partial x} + \frac{\partial u}{\partial z} \right) \end{aligned} \quad (3.8)$$

Substituting both normal and shear stress components, equations (3.5) and (3.8) respectively, into the Equation of Equilibrium, equation (3.2), the following modified Equation of Equilibrium is obtained as:

$$\begin{aligned} (\lambda + G) \frac{\partial e}{\partial x} + G \nabla^2 u + X &= 0 \\ (\lambda + G) \frac{\partial e}{\partial y} + G \nabla^2 v + Y &= 0 \\ (\lambda + G) \frac{\partial e}{\partial z} + G \nabla^2 w + Z &= 0 \end{aligned} \quad (3.9)$$

where,  $\frac{\partial e}{\partial x}$  is the rate of change in volume expansion and  $\nabla^2 = \frac{\partial^2}{\partial x^2} + \frac{\partial^2}{\partial y^2} + \frac{\partial^2}{\partial z^2}$  is the summation of second derivative with respect to x, y and z.

If body forces are not considered, i.e. gravitational forces have no effect on the stress change of the body, and the effective external forces are surface forces which are located on the surface boundaries of the body,  $X$ ,  $Y$  and  $Z$  can be eliminated for the internal elements, and substituted with surface forces,  $\bar{X}$ ,  $\bar{Y}$  and  $\bar{Z}$ , for the infinitesimal tetrahedral elements on the boundary surface of the body[2]. In this case, all of the infinitesimal elements come to equilibrium with the external forces in each direction when they are added together. Therefore, equilibrium is still maintained at each of these elements without the existence of body forces, and the *Equation of Equilibrium* in terms of displacements will be;

$$\begin{aligned} (\lambda + G) \frac{\partial e}{\partial x} + G \nabla^2 u &= 0 \\ (\lambda + G) \frac{\partial e}{\partial y} + G \nabla^2 v &= 0 \\ (\lambda + G) \frac{\partial e}{\partial z} + G \nabla^2 w &= 0 \end{aligned} \quad (3.10)$$

If differentiating these equations, (3.10), with respect to  $x$ ,  $y$  and  $z$  respectively, and adding the differentiated values together, the *Equation of Equilibrium* will become;

$$(\lambda + 2G) \nabla^2 e = 0 \quad (3.11)$$

This means that  $\nabla^2 e = 0$ , and the rate of volume expansion  $\nabla e$  is also zero since the volume expansion  $e = \varepsilon_x + \varepsilon_y + \varepsilon_z$  is a constant value.

### 3.1.1 Solving the Elastic Body Problem

In order to solve the problem of the elastic body, the equation of equilibrium (3.10) for the body and equation (3.9) for its boundaries, substituting the surface forces  $\bar{X}$ ,  $\bar{Y}$  and  $\bar{Z}$  for the body forces, must all satisfy the 6 conditions of compatibility, which are:

$$\begin{aligned} \frac{\partial^2 \varepsilon_x}{\partial y^2} + \frac{\partial^2 \varepsilon_y}{\partial x^2} &= \frac{\partial^2 \gamma_{xy}}{\partial x \partial y}, & \frac{\partial^2 \varepsilon_y}{\partial z^2} + \frac{\partial^2 \varepsilon_z}{\partial y^2} &= \frac{\partial^2 \gamma_{yz}}{\partial y \partial z}, & \frac{\partial^2 \varepsilon_z}{\partial x^2} + \frac{\partial^2 \varepsilon_x}{\partial z^2} &= \frac{\partial^2 \gamma_{xz}}{\partial x \partial z}, \\ 2 \frac{\partial^2 \varepsilon_x}{\partial y \partial z} &= \frac{\partial}{\partial x} \left( -\frac{\partial \gamma_{yz}}{\partial x} + \frac{\partial \gamma_{xz}}{\partial y} + \frac{\partial \gamma_{xy}}{\partial z} \right), & 2 \frac{\partial^2 \varepsilon_y}{\partial x \partial z} &= \frac{\partial}{\partial y} \left( \frac{\partial \gamma_{yz}}{\partial x} - \frac{\partial \gamma_{xz}}{\partial y} + \frac{\partial \gamma_{xy}}{\partial z} \right) \text{ and} \\ & & 2 \frac{\partial^2 \varepsilon_z}{\partial x \partial y} &= \frac{\partial}{\partial z} \left( \frac{\partial \gamma_{yz}}{\partial x} + \frac{\partial \gamma_{xz}}{\partial y} - \frac{\partial \gamma_{xy}}{\partial z} \right) \end{aligned} \quad (3.12)$$

Using algebraic methods, there must be sufficient equations to solve for the unknowns of stress, strain and displacement components. There are 6 stress components, 6 strain components and 3 displacement components, which need to be determined using the 3 equilibrium equations (3.10), the 6 compatibility equations (3.12), the 6 strain-displacement relations, (3.3) & (3.6) and the 6 constitutive relations, (3.5) & (3.7).

There are different Algebraic methods to solve for these unknowns, which can be found in the references of the subject of Continuum Mechanics [3,4,5,6].

## 3.2 DIFFERENTIAL EQUATIONS FOR EQUILIBRIUM OF DYNAMIC FORCES IN ISOTROPIC ELASTIC MEDIUM

For an isotropic elastic body subjected to a *small motion loading* such as sudden displacements, the inertia forces;  $m\ddot{u}$ ,  $m\ddot{v}$  and  $m\ddot{w}$  are considered as the external *Body forces* in three directions, and are added to the *Equation of Equilibrium* (3.10) in terms of displacements. This will result the following *Equation of Motion*:

$$(\lambda + G) \frac{\partial e}{\partial x} + G \nabla^2 u - \rho \frac{\partial^2 u}{\partial t^2} = 0$$

$$(\lambda + G) \frac{\partial e}{\partial y} + G \nabla^2 v - \rho \frac{\partial^2 v}{\partial t^2} = 0 \quad (3.13)$$

$$(\lambda + G) \frac{\partial e}{\partial z} + G \nabla^2 w - \rho \frac{\partial^2 w}{\partial t^2} = 0$$

where,  $\frac{m}{V} \ddot{u} = \rho \frac{\partial^2 u}{\partial t^2}$ ,  $\frac{m}{V} \ddot{v} = \rho \frac{\partial^2 v}{\partial t^2}$  and  $\frac{m}{V} \ddot{w} = \rho \frac{\partial^2 w}{\partial t^2}$  are the inertia forces,  $m$  is the mass,  $V$  is the volume and  $\rho$  is the density.

The forces in the equation of Motion can be physically interpreted as forces applied normal to the infinitesimal surfaces, and thus, transfer as stress waves propagating in the elastic volume. Such propagation can be in either a longitudinal or a transversal manner, as will be briefly explained.

### 3.2.1 The Propagation of Waves of Distortion in the Elastic Medium

In case where no volume expansion exists such as in Von-Mises materials, the volume change  $= \varepsilon_x + \varepsilon_y + \varepsilon_z = 0$ . This means that the deformation is either shearing distortion due to shear stresses, rotation due to torsion stresses or both shearing and rotational distortion, and therefore, no *Dilation* could occur. Thus, the *Equation of Motion* will be:

$$\begin{aligned} G \nabla^2 u - \rho \frac{\partial^2 u}{\partial t^2} &= 0 \\ G \nabla^2 v - \rho \frac{\partial^2 v}{\partial t^2} &= 0 \\ G \nabla^2 w - \rho \frac{\partial^2 w}{\partial t^2} &= 0 \end{aligned} \quad (3.14)$$

This is called the *Equation of Equivoluminal Waves* or the *Equation of Distortion Waves*.

### 3.2.2 The Propagation of Waves of Dilation in the Elastic Medium

In case that volume expansion exists, such as in Quasi-brittle materials, the volume change  $e = \varepsilon_x + \varepsilon_y + \varepsilon_z \neq 0$ , and deformation has a *Dilation* feature. This indicates that the volume expansion is a constant value, i.e. there is a volume change when the material is compressed (or tensioned). This is true for quasi-brittle material such as concrete, where its Poisson's ratio reaches 0.3. However, incompressible materials with zero volume change,  $e = 0$ , have their Poisson's ratio approaching 0.5.

The *Equation of Motion* is the same as was first defined, and it can be substituted by the following terms:  $\frac{\partial e}{\partial x} = \nabla^2 u$ ,  $\frac{\partial e}{\partial y} = \nabla^2 v$  and  $\frac{\partial e}{\partial z} = \nabla^2 w$ . The *Equation of Motion* is re-written as follows:

$$\begin{aligned}(\lambda + 2G)\nabla^2 u - \rho \frac{\partial^2 u}{\partial t^2} &= 0 \\(\lambda + 2G)\nabla^2 v - \rho \frac{\partial^2 v}{\partial t^2} &= 0 \\(\lambda + 2G)\nabla^2 w - \rho \frac{\partial^2 w}{\partial t^2} &= 0\end{aligned}\tag{3.15}$$

This is called the *Equation of Irrotational Waves* or the *Equation of Dilation Waves*.

### 3.2.3 Longitudinal and Transversal Propagation of Stress Waves

The general case of propagation of waves in an elastic medium is obtained by the superposition of both *waves of Distortion and Dilation*, which can be written as follows:

$$\frac{\partial^2 r}{\partial t^2} = a^2 \nabla^2 r\tag{3.16}$$

Where,  $r$  is the displacement,  $a = c_1 = \sqrt{\frac{\lambda+2G}{\rho}}$  in case of waves of Dilation and  $a = c_2 = \sqrt{\frac{G}{\rho}}$  in case of waves of Distortion.  $c_1$  and  $c_2$  are the velocities of propagation of the plane waves. This equation is representing the earthquake vibration motion in the soil medium, which can be recorded on a seismograph.

In simpler terms, for a one dimensional motion,  $v = w = 0$  and the equation of motion will be represented as follows:

$$\frac{\partial^2 u}{\partial t^2} = a^2 \nabla^2 u\tag{3.17}$$

Stress waves propagate from the *centre of disturbance* at which external forces apply. The *Equation of Motion* assumes two kinds of wave propagation in the plane of an elastic medium, according to the type of material of the medium. As shown in Figure 3.2, the first kind is the motion of *Longitudinal waves* which propagate in parallel to the direction of plane propagation lines, causing *Dilation* strains which involve the parameter of  $c_1 = \sqrt{\frac{\lambda+2G}{\rho}}$  in the equation of motion. The second kind is the motion of *Transversal waves* which propagate perpendicular to the direction of plane propagation lines, causing *Distortion* strains which involve the parameter  $c_2 = \sqrt{\frac{G}{\rho}}$  in the equation of motion.



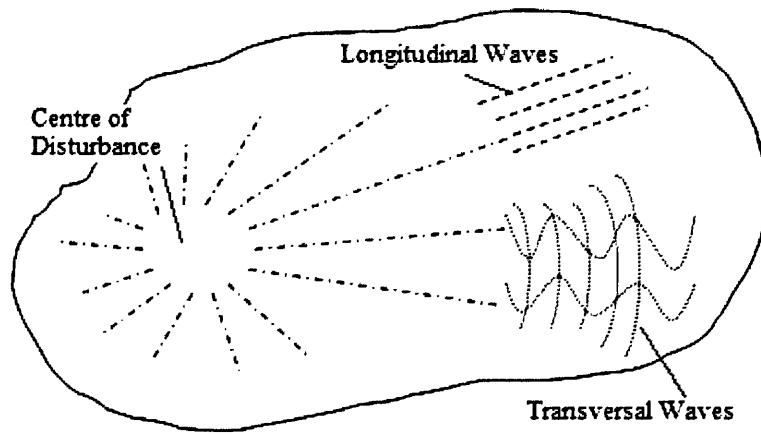


Figure 3.2 Propagation of stress waves in an elastic medium; Longitudinal and Transversal waves

### 3.2.4 The Propagation of Waves in Isotropic Elastic structures

Structural members depend on their *Modulus of Rigidity* to resist against the propagation of waves in the elastic range of loading. The *Modulus of Rigidity* for a member, also known as member's *stiffness*, depends on the method of loading. The *Modulus of Rigidity* for a member is: its *axial rigidity*  $EA$  in a pure axial loading, its *shear rigidity*  $GA$  in a pure shear loading, its *shear rigidity*  $GI$  in shear with bending, its *torsional rigidity*  $GJ_o$  in a torsional loading and its *flexural rigidity*  $EI$  in a flexural bending moment loading.

In general, the stiffness matrix of a structural member in the *Equation of Motion* is analogous to the term  $a^2\nabla^2$  in the elastic medium, which is a function of the mechanical properties of the material multiplied by the second order gradient. However, *stiffness matrix* for a member is a function of its geometry, material properties and degrees of freedom.

## 3.3 THE EQUATION OF MOTION FOR THE DYNAMIC BODY (a different approach)

This is a different approach for determining the dynamic forces in the isotropic elastic medium. In seismic problems, responses of excited bodies are studied as elastic non-rigid bodies, which are structured with single or multiple degrees of freedoms. All forces affecting the body's responses need to be determined including those existing before the dynamic excitation, i.e. the elastic stiffness of the structure in the static stage of the problem. Both static and dynamic responses (results) of the structure are directly added up for every degree

of freedom in order to obtain the overall response. This direct superposition of the results is valid for linear systems only. However, non-linear systems, such as structures with plastic design need to be analysed collectively for both the static and dynamic cases.

Since we are not interested in studying the motion of rigid bodies, but rather the elastic and plastic behaviour in all points of the moving body, together with its mass inertia and other possible resisting forces, equilibrium of the forces on an infinitesimal 3D element, shown in Figure 3.3, can be derived in 1D [9] first as:

$$P = \sigma A = EA \varepsilon = EA \frac{\partial u}{\partial x} \tag{3.18}$$

where,  $P$  is the force acting in the infinitesimal element.

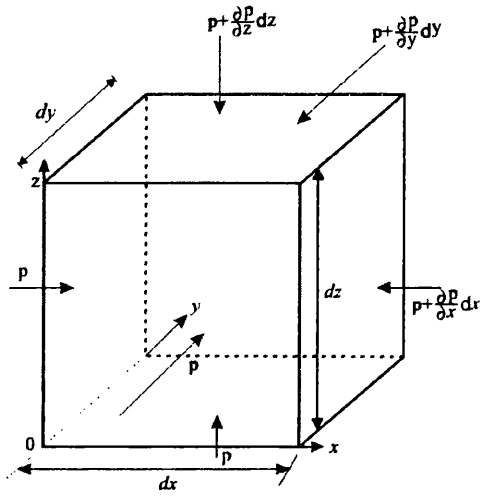


Figure 3.3 Stresses on a cube element.

To maintain equilibrium in the x-direction, body forces  $Q_x$  (per derivative length  $\partial x$ ), such as gravitational or inertia forces, counteracting the acting derivative forces  $\partial P_x$  (per derivative length  $\partial x$ ) as follows:

$$\frac{\partial P_x}{\partial x} + Q_x = 0 \tag{3.19}$$

Substituting;

$$EA \frac{\partial^2 u}{\partial x^2} + Q_x = 0 \tag{3.19'}$$

If the body forces are considered as inertia forces only, they can be represented by using the Newton's Law for the force per unit length  $Q_x$  as  $Q_x = \frac{\text{mass}}{\text{unit length}} \times \text{acceleration}$ . Then, equation (3.19') becomes:

$$EA \frac{\partial^2 u}{\partial x^2} + \rho A \frac{\partial^2 u}{\partial t^2} = 0 \quad (3.20)$$

where,  $\rho$  is the mass per unit volume and  $A$  is the area of the cube surface.

In a more general case, the damping forces are also added to the inertia forces and the stiffness forces. In case of a forced vibration, external forces are added to the right hand side, and the equation of motion can be written in the 3D formulation as follows:

$$\begin{aligned} \rho A \frac{\partial^2 u}{\partial t^2} + c \frac{\partial u}{\partial t} + EA \frac{\partial^2 u}{\partial x^2} &= F_x \\ \rho A \frac{\partial^2 v}{\partial t^2} + c \frac{\partial v}{\partial t} + EA \frac{\partial^2 v}{\partial y^2} &= F_y \\ \rho A \frac{\partial^2 w}{\partial t^2} + c \frac{\partial w}{\partial t} + EA \frac{\partial^2 w}{\partial z^2} &= F_z \end{aligned} \quad (3.21)$$

where,  $c$  is the damping factor, and  $F_x$ ,  $F_y$  and  $F_z$  are the external forces (driving forces ) per unit length. The driving forces together with the stiffness, damping and inertia forces, will form the equation of motion in its 2nd order time-dependant form of a partial differential equation.

To solve the equation of motion for  $u$ ,  $v$  and  $w$  displacements, numerical methods are used to build an analytical model to simulate loading and material response within the geometric context and boundary conditions of the problem. This is done in the following two steps:

1. Finite element discretization level; Transforming the partial differential equations PDE's which are governing the infinitesimal elements (infinite elements) of the body volume into ordinary differential equations ODE's that govern a context of finite elements FE's. such finite elements could be in the form of:
  - A discrete system of multiple degrees of freedoms (MDOF) for discrete (skeleton) structures such as frames and converted pendulums, or
  - A finite element form, or fibre element form for elastic continuum systems.
2. Solution level; Solving the discretized body volume by using Newmark's Method, which is one of the most popular time-stepping methods for solving dynamic problems.

In the discretization process the body mass is to be divided into small masses, each is "lumped" to a node which would control its movement and response. Therefore, equation (3.21) is linearized by discretising  $u$ ,  $v$  and  $w$  in the finite elements. The equation of motion for each *local finite element* would be written in a *matrix form* as:

$$\mathbf{m} \frac{\partial^2 \mathbf{u}}{\partial t^2} + \mathbf{c} \frac{\partial \mathbf{u}}{\partial t} + \mathbf{k} \mathbf{u} = \mathbf{F} \quad (3.22)$$

where,  $\mathbf{u} = [u \ v \ w]^T$  is the nodal displacements,  $\mathbf{m}$  is the local matrix of material mass inertia for an element,  $\mathbf{c}$  is the local matrix of material damping for an element,  $\mathbf{k}$  is the local matrix of material stiffness for an element and  $\mathbf{F} = [F_x \ F_y \ F_z]^T$  is the nodal forced vibrations. Noting that  $\mathbf{F}$  is representing the forces applied on the nodes, and is equivalent to the effect of earthquake ground motion on the structure.

For simplicity, consider a structure system with multiple degrees of freedom (MDOF), to be *generalized* in one degree of freedom at each node. The equation of motion (3.22) that controls any vibration (periodic or non-periodic) for a structure with single degree of freedom (SDOF) is reduced for the single freedom to:

$$m \ddot{u} + c \dot{u} + k u = p(t) \quad (3.23)$$

For simplicity, consider a SDOF structure with un-damped forced vibration, which will have the equation of motion as:

$$m \ddot{u} + k u = p(t) \quad (3.23')$$

The equation of motion for a node subjected to a ground acceleration  $\ddot{u}_g(t)$  is given as:

$$m \ddot{u} + k u = -m \ddot{u}_g = p(t)_{eff} \quad (3.24)$$

Where,  $p(t)_{eff}$  is the *effective force* that causes *the same effect on a stationary structure* as the earthquake does.

In a *local matrix form*, the equation of motion for one local element with more than 2 DOF's is written (in the italic bold face) as [10]:

$$\mathbf{m} \ddot{\mathbf{u}} + \mathbf{k} \mathbf{u} = -\mathbf{m} \mathbf{l} \ddot{u}_g = \mathbf{p}(t)_{eff} \quad (3.24')$$

And in a *global matrix form*, the equation of motion for the whole MDOF structure is to be written (in the bold face) as:

$$\mathbf{m} \ddot{\mathbf{u}} + \mathbf{k} \mathbf{u} = -\mathbf{m} \mathbf{l} \ddot{u}_g = \mathbf{P}(t)_{eff} \quad (3.24'')$$

where  $\mathbf{l}$  is the influence vector which equals 0's and  $\pm 1$ 's as according to the DOF of the structure, and  $\mathbf{m} \mathbf{l}$  is known as the spatial distribution for the system which determines the existence of mass inertia forces in the right degree of freedom.

### **3.4 FAILURE AND NON-LINEAR BEHAVIOUR IN THE ISOTROPIC MATERIALS**

Failure of isotropic materials occurs when the waves of *Distortion*, *Dilation* or both become large enough to cause the initiation of micro-cracks by starting the plastic softening or hardening stage. In this stage the *Equation of Motion* is not valid via the elastic stiffness, since that the elastic potential of the material is not totally conserved, and the material's ultimate strength is degraded via residual strains when the structure is un-loaded and re-loaded during the plastic stage.

To determine the internal stresses in this stage, at first; failure criteria such as Mohr-Coulomb and Rankine are needed in case of quasi-brittle materials, so as to predict the failure in the overstressed zones which develop *Distortion* and *Dilation* strains. Secondly; the numerical time-stepping techniques for integrating differential equations are still needed, to apply the *Equation of Motion* under certain conditions of degraded stiffness and strength of the material, and determine the resulting displacements in such non-linear stage. The last stage is the post-failure stage in which the material strength is totally lost and micro-cracks develop to become visible cracks. In this stage the material fracture energy which bonds the elements together is violated, and a new stage of discrete elements is reached. Failure criteria, non-linearity and fracturing of the material are important issues in the proposed RC problem, and are discussed in the successive chapters in this research.

### **3.5 SOLVING THE EQUATION OF MOTION FOR NON-PERIODIC RESPONSES OF MDOF STRUCTURES SUBJECT TO EARTHQUAKE LOADING**

Non-periodic responses such as those gained by seismic loading have no exact solutions since the frequency for the forced vibration cannot be defined. Non-periodic response of MDOF structures are even more complex to solve, since they will have more than one modal frequency response and more than one modal shape. Therefore only approximate solutions can be obtained for this case of loading. There are several approximate methods to solve equation (3.24, 3.24' and 3.24'') numerically for the nodal displacements:

- The *Modal Superposition Method*,
- The *Direct Integration Methods*, using *Newmark Method* with the Explicit integration, Implicit Integration or mixed Explicit/Implicit Integration method.

In the following two sections, both methods will be discussed briefly.

### 3.5.1 Applying the Modal Superposition Method for Solving a Non-Periodic Response of MDOF Structures Subject to Earthquake Loading

Since it is possible to obtain the exact solution for harmonic loading problems, the *Modal Superposition Method* is associated with the concept of *Modal Expansion*, which depends on the superposition of *all* possible harmonic responses of the structure. The equation of motion for MDOF systems can be solved numerically by decomposing the MDOF equation into independent equations for the coupled nodes. This is done by using the *Modal Decomposition Principle*. In this way, a MDOF structural system is decomposed into several SDOF systems which can be solved independently, and thus the differential equations for the multiple systems can be solved independently and numerically. From the previous briefing, 4 steps are to be performed [10,11]:

1. Applying the concept of modal expansion of MDOF responses
2. Decomposition of the MDOF equation of motion into independent uncoupled equations
3. Solving for the harmonic responses for all modes.
4. Superposition of the expanded SDOF equations

Before proceeding to further explanation, it should be known that the *Modal Superposition Method* is valid for elastic analysis only, and cannot be used for inelastic analysis. Therefore, this method is not used in this research. Alternatively, Newmark's method is then discussed and applied.

#### 3.5.1.1 Applying the concept of modal expansion of MDOF responses

In this principle, superposition of all harmonic responses, namely; the modal coordinate  $q_n(t)$  times the modal shape  $\phi_{jn}$  will produce the displacement response  $u_j(t)$  for any given non-periodic motion, (e.g. responses to earthquakes), for a structure at any time  $t$ . This displacement is to be determined by summing up the scalar products of all modal shapes and coordinates at a time, as follows:

$$u_j(t) = \sum_{n=1}^N \phi_{jn} q_n(t) \quad (3.25)$$

Or, in a matrix form;  $\mathbf{u} = \Phi \cdot \mathbf{q}$  (3.25')

$$\begin{Bmatrix} u_1(t) \\ u_2(t) \\ \vdots \\ u_j(t) \end{Bmatrix} = \begin{bmatrix} \phi_{11} & \phi_{12} & \dots & \phi_{1n} \\ \phi_{21} & \phi_{22} & \dots & \phi_{2n} \\ \vdots & \vdots & \ddots & \vdots \\ \phi_{j1} & \phi_{j2} & \dots & \phi_{jn} \end{bmatrix} \begin{Bmatrix} q_1(t) \\ q_2(t) \\ \vdots \\ q_n(t) \end{Bmatrix}$$

where,

- $q_n(t)$  = generalized displacement at time t, also known as modal coordinate, or coordinate at n. It equals the extreme displacement if  $\phi_{jn}$  is normalized, but it can be any displacement value if  $\phi_{jn}$  is not normalized.
- $\phi_{jn}$  = modal deflected shape, which is a ratio representing relative displacements at different DOFs in the structure.  $\phi_{jn}$  is independent of time, and normalized shapes rank from 0 to 1.0.

### 3.5.1.2 Decomposition of the MDOF equation of motion into independent uncoupled equations

Now; introducing the Modal Superposition principle in order to have the equation of motion solved for a non-periodic response, i.e. response due to earthquake loading. Substituting equation (3.25') into equation (3.24'');

$$\mathbf{m} \cdot \Phi \cdot \ddot{\mathbf{q}} + \mathbf{k} \cdot \Phi \cdot \mathbf{q} = -\mathbf{m} \cdot \mathbf{l} \cdot \ddot{u}_g(t) \quad (3.26)$$

Multiplying both sides by  $\Phi^T$ ; the transposed modal shape matrix;

$$\Phi^T \cdot \mathbf{m} \cdot \Phi \cdot \ddot{\mathbf{q}} + \Phi^T \cdot \mathbf{k} \cdot \Phi \cdot \mathbf{q} = -\Phi^T \cdot \mathbf{m} \cdot \mathbf{l} \cdot \ddot{u}_g(t) \quad (3.27)$$

Or  $\mathbf{M} \cdot \ddot{\mathbf{q}} + \mathbf{K} \cdot \mathbf{q} = -\mathbf{L} \cdot \ddot{u}_g(t)$  (3.28)

where,

$$\mathbf{M} = \Phi^T \cdot \mathbf{m} \cdot \Phi$$

$$\mathbf{K} = \Phi^T \cdot \mathbf{k} \cdot \Phi$$

$$\mathbf{L} = \Phi^T \cdot \mathbf{m} \cdot \mathbf{l}$$

Dividing by  $\mathbf{M}$  ;  $\ddot{\mathbf{q}} + \mathbf{\Omega}^2 \cdot \mathbf{q} = -\mathbf{\Gamma} \cdot \ddot{u}_g(t)$  (3.29)

where,  $\mathbf{\Gamma} = \frac{\mathbf{L}}{\mathbf{M}} = \frac{\Phi^T \cdot \mathbf{m} \cdot \mathbf{l}}{\Phi^T \cdot \mathbf{m} \cdot \Phi}$  = modal participation factor

Equation (3.29) is the *modal form* of equation of motion for a forced vibration which does not contain any *coupled coefficients* of a matrix, since the spectral matrix  $\mathbf{\Omega}^2$  is diagonal, and  $\mathbf{L}$  and  $\mathbf{M}$  depend on the modal matrix  $\Phi^T$  which is uncoupled as well.

However, equation (3.29) has been derived from equation (3.24'') which contains the stiffness matrix  $\mathbf{k}$  with *coupled coefficients*. Having obtained the equation of motion (3.29) with *uncoupled matrix coefficients*, it is very usual to have it solved for  $\mathbf{q}$  on single basis, i.e. as a SDOF system. Therefore, equation (3.29) is now reduced to the modal level of a SDOF system as follows:

$$\ddot{q}_n(t) + \omega_n^2 q_n(t) = -\Gamma_n \cdot \ddot{u}_g(t) \quad (3.30)$$

where;  $\Gamma_n = \frac{L_n}{M_n} = \frac{\phi_{jn}^T \cdot m \cdot l}{\phi_{jn}^T \cdot m \cdot \phi_{jn}}$  = modal participation factor

### 3.5.1.3 Solving for the harmonic responses for all modes

As an example, the equation of motion for an undamped structure with natural angular frequency ( $\omega_n$ ), and subjected to a step force  $P_o$  is  $m \ddot{u} + k u = P_o$ . This is a 2<sup>ed</sup> order homogeneous DE that has an exact solution consisting of the summation of the particular and complementary solutions to be:  $u(t) = \frac{P_o}{k} (1 - \cos \omega_n t)$ .

Similarly, when  $\ddot{q}_n(t) = 0$ , the particular solution is :

$$q_n(t)_p = -\frac{\Gamma_n}{\omega_n^2} \cdot \ddot{u}_g(t) \quad (3.31)$$

the complementary solution is:  $q_n(t)_c = A \cos \omega_n t + B \sin \omega_n t$

and the complete solution is :  $q_n(t) = A \cos \omega_n t + B \sin \omega_n t + -\frac{\Gamma_n}{\omega_n^2} \cdot \ddot{u}_g(t)$

Applying the I.C. ;  $q(0) = 0$  &  $\dot{q}(0) = 0$  at which the SDOF system is initially at rest:

$$q(0) = 0 = A \cos 0 + B \sin 0 + -\frac{\Gamma_n}{\omega_n^2} \cdot \ddot{u}_g(t) \rightarrow A = \frac{\Gamma_n}{\omega_n^2} \cdot \ddot{u}_g(t)$$

$$\dot{q}(0) = 0 = -\omega_n A \sin 0 + \omega_n B \cos 0 + 0 \rightarrow B = 0$$

Substituting A & B;

$$q_n(t) = \frac{\Gamma_n}{\omega_n^2} \cdot \ddot{u}_g(t) ( \cos \omega_n t - 1 ) \quad (3.32)$$



### 3.5.1.4 Superposition of the expanded SDOF equations

As substituting (3.32) into equation (3.25'), in which equations of (3.25):  $u_j(t) = \phi_{jn} q_n(t)$  are summed in a superposition method for all times (t) given for a ground acceleration interval. Thus,  $u_j(t)$  can be determined. It should be known that the modal superposition method is valid for elastic behaviour only.

### 3.5.2 Applying the Direct Integration Method, by using Newmark's Method with Implicit Integration, for Solving a Non-Periodic Response of MDOF Structures Subject to Earthquake Loading

The *Newmark Method* is more popular with less complex calculations, and will be discussed in this section briefly. The equation of motion is the 2ed order time-dependant equation, and written in its global matrix form as:

$$\mathbf{M} \frac{\partial^2 \mathbf{r}}{\partial t^2} + \mathbf{C} \frac{\partial \mathbf{r}}{\partial t} + \mathbf{K} \mathbf{r} = \mathbf{F}(t) \quad (3.33)$$

where;  $\mathbf{r}$  is the displacement vector in the global structure. By using the *Implicit Integration* scheme, this equation is re-written numerically in a linear interpolation in time by involving a scalar parameter  $\theta$  varying between 0.5 and 1, thus a class of *Recurrence Relations* based on this linear interpolation is obtained [9]. The equation of motion is re-written at two numerical stations; '0' and '1' as follows:

$$\mathbf{M} \frac{\partial^2 \mathbf{r}_0}{\partial t^2} + (\alpha \mathbf{M} + \beta \mathbf{K}) \frac{\partial \mathbf{r}_0}{\partial t} + \mathbf{K} \mathbf{r}_0 = \mathbf{F}_0 \quad (3.34.a)$$

$$\mathbf{M} \frac{\partial^2 \mathbf{r}_1}{\partial t^2} + (\alpha \mathbf{M} + \beta \mathbf{K}) \frac{\partial \mathbf{r}_1}{\partial t} + \mathbf{K} \mathbf{r}_1 = \mathbf{F}_1 \quad (3.34.b)$$

where,  $\alpha$  and  $\beta$  are the inertia and stiffness Rayleigh damping coefficients respectively. The linear interpolation in time involving  $\theta$  between 0.5 and 1 for the displacement and velocity can be written as:

$$\mathbf{r}_1 = \mathbf{r}_0 + \Delta t \left[ (1 - \theta) \frac{\partial \mathbf{r}_0}{\partial t} + \theta \frac{\partial \mathbf{r}_1}{\partial t} \right] \quad (3.35.a)$$

$$\frac{\partial \mathbf{r}_1}{\partial t} = \frac{\partial \mathbf{r}_0}{\partial t} + \Delta t \left[ (1 - \theta) \frac{\partial^2 \mathbf{r}_0}{\partial t^2} + \theta \frac{\partial^2 \mathbf{r}_1}{\partial t^2} \right] \quad (3.35.b)$$

Substituting these two equations into the two numerical stations '0' and '1', equations 3.34.a and 3.34.b, will construct the following *three Recurrence Relations*, as follows:

$$\left[ \left( \alpha + \frac{1}{\theta \Delta t} \right) \mathbf{M} + (\beta + \theta \Delta t) \mathbf{K} \right] \mathbf{r}_1 =$$

$$\theta \Delta t \mathbf{F}_1 + (1 - \theta) \Delta t \mathbf{F}_0 + \left( \alpha + \frac{1}{\theta \Delta t} \right) \mathbf{M} \mathbf{r}_0 + \frac{1}{\theta} \mathbf{M} \frac{\partial \mathbf{r}_0}{\partial t} + [\beta - (1 - \theta) \Delta t] \mathbf{K} \mathbf{r}_0 \quad (3.36.a)$$

$$\frac{\partial \mathbf{r}_1}{\partial t} = \frac{1}{\theta \Delta t} (\mathbf{r}_1 - \mathbf{r}_0) - \frac{1 - \theta}{\theta} \frac{\partial \mathbf{r}_0}{\partial t} \quad (3.36.b)$$

$$\frac{\partial^2 \mathbf{r}_1}{\partial t^2} = \frac{1}{\theta \Delta t} \left( \frac{\partial \mathbf{r}_1}{\partial t} - \frac{\partial \mathbf{r}_0}{\partial t} \right) - \frac{1 - \theta}{\theta} \frac{\partial^2 \mathbf{r}_0}{\partial t^2} \quad (3.36.c)$$

By means of the recurrence relations, the values of displacement (3.36.a) and its derivatives (3.36.b and c) at one instant in time are sufficient to determine these values at the subsequent instant, i.e. giving implicitly one equation solution per each time-step. This method was formulated into a FE computational code by using the MatLab program, and was applied to solve a simple forced vibration problem, by using an elasto-plastic solid in plane strain with 8-noded quadrilateral elements and lumped masses. The aim of this analysis was to understand more about Newmark's method with implicit integration and to be able to determine the behaviour of two different materials; namely concrete and a steel bar, with interface elements in between, under forced vibrations to simulate the damping influence due to the bond effect between concrete and steel bars. The simulation was verified by published results, but no further investigations were conducted in this direction, since it was diverting from the main topic of this research, but could be carried out in other future work.

## 3.6 TOPICS IN EARTHQUAKE ENGINEERING

### 3.6.1 Equation of Motion of a SDOF Structural System

It is important to physically understand the governing equation of a SDOF structural system subjected to ground accelerations and how the equation's parameters are formulated for an equivalent structure with a stationary base. When a portal frame structure with a SDOF is subjected to a ground acceleration motion  $\ddot{u}_g$  for a period of time, i.e. a number of time-steps, the corresponding response that's documented for a single time-step can be divided into two different stages:

- 1- A rigid absolute motion with  $u_g$  displacement, that is caused by a ground force  $m \ddot{u}_g$ , where  $m$  is the structure's lumped mass.
- 2- A flexible relative motion with  $u$  displacement, that is caused also by the ground force  $m \ddot{u}_g$ , which is resisted by two different types of forces;
  - external, which is known as the mass inertia  $m \ddot{u}$ , also described as fictitious since it is not expressed alike others by a spring or a dashpot.
  - internal, which has two parts; a damping force  $c \dot{u}$  and a restoring force  $ku$ . The former is expressed by a dashpot and the latter is expressed by a spring in a rheological model.

The overall resisting forces are summed up and known as the effective forces since they indicate the forces that cause the relative motion only;  $P_{eff} = m \ddot{u} + c \dot{u} + k u$ . The force diagram of the dynamic structure in Figure 3.4 shows 3 movements of the structure mass in the moving ground diagram; a) initial, b) rigid and c) deforming cases. In this motion diagram the inertia force is resisted by the effective force and equilibrium is reached after the relative motion stops at position c. Equivalent to that is the force diagram in the stationary base, in which the two forces are equal and summed up as:  $m \ddot{u}_g + P_{eff} = 0$ .

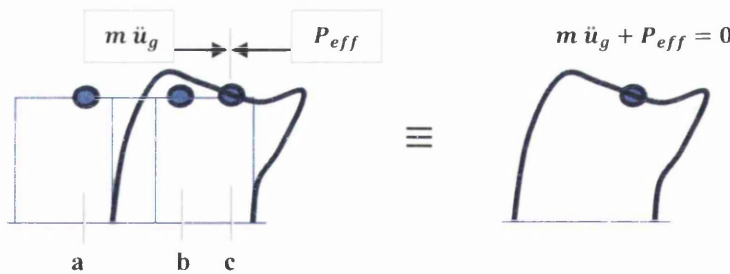


Figure 3.4 Force diagram for the moving ground and for the equivalent stationary base

Substituting; 
$$m \ddot{u}_g + m \ddot{u} + c \dot{u} + k u = 0$$

Or 
$$m \ddot{u} + c \dot{u} + k u = -m \ddot{u}_g \quad (3.37)$$

The minus sign is only a convention indicating that the resisting effective forces  $P_{eff}$  and ground forces  $m \ddot{u}_g$  are equal and acting opposite to each other, or  $m \ddot{u}_g + -m \ddot{u}_g = 0$ . The total displacement of a structure is equal to the relative structural motion displacement  $u$  and the rigid ground motion displacement  $u_g$  as follows:  $u^t = u + u_g$ .

In a dynamic analysis the rigid absolute motion  $u_g$  is ignored, but its force effect  $m \ddot{u}_g$  is used as an applied load subjected on the lumped mass structure on a stationary base. The structural response of any point on the structure is computed relative to the stationary base. The resisting relative forces will have different contributions according to the inertia, damping and stiffness of the structure. They are namely the inertia, damping and restoring forces and their summation is the total effective force. They are plugged in the equation of motion as follows:

$$f_I + f_D + f_S = -m \ddot{u}_g \quad (3.38)$$

### 3.6.2 Rotational Motion

Although ground rotation  $\theta_g$  does not exist, it is worth it to apply the previous concept of dynamic analysis on the rotational motion of a cantilever structure such as an elevated water tank. The total displacement (rigid & flexible) is  $u_t = u + h \theta_g$  and the total rotation is  $\theta_t = \theta + \theta_g$ , as shown in Figure 3.5. By applying the equation of motion for the moments and rotational response the following equations are obtained [10]:

$$M_I + M_D + M_S = -m \ddot{\theta}_g \quad (3.39)$$

$$m \ddot{\theta} + c_\theta \dot{\theta} + k_\theta \theta = -m \ddot{\theta}_g = M_{eff} \quad (3.40)$$

where,  $c_\theta$  and  $k_\theta$  are the rotational damping and rotational stiffness respectively. However, the transitional relative forces and effective force  $P_{eff}$  can also be calculated from the assumed ground rotation as follows:

$$m \ddot{u} + c \dot{u} + k u = -m h \ddot{\theta}_g = P_{eff} \quad (3.41)$$

where,  $h$  is the height of the lumped mass from the stationary base.

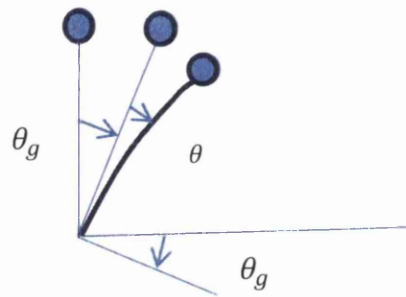


Figure 3.5 Rotational motion diagram

It should be noted that measurements of rotational parameters for a SDOF cantilever structures are preferred for many researchers since  $\theta$  is a good indicator for a structural damage index and more significant hysteresis loops are attained from  $M_S - \theta$  curve representation more than  $f_S - u$  curves. A hysteresis curve of base moment vs. curvature ( $M_S - \theta$  curve) is used to produce a hysteresis curve of base shear vs. displacement ( $f_S - u$  curve), by dividing  $M_S/h$  to obtain the base shear and multiplying  $\theta * h$  to obtain the displacement.

### 3.6.3 Ductility: the Capacity and Demand

The inelastic response of the structure is fundamentally important in earthquake engineering. From the design aspect, earthquake engineering mainly considers that the seismic capacity of the structure to be larger than the seismic demand on the structure.

Theoretically, if the demand is larger than the capacity, the structure would suffer damage as a result of exceeding the capacity limit. However, this may not be feasible in all cases, since low damage can occur even before reaching the capacity of the structure yet acceptable from the design aspect. The question is: how much damage could result at low or high levels of the demand versus capacity? The scope of this research focuses mainly on this subject. From a different aspect, engineers choose to keep their work under the design criterion for ductility. The challenge to the engineer is to design the structure with damage that is controlled to some acceptable degree. Ideally, the designed structure is aimed to be safe and damage-free. Design-wise, this should be approved if:

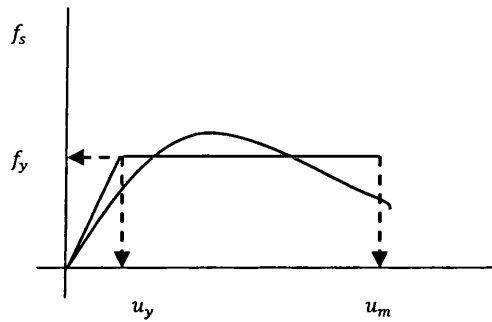
$$\mu_{Capacity} > \mu_{Demand} \quad (3.42)$$

Where,  $\mu$  is the Ductility factor, which is the capacity of an inelastic structural system to deform beyond its elastic level. This implies determining the inelastic range for the structure when it is subjected to the ground shaking and is defined as [10]:

$$\mu = \frac{u_m}{u_y} \quad (3.43)$$

where,  $u_m$  is the maximum inelastic displacement and  $u_y$  is the yield displacement of the structure. Ductility, in this sense, is the inelastic displacement normalized to the elastic displacement limit of the structure. For the whole structure, it is very suitable to plot the

force-deformation curve as a global indication for the hysteresis behaviour of the structure in resisting the seismic loading as in Figure 3.6.



**Figure 3.6 First response stages of force-deformation curve: actual and elastoplastic idealization**

An approximation to the actual force-deformation curve, Figure 3.6, is known as Elastoplastic idealization, or linearized inelastic system, which considers the yielding force as the resisting force during the inelastic phase. The condition is to keep the same area under both curves, since it expresses both the strain recovery Energy  $E_s$  and the Dissipative Yield Energy  $E_y$ .

### 3.6.4 Yield Strength and Ductility Relation

Two important measures for determining the inelastic responses are; the Ductility factor  $\mu$  and the Yield Strength factor  $f_y$ . The combination of both measures is so important in designing inelastic systems. *They simply lead to control the yield displacement  $u_y$  of the inelastic structure.* However, if  $\mu$  and  $f_y$  are provided in inadequate values, the structure may not respond to the seismic loading sufficiently and the resulting damage could be very severe. For design purposes, it is important to determine the yield displacement  $u_y$  for the structure, in order to limit the ductility demand imposed by the earthquake loading, so that it should be always less than the ductile capacity of the structure.

In this sense, it is important to normalize both the ductility  $\mu$  and yield strength  $f_y$  of a SDOF inelastic structure, corresponding to the parameters of a SDOF elastic structure that has the same dynamic characteristics; frequency  $\omega_n$  (with small amplitudes), damping ratio  $\zeta$ . Both systems, elastic and inelastic, are of course subjected to the same ground acceleration  $\ddot{u}_g$ .

The yield strength  $f_y$  is normalized to measure the elastoplastic system in relation to the elastic system, as follows [10]:

$$\bar{f}_y = \frac{f_y}{f_o} = \frac{u_y}{u_o} \tag{3.44}$$

Where,  $f_o$  is the minimum strength required for the structure to remain elastic and  $u_o$  is the corresponding elastic displacement.

The normalized yield strength is restrained to be;  $0 < \bar{f}_y < 1$ . However, it is more suitable to use the yield strength reduction factor, which is restrained between  $1 < R_y < \text{positive number}$ , and equals

$$R_y = \frac{1}{\bar{f}_y} = \frac{f_o}{f_y} \tag{3.45}$$

Similarly, the ductility factor is restrained to be;  $1 < \mu < \text{positive number}$ , and equals

$$\mu = \frac{u_m}{u_y} \tag{3.46}$$

where,  $u_m$  is the maximum displacement response. When  $R_y = 1$ , the system is not elastoplastic, but when  $R_y$  equals 4 for example, this means that the yield strength of the proposed system is reduced 4 times below the elastic strength of its *corresponding* elastic system. Similarly, if the ductility  $\mu$  of this elastoplastic system is computed and found to be 3.11 for example, this means that a seismic demand is imposed on this structure to deform 3.11 times beyond the elastic limit  $u_y$  of this elastoplastic structure. In Figure 3.7, shown the force-deformation relation for the elastoplastic (or elastic perfectly-plastic) system and its *corresponding* elastic system. The force  $f_s$  is the resisting force, or the strength required by any of the two structures to resist the seismic loading.

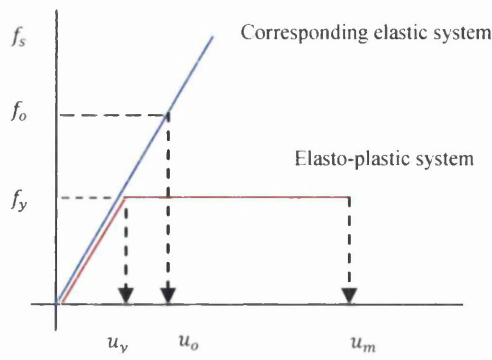


Figure 3.7 An elastoplastic system and its corresponding linear system

The linear parameters are used as references for the ductility factor  $\mu$  and the reduction factor  $R_y$ , to evaluate the behaviour of the non-linear system. These factors are very useful to construct the Inelastic Design Spectrum from the Elastic Design Spectrum. This topic is not relevant to the scope of this research but the Inelastic Design Spectrum, provided with the ductility range, is significantly practical in determining the demand quantities (yield strength  $f_y$  and stiffness) for the structure.

### 3.6.5 The Equation of Motion for an Elastic System

The governing equation of motion of a linear SDOF system subjected to a ground acceleration  $\ddot{u}_g$  is

$$m \ddot{u} + c \dot{u} + k u = -m \ddot{u}_g \quad (3.37)$$

If divided by the mass  $m$ , the following formula is obtained:

$$\ddot{u} + 2 \zeta \omega_n \dot{u} + \omega_n^2 u = -\ddot{u}_g \quad (3.47)$$

where,  $\omega_n = \sqrt{\frac{k}{m}}$  and  $\zeta = \frac{c}{2m\omega_n}$ .

As a conclusion, the deformation response  $u$  for an elastic (linear) structural system depends on 2 system parameters; the natural period  $T_n$  of the system (or its natural angular frequency  $\omega_n$ ) and its damping ratio  $\zeta$  only, in addition to the time of motion  $t$ .

Therefore, for an earthquake with ground acceleration  $\ddot{u}_g$ , the deformation response for a linear system is formally written as [10]:  $u(t, T_n, \zeta)$ .

Consequently, for any two structural systems having the same values of natural period  $T_n$  and damping ratio  $\zeta$ , they should have the same deformation response  $u$  even if one system is stiffer or more massive than the other. This is true when the structure is dynamically activated. However, when structures with different stiffness values  $k_1, k_2, k_3, \dots \dots k_N$  are subjected to the same static loading they will produce different deformation responses  $u_1, u_2, u_3, \dots \dots u_N$ . This is one of the main differences between dynamic and static actions [10].



### 3.6.6 Equation of Motion for an Inelastic System

The resisting force  $f_s$  in the inelastic systems extends to the yielding phase especially at large displacement responses. The yielding property in the material is corresponding to the ductile property of the whole structure. The resisting force  $f_s$  of the whole structure will be dependent on both the displacement and velocity in the inelastic range and is written as  $f_s(u, \dot{u})$ . This is because determining  $f_s$  in the inelastic phase for the dynamic loading depends on whether  $u$  is increasing, which means positive velocity  $+\dot{u}$ , or decreasing, which means negative velocity  $-\dot{u}$ . Hence, the resisting force  $f_s$  is not a single valued vector, since it depends on the history of the deformation response in the inelastic phase. The equation of motion for a SDOF structure subject to a ground motion  $\ddot{u}_g$  is [10]:

$$m \ddot{u} + c \dot{u} + f_s(u, \dot{u}) = -m \ddot{u}_g \quad (3.37')$$

If divided by the mass  $m$ , the following formula is obtained:

$$\ddot{u} + 2 \zeta \omega_n \dot{u} + \omega_n^2 u_y \tilde{f}_s(u, \dot{u}) = -\ddot{u}_g \quad (3.48)$$

where,  $u_y$  is the yield deformation limit,  $\tilde{f}_s(u, \dot{u}) = \frac{f_s(u, \dot{u})}{f_y}$  is a dimensionless quantity that's multiplied by  $u_y$  to estimate the deformation  $u$  and  $f_y$  is the yield strength of the system.

When the system is working plastically,  $\tilde{f}_s(u, \dot{u}) \geq 1$  and the plastic deformation is estimated according to this ratio.

$\omega_n$  is the natural frequency of the inelastic system vibrating within its linearly elastic range, when  $u < u_y$ , or the natural frequency of the corresponding elastic system. Similarly,  $\zeta$  is the damping ratio of the inelastic system vibrating within its linearly elastic range, when  $u < u_y$ , or the damping ratio of the corresponding elastic system.

In the plastic range for an inelastic system, ductility factor  $\mu$  is a dimensionless ratio that measures how much the system will deform beyond its elastic limit. For  $u > u_y$ , substituting  $u = u_y \cdot \mu$  and its derivatives too, then dividing by  $u_y$ , the equation of motion becomes:

$$\ddot{\mu} + 2 \zeta \omega_n \dot{\mu} + \omega_n^2 \tilde{f}_s(u, \dot{u}) = -\frac{\ddot{u}_g}{u_y} \quad (3.49)$$

Since  $\frac{1}{u_y} = \frac{k}{f_y} = \frac{\omega_n^2 m}{f_y} = \frac{\omega_n^2}{a_y}$ , the previous equation can be re-written in the following form:

$$\ddot{\mu} + 2 \zeta \omega_n \dot{\mu} + \omega_n^2 \tilde{f}_s(u, \dot{u}) = -\omega_n^2 \frac{\ddot{u}_g}{a_y} \quad (3.50)$$

where,  $a_y = \frac{f_y}{m}$  is interpreted as the acceleration of the mass necessary to produce the yield force  $f_y$ .

The next step is to substitute the yield force by the normalized yield force  $\bar{f}_y = \frac{f_y}{f_o} = \frac{u_y}{u_o}$ , where  $f_o$  and  $u_o$  are the resisting force and deformation, respectively, in the *corresponding* elastic linear system. From this equation, it is clear that the ductility  $\mu$  depends on the following parameters:  $\omega_n$ ,  $\zeta$  and  $a_y$ .

Substituting  $\bar{f}_y$  for  $f_y$  and  $\frac{k}{\omega_n^2}$  for  $m$ ,  $a_y$  is re-written as follows:

$$a_y = \frac{\bar{f}_y f_o}{m} = \frac{\omega_n^2}{k} \bar{f}_y f_o = \frac{\omega_n^2 u_o}{f_o} \bar{f}_y f_o = \omega_n^2 u_o \bar{f}_y \quad (3.51)$$

Therefore, the equation of motion for the inelastic system is now re-written as:

$$\ddot{u} + 2 \zeta \omega_n \dot{u} + \omega_n^2 \tilde{f}_s(u, \dot{u}) = - \frac{\ddot{u}_g}{u_o \bar{f}_y} \quad (3.52)$$

As a conclusion, the deformation response  $u$  for an inelastic (non-linear) structural system depends on the ductility factor  $\mu$ , which depends on 3 system parameters; the natural period  $T_n$  of the system ( or its natural angular frequency  $\omega_n$  ), its damping ratio  $\zeta$  and the normalized yield strength of the system  $\bar{f}_y$ . Therefore, for an earthquake with a ground acceleration  $\ddot{u}_g$ , the deformation response for an inelastic system is formally written as:  $u(t, T_n, \zeta, \bar{f}_y)$ .

It is now concluded that for an earthquake with a ground acceleration  $\ddot{u}_g$ , the ductility  $\mu$  of an inelastic structural system depends on  $T_n, \zeta$  and  $\bar{f}_y$ , or formally written as  $\mu(T_n, \zeta, \bar{f}_y)$ .

### 3.6.7 Ductility Factor $\mu$ and Yield Strength Reduction Factor $R_y$

For an inelastic system, ductility is then depending on the normalized yield strength  $\bar{f}_y = \frac{1}{R_y}$

since that  $\bar{a}_y = \frac{\bar{f}_y}{m}$  and  $\bar{f}_y = \frac{f_y}{f_o} = \frac{u_y}{u_o}$ . This leads to the conclusion that the Ductility

Demand Factor  $\mu$  and the Yield Strength Reduction Factor  $R_y$  are correlated. They are proportionally related as follows [10]:

$$\frac{\mu}{R_y} = \frac{\frac{u_m}{u_y}}{\frac{u_o}{u_y}} = \frac{u_m}{u_o} \quad (3.53)$$

which means that the maximum inelastic displacement  $u_m$  of the inelastic system can be related to the maximum elastic displacement  $u_o$  of the corresponding elastic system.

The corresponding elastic system is not meant to be an alternative to the inelastic systems. It however, has no physical benefit except as being a reference to the inelastic systems. This helps researchers comparing between different inelastic systems, through the ductility factors  $\mu$  and yield strength reduction factors  $R_y$  for a specific ground motion. More reduction in the yield strength allows for more ductility values for systems subject to the same ground excitement.

Both  $\mu$  and  $R_y$  parameters are mainly used to construct the Inelastic Response Spectrum (Actual & Design Spectrum) from the Elastic Response Spectrum. Both spectra are significantly useful for engineers, and are widely approved by many international codes for seismic structural design. None of these applications are within the scope of this research.

The  $\mu - R_y$  relation is significantly explored via the frequency domain for the SDOF structures. This subject is also not within the scope of this research. [10, p.274].

However, some typical design approaches consider that the reduction factor is assigned equal to the ductility factor, as shown in Figure 3.8.a, in order to obtain an optimum design in which the demand is less than or equal to the capacity, therefore,  $R_y \equiv \mu$ .

This is not necessarily the case for all structures, since some structures could have their ductility capacity exceeded at  $R_y \equiv \mu$  and it is preferable to have the reduction factor much less than the ductility, as shown in Figure 3.8.b, in order to obtain the optimum design in which the demand is less than or equal to the capacity, therefore,  $R_y \ll \mu$ .

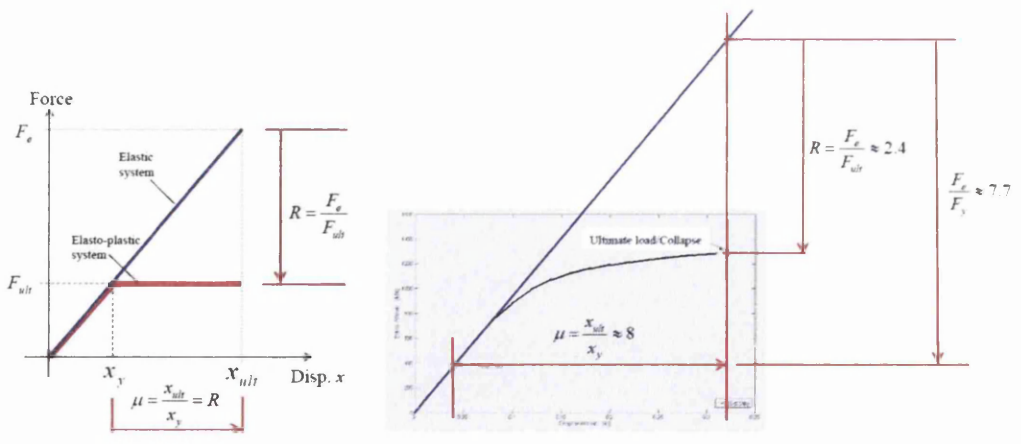


Figure 3.8 The reduction factor and the ductility factor, a)  $R_y \equiv \mu$ , b)  $R_y \ll \mu$ . [14]

### 3.6.8 Base Shear Coefficients and Ductility

The combined D-V-A Elastic Design Spectrum curves are the peak Displacement response, peak Velocity response and peak Acceleration response in the natural period domain  $T_n$  for a SDOF structure with a given damping ratio and subjected to a ground motion record  $\ddot{u}_g(t)$ . The combined D-V-A Elastic Design Spectrum shown in Figure 3.9 is for a ground motion record  $\ddot{u}_g(t)$  with peak ground acceleration PGA  $\ddot{u}_{g_o} = 1g$ . These peak responses are reduced by few reduction factors  $R_y$  to create the combined D-V-A Inelastic Design Spectrum curves, corresponding to a variety of given ductility factors. The elastic and inelastic curves are obviously applied for elastic and inelastic systems respectively. It should be noted that Design Spectra are the simplified versions of the Actual Responses Spectra for the same SDOF structure with a given damping ratio, and subjected to a ground motion record  $\ddot{u}_g(t)$ . However, errors could exist because of these simplifications especially, in the velocity-sensitive and displacement-sensitive ranges of the natural period of the spectrum[10].

Design Spectrum curves or, alternatively, Response Spectrum curves, are used to determine the Base Shear Coefficient  $\frac{A}{g}$ , which is used to determine the peak base shear  $V_{b_o}$  and peak base moment  $M_{b_o}$  for the structural columns. Where,  $A$  is the peak pseudo acceleration of the structure at its top level and  $g$  is the ground acceleration =  $9.81 \text{ kg.m/s}^2$ . It should be known that the peak pseudo acceleration  $A$  is not equal to the peak acceleration response  $\ddot{u}_o^t$  even though both have the same units. Peak pseudo acceleration =  $\omega_n^2 D$ , where  $D = u_o$  is the peak displacement response of the structure at its top level and  $\ddot{u}_o^t \neq A = \omega_n^2 D$ .

### 3.6.9 Procedures for Strength-based Seismic Design

For a given column section design, the next steps are typically followed to determine the peak base shear  $V_{b_o}$  and check the validity of the given section:

- 1- Given the geometric properties for a generalized SDOF structure; moment of inertia  $I$ , elastic modulus  $E$ , moment arm  $y$  and structure's height  $h$ .
- 2- Determine the structural stiffness  $k$  for a generalized SDOF structure of an inverted pendulum fixed at base =  $\frac{3EI}{h^3}$ .

- 3- Determine the natural period for the structure  $T_n = \frac{2\pi}{\omega_n} = \frac{2\pi}{\sqrt{\frac{k}{m}}}$ .
- 4- Using  $T_n$  in the Elastic Design Spectrum, determine the Base Shear Coefficient  $\frac{A}{g}$ .
- 5- Determine the peak base shear  $V_{b_o} = \frac{A}{g} w$ , where,  $w$  is the total weight of the structure.
- 6- Find the peak base moment  $M_{b_o} = V_{b_o} \cdot h$  for the structure.
- 7- Find the axial stress on the structural section due to applied moment,  $\sigma_{axial} = \frac{M_{b_o} \cdot y}{I}$  and check its validity with the allowable stress  $\sigma_{allowable}$ . If  $\sigma_{axial} \geq \sigma_{allowable}$  the section should be revised.
- 8- Using  $T_n$  in the Elastic Design Spectrum Response curves, with  $\mu = 1$ , determine the peak displacement response of the structure at its top level,  $u_o = D$  and check its serviceability with the allowable lateral displacement. If  $u_o \geq u_{allowable}$  the section should be revised.

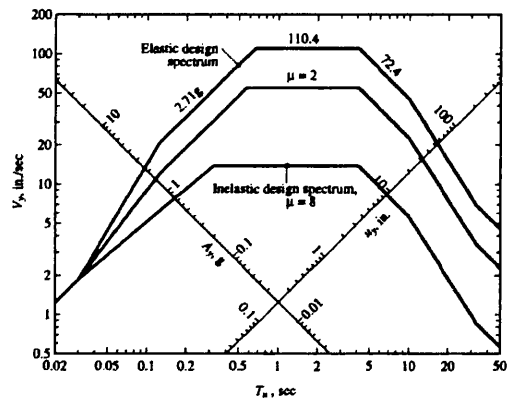
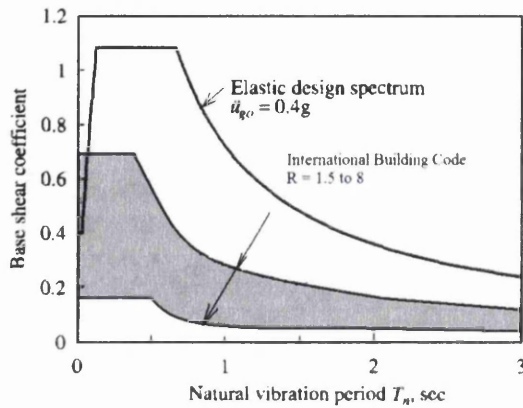


Figure 3.9 Elastic and Inelastic Design Spectra for ground motion record  $\ddot{u}_g(t)$  with  $\ddot{u}_{g_o} = 1g$ ,  $\dot{u}_{g_o} = 48 \frac{in}{s}$  and  $u_{g_o} = 36 in$ ;  $\mu = 1, 2$  and  $8$ ;  $\zeta = 5\%$ . [10]

### 3.6.10 Procedures for Ductility-based Seismic Design

In addition to strength based design, the capability of elastoplastic systems to resist earthquake loads is verified by Ductility-based seismic design, which is used to determine the initial stiffness  $k$  and yield strength of the structure  $f_y$  necessary to limit the maximum deformation  $u_m$  to an acceptable value. It should be noted that seismic codes introduce reduced base shear coefficients which are smaller than the elastic base shear coefficients that are associated with the strongest shaking that can occur at the site [10]. The 2000

*International Building Code* has a range of base shear coefficients reduced between  $R=1.5$  to 8 from the elastic design spectrum for ground motion record  $\ddot{u}_g(t)$  with  $\ddot{u}_{g_o} = 0.4g$ , as can be seen in Figure 3.10.



**Figure 3.10 Comparison of base shear coefficients from elastic design spectrum and International Building Code [10]**

Therefore, structures that are designed according to many building codes, such as the *International Building Code* exhibiting reduced base shear coefficients, must act beyond the limit of elastic behaviour when subjected to ground motion with  $\ddot{u}_{g_o} = 0.4g$ . Consequently, buildings are vulnerable to suffer damages when subjected to severe earthquake ground motions such as with peak ground acceleration PGA  $\ddot{u}_{g_o} = 0.4g$  due to their obliged elastoplastic behaviour, but the challenge is to design the structure with such controlled damage that is acceptable according to the Performance Based Seismic Evaluation PBSE. The goal of a performance-based seismic design is to maintain the building or structure within its safety and serviceability performance during and after the earthquake event.

For an unknown column section, the following steps represent the sequence of the flow chart in Figure 3.11, which shows seismic design procedures that could be followed in order to determine the initial stiffness  $k$  and yield strength of the structure  $f_y$  necessary to limit the maximum deformation  $u_m$  to an acceptable value. The procedures are divided into two parts; determining the seismic demand and the seismic capacity parameters, as follows:

- 1- The yield displacement  $u_y$  and maximum deformation response  $u_m$  are assumed so as to assume the ductility demand  $\mu$  for the structure.

- 2- From the combined D-V-A Inelastic Design Spectrum curves, with a variety of ductility factors, the natural period  $T_n$  can be determined and thus, the initial stiffness of the structure is estimated as  $k = \left(\frac{2\pi}{T_n}\right)^2 m$ .
- 3- By solving the stiffness equation, the yield strength of the structure  $f_y$  is obtained.
- 4- The seismic demand parameters of strength  $f_y$  and ductility  $\mu$  are validated by their correspondents from the seismic capacity parameters, in order to ensure the workability of the flexural and lateral strength of the designed section. If the demand is not less than the capacity, either a new ductility factor  $\mu$  is assumed or the section is revised.

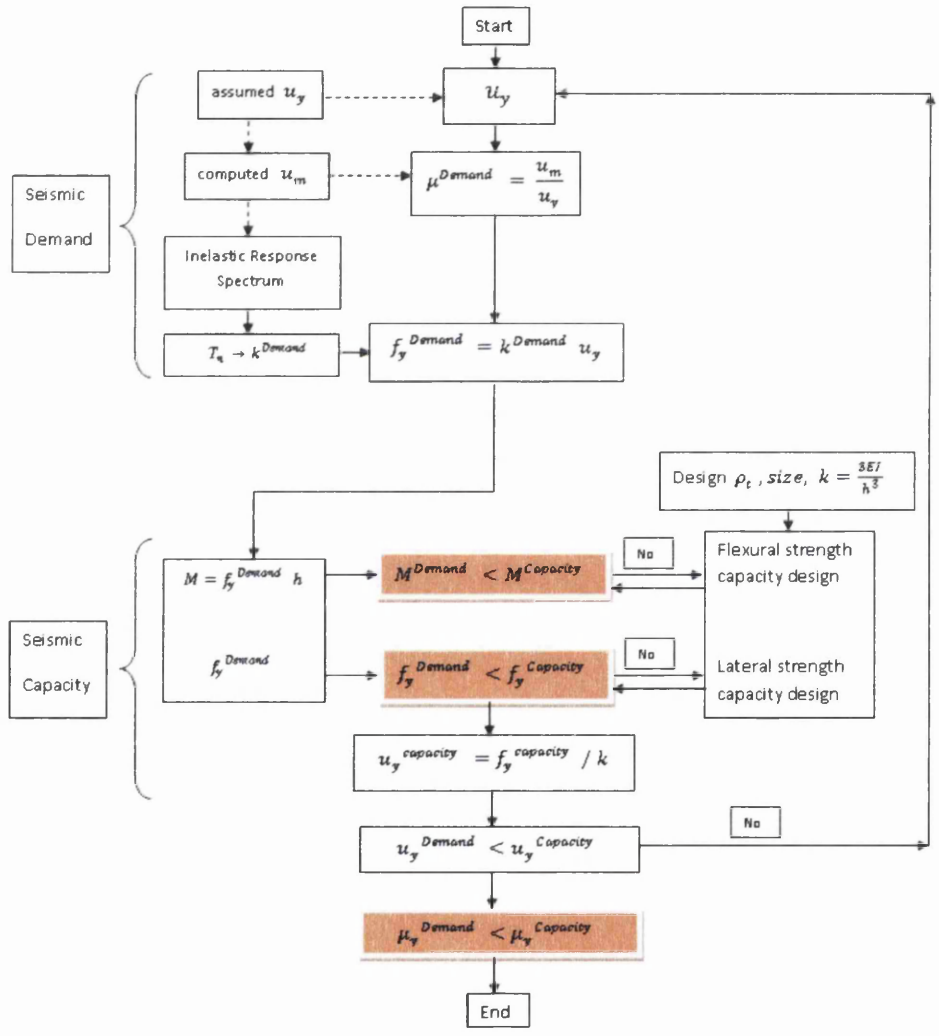


Figure 3.11 Flow chart of ductility-based seismic design for elastoplastic systems

# 3.7 FRACTURE

## 3.7.1 The Energy Balance Approach

The Griffith Theory is designed to explain the tensile fracture mode only, (or Mode I), and the two other modes of twisting and shear, as illustrated in Figure 3.12, are less dominant in brittle materials and will not be considered as a fracture-induced mechanism, but rather leading to failure, such as shear stresses exceeding the Mohr-Coulomb criterion [20].

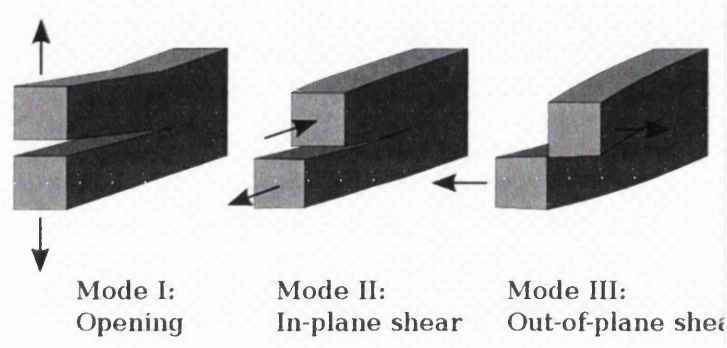


Figure 3.12 Types of fracture modes

Considering a 2D brittle material specimen with a unit thickness and width, that is *remotely* loaded by a tensile loading of  $\sigma$  and causing an initiation of a central crack with a very small crack length of  $2a$ , where  $2a \ll \text{width}$  [20], as in Figure 3.13.

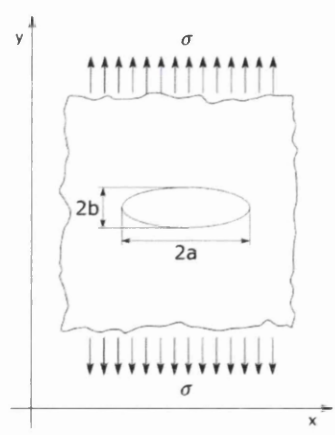


Figure 3.13 Central crack in an infinite plate due to a remote load  $\sigma$

When a crack starts to grow, the circular area around the crack is driven to have significantly low vertical stresses that will reach zero especially near the crack flanks. This stress drop



would decrease the stored elastic strain energy of the material in that region. The energy change (per unit volume) would be:

$$\frac{1}{2} \sigma \varepsilon = \frac{\sigma^2}{2E} \quad (3.54)$$

Since the circular area around the crack is the area with stress drop, the energy change for that cylindrical volume (or area multiplied by unit thickness  $t=1$ ) is:

$$(\pi a^2 \cdot t) \frac{\sigma^2}{2E} \rightarrow \frac{\pi \sigma^2 a^2}{2E}$$

This is only an approximation because the stress field becomes non-homogeneous near the crack. Therefore, (Griffith) used a stress analysis developed by (Inglis) to obtain a more accurate amount for the elastic energy change for an infinite plate:

$$U_a = -\frac{\pi \sigma^2 a^2}{E} \quad (3.55)$$

where  $U_a$  is the change in elastic strain energy (energy drop).

In order to have the crack extended, Griffith assumes that the elastic energy drop (elastic energy change)  $U_a$  should be larger than the tensile surface energy change  $U_\gamma$ , which acts in the opposite direction of the flanks opening process, and tends to close the crack flanks back to their non-cracking position. Thus;

$$U_\gamma = 4 a \cdot \gamma_e \quad (3.56)$$

Where,  $\gamma_e$  is the surface energy per unit area, (or surface tension), and  $4 a$  is the approximate area of the surface tension of the existing crack with a length of  $2a$ , i.e. total surface area is  $(2a + 2a)t = 4a$ .

The total energy  $U$  for a specimen with finite dimensions, loaded with a “fixed grip” condition and has its first crack initiated is:

$$U = U_o + U_a + U_\gamma - Work \quad (3.57)$$

where,  $U_o =$  (a constant value) total energy of specimen + its loading system, *before* the crack is introduced. *Work* = work performed by the loading system *during* the introduction

of the crack = load x displacement. Since the loading system on the specimen is a fixed grip type, it is defined as a constant displacement loading system. Since the elastic stresses at that region will drop due to the crack initiation, the work performed by the loading system, fixed grip, will also drop as no displacement would occur. Therefore,  $Work = 0$ . Substituting 3.55 and 3.56 into 3.57, the total load is [20]:

$$U = U_o - \frac{\pi \sigma^2 a^2}{E} + 4 a \cdot \gamma_e \quad (3.58)$$

### 3.7.2 A Crack Growth

A crack would grow if the total energy  $U$  decreases. Considering an increase in the crack length by  $d(2a)$ . Equation 3.58 can be differentiated with respect to  $(2a)$  to obtain the rate of decrement of the total energy as:

$$\frac{dU}{d(2a)} < 0 \quad (3.59)$$

The driving force for a crack extension exists due to the decrease in the elastic energy rate  $\left(\frac{dU_a}{d2a}\right)$  that counteracts the tension energy rate  $\left(\frac{dU_\gamma}{d2a}\right)$  of the crack surface. This is the principle of *Energy Balance*, which can also be illustrated in the Figure 3.14, when the slope of the total energy decreases, the crack will experience unstable crack propagation.

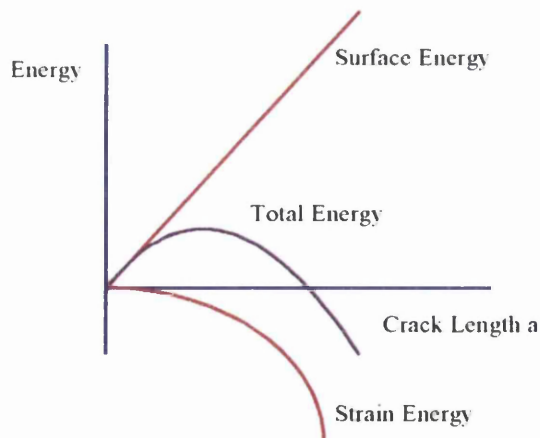


Figure 3.14 Energy Balance between Stable and Instable Crack Propagation [21]

This concept can be explained as follows. The total energy rate due to crack growth of  $d(2a)$ , i.e. slope of the curve, decreases such as:

$$\frac{dU}{d(2a)} = \frac{dU_a}{d(2a)} + \frac{dU_\gamma}{d(2a)} < 0 \quad (3.60)$$

Since  $U_o$  is constant,  $\frac{dU}{d(2a)}$  is zero, and by substituting for the other terms we obtain:

$$\begin{aligned} \frac{d}{d(2a)} \left( -\frac{\pi \sigma^2 a^2}{E} + 4 a \cdot \gamma_e \right) < 0 \quad \text{or,} \\ \frac{\pi \sigma^2 a}{E} > 2 \gamma_e \end{aligned} \quad (3.61)$$

This implies that a crack growth occurs when:

The rate of fracture energy (energy release rate  $G$ )  $> 2$  (surface energy per unit area, i.e. surface tension  $\gamma_e$ ).

Irwin designated the left hand side of equation (3.61) as the energy release rate  $G$ , representing the energy per unit *new* crack area *available* for the crack extension. The right hand side represents the crack resistance  $R_s$ , representing the surface energy increase per unit *new* crack area that is *required* to allow for an extension. Therefore, a crack will extend when the *available* energy rate is *greater than* the *required* energy rate. If  $R_s$  is constant, then  $G$  should be larger than some critical value  $G_c$  which is equal to  $R_s$ , i.e.  $G > G_c = R_s$

Equation (3.61) can be re-written as:

$$\sigma \sqrt{a} > \sqrt{\frac{2 E \cdot \gamma_e}{\pi}} \quad (3.62)$$

$\sqrt{\frac{2 E \cdot \gamma_e}{\pi}}$  is purely material properties which has a constant value that should be violated by  $\sigma \sqrt{a}$  to allow for a crack growth extension.

### 3.8 REFERENCES

- [1] S. P. Timoshenko, J. N. Goodier. Theory of Elasticity, 3rd edition, McGraw-Hill 1970.
- [2] D. R. Owen. Lecture notes on structural Mechanics. College of Engineering, Swansea University, 2010.
- [3] H. O. Kirchner, M. A. Meyers, R. W. Armstrong. Mechanics and Materials: Fundamentals and Linkage. New York ; Chichester: Wiley, 1999.
- [4] A. C. Ugural, S. K. Fenster. Advanced strength and applied elasticity. Third edition, Prentice-Hall, Inc. 1995.
- [5] G. Eason, R. W. Ogden, Elasticity Mathematical Methods and Applications, Ellis Horwood Publishers, 1990.
- [6] A. P. Boresi, O.M. Sidebottom. Advanced mechanics of materials. Fourth edition, John Wiley and Sons, Inc., 1985.
- [7] W. F. Chen, A. F. Saleeb. Constitutive Equations for Engineering Materials. John Wiley & Sons. Inc., 1982.
- [8] E. S. Neto, D. Perić, D. Owens, Computational methods for plasticity: theory and applications. 2008, Chichester: Wiley.
- [9] I. M. Smith, D. V. Griffith. Programming the finite element method. Second edition, John Wiley & Sons Ltd., 1988
- [10] A. K. Chopra, Dynamics of Structures, Pearson Education, Inc., third edition, 2007.
- [11] R. W. Clough, J. Penzien. Dynamics of structures. McGraw-Hill, Inc., international edition, 1993.
- [12] N. M. Newmark, E. Rosenblueth. Fundamentals of Earthquake Engineering. Englewood Cliffs, N.J.: Prentice-Hall, 1971.
- [13] Y. Feng. Lecture notes on Dynamics of Structures. College of Engineering, Swansea University, 2009.
- [14] N. Alexander. Structural Dynamics for Seismic Problems, ICE Earthquake Seminar, University of Bristol, March 2010
- [15] A. H. Barbat, J. M. Canet. Structural Response Computations in Earthquake Engineering. Swansea: Pineridge Press, 1989.
- [16] A. J. Kappos. Dynamic loading and design structures. Spon press, 2002.
- [17] D. Halliday, R. Resnick, J. Walker. Fundamentals of physics. 5th edition, John Wiley & Sons, Inc., 1977.

- [18] M. Geradin, D. Rixen. Mechanical vibrations: Theory and application to structural dynamics. 2ed edition, John Wiley & Sons Ltd., 1997.
- [19] C. F. Gerald, P.O. Wheatley. Applied Numerical Analysis. 3rd ed. Reading, Mass.: Addison-Wesley Publishing Co., 1984.
- [20] M. Janssen, J. Zuidema, R. Wanhill. Fracture mechanics. 2ed edition, Spon press, 2004.
- [21] Lecture notes on Fracture mechanics.

# Chapter 4

---

## Fibre Element Method for Dynamic Non-Linear Problems

---

### Contents

- 4.0 INTRODUCTION ..... 107
- 4.1 NUMERICAL-INTEGRATION SOLUTIONS FOR DYNAMIC PROBLEMS ..... 108
  - 4.1.1 Newmark Method for Linear Systems ..... 108
  - 4.1.2 Newmark Method for Non-Linear Systems ..... 109
- 4.2 THE FIBRE ELEMENT METHOD FOR SOLVING NON-LINEAR DYNAMIC ANALYSIS ..... 110
  - 4.2.1 Initiation of the Hysteresis and Employment of the Built-in Hysteresis in the Fibre Element Method ..... 110
  - 4.2.2 Fibre/Beam-Column Elements with Two Nodes ..... 111
  - 4.2.3 The Stiffness Matrix of the Two-dimensional Fibre Element ..... 112
  - 4.2.4 Envelope Curves of Concrete Stress-strain Model ..... 113
  - 4.2.5 Simplified Concrete Stress-strain Envelop ..... 114
  - 4.2.6 Simplified Constitutive Un-loading and Re-loading Paths for Concrete ..... 115
  - 4.2.7 Simplified Constitutive Un-loading and Re-loading Paths for Steel Rebars ..... 116

- 4.2.8 Algorithm and Flow Chart ..... 117
- 4.2.9 Flow Chart for the Code Algorithm ..... 119
  - 4.2.9.1 Damage ..... 120
  - 4.2.9.2 Programming Issues ..... 120
- 4.3 THE PROPOSED PROBLEM ..... 121
  - 4.3.1 The Structure Model ..... 122
    - 4.3.1.1 Assumptions of the Fibre Element Model in the MatLab Code ..... 123
  - 4.3.2 Results and Discussion ..... 125
    - 4.3.2.1 The Number of Elements and the Number of Fibres ..... 128
    - 4.3.2.2 Differences Between the MatLab code and the SeismoStruct Model ..... 130
    - 4.3.2.3 Diagram Representations of Results for all Elements at all Times, and for all Fibres at all Times ..... 131
    - 4.3.2.4 Stiffness matrix effect on the hysteresis curve of quasi-brittle material ..... 132
- 4.4 CONCLUSIONS ..... 134
- 4.5 REFERENCES ..... 135

## 4.0 INTRODUCTION

The analytical exact solution for the Equation of Motion can be determined usually for periodically loaded problems of linear systems. However, such solutions are not possible in cases of arbitrarily time-varying excitation forces such as ground acceleration  $\ddot{u}_g$ , or if the system is non-linear. Therefore, only numerical time-stepping methods for integrating the differential equation of motion are applicable, giving approximate solutions. The numerical solution of such a differential equation requires the equation to be represented in an incremental procedure [1].

Numerical time-stepping methods apply the time interval  $\Delta t_i = t_{i+1} - t_i$  as a constant value. The response of a structure is to be known at a discrete time instant  $t_i$  as  $u_i, \dot{u}_i$  and  $\ddot{u}_i$ , which are satisfying the elastic system governed by this equation of motion at time  $t_i$ :

$$m \ddot{u}_i + c \dot{u}_i + (f_s)_i = p_i \quad (4.1)$$

where,  $(f_s)_i$  is the resisting elastic force that equals  $k u_i$  at time  $t_i$  for a linearly elastic system. However, for an inelastic system the resisting force is  $(f_s(u, \dot{u}))_i$  which depends on the prior history of displacement and on the velocity.

The system is assumed to have linear viscous damping coefficient  $c$  which is determined approximately, since the exact damping value is still lacking information and needs to be approximated to predict the magnitude of energy absorption that's associated with the damping effect, especially at large amplitudes of motion [2].

By using the time-stepping procedure, the response of the structure  $u_{i+1}, \dot{u}_{i+1}$  and  $\ddot{u}_{i+1}$ , at time  $t_{i+1}$  are to be determined by satisfying the equation of motion as follows:

$$m \ddot{u}_{i+1} + c \dot{u}_{i+1} + (f_s)_{i+1} = p_{i+1} \quad (4.2)$$

If the equation of motion at time  $t_i$  is subtracted from this equation, the incremental equation of motion is obtained as:

$$m \Delta \ddot{u}_i + c \Delta \dot{u}_i + (\Delta f_s)_i = \Delta p_i \quad (4.3)$$

It should be known that stepping the equation from time  $t_i$  to time  $t_{i+1}$  is an approximate procedure that needs the conditions of convergence, stability and accuracy to be successful. Convergence imposes approaching towards the exact solution as the time-step decreases. Stability means that the solution should be stable in the presence of numerical round-off errors. Accuracy is how close the approximate solution is to the exact solution [2].



## 4.1 NUMERICAL-INTEGRATION SOLUTIONS FOR DYNAMIC PROBLEMS

There are different types of time-stepping procedures. Generally, they are:

- Procedures based on interpolation of the excitation function.
- Procedures based on finite difference of velocity and acceleration.
- Procedures based on assumed variation of acceleration, which is known as Newmark Method. These procedures have two kinds; the Linear Acceleration Method and the Average Acceleration Method. The following section will consider a time-stepping procedure based on the Average Acceleration Method since it is numerically stable under any time interval [2]. This method is applied in this chapter to solve the proposed example numerically.

### 4.1.1 Newmark Method for Linear Systems

Newmark (1959) developed a time-stepping method based on the integration of an approximated acceleration value  $\ddot{u}(\zeta)$  at time  $\zeta$  between time  $t_i$  and  $t_{i+1}$ . The integration produced the following approximate *Recurrence Equations* for velocity and displacements at time  $t_{i+1}$  :

$$\dot{u}_{i+1} = \dot{u}_i + [(1 - \gamma)\Delta t] \ddot{u}_i + \gamma\Delta t \ddot{u}_{i+1} \quad (4.4.a)$$

$$u_{i+1} = u_i + \Delta t\dot{u}_i + [(0.5 - \beta)(\Delta t)^2]\ddot{u}_i + [\beta(\Delta t)^2]\ddot{u}_{i+1} \quad (4.4.b)$$

Where, the parameters  $\gamma$  and  $\beta$  determine the type of approximation for the acceleration over a time step. The parameters  $\gamma = \frac{1}{2}, \beta = \frac{1}{4}$  are for average acceleration and  $\gamma = \frac{1}{2}, \beta = \frac{1}{6}$  are for linear acceleration, and they determine the stability and accuracy of the method. It is important to know that the average acceleration method is stable for any  $\Delta t$ , even if it is relatively large. However, the solution will be accurate only if  $\Delta t$  is small enough [2]

By introducing an incremental form such as  $\Delta u_i = u_{i+1} - u_i$  for all of the time-dependant parameters  $u_i, \dot{u}_i, \ddot{u}_i$  and  $p_i$ , the *Recurrence Equations* are re-written as follows:

$$\Delta\ddot{u}_i = \frac{1}{\beta(\Delta t)^2} \Delta u_i - \frac{1}{\beta\Delta t} \dot{u}_i - \frac{1}{2\beta} \ddot{u}_i \quad (4.5.a)$$

$$\Delta\dot{u}_i = \frac{\gamma}{\beta\Delta t} \Delta u_i - \frac{\gamma}{\beta} \dot{u}_i + \Delta t \left(1 - \frac{\gamma}{2\beta}\right) \ddot{u}_i \quad (4.5.b)$$

Which are substituted into the incremental equation of motion;  $\Delta\ddot{u}_i + c \Delta\dot{u}_i + k \Delta u_i = \Delta p_i$ , where,  $(\Delta f_s)_i = k \Delta u_i$ . This will produce a relationship that contains the incremental

displacement  $\Delta u_i$ , and is considered as the *key equation*, that is, implicitly, solved at each time step in Newmark's Method. This *key equation* is:

$$\hat{k} \Delta u_i = \Delta \hat{p}_i \quad (4.6)$$

where,  $\hat{k} = k + \frac{\gamma}{\beta \Delta t} c + \frac{1}{\beta (\Delta t)^2} m$  which is constant in the elastic system analysis, and

$$\Delta \hat{p}_i = \Delta p_i + \left( \frac{1}{\beta \Delta t} m + \frac{\gamma}{\beta} c \right) \dot{u}_i + \left[ \frac{1}{2\beta} m + \Delta t \left( \frac{\gamma}{2\beta} - 1 \right) c \right] \ddot{u}_i .$$

Therefore, the solution is then found by adding the incremental displacement  $\Delta u_i$  to the solution of the previous step as follows:

$$u_{i+1} = u_i + \Delta u_i \quad (4.7.a)$$

By substituting the incremental velocity and acceleration at each time step  $i$ , the rest of the solution is similarly found as:

$$\dot{u}_{i+1} = \dot{u}_i + \Delta \dot{u}_i \quad (4.7.b)$$

$$\ddot{u}_{i+1} = \ddot{u}_i + \Delta \ddot{u}_i \quad (4.7.c)$$

#### 4.1.2 Newmark Method for Non-Linear Systems

The previous solution can be extended to be applicable to a non-linear response by modifying the incremental resisting force  $(\Delta f_s)_i$  to become a function of the incremental displacement, using a time-varying variable as follows:

$$(\Delta f_s)_i \cong (k_i)_t \Delta u_i \quad (4.8)$$

where,  $(k_i)_t$  is the tangential stiffness at time-step  $i$ , which is changing at each time-step. However, the incremental displacement must first be calculated from the *key equation*, which is also re-written as:

$$(\hat{k}_i)_t \Delta u_i = \Delta \hat{p}_i \quad (4.6')$$

and consequently,  $(\hat{k}_i)_t = (k_i)_t + \frac{\gamma}{\beta \Delta t} c + \frac{1}{\beta (\Delta t)^2} m$ .

The resulting errors in the approximate incremental resisting force  $(\Delta f_s)_i$  are due to the linearity of the tangential stiffness, which is assumed to be approximate to the secant stiffness as follows:

$$(k_i)_t \cong (k_i)_s \quad (4.9)$$

where, the secant stiffness  $(k_i)_s$  is assumed as the exact representation of the element stiffness. This assumption introduces numerical errors, which can be minimized by reducing the time-step interval  $\Delta t_i = t_{i+1} - t_i$  to a relatively small value. This technique is quite useful and easy to consider, it can be used to solve non-linear problems with very small errors.

However, these errors can also be minimized by using an iterative procedure in which the key equation is iterated a number of times within every time interval  $\Delta t_i$ , until convergence is reached by some tolerance value. This can be processed by using the technique of Newton-Raphson or modified Newton-Raphson iterative methods. However, no iterative procedure has been adopted in the proposed computer code of this problem, but rather reducing the time-step interval  $\Delta t_i = t_{i+1} - t_i$  to a relatively small value, to minimize the expected errors.

## **4.2 THE FIBRE ELEMENT METHOD FOR SOLVING NON-LINEAR DYNAMIC ANALYSIS**

The response of reinforced concrete columns under dynamic loading can be predicted numerically by using the fibre element models. The linear and non-linear responses such as force versus displacement hysteresis and time history are determined.

A fibre element is a beam element that consists of a number of 'fibres'. Each of the fibres is assigned a uni-axial constitutive model corresponding to the material it represents. The fibres are grouped in an element section and the fibres' properties are summed together to form the stiffness matrix of the element. It is significantly practical to use fibres in order to model the reinforcement bars of different diameters within the reinforced concrete section. Fibre modelling is also useful to represent the degradation of stiffness of the section during the non-linear process. Gradual degradation of the element stiffness is a consequence of failure of those fibres that reached the ultimate axial strength. It is therefore, possible to examine the failed concrete or steel fibres at any stage of loading and obtain useful conclusions for the analysed structure. Many researchers adopt fibre element analysis in non-linear dynamic problems especially for the analysis of reinforced sections.

### **4.2.1 Initiation of the Hysteresis and Employment of the Built-in Hysteresis in the Fibre Element Method**

The Difference between non-linear analysis with a pre-defined hysteretic rule and the non-linear analysis with fibrous elements is that, in fibrous elements the stiffness depends on the state of the computed elastic modulus  $E$ , which depends on the stress-strain state at each time-step and the axial stress-strain behaviour depends on the given material model. While, in a non-linear analysis with a pre-defined hysteretic rule, the stiffness alternates according to

a given load-displacement (hysteresis) curve, that's extracted from the hysteresis theory. The hysteresis can also be extracted from experimental data of a SDOF inelastic system. In this case, the stiffness response is not calculated, but simulated according to a previous model, which may differ in the hysteretic behaviour from the analysed problem.

#### 4.2.2 Fibre/Beam-Column Elements with Two Nodes

The applied two-dimensional fibre element has two nodes at its ends, with a total of 6 degrees of freedom DOF. The non-linearity of the element is assumed in the middle cross section of the element, as shown in Figure 4.1.a and 4.1.b.

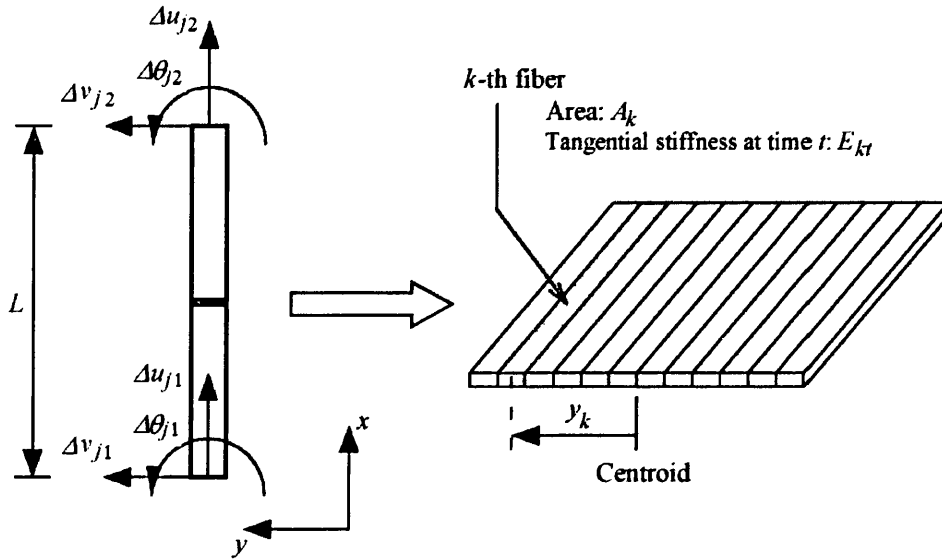


Figure 4.1.a) Two-dimensional fibre element. b) Fibre section of the element.

The incremental axial strain at the centroid of the element  $\Delta\varepsilon_a$  and incremental curvature  $\Delta\phi$  of an element between time  $t$  and  $t + \Delta t$  are as follows:

$$\Delta\varepsilon_a = \frac{\Delta u_{j2} - \Delta u_{j1}}{L} \quad (4.10)$$

$$\Delta\phi = \frac{\Delta\theta_{j2} - \Delta\theta_{j1}}{L} \quad (4.11)$$

where  $L$  is the element length,  $\Delta u_{j1}$  and  $\Delta u_{j2}$  are the incremental nodal axial displacements at joints  $j1$  and  $j2$ , respectively, and  $\Delta\theta_{j1}$  and  $\Delta\theta_{j2}$  are the incremental nodal rotations at joints  $j1$  and  $j2$ , respectively.

By employing the assumption of plane sections remaining plane after deformation, the axial strains in all fibres of the section are linearly proportional as shown in Figure 4.2. The incremental axial strains of the  $k$ -th fibre is the difference between the incremental axial strains due to axial force and the incremental axial strains due to bending moment. This can be obtained as follows:

$$\Delta\varepsilon_k = \Delta\varepsilon_a - y_k \cdot \Delta\phi \quad (4.12)$$

where,  $y_k$  is the distance from the element centroid to the  $k^{\text{th}}$  fibre. It is assumed that  $\Delta\phi = \sin \Delta\phi$  having the condition that  $\Delta\phi$  is very small and must be in radians. The value of  $\Delta\phi$  is very small for such problems, but if  $\Delta\phi$  is in degrees, it must be substituted with  $\sin \Delta\phi$  in the previous equation.

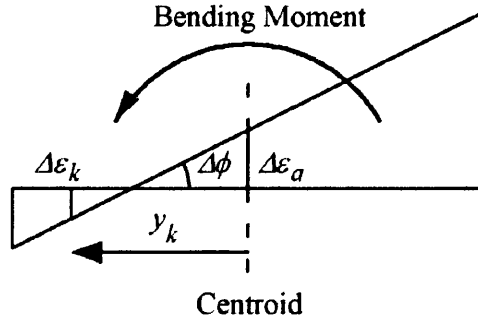


Figure 4.2 Diagram of incremental axial strain of the  $k^{\text{th}}$  fibre.

### 4.2.3 The Stiffness Matrix of the Two-dimensional Fibre Element

The stiffness of the fibre element defines the function between the applied forces and corresponding displacement and rotation responses. For a 6 DOF element with nodal freedoms  $\{n1, n2, n3, n4, n5, n6\}$ , the stiffness matrix defines the function between the following couples:

- The incremental axial force  $\Delta N_j$  and the nodal incremental vertical displacement  $\Delta u_j$ ,
- The incremental nodal lateral force  $\Delta Q_j$  and the incremental nodal lateral displacement  $\Delta v_j$ , and
- The incremental bending moment  $\Delta M_j$  and the incremental nodal curvature  $\Delta\theta_j$ .

The forces-displacements relationship for the element can be written in a matrix form as:

$$\{\Delta f\} = [k_t] \{\Delta u\} \quad (4.13)$$

where,  $k_t$  is the tangential stiffness for the element,  $\Delta f$  is the incremental nodal forces and  $\Delta u$  is incremental nodal responses, or

$$\{\Delta f\} = \{\Delta N_{j1}, \Delta Q_{j1}, \Delta M_{j1}, \Delta N_{j2}, \Delta Q_{j2}, \Delta M_{j2}\}^T \quad (4.14)$$

$$\{\Delta u\} = \{\Delta u_{j1}, \Delta v_{j1}, \Delta\theta_{j1}, \Delta u_{j2}, \Delta v_{j2}, \Delta\theta_{j2}\}^T \quad (4.15)$$

The stiffness matrix is derived from the force-stress and the moment-stress relations. By substituting equation 4.12 into these relations the following is obtained:

$$\Delta N = \int \Delta \sigma dA = \sum_{n=1}^k (\Delta \varepsilon_k E_k A_k) = EA_t^* \Delta \varepsilon_c - EG_t^* \Delta \phi \quad (4.16)$$

$$\Delta M = - \int \Delta \sigma .y. dA = - \sum_{n=1}^k (\Delta \varepsilon_k E_k A_k y_k) = -EG_t^* \Delta \varepsilon_c + EI_t^* \Delta \phi \quad (4.17)$$

Where,

$$EA_t^* = \sum_{n=1}^k (E_k A_k) \quad (4.18)$$

$$EG_t^* = \sum_{n=1}^k (E_k A_k y_k) \quad (4.19)$$

$$EI_t^* = \sum_{n=1}^k (E_k A_k y_k^2) \quad (4.20)$$

are the parameters of the stiffness matrix. Where,  $E_k$  is the elastic modulus of the  $k^{th}$  fibre material, and  $A_k$  is the cross section area of the k-th fibre. Using these relations and using polynomial formulae for the assumed deformed shape of the element in  $u$  and  $v$ , the stiffness matrix of the two-dimensional fibre element with 6 DOF's  $[k_t]$  can be expressed as:

$$\begin{bmatrix} \frac{EA_t^*}{L} & 0 & -\frac{EG_t^*}{L} & -\frac{EA_t^*}{L} & 0 & \frac{EG_t^*}{L} \\ 0 & \frac{12EI_t^*}{L^3} & \frac{6EI_t^*}{L^2} & 0 & -\frac{12EI_t^*}{L^3} & \frac{6EI_t^*}{L^2} \\ -\frac{EG_t^*}{L} & \frac{6EI_t^*}{L^2} & \frac{4EI_t^*}{L} & \frac{EG_t^*}{L} & -\frac{6EI_t^*}{L^2} & \frac{2EI_t^*}{L} \\ -\frac{EA_t^*}{L} & 0 & \frac{EG_t^*}{L} & \frac{EA_t^*}{L} & 0 & -\frac{EG_t^*}{L} \\ 0 & -\frac{12EI_t^*}{L^3} & -\frac{6EI_t^*}{L^2} & 0 & \frac{12EI_t^*}{L^3} & -\frac{6EI_t^*}{L^2} \\ \frac{EG_t^*}{L} & \frac{6EI_t^*}{L^2} & \frac{2EI_t^*}{L} & -\frac{EG_t^*}{L} & -\frac{6EI_t^*}{L^2} & \frac{4EI_t^*}{L} \end{bmatrix}$$

#### 4.2.4 Envelope Curves of Concrete Stress-strain Model

It should be noted that the equations for the constitutive model described by Sakai & Mahin [3] represent comprehensive formulae for linear and all probable non-linear stress-strain paths. They describe 7 paths in the compressive field, and they are listed as follows:

- elastic stress-strain path,
- idealized unloading path,
- unloading path from re-loading path,
- re-loading path from zero stress, Figure 4.3.a,
- re-loading path from un-loading path, Figure 4.3.b,
- post un-loading from envelope curve and
- post un-loading from re-loading path.

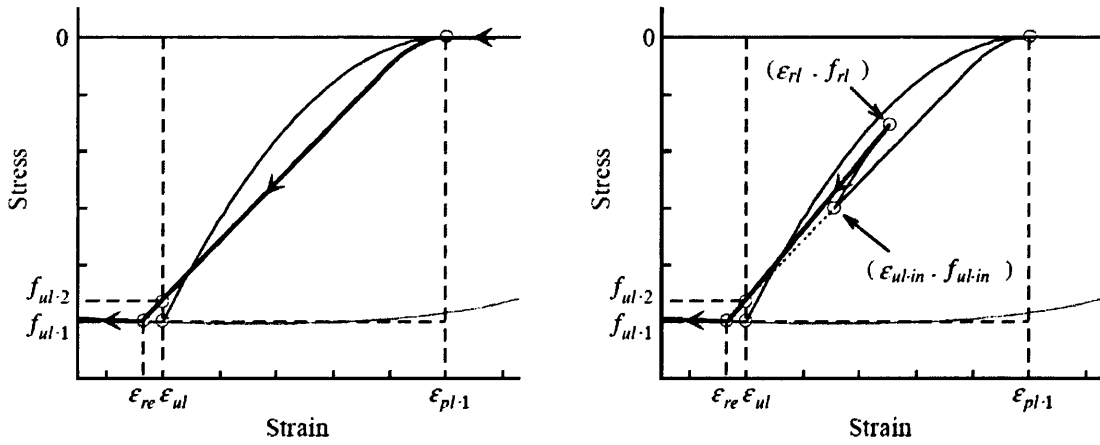


Figure 4.3.a and 4.3.b Idealized re-loading paths [3]

Such lengthy detailed formulae can estimate the expected non-linear behaviour more approximately, but they need longer computer programming sections than the scope of this chapter. However, a more simplified loading, un-loading and re-loading path of the stress-strain relationship has been used, in order to bring the calculations to an acceptable standard, and then, determine the level of approximation that can be reached.

**Assumptions:**

There are two important assumptions that have been made in the proposed computer code so as to determine the level of acceptable approximation that's required to solve the dynamic non-linear problem. They are:

1. No iterative procedure has been adopted in the proposed computer code of this problem, but rather reducing the time-step interval  $\Delta t_i = t_{i+1} - t_i$  to a relatively small value, 0.01 seconds, in order to minimize the expected errors made due to the assumption of adopting the tangential stiffness as equal to the secant stiffness, or  $(k_i)_t \cong (k_i)_s$ , as previously discussed.
2. A more simplified formula for the probable non-linear stress-strain paths has been adopted, which is more suitable to the proposed computer code.

**4.2.5 Simplified Concrete Stress-strain Envelop**

The adopted simplified envelopes of the constitutive law for the concrete column are based on the idealized linear stress-strain curve of the concrete core and the concrete cover of the column. The shown Figure 4.4 will have the stress-strain curve envelop in the non-linear strains, where  $\epsilon_i < \epsilon_{cc}$  for confined concrete core, and  $\epsilon_i < \epsilon_{sp}$  for un-confined concrete cover. However, the numbers in the figure were changed to suit the proposed problem. At

time-step  $i$ , elastic stresses are obtained from Hook's law, and the stress envelop is obtained from the following formulae, as a function of strain:

For concrete cover:  $\sigma_i = -7.00E09 \varepsilon_i - 5.6E07$

For concrete core:  $\sigma_i = -11.5E09 \varepsilon_i - 5.75E07$

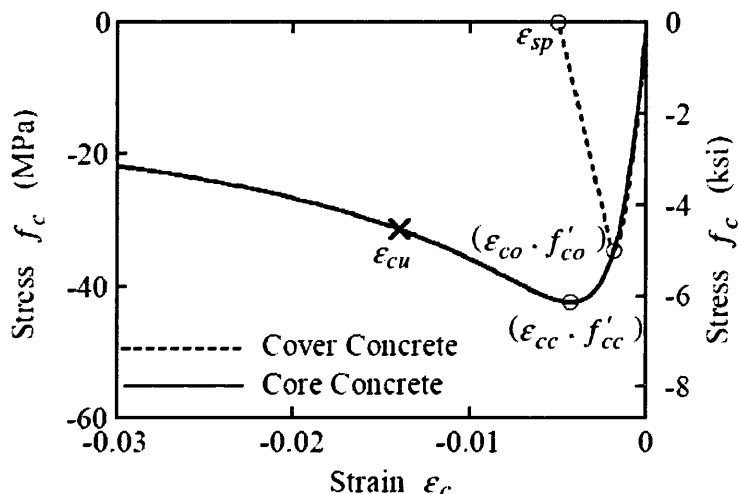


Figure 4.4 Envelope curves of concrete stress-strain model [3]

**Confinement:**

The confinement of a concrete core section increases its ultimate strength according to two main factors; firstly, the transverse reinforcement properties; yield strength, cross section area and spacing, secondly, the axial stress on the column section. However, confinement is not effective when the axial stress is relatively low, less than 10% of the column compressive strength [4]. In general, confinement increases as more axial forces are applied on the column. In the proposed problem less than 3% of the column compressive strength is applied as axial stresses, and thus very low confinement is activated by the transverse reinforcement on the core section. Thus, the stress envelop is obtained from the following formula:

For concrete core:  $\sigma_i = -11.5E09 \varepsilon_i - 5.75E07$ .

**4.2.6 Simplified Constitutive Un-loading and Re-loading Paths for Concrete**

For every time-step  $i$  strain is produced to fall into one of 5 parts of the simplified constitutive curve to define its corresponding stress. For concrete modelling, the 5 parts are:

1. **Tension strains part:** In this range stresses are ignored and set equal to zero.
2. **Linear Loading, Un-Loading and Re-Loading part:** In this range of strains the behaviour is considered linear as long as they lie between two determined boundary



values of strains; lower and upper strain limits. The lower-limit strain value corresponds to a stress value on the envelope, and the upper-limit strain value corresponds to a zero-stress value. These two strain values are updated in the code at each new lower strain exceeding the previous lower-limit on the softening envelope. They are also updated at each time a new higher strain exceeds the upper-limit on the zero-stress line. Therefore, these two limits should be previously updated for the 3rd or 4th parts for the current iteration.

It should be noted that this part is idealized differently by researchers to obtain the path functions in the un-loading and re-loading processes, such as Sakai & Mahin [3] who developed parabolic stress-strain paths for the unloading process and linear paths for the re-loading process. In this model, both unloading and reloading paths are considered linear, with a slope parallel to the concrete linear elastic stiffness. Such approximation is adopted to reduce the size and complexity of calculations, since paths with parabolic functions are very close to the linear behaviour.

### **3. Envelope stresses with softening strains (strains below the lower-limit):**

These softening points lie on the softening envelope, and they are updated at each time-step. Confined concrete fibres have a different softening envelope from that of the unconfined fibres, which are in the column outer cover and are more vulnerable to dissipate energy than the concrete in the column core.

### **4. Unloading and reloading beyond the zero stresses (strains above the upper-limit):**

If the concrete model is unloaded to reach strains beyond the zero-stress point, i.e. strains exceeding the upper-limit and re-loaded again, a new linear path with new upper and lower limits is updated. Such a path is followed for the re-loading and un-loading processes as far as limits are not exceeded.

### **5. Crushing strains:**

Once the fibres are strained to a crushing value of the concrete, -0.008, all successive points will have a zero-stress value, since fibres are considered fully fractured and have absorbed energy equal to their fracture energy.

## **4.2.7 Simplified Constitutive Un-loading and Re-loading Paths for Steel Rebars**

The adopted stress-strain constitutive Model for Steel Rebars is also simplified by considering idealized linear loading, un-loading and re-loading paths, in addition to considering zero-slope envelope at the ultimate strength of the steel material. However, more

complex paths are adopted by researchers for these path functions for steel, such as the one adopted by Sakai & Mahin [3] who modified a stress-strain model based on Mongetto & Pinto model and Sakai & Kawashima model.

A steel fibre strain is introduced to fall into one of 3 parts of the simplified constitutive curve to define its corresponding stress. For the steel rebars modelling, the 3 parts are:

1. **Tension strains part:** In this range, stresses are either linear which follow the linear stress-strain relation of uni-axial loading, or non-linear, with strains exceeding the tensile yield stress value of steel.
2. **Compressive loading part:** In this range stresses are either linear which follow the linear stress-strain relation of uni-axial compressive loading, or non-linear, with strains exceeding the compressive yield stress value of steel.

**3. Un-loading and Re-loading part:**

This range falls between the tensile and compressive yield stresses. All constitutive points within this range follow a linear path in this model. The linear path is taken as parallel to the initial elastic stiffness rate of the steel. All un-loading and re-loading points behave linearly as far as they do not exceed the upper or lower limits of the strains.

#### 4.2.8 Algorithm and Flow Chart

In addition to the previous explanation of Newmark's method, fibre element modelling for non-linear dynamic analysis and the simplified constitutive modelling of envelop curves for concrete and steel, the following explanation is concerned with the code algorithm that has been built using MatLab programming to solve and analyse a nonlinear RC column problem under dynamic loading. Appendix [A] shows a complete list of the written code.

In general, the code follows the major steps given by Chopra [2], which are listed below with an important explanation of the necessary steps required for the iteration loops, fibre loops and formation of the global matrices. They are three major steps as follows:

- 1.0** Given are the initial conditions:  $p_o$ ,  $f_{s_o}$ ,  $\dot{u}_o$  which are the initial load, initial restoring forces and initial velocities respectively. The initial accelerations are then calculated as:

$$\ddot{u}_o = \frac{p_o - c \cdot \dot{u}_o - f_{s_o}}{m}$$

Where  $c$  and  $m$  are the damping and mass matrices for one element.

- 2.0** For all time-steps iteration, beginning from  $i=1$  to the end, with time-step  $\Delta t$ :

- 2.1** Obtain the local and global grand load increment  $\Delta \hat{p}_i$  as

$$\Delta \hat{\mathbf{p}}_i = \Delta \mathbf{p}_i + a \cdot \dot{\mathbf{u}}_i + b \cdot \ddot{\mathbf{u}}_i$$

$$\Delta \hat{\mathbf{p}}_i = \Delta \mathbf{p}_i + a \cdot \dot{\mathbf{u}}_i + b \cdot \ddot{\mathbf{u}}_i$$

where,  $a = \frac{1}{\beta \Delta t} m + \frac{\gamma}{\beta} c$  and  $b = \frac{1}{2\beta} m + \Delta t \left( \frac{\gamma}{2\beta} - 1 \right) c$

**2.2** Obtain the global stiffness matrix  $\mathbf{k}_i$  from the previous time step.

**2.3** Obtain the global grand stiffness matrix as follows:

$$\hat{\mathbf{k}}_i = \mathbf{k}_i + \frac{\gamma}{\beta \cdot \Delta t} \cdot \mathbf{c} + \frac{1}{\beta \cdot \Delta t^2} \cdot \mathbf{m}$$

$\hat{\mathbf{k}}_i$  needs to be reduced into  $\hat{\mathbf{k}}_i^r$  by deleting terms of boundaries constraints in order to avoid singularity when inverted in the next step 2.4.

**2.4** Solve the key equation for the global displacement increment  $\Delta \mathbf{u}_i$  for the whole structure as follows:

$$\Delta \mathbf{u}_i = \left[ \hat{\mathbf{k}}_i^r \right]^{-1} \cdot \Delta \hat{\mathbf{p}}_i^r$$

Start of fibre-level loop. Obtain the global stiffness matrix and the global displacements for the next time-step iteration, from 2.4.a) to 2.4.c) :

**2.4.a)** Obtain the strain increment of this iteration  $(\Delta \varepsilon_k)_i$  for each fibre in the element as:

$$(\Delta \varepsilon_k)_i = (\Delta \varepsilon_a - y_k \cdot \Delta \phi)_i$$

where,  $(\Delta \varepsilon_a)_i = \frac{(\Delta u_{j2} - \Delta u_{j1})_i}{L}$  ,  $(\Delta \phi)_i = \frac{(\Delta \theta_{j2} - \Delta \theta_{j1})_i}{L}$  and ,  $y_k$  is the distance from the element centroid to the k-th fibre.

Where  $L$  is the element length.  $\Delta u_{j2}$  and  $\Delta u_{j1}$  are the incremental nodal displacements at the nodal freedoms n4 and n1, respectively.  $\Delta \theta_{j2}$  and  $\Delta \theta_{j1}$  are the incremental nodal rotations at the nodal freedoms n6 and n3, respectively. The nodal freedoms {n1, n2, n3, n4, n5, n6} in the code terms correspond to the incremental nodal responses  $\{\Delta u_{j1}, \Delta v_{j1}, \Delta \theta_{j1}, \Delta u_{j2}, \Delta v_{j2}, \Delta \theta_{j2}\}$  in the theoretical terms, respectively.

Now, obtain the strains of the next iteration  $(\varepsilon_k)_{i+1}$  for each fibre in the element as:

$$(\varepsilon_k)_{i+1} = (\Delta \varepsilon_k)_i + (\varepsilon_k)_i$$

**2.4.b)** Obtain the stresses of the next iteration  $(\sigma_k)_{i+1}$  for each fibre in the element from the provided concrete & steel simplified constitutive models.

**2.4.c)** Obtain the updated stiffness modulus for every concrete and steel fibre in the element as follows:

$$E_{i+1} = \frac{(\sigma_k)_{i+1}}{(\varepsilon_k)_{i+1}}$$

**2.4.d)** End of fibre-level loop. Repeat all steps from 2.4.a) to 2.4.c) for the next fibre.

**2.4.e)** Form the global stiffness matrix as in the following steps:

*step(1):* Construct the element stiffness matrix  $k_{i+1}$  as a function of  $EA_t^*$ ,  $EG_t^*$ ,  $EI_t^*$  and  $L$  using the updated stiffness modulus  $E_{i+1}$ .

*step(2):* Transform element stiffness matrices to global coordinates (NOT NEEDED).

*step(3):* Combine element stiffness matrices to form global stiffness matrix  $k_{i+1}$ .

*step(4):* Reduce global stiffness matrix with constraints.(NOT NEEDED here, but needed for the Grand global stiffness matrix in step 2.3).

**2.4.f)** Obtain the global displacements vector  $\mathbf{u}_{i+1}$  for the next iteration as:

$$\mathbf{u}_{i+1} = \Delta \mathbf{u}_i + \mathbf{u}_i$$

**2.4.g)** Solve for the global restoring forces vector  $(\mathbf{f}_s)_{i+1}$  as follows:

$$(\mathbf{f}_s)_{i+1} = \mathbf{k}_{i+1} \cdot \mathbf{u}_{i+1}$$

**2.5** Obtain the global incremental velocities and accelerations vectors as:

$$\Delta \dot{\mathbf{u}}_i = \frac{\gamma}{\beta \Delta t} \Delta \mathbf{u}_i - \frac{\gamma}{\beta} \dot{\mathbf{u}}_i + \Delta t \left(1 - \frac{\gamma}{2\beta}\right) \ddot{\mathbf{u}}_i$$

$$\Delta \ddot{\mathbf{u}}_i = \frac{1}{\beta (\Delta t)^2} \Delta \mathbf{u}_i - \frac{1}{\beta \Delta t} \dot{\mathbf{u}}_i - \frac{1}{2\beta} \ddot{\mathbf{u}}_i$$

**2.6** Obtain the global velocities vector for the next iteration as:

$$\dot{\mathbf{u}}_{i+1} = \Delta \dot{\mathbf{u}}_i + \dot{\mathbf{u}}_i$$

**2.7** Obtain the global accelerations vector for the next iteration as:

$$\ddot{\mathbf{u}}_{i+1} = \Delta \ddot{\mathbf{u}}_i + \ddot{\mathbf{u}}_i$$

**3.0** End of time-step iteration loop. Repeat all steps from 2.1 to 2.7 for the next time-step.

## 4.2.9 Flow Chart for the Code Algorithm

Solving the proposed non-linear dynamic problem requires several computational tasks. The main tasks can be summarised in the following points:

1. Defining initial values, Newmark's constants, input and output parameters, and configure them in the correct arrays dimension. This also includes configuring the geometry of element fibres and assembling the global matrices.
2. Constructing constant and varying global matrices; mass, damping and stiffness matrices. The global stiffness matrix is constructed twice; the first time is to solve for unknowns in the static analysis under the permanent loading of gravity, the second time is during an iterative updating process to solve for unknowns in the non-linear dynamic analysis under dynamic loading.

Updating the stiffness matrix is processed at every time-step, and depends on computing the updated elastic modulus, which depends on the simplified constitutive models built-in for the concrete and steel fibres.

The global stiffness equation, known as key equation, is solved iteratively, and the solution is used to determine and update the fibres' strains and stresses, which are used to determine and update the elastic modulus.

The hysteresis curves can be obtained from solving the stiffness equation again. Damage could also be estimated according to those stresses falling in the stage of softening strains.

The sequence for handling these tasks can be briefly described using the flow chart shown in Figure 4.5.

#### 4.2.9.1 Damage

According to the concrete constitutive curve, the fibres are not designed to resist the tensile stresses, but rather resist compressive stresses until some strain crushing limit -0.008, after which the fibres are banned from resisting any more loads since they are considered fully damaged. However, even though fibres that have experienced tensile strains are theoretically damaged, they are not banned from resisting further compressive stresses at further time-steps. This is because they attain small hair cracks in reality, and are not considered fully damaged. In this fibre element model, damage is not estimated but rather its effect is encountered within the updated stiffness matrix for each element.

#### 4.2.9.2 Programming Issues

- Solving for the displacement increment for the whole structure in step (2.4) is obtained from the reduced grand (cap) stiffness matrix  $\hat{\mathbf{k}}_i^r$  and reduced grand loading vector  $\Delta\hat{\mathbf{p}}_i^r$ . This is done by using the key equation.
- After using a MatLab function file to produce the stresses from strains, it is necessary to update every strain value for the next time-step before entering the fibres' loop of the next iteration. This should be done for each element otherwise, strains would not be updated for the next iteration.
- The global restoring forces vector  $(\mathbf{f}_s)_i$  and the global displacements vector  $\mathbf{u}_i$  in steps 2.4.f) and 2.4.g) respectively, are plotted to obtain the hysteresis curve for the structure for all time-steps.
- The updated stiffness modulus  $E_{i+1}$  in step 2.4.c) is the damaged modulus  $E^D$  if the fibres strains exceed the elastic limit and fall into the softening strain stage.

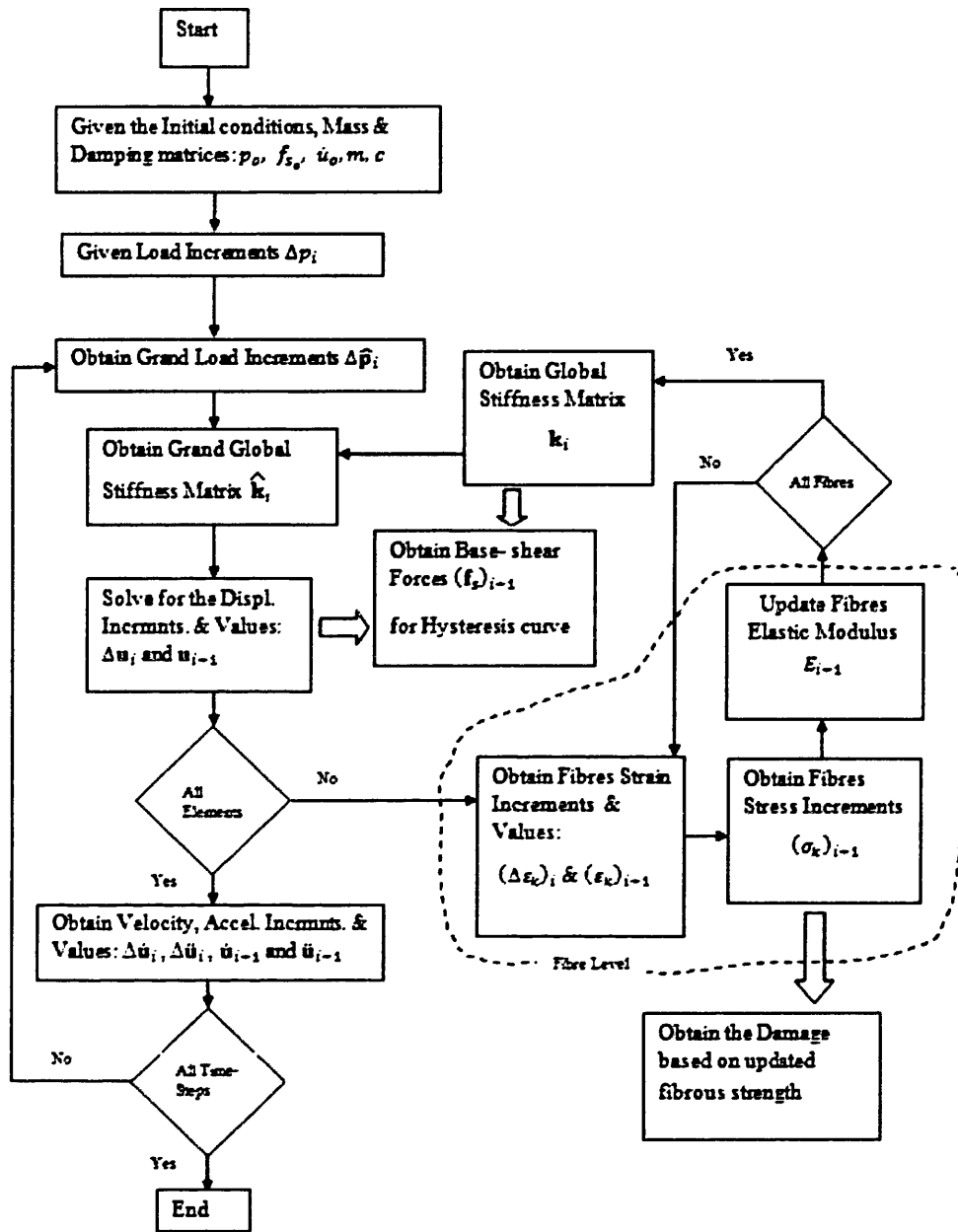


Figure 4.5 Flow Chart for non-linear dynamic solver using the Finite Fibre Elements

### 4.3 THE PROPOSED PROBLEM

The proposed problem is a reinforced concrete column with a mass lumped at the top of the column and complete fixation at the base. The top mass is subjected to an effective dynamic lateral load equivalent to an artificial ground acceleration record of 6 to 8 seconds long. The structure has a fundamental vibration period of 0.375 seconds for the first of mode 1, and is analysed with a damping ratio of 5% using the mass-proportional damping type with mass parameter 1.66221693. The column is 6 meters long, and its cross section is (0.70m x 0.70m)

with 0.025m cover and 16 No.14 steel rebars of diameter 25 mm, as shown in Figures 4.6.a & b.

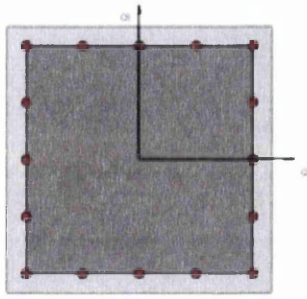


Figure 4.6.a) RC column cross section,



b) Column structure

### 4.3.1 The Structure Model

The model for the proposed problem was built and analysed by using MatLab programming, and verified using the SeismoStruct model. The Seismostruct software is one of the successful and robust non-linear dynamic solvers. It is designated to perform seismic analyses for RC and steel structures under seismic loading. The Seismostruct Modelling is based on the Finite Fibres Elements which are very suitable for modelling of 2D and 3D RC frame structures. As can be seen from Figure 4.7, the fibre-elements modelling for a RC member is based on discretization of the member's section into 2D fibres which are entitled the elastoplastic properties of the material [5]. The program accounts for both material inelasticity and geometric nonlinearity, following the constitutive relationship for the materials in their elastoplastic behaviour. Several seismic tasks can be performed by the Seismostruct such as dynamic, quasi-static, static time-history, and Eigen analyses. Two schemes of solutions are available; the displacement-based and force-based schemes, with and without involving the plastic hinge properties. The force-based scheme is very successful in solving non-linear dynamic problems since it converges with a very few number of elements, and is recommended by the User's manual for solving non-linear problems when applying dynamic and quasi-static analyses.

Two of the SeismoStruct contesters won the 'Award of Excellence' in the 'blind prediction contest' carried out by PEER and NEES in 2010 for analysing the shaking-table test of a full-scale RC column. In 2012, The Seismostruct software was also awarded in the '15th World Conference on Earthquake Engineering' for estimating, with unmatched accuracy, the

dynamic response of two full-scale reinforced concrete frames designed for low and high ductility levels, and tested on a shaking-table.

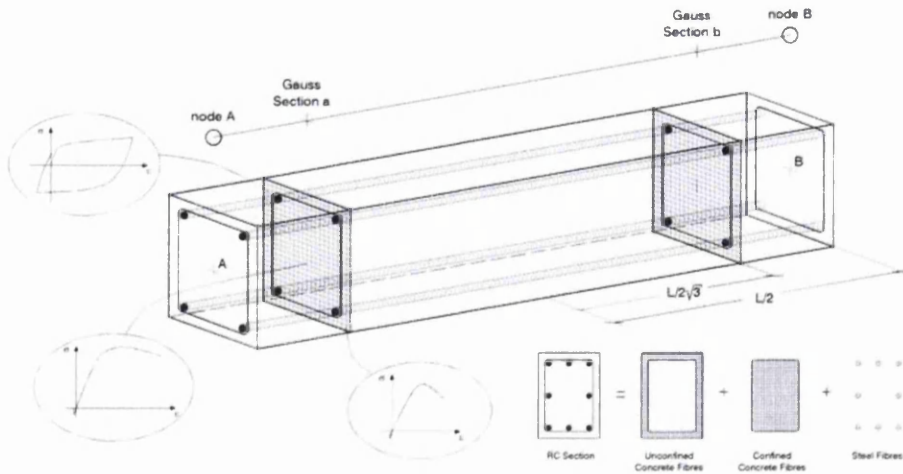


Figure 4.7 Modelling components of RC members by fibre elements [5]

#### 4.3.1.1 Assumptions of the Fibre Element Model in the MatLab Code

##### Elements and Nodes:

Number of elements=5, number of DOF per element=6, total number of DOF=18, number of restrained DOF=3 at the base of the column.

Length of element  $L=1.2$  m, width of element= width of column cross section= $0.70$  m

##### Fibres:

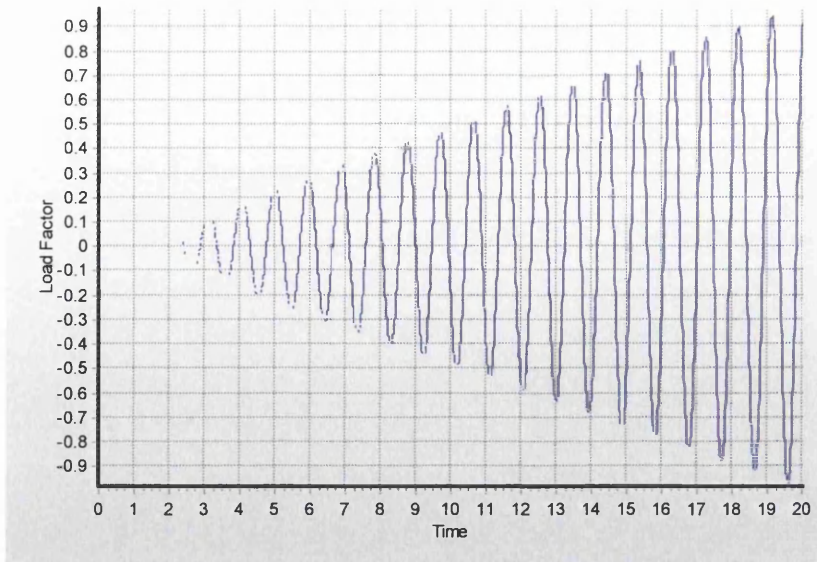
Number of fibres per element=57, width of each fibre= $0.0125$  m.

Diameter of steel bars= $0.025$ m, number of bars at each side of section = 7 bars.

**Axial loading:** Axial load is the dead gravity load of the top mass, and is placed at top node 16 with a value of  $(-30,000 \times g)$  N, where  $g$  is the ground gravity= $9.81$  kg/m.s<sup>2</sup>. In order to have the axial load as a permanent gravity value, that's maintained during the time of analysis, it is applied as a static loading, and solved with the reduced stiffness equation to obtain the displacements, which are added to the displacements obtained from the dynamic loading.

**Lateral loading:** Lateral loads are calculated by multiplying the lumped mass of every node by an artificial ground acceleration record of 6 to 8 seconds long, as shown in Figure 4.8. Loads are applied at the lateral DOF number 14 at the column top node, with a magnitude of  $(30000 \times g \times \text{Load Factor changing per time})$ .





**Figure 4.8 Artificial ground acceleration record**

**Time-step:** The total time of curve loading = time step (0.01 sec) x size(600-800 time-steps) = 6-8 seconds, where, the interval of time step = 0.01 seconds and size of the problem = 600-800 time-steps.

**Material properties:**

Concrete elastic modulus  $E_{conc} = 21000 \text{ MPa} = 2.10 \times 10^{10} \text{ Pa (N/m}^2\text{)}$

Concrete Axial Strength  $F_c = -4.2 \times 10^7 \text{ Pa}$

Steel elastic modulus  $E_{steel} = 175000 \text{ MPa} = 1.75 \times 10^{11} \text{ Pa}$

Steel Axial Strength  $F_y = 3.5 \times 10^8 \text{ Pa}$

Lumped mass at top node = 30000 kg, rotational mass = 43200 kg.m<sup>2</sup>[6,7].

Lumped mass at column nodes = 735 kg, rotational mass = 1058 kg. m<sup>2</sup>

**Damping factor:**

The damping matrix  $c$  can be formed by different formulae according to different assumptions. For a 5% damping ratio the following formulae are obtained:

$$c = 0.231 m + 0.00501 k \text{ Rayleigh damping, calculated from Chopra [2, eq.11.4.10]}$$

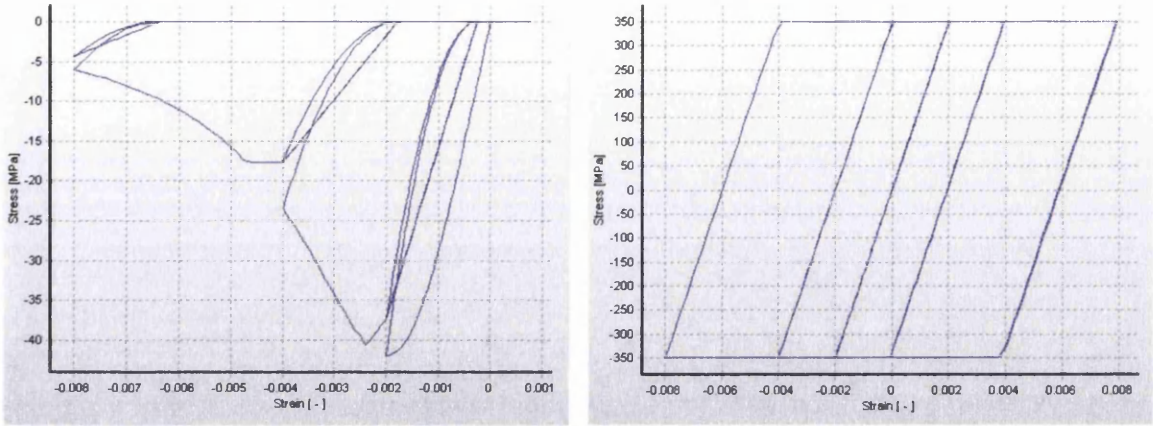
$$c = 0.2138 m + 0.00524 k \text{ Rayleigh damping, obtained from SeismoStruct.}$$

$$c = 0.00601 k \text{ Stiffness-proportional damping, obtained from SeismoStruct.}$$

$c = 1.662217 m$  Mass-proportional damping, obtained from SeismoStruct. The mass-proportional damping type was used to avoid possible numerical instability.

### Constitutive Models in SeismoStruct:

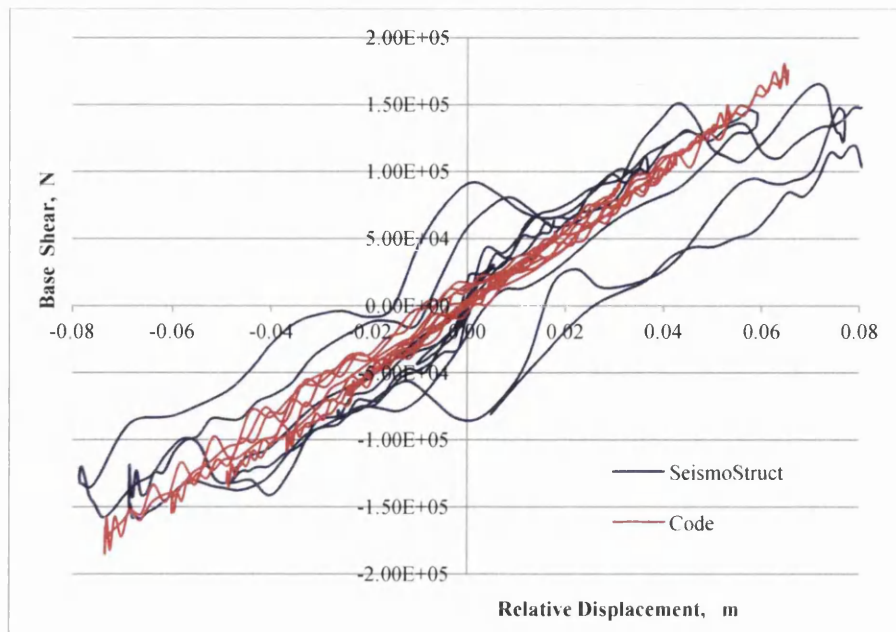
The constitutive models used by the SeismoStruct for concrete and steel have been chosen as most simplified ones, as shown in Figures 4.9.a and 4.9.b, and are given the same properties in the code.



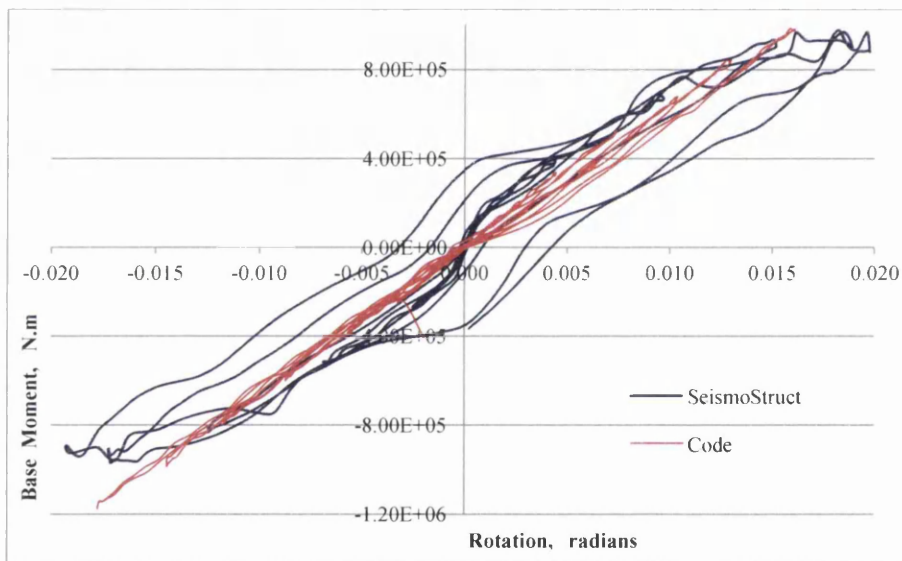
Figures 4.9.a and 4.9.b Constitutive models used by the SeismoStruct for concrete and steel, respectively

### 4.3.2 Results and Discussion

Figure 4.10 shows the hysteresis curve for the relative lateral displacement versus the base shear by both MatLab code and SeismoStruct analyses. The hysteretic loops tend to degrade as the dynamic loading increases every time step. This is due to the fact that the global stiffness matrix is updated according to the changes in the elastic moduli of the loaded fibres. According to the concrete constitutive models assigned for the column core and cover, fibres must lose their elastic strength when subjected to any tensile strains. This would, eventually, cause the degradation of the global stiffness matrix as fibres strain in the tensile direction. This can also be seen in the base-moment/rotation hysteresis curve in Figure 4.11.

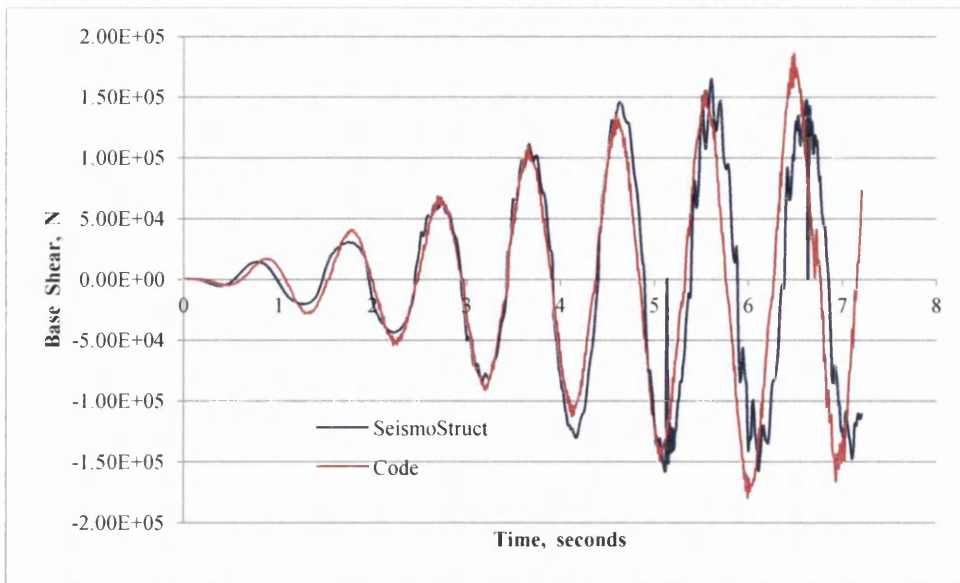


**Figure 4.10 Base-shear/displacement hysteresis curve**

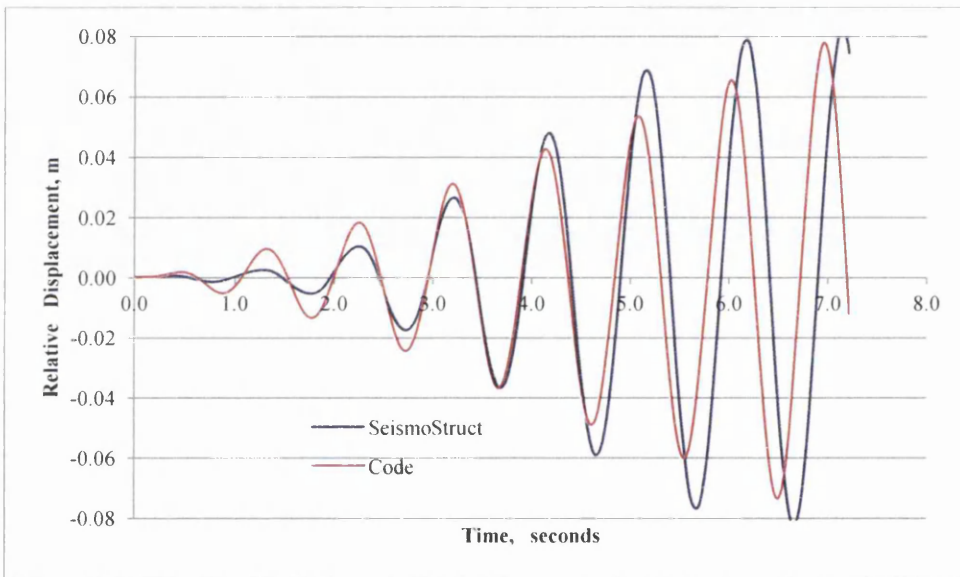


**Figure 4.11 Base-moment/rotation hysteresis curve**

Figures 4.12 and 4.13 show comparisons of different responses of base shear forces and displacements, between the MatLab code and SeismoStruct analyses. It can be seen that displacements do not agree in the beginning of the response, but relatively agree in further stages.



**Figure 4.12** Base shear forces by SeismoStruct and code analyses.



**Figure 4.13** Relative displacements by SeismoStruct and code analyses.

At the first element, the fibres at the end of the element section will have concrete and steel stress-strain curves that look like Figures 4.14 and 4.15. The curves follow the assigned constitutive models for concrete and steel linear and non-linear paths successfully. However, concrete stress-strain curves of the two analyses do not coincide even though the overall results are approximately close. This is because the concrete elastic modulus in the code is linearly plotted, and not processed with non-linearity curving as in the SeismoStruct concrete constitutive model, as can be seen in Figure 4.9.a.

In general, the limited non-linear behaviour in the softening stage of the concrete fibres is due to the problem input parameters such as loading, geometry, material and rate of loading.



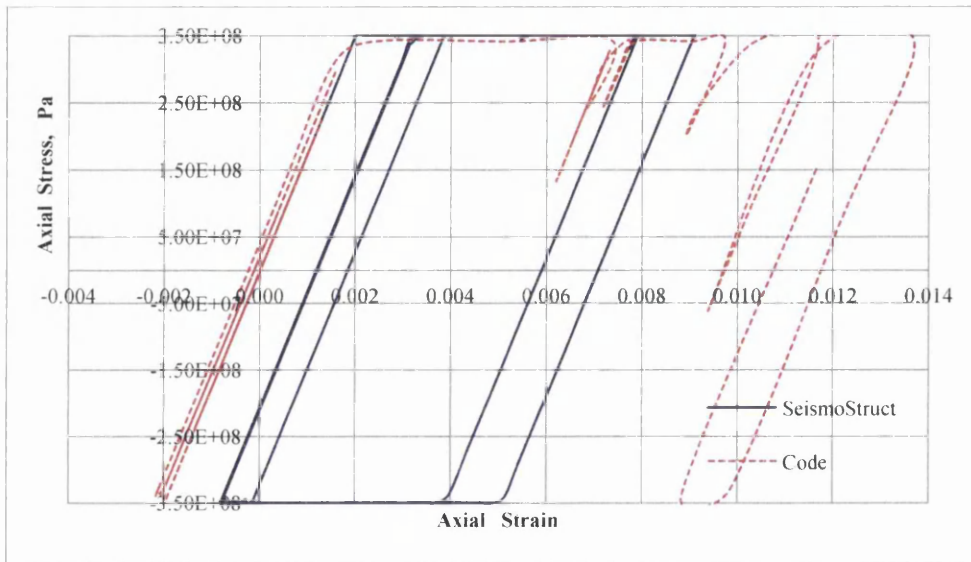
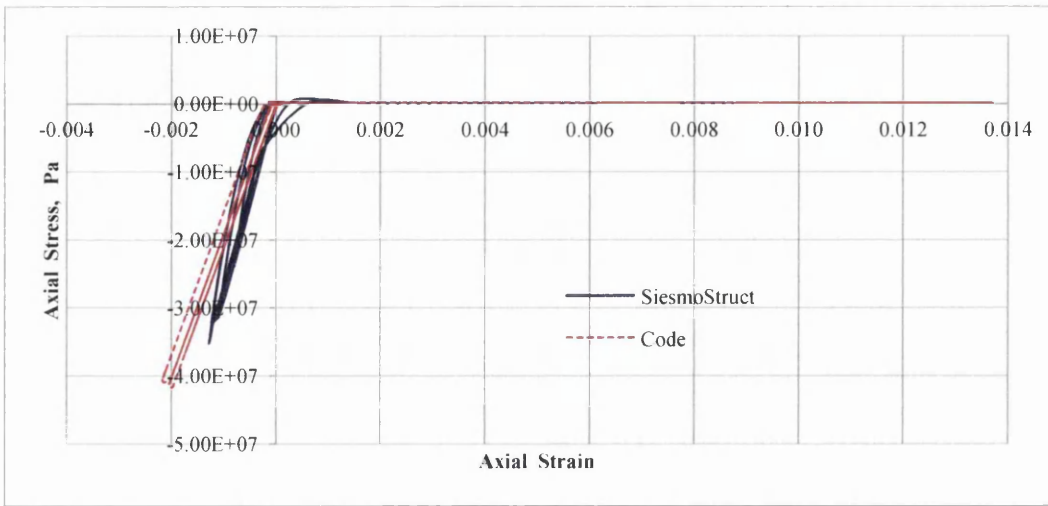


Figure 4.14 and 4.15 Constitutive curves for concrete and steel end fibres in the first element in both SeismoStruct and code analyses

#### 4.3.2.1 The Number of Elements and the Number of Fibres

It is typically known in numerical modelling that the increase of elements should improve the performance of analysis. In the proposed dynamic problem, this has been found true for elastic analysis only, and when implying the Displacement-Based Scheme for computing the numerical integration. In contrary to this, increasing the number of elements will lead to incorrect results in a non-linear plastic analysis, and it is preferred to keep a lower number of elements for this problem since the plastic stage is applied at most of the analysis.

Another important conclusion is related to the number of fibres assigned to the element section. It has been found that increasing the number of fibres will improve the non-linear

performance of the analysis, since the degradation of the global stiffness matrix would become gradual, giving more continuity to the produced curves.

As a rule of thumb, single-material sections will usually be adequately represented by 100 fibres, whilst more complicated sections, subjected to high levels of inelasticity, will normally employ more than 200 fibres. Therefore, only a sensitivity study on a case-by-case basis can establish the optimum number of section fibres [5]

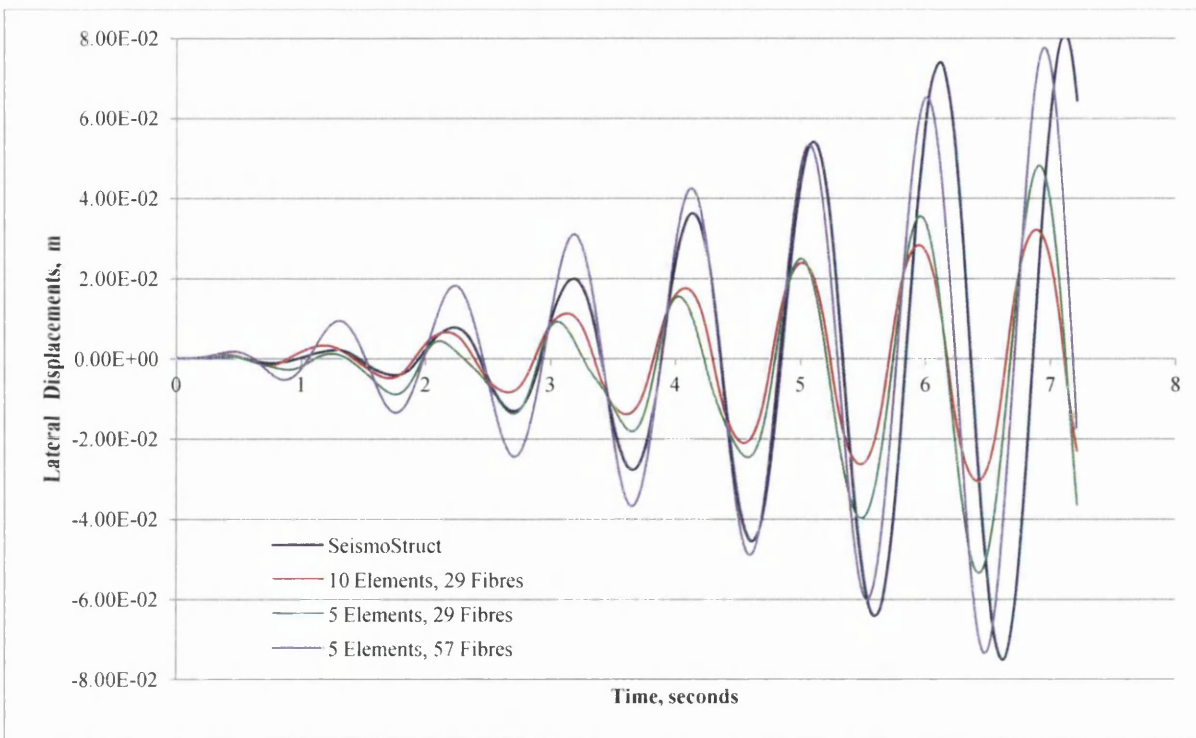
Figure 4.16 shows a comparison of displacement responses obtained from different analyses for the same problem. The analyses are for 10 elements with 29 fibres, 5 elements with 29 fibres and 5 elements with 57 fibres, which are all to be compared with results by the SeismoStruct analysis. SeismoStruct analysis is performed by using 2 elements only since it employs the Force-based Method, and the section is provided with 200 fibres. From comparison, the closest to the SeismoStruct is the analysis with the 5 elements and 57 fibres.

A useful conclusion has been made upon several computer runs that have been carried out for different numbers of elements and fibres to different dynamic non-linear problems, that there's no rule of thumb that generalises a main refinement of the elements and fibres to attain acceptable solutions. However, a sensitivity study for each specific problem must be carried out in a case-by-case basis in order to establish the optimum number of elements and section fibres for such a problem.

In mathematical terms, the need for a lower number of elements to obtain a better non-linear simulation, can be interpreted from the fact that larger incremental rotational strains  $\Delta\phi$  will increase if taller element fibres are used, and thus, less number of elements are required.

As can be seen from the definition of incremental rotational strains;  $(\Delta\phi)_i = \frac{(\Delta\theta_{j6} - \Delta\theta_{j3})_i}{L}$ , the difference between the incremental rotations  $\Delta\theta$  for the two element ends should be large enough to produce large rotational incremental strains;  $\Delta\phi$ , and thus, produce large incremental axial strains;  $y_k \cdot \Delta\phi$  at each time-step. This will, consequently, increase the overall incremental axial strains  $\Delta\varepsilon_k$  as follows:

$$(\Delta\varepsilon_k)_i = (\Delta\varepsilon_a - y_k \cdot \Delta\phi)_i$$



**Figure 4.16** A comparison of displacement responses

In the proposed problem,  $\Delta\varepsilon_k$  will increase since  $\Delta\varepsilon_a$  has relatively small values, and when  $y_k$  is negative. Thus, the axial strains  $(\varepsilon_k)_i$  increase when accumulating.

On the other hand, if shorter element fibres are applied, i.e. more elements are used, smaller incremental rotational strains  $\Delta\phi$  are produced, and thus, the axial strains  $(\varepsilon_k)_i$  decrease when accumulating. Such a case has occurred when 10 elements were modelled for the same proposed problem.

#### 4.3.2.2 Differences Between the MatLab code and the SeismoStruct Model

In general, the differences in results between the two analyses by SeismoStruct and MatLab code, can be attributed to many issues:

1. The most suspected reason creating such differences is using different methods of problem-solving. The code employs the Displacement-based Method with 5 elements, while the SeismoStruct employs the Force-based Method with only 2 elements, which is recommended for the simulation of dynamic non-linear analysis by [5].
2. The number of fibres in an element section is assumed 57 in the code, while in the SeismoStruct analysis it is taken as 200-300 fibres with 3-4 integration sections in each element.

3. The constitutive models of concrete and steel are very simple in the code, while they are complex in the Seismostruct.
4. There is no iterative process, such as Newton-Raphson, used in the code to minimise the errors due to the assumed approximation between the secant stiffness and tangential stiffness:

$$(k_i)_t \cong (k_i)_s$$

but only small time-step interval (0.01 seconds) to compensate for that simplification. While, an iterative strategy is used in the Seismostruct with a small tolerance (1e-05) for convergence.

5. Mass matrix in the code is based on a lumped mass approach by having the element masses lumped in the nodes, while it is based on the distributed mass approach in Seismostruct, in representing both transitional and rotational mass parameters at the nodes.
6. SeismoStruct applies geometric non-linearity, while it is not applied in the code.

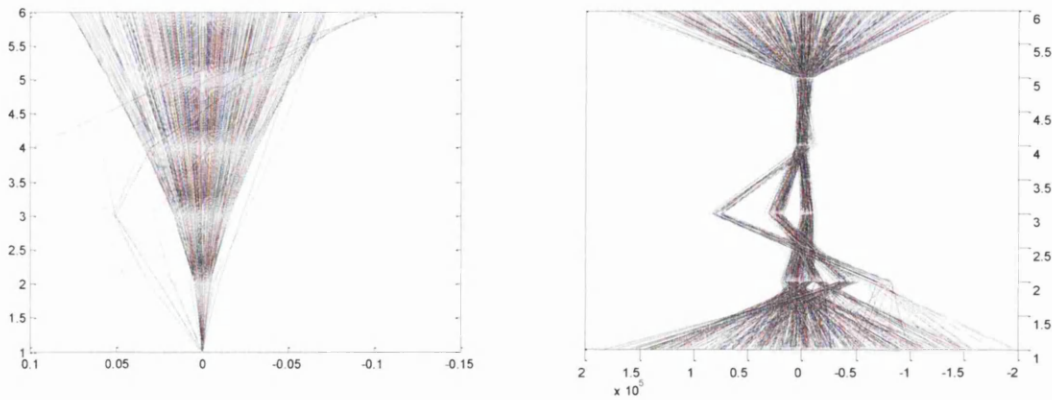
All these differences can produce the mismatch in the comparison between the two analyses, especially the difference in the applied constitutive models, which largely affect the non-linearity process and ductility of the structure.

#### **4.3.2.3 Diagram Representations of Results for all Elements at all Times, and for all Fibres at all Times**

In the non-linear dynamic analysis for the RC column example with 10 elements and 29 fibres per element, Figures 4.17 and 4.18 represent the lateral displacements  $v_j$  and resisting shear forces  $Q_j$  for all of the element nodes, respectively, at all of the analysing times.

The modal shape of the structure across the 6-meters height of the analysed column has the first modal shape for an inverted pendulum problem. However, it can be observed that the modal shape starts to change at the last stages of loading, as in Figure 4.17. The change in modal shape is due to strength degradation of the elements due to the increase in dynamic loading. Consequently, the resisting shear forces  $Q_j$  for all of the element nodes tend to increase at the very last stages of the dynamic loading, as in Figure 4.18. Strength degradation is an indication of the occurrence of damage in element fibres.

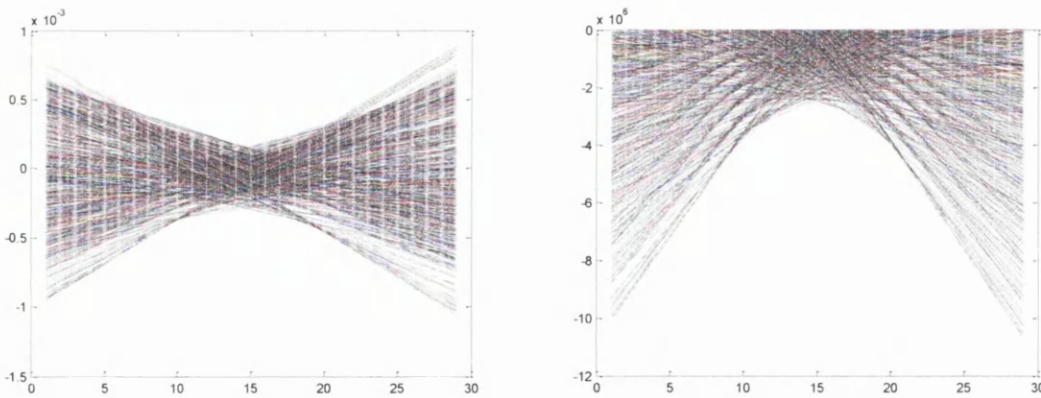




**Figure 4.17** Lateral displacements of all elements. **Figure 4.18** Resisting forces for all elements

Figures 4.19 and 4.20 show the axial strains and corresponding axial stresses diagrams, respectively, for all of the 29 fibres of one element at all of the analysed times. The selected element is the one with the plastic hinge (PH) to observe the plastic strains behaviour.

It can be noticed that the centre of the strain diagram is moved off the centroid of the element at the last stage of loading, indicating the occurrence of strength degradation, which indicates damage in the plastic hinge PH.



**Figures 4.19 and 4.20** Axial strains and axial stresses of all fibres at PH element, respectively.

#### 4.3.2.4 Stiffness matrix effect on the hysteresis curve of quasi-brittle material

It is known that the stiffness matrix terms are coupled, since axial displacements are due to axial forces, and curvature of the elements are due to both lateral forces and moments. However, another term, the shear modulus term  $EG_t^*$ , is added to the applied stiffness matrix, which is relating the curvature rotation to the axial forces, and will affect the hysteresis behaviour in a quasi-brittle structure significantly. This is because the elastic modulus  $E$  will become zero in the fibres under tension, and remains the same in the compressed fibres, thus

making the stiffness term  $EG_t^* = \sum_{n=1}^k (E_k A_k y_k)$ , fluctuate between +ve and -ve values, since  $y_k$  has different signs according to fibres positions. More fluctuation can also occur when the compressed fibres exceed the elastic limit, and  $E_k$  for those fibres become degraded. Generally, if the shear modulus term  $EG_t^*$  is not included, the hysteresis mode of the lateral forces will not be affected, and will appear in an undisturbed mode, as shown in Figure 4.21, for the structure under cyclic loading. However if term  $EG_t^*$  is included, but the elastic modulus  $E$  remains elastic at all time-steps; i.e.  $E$  is the same under both tensile and compressed fibres, the hysteresis of the lateral forces will also be undisturbed, and will show an elastic dynamic response as shown in Figure 4.22.

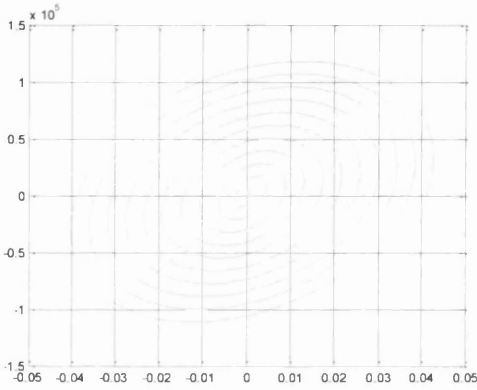


Figure 4.21 Hysteresis with  $EG_t^*$ -term = 0

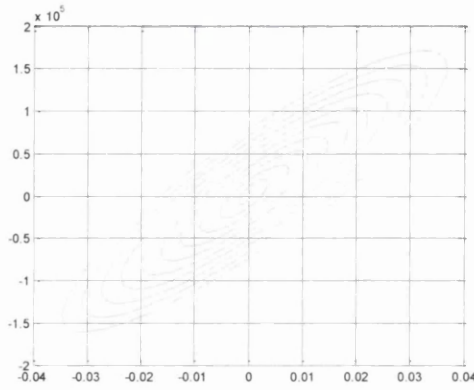


Figure 4.22 Elastic Hysteresis with  $EG_t^*$ -term

In general, the inclusion of the  $EG_t^*$  term in the stiffness matrix will disturb the lateral-forces hysteresis of the structure by establishing axial forces due to the moments, or  $-EG_t^* \cdot \Delta\theta_{j1}$  and  $EG_t^* \cdot \Delta\theta_{j2}$ , and by establishing moments due to the axial forces, or  $-EG_t^* \cdot \Delta u_{j1}$  and  $EG_t^* \cdot \Delta u_{j2}$ , as can be seen in the solution of the stiffness equations at one node:

$$\Delta N_{j1} = \frac{1}{L}(EA_t^* \cdot \Delta u_{j1} + 0 + -EG_t^* \cdot \Delta\theta_{j1}) + \frac{1}{L}(EA_t^* \cdot \Delta u_{j2} + 0 + EG_t^* \cdot \Delta\theta_{j2}) \quad (4.21)$$

$$\Delta M_{j1} = \frac{1}{L} \left( -EG_t^* \cdot \Delta u_{j1} + \frac{6EI_t^*}{L} \cdot \Delta v_{j1} + \frac{4EI_t^*}{L} \cdot \Delta\theta_{j1} \right) + \frac{1}{L} \left( EG_t^* \cdot \Delta u_{j2} + -\frac{6EI_t^*}{L} \cdot \Delta v_{j2} + \frac{4EI_t^*}{L} \cdot \Delta\theta_{j2} \right) \quad (4.22)$$

The incremental lateral forces are not directly related to the axial forces, as can be seen from the stiffness matrix, but since the axial force and moment are coupled, the incremental lateral force  $\Delta Q$  is also affected by  $\Delta\theta$ , as can be seen from the solution of the stiffness equations at one node:

$$\Delta Q_{j1} = \frac{1}{L} \left( 0 + \frac{12EI_t^*}{L} \cdot \Delta v_{j1} + \frac{6EI_t^*}{L} \cdot \Delta\theta_{j1} \right) + \frac{1}{L} \left( 0 + -\frac{12EI_t^*}{L} \cdot \Delta v_{j2} + \frac{6EI_t^*}{L} \cdot \Delta\theta_{j2} \right) \quad (4.23)$$

In this case, the vertical displacements of the analysed structure, also known as rocking motion, will differentiate largely between the upper (top) and lower (base) nodes of the structure, which will disturb the lateral-forces hysteresis as  $E$  is fluctuating between tensioned and compressed fibres in quasi-brittle materials.

## 4.4 CONCLUSIONS

- The fibre element method is an effective method for modelling RC framed structures under dynamic loading. It is widely used by researchers and engineers, with many developed versions, but its powerful performance can also be achieved under simplified assumptions. Modelling of dynamic problems was performed with linearized assumptions for more simplification. The possible errors due to linearization of the tangential stiffness can be minimized by reducing the time-step interval to a relatively small value. This technique is quite useful and easy to consider, and can be used to solve non-linear problems with small errors.
- The un-loading and re-loading of non-linear paths for the material in problems of RC sections can also be simplified by linearising the constitutive concrete and steel models. Such simplifications can be implemented into a fibre element low-fidelity model to analyse non-linear dynamic problems, yet producing acceptable approximate results.
- Increasing the number of fibres will improve the non-linear performance of the analysis and give more continuity to the produced curves by gradual degradation of the global stiffness matrix.
- There's no rule of thumb to generalize refinement of the fibres to attain acceptable solutions, but rather a sensitivity study for each specific problem should be carried out in a case-by-case basis in order to establish an optimum number of elements and section fibres for each specific non-linear dynamic problem.
- In the proposed problem, less than 3% of the column compressive strength is applied as axial stresses, and thus very low confinement is obtained by the transverse reinforcement on the core section.
- In this fibre element model, damage is not estimated but rather its effect is reflected as the stiffness matrix for each element is updated due to the degradation process.

## 4.5 REFERENCES

- [1] R. W. Clough, J. Penzien. Dynamics of Structures, McGraw-Hill, Inc., 1993.
- [2] A. K. Chopra. Dynamics of Structures, Theory and Applications to Earthquake Engineering, 3ed edition, Pearson Prentice Hall 2007.
- [3] J. Sakai, S. A. Mahin. Analytical investigations of new methods for reducing residual displacements of reinforced concrete bridge columns, Pacific Earthquake Engineering Research Centre, PEER Report 2004/02.
- [4] E. Erduran, A. Yakut. Component damage functions for reinforced concrete frame structures. Engineering Structures, 2007. 29(9): p. 2242-2253.
- [5] Bibliography of SeismoStruct Earthquake engineering Software, SeismoStruct v5.2.2 Official release of 22/08/2011Koys.
- [6] W.D. Pilkey. Formulas for Stress, Strain, and Structural Matrices, John Wiley & Sons, New York.1994.
- [7] J.M. Gere, Timoshenko S.P. [1997] Mechanics of Materials, 4th Edition.

# Chapter 5

---

## Non-Linear Numerical Analysis and Damage Assessment

---

### Contents

- 5.0 INTRODUCTION ..... 138
- 5.1 VERIFICATION OF NON-LINEAR ANALYSES..... 138
  - 5.1.1 Example By Erduran and Yakut [1]..... 138
  - 5.1.2 Example by Sakai and Unjoh [2]..... 140
- 5.2 COMPUTATION OF ENERGY AND SEPARATION OF ENERGY QUANTITIES 142
  - 5.2.1 Mass Inertia Forces and the Kinetic Energy ..... 143
  - 5.2.2 Damping Forces & Energy ..... 144
  - 5.2.3 Accumulated Energy Curve..... 144
- 5.3 DAMAGE CURVES BASED ON HYSTERESIS OF THE STRUCTURE ..... 145
- 5.4 CASE STUDY 1: NUMERICAL ANALYSIS ..... 149
  - 5.4.1 RC column Under quasi-static loading..... 150
    - 5.4.1.1 Global Damage (Energy-Based Approach) ..... 151
    - 5.4.1.2 Local Damage (Stress-Based Approach)..... 152
    - 5.4.1.3 Damage Assessment ..... 154
  - 5.4.2 RC Column Under Dynamic Loading ..... 155
- 5.5 CASE STUDY 2: SHAKING TABLE EXPERIMENT..... 159

- 5.5.1 Accumulated Dissipating Yield Energy Curve..... 160
- 5.5.2 Yield Energy Curves and the Damage State in the Shaking Table Experiment..... 162
- 5.5.3 Discussion of Results..... 164
- 5.6 SEISMIC ISOLATION BEARINGS (SIB)..... 164
- 5.6.1 Introduction..... 164
  - 5.6.1.1 Future research point..... 167
- 5.6.2 Damage in the Isolated and Non-Isolated Systems..... 168
- 5.6.3 A Low Fidelity Model Representing an Ideal Seismic Isolation System ..... 170
  - 5.6.3.1 A simplified moment-curvature damage model for bridges subject to seismic loads ..... 171
- 5.6.4 A Numerical Example..... 174
  - 5.6.4.1 Single RC Column with a Seismic Isolated Bearing System ..... 174
  - 5.6.4.2 Single RC Columns with a Seismic Isolated Bearings System ..... 177
  - 5.6.4.3 Discussion of Results..... 179
- 5.7 CONCLUSION & RECOMMENDATIONS ..... 180
- 5.8 REFERENCES ..... 182

## **5.0 INTRODUCTION**

The input energy imposed on an inelastic structural system by a dynamic cyclic loading is dissipated by both viscous damping and yielding energy; also known as hysteretic energy. However, mass inertia forces also resist the applied loading and affect the hysteretic performance of the structure. However, hysteretic curves are different in a statically loaded structure since the resistance of mass inertia does not exist. The hysteretic curves depend on the geometry of a structural system and its material strength and ductility, and they can reflect the overall damaging behaviour that a structural system may have under the lateral static or dynamic loading.

There are several measures for damage due to lateral loading applied on reinforced concrete structures. Engineering-based measures depend on empirical results which justify the damage according to both ductility and hysteresis parameters. For example, Park & Ang damage index is one of the popular damage measures, which is based on both ductility and energy dissipation of the structure. However, it does not take into account the plastic cycles' distribution, but rather considers the global amount of the dissipated energy [1]. In fact, analytical damage calculations consider the non-linear hardening, softening and unloading behaviour, and give a more accurate definition for the damage.

### **5.1 VERIFICATION OF NON-LINEAR ANALYSES**

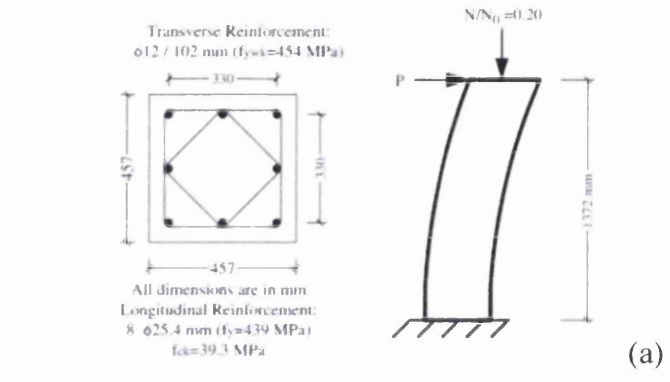
In the following sections, two examples are modelled and analysed by using the Seismostruct software in order to verify the published numerical and experimental results.

#### **5.1.1 Example By Erduran and Yakut [1]**

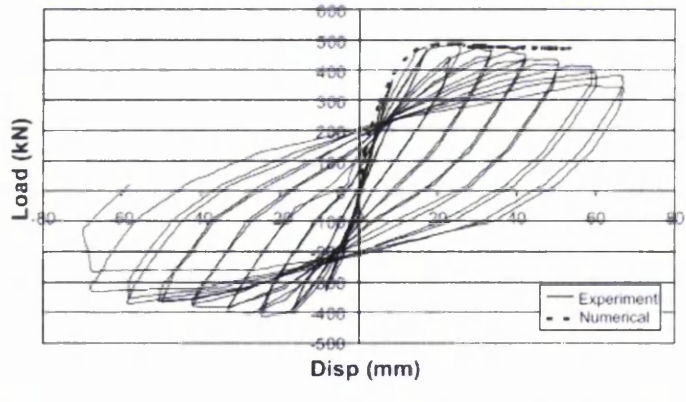
The example is a verification of numerical and experimental load–displacement curves obtained for a referenced RC column problem. The selected column is experimentally tested by Azizinamini et al [1], and is subjected to a cyclic loading of a quasi-static nature. The numerical non-linear analysis carried out by Yakut [1] is obtained by a FE model with longitudinal reinforcement modelled as smeared through the column section, and is able to simulate the cracking and crushing of concrete. The small difference between these two analyses is due to the method of loading and nature of analytical analysis. The monotonic

one-way static loading in the FE analysis does not take the strength degradation into account, hence it overestimates the column strength.

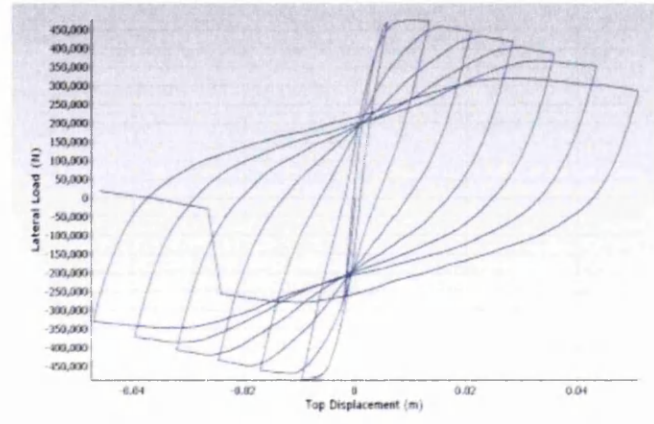
Using the Seismostruct, the obtained hysteretic curve is following similar behaviour of the published numerical and experimental Push-over and hysteretic curves respectively. However, even though the loading cycles are different but they agree at the negative values of displacements and loads. The program terminates before reaching the end of the analysis due to lack of convergence because of failure of most of the concrete fibres. Figure 5.1. The axial applied load is 20% of the column capacity, and is affecting the hysteresis loops significantly.



(a)



(b)



(c)

Figure 5.1 a) Properties of specimen, b) Published results [1] c) Hysteresis by the SeismoStruct



### 5.1.2 Example by Sakai and Unjoh [2]

Junichi Sakai and Shigeki Unjoh [2] conducted a shaking table experiment for a RC circular column specimen, subjected to the strong ground motions that were recorded near Tsugaru Bridge during the 1983 Nihonkai Chubu in Japan. The earthquake record was scaled up by 400%, since the tested specimen was a  $\frac{1}{4}$ -scaled model. Junichi Sakai and Shigeki Unjoh also introduced a numerical model for the same problem using a mathematical model of fibre element with lumped masses, which verified the testing results [2]. The top inertia mass is 27000 kg, and is inducing an axial force dead load at the bottom of the column of 280 kN. The cylinder concrete strength is 41.7 MPa, and the yield strength of the longitudinal and transversal reinforcement bars are 351 MPa and 340 MPa respectively. Figure 5.2 shows the  $\frac{1}{4}$ -scaled ground accelerations. Figure 5.3.a shows the geometric set up of the scaled specimen, the column cross section and reinforcement details. This test was performed mainly to investigate the multi-directional effect of the seismic loading on the RC circular column, since no method properly evaluates the effect of multidirectional dynamic loading that has been developed until 2006 [2].

The SeismoStruct model also came into a fair agreement with the test results, and with a better agreement with the numerical results. The differences in the base shear magnitudes are attributed mainly to the unpredictable crack growth that governs the post-softening stage of the process. The analytical rules that govern strength degradation of the column at the softening stage are different from those due to real fracture in the test. Furthermore, the assumed length of the modelled plastic hinge PH and assumed damping ratio have also significant effects on the final results.

Figure 5.3.b shows the time history results obtained from experiment and numerical analysis by Sakai and Unjoh. Figure 5.4.a shows the fibre element model by the Seismostruct, and Figures 5.4.b and 5.4.c show the time history results obtained from numerical analysis by SeismoStruct dynamic solver in the x and y directions respectively. Both numerical analyses use the fibre element technique but with lumped mass in the former and distributed mass in the latter.

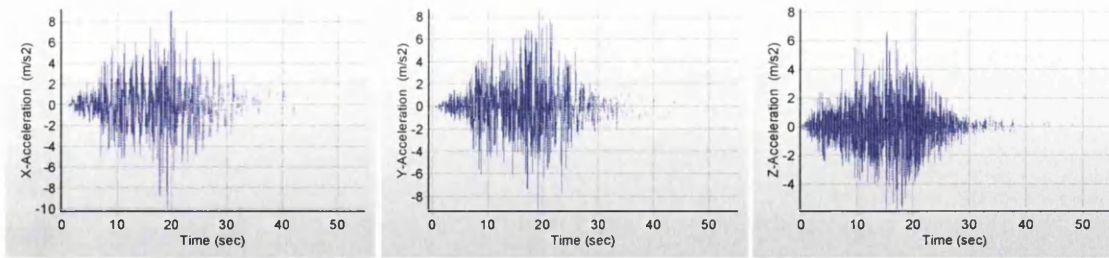


Figure 5.2 400%-Scaled ground accelerations in the x, y and z directions.

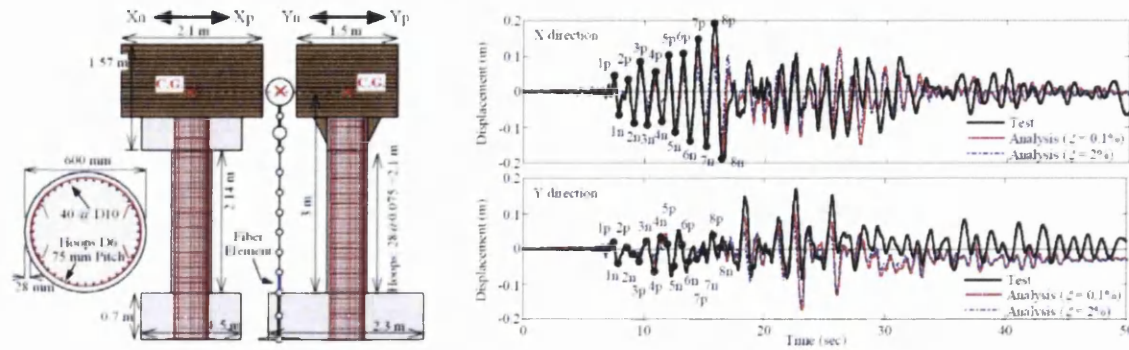


Figure 5.3.a) Shaking table specimen b) x & y-Displacement responses at the c.g. of the structure [2].

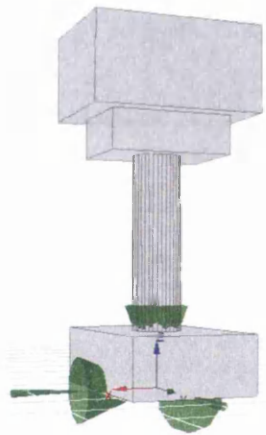


Figure 5.4.a Seismostruct fibre model

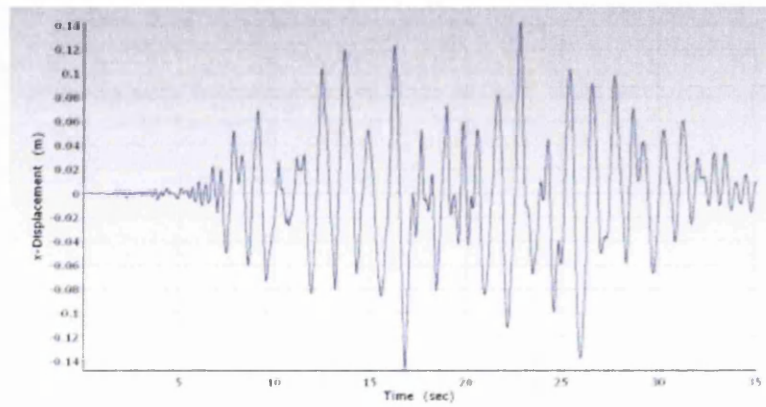


Figure 5.4.b x-Displacement responses at the c.g. of the structure, modelled by Seismostruct.

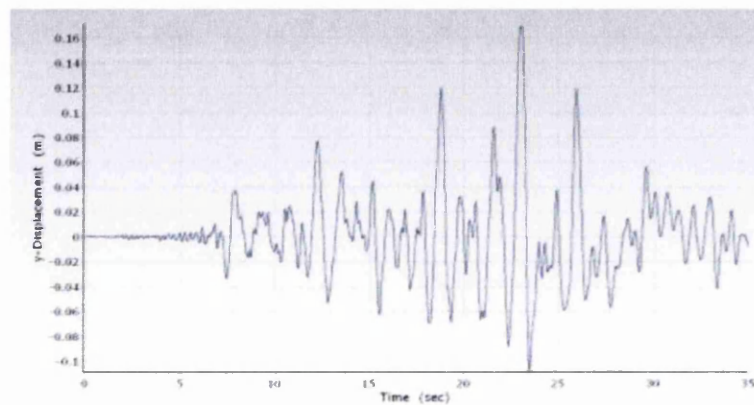


Figure 5.4.c y-Displacement responses at the c.g. of the structure, modelled by Seismostruct.

## 5.2 COMPUTATION OF ENERGY AND SEPARATION OF ENERGY QUANTITIES

The seismic energy demand that is imposed on an inelastic structural system, such as a RC multi-column bridge, is released, or dissipated by the structural response into elastic, kinetic, damping and yield energy. This occurs according to the capacity of the system, but the main dissipation is released by both viscous damping and yielding energy quantities [3].

The equation of motion for a structure with mass  $m$  and damping factor  $c$  is written as:

$$\ddot{u} + c \dot{u} + f_S(u, \dot{u}) = -m \ddot{u}_g \quad (5.1)$$

where, both the elastic and yield forces  $f_S(u, \dot{u})$  are the RC column restoring internal forces, that are produced by the initial stiffness and yielded stiffness of the column. By integrating the equation of motion with respect to the displacement  $u$  for an inelastic system subjected to the ground acceleration  $\ddot{u}_g$ , the work done by each of the resisting forces can be calculated as follows:

$$\int_0^u m \ddot{u} du + \int_0^u c \dot{u} du + \int_0^u f_S(u, \dot{u}) du = - \int_0^u m \ddot{u}_g du \quad (5.2)$$

Or can be re-written by integrating with respect to time, which is more convenient for numerical computations. This is written in terms of the time step  $dt$  and velocity as follows:

$$\int_0^t m \ddot{u} \dot{u} dt + \int_0^t c \dot{u} \dot{u} dt + \int_0^t f_S(u, \dot{u}) \dot{u} dt = - \int_0^t m \ddot{u}_g \dot{u} dt \quad (5.3)$$

The first term is the kinetic energy,  $E_K$ , the second term is the damping energy,  $E_D$ , the third term is the sum of the energy dissipated by both yielding,  $E_Y$ , and recoverable strain energy of the system,  $E_S$ .

Thus the dissipating energy by yield is:

$$E_Y = \left[ \int_0^t f_S(u, \dot{u}) \dot{u} dt \right] - E_S \quad (5.4)$$

where, the recoverable strain energy can be established by determining the initial stiffness  $k$  of the system as follows:

$$E_S = \int_0^u f_S du = \int_0^u k u du = \frac{1}{2} k u^2 \quad (5.5)$$

When  $k$  becomes inelastic  $E_S$  is set to zero, and  $f_S$  is considered purely inelastic and not associated with any elastic restoring forces. In this way  $E_Y$  can be separated and defined for the inelastic system.

However,  $E_Y$  can also be obtained directly by considering only the forces that exceed the elastic limit  $f_y$  of the structural system, and not by considering those lying before that limit on the time-history graph of the restoring forces. This method is also used to determine the

graph of time intervals yielding for an idealized elastic perfectly-plastic structural system [3, 4]. However, this method is approximate since it considers all forces that are within the elastic limit as elastic even if they are unloading force responses occurring in the inelastic stage. This is also a basic definition in both cases of ‘kinetic non-linearity’ and ‘isotropic non-linearity’ curves under static loading, in which all unloaded responses are considered elastic when they are within the elastic limit [5].

In order to determine and graph the energy curves, it is important to separate the linear elastic and non-linear inelastic force diagrams at first. To do this, it is important to define the elastic limit  $f_y$  for the structural system.

The elastic limit for a monolithic structure such as steel, is a well pre-defined parameter, but for combined-section structures such as RC columns,  $f_y$  must be defined independently as according to each structure. This is defined by either quasi-static or push-over analysis, which is used to draw the ‘envelope curve’ of the linear and non-linear behaviour in a load-deflection curve [6]. The connection point between the linear and non-linear envelopes in a load-deflection curve, hysteresis curve, is the elastic limit  $f_y$  for the system.

### 5.2.1 Mass Inertia Forces and the Kinetic Energy

From the integrated equation of motion, the kinetic energy is determined as:

$$E_K = \int_0^u f_I du = \int_0^u m \ddot{u} du = \int_0^u m \frac{d\dot{u}}{dt} du = \int_0^{\dot{u}} m \dot{u} d\dot{u} = \frac{1}{2} m \dot{u}^2 \quad (5.6)$$

Together with the restoring force  $f_S$  and damping force  $f_D$  the mass inertia  $f_I$  are resisting the motion induced by an external effective force  $P_{eff}$ .

According to the first law of Newton, mass inertia force resists the forced motion and the forced state of rest. Therefore, the inertia force, together with the restoring force and damping force are internal forces that always resist the external forces, since the system is a forced vibration system. However, in a free vibration system, mass inertia forces resist internal restoring forces  $f_S$  when motion is triggered by the stiffness potential of the oscillated column. Meanwhile, mass inertia force also triggers motion since mass has gained acceleration as returning to its original position. Thus a fluctuating manner of forced and resisting modes of motion is found in the free vibration system.

In a damped inelastic structural system, both yielding and damping energy dissipate all the seismic energy at the end of the earthquake excitation event. This is true since the kinetic energy  $E_K$  and recoverable strain energy  $E_S$  diminish near the end of the ground shaking

process [3]. This can be proved for a steady state motion of a SDOF elastic system represented by a mass-spring-damper system [3].

From personal practice,  $f_y$  can also be defined by drawing the recoverable strain energy  $E_S$  that shows the best diminishing level of energy by end of the time history of the dynamic analysis. This is done by first assigning a trial-and-error value for  $f_y$  in the energy calculations, and then plotting the recoverable strain energy  $E_S$  that fits the best diminishing energy value at the curve end. Even though this was successful for some dynamic problems but it was also very sensitive to the number of hysteretic loops and load intensity of the problem. Therefore, no theoretical evidence could be obtained to support this technique, and it may not be reliable for all cases.

### 5.2.2 Damping Forces & Energy

Dampers are special devices that mitigate a structure's velocity response. They also play a vital role in absorbing the seismic shock, thus a large part of the seismic energy is dissipated by the damper. However, damping forces can also be produced by the internal friction of material's particles and the bond frictional forces between reinforcement bars and the concrete [7].

In general there are three types of dampers; viscous and viscoelastic dampers, metallic dampers and friction dampers [3]. A useful quality in damping devices is that destroyed dampers can easily be replaced by new substitutes at the retrofit of a structure. This gives a significant flexibility for designers to work for a performance-based seismic design with lower rates of strength and ductility.

The damping energy can be determined as follows:

$$E_D = \int_0^t f_D \dot{u} dt = \int_0^t c \dot{u} \dot{u} dt \quad (5.7)$$

### 5.2.3 Accumulated Energy Curve

In general, energy quantities express the work done by each resisting force, and can be represented as follows:

$$E_I = E_K + E_D + E_S + E_Y \quad (5.8)$$

where,  $E_I$  is the energy input for the structure since the earthquake excitation begins, and can be expressed in terms of the effective forces  $p_{eff}$  which can be alternatively applied on the c.g. of a SDOF structure as equivalent to the ground excitation as follows:

$$E_I = - \int_0^t p_{eff} \dot{u} dt = - \int_0^t m \ddot{u}_g \dot{u} dt \quad (5.9)$$

It is good practice to compute and plot the accumulating energy quantities versus time of analysis, when it is desirable to find out the contribution of each force-type to resist the seismic demand during the earthquake event.

### 5.3 DAMAGE CURVES BASED ON HYSTERESIS OF THE STRUCTURE

Sadeghi [8] introduced a method of assessment of global damage for structures, based on the global degradation of strength in structures under cyclic loading. This can be detected from the hysteresis representation, which is a load-deflection relationship represented by the displacements of the top of the structure and the base shear forces at the bottom of the structure.

From the graph of hysteresis loops, the area under the first loop represents the dissipating energy that could cause the first damage. The following loops with strength degradation indicate occurrence of successive damages. When the structure is unloaded some of this energy is recovered, and the rest of it is absorbed by the structural stiffness potential, but the damage would retain as it first occurred. It should be noted that damage is a residual quantity, and cannot be partially or fully recovered or recurred when energy or some of the energy is recovered.

The relationship between those three kinds of energy can be formulated in an inelastic system as follows:

$$E_{Absorbed} = E_{Dissipated} - E_{Recovered} \quad (5.10)$$

In general, a structure absorbs all of the dissipated energy unless some of it gets recovered by an un-loading process. For the purpose of simplification of this concept, three theoretical assumptions of hysteresis are now introduced, and the load-deflection curves are shown for one side only. Figure 5.5.a shows the dynamic load-deflection behaviour of an irrecoverable inelastic system with zero recovered energy,  $E_{Recovered} = 0$ . Figure 5.5.b shows the dynamic load-deflection behaviour of a fully recoverable inelastic system with zero energy absorption,  $E_{Absorbed} = 0$ .

Figure 5.5.c shows the dynamic load-deflection behaviour for an inelastic system with partial recovery, in which some of the dissipated energy is recovered and the rest is absorbed. The absorbed energy sustains a residual deformation  $R_d$  when the system is un-loaded until zero loading. Moreover, the absorbed energy increases and sustains a residual stress  $R_s$  when the

system is further un-loaded and returns back to its original position, i.e. at zero displacement. In both residual cases the damage potential exists unless all absorbed energy is fully recovered alike in the case of fully recoverable inelastic or elastic systems, as mentioned earlier.

Figure 5.5.d shows the dissipated, recovered and absorbed energy quantities on the second degraded hysteretic loop. It should be known that such degradation reflects the degradation of both stiffness and strength in the structure. Degradation of strength occurs usually in RC structures due to the initiation of fracture in concrete. This indicates that part of the dissipated energy is due to damage in the concrete, while in steel structures, for example, no strength degradation exists apart from stiffness degradation due to the yielding influence.

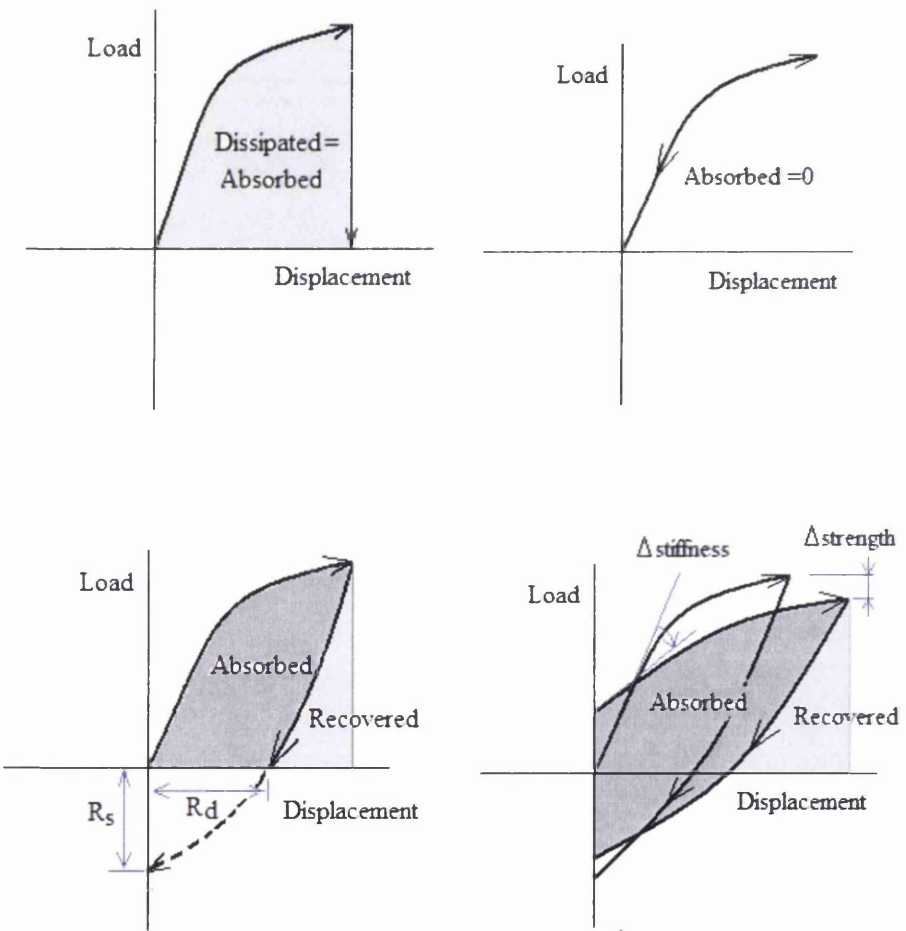


Figure 5.5 a) Full energy absorption b) Full energy recovery c) Partial energy recovery with residuals d) Degradation of stiffness and strength in successive loops.

To conclude and further explain, an important summary is given as follows:

- Hysteresis occurs when the state of a system (deformation) depends on its history of the environment (loading), as when dynamic loading is applied on elastic systems. This is

known as the Dynamic Hysteresis since loop area is proportional to the excitation frequency  $\omega$  [3], and thus, the load-deformation curve is hysteretic and not a single-valued curve, like when static loading is applied on elastic systems; i.e. no hysteresis loops since  $\omega = 0$ . Hysteresis, therefore, is due to the dissipation of energy in systems under dynamic loading.

- In elastic structures under dynamic loading, the energy is dissipated due to influence of viscous damping, kinetic and strain energy only. The hysteresis loops maintain their shape by having the same stiffness and same strength unchanged.
- Elastoplastic (or, inelastic) systems dissipate the input energy as they are loaded dynamically. They tend to retain absorbed energy and recovered energy when unloaded. These systems are partially recovered with residual deformations or, strains.
- In elastoplastic systems such as steel structures, the input energy is dissipated due to kinetic, strain and damping energy, in addition to (yielding) energy, which is reflected in the hysteresis graph by the ‘degradation of stiffness’.
- In structures such as RC members, the input energy is dissipated due to kinetic, strain, damping and (yielding) energy seen by ‘degradation of stiffness’, in addition to the (fracturing) energy seen by ‘degradation of strength’.
- Residual deformations  $R_d$  and residual stresses  $R_s$  sustain the potential of damage. When damage occurs in RC structures due to these residuals, it is not recoverable by any recovered energy with further unloading process. Therefore, it is possible to record such damage at every newly dissipated energy, regardless of any further recovering of energy.
- As an exception to the previous rules, structures under quasi-static loading can be considered to have ‘dynamic hysteresis’ since they involve pseudo time with the applied cyclic loading during the analysis. The exception here is that damping, kinetic and strain energy do not exist since there is no real time involved in the calculations. This means that the hysteresis in quasi-static analysis for a RC structure is dissipating only (yielding) energy seen by the ‘degradation of stiffness’, in addition to the (fracturing) energy seen by ‘degradation of strength’. Both of these energy quantities are referred to in the literature as (yield) or (hysteretic) energy.
- An important result that will be concluded in the following sections is that both dynamic and quasi-static analysis can have close quantities of the dissipated energy since strain, kinetic and viscous damping in RC box-girder bridge columns are not relatively large, and the yield energy has the major contribution in dissipated energy.



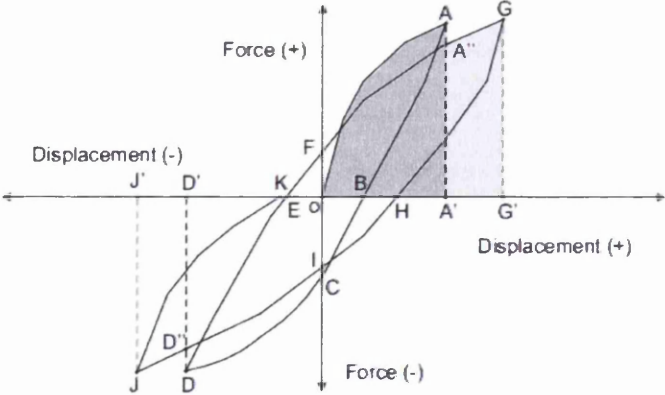
Back to Sadeghi's method of assessment of global damage, the damage is now determined as it corresponds to energy dissipation before any energy recovery takes place. This is necessary since no damage is recovered even when part of the energy is recovered, or when:

$$E_{\text{Absorbed}} = E_{\text{Dissipated}} \tag{5.11}$$

The global damage index  $D_i$  for any loop cycle (i) is defined as the ratio between the summation of the dissipating energy  $E_{d,i}$  and the total energy dissipated by the system for all cycles (n), or summation of  $E_{d,n}$ , or:

$$D_i = \frac{\sum_i E_{d,i}}{\sum_n E_{d,n}} \tag{5.12}$$

Figure 5.6 shows two hysteretic cycles from which the damage can be determined for each time step. The dissipated energy  $E_{d,1}$  for the first cycle is the area under the curve OAA', and the dissipated energy  $E_{d,2}$  for the second cycle is the area under the curve A'A''G G'. The sum of the dissipated energy until the last cycle must be the area under all those limited curves in the shown primary half cycle PHC [8]. The global damage index can be determined for each side of the oscillation axis of the structure. In inverted pendulum structures such as bridge columns, each side should represent the global damage in the structure since the energy dissipation is the same in both sides with cyclic loading of a quasi-static analysis.



**Figure 5.6** Damage as corresponding to the dissipating energy before recovery, on one side of the hysteresis [8]

The global damage index can be graphed versus the lateral displacement or rotational curvature that causes the damage value at each progressive movement. The damage index can also be graphed versus the time-step of the analysis, bearing in mind that only those time-steps with the progressive movements are considered, and not those at the un-loading processes or those occurring on the other side of the oscillation axis. It is also important to

know that the damage index is plotted versus pseudo time abscissa since it is exhibited for a structure under quasi-static analysis.

In following section, Sadeghi’s method to produce an energy-based damage curve [8] is applied. The global damage is calculated for a RC bridge column structure exhibiting an oscillation movement due to a cyclic loading effect. The steps for calculating the global damage from a hysteresis curve are written in a MatLab program, and documented in Appendix [B].

### 5.4 CASE STUDY 1: NUMERICAL ANALYSIS

A designed RC bridge column with aspect ratio AR=6 and geometric properties shown in Figure 5.7, is selected from an analytical research study on 8 different column structures [9], which have the same section geometry and reinforcement but vary in the aspect ratio AR ranging between 3 and 10. To determine the damage curve for this column, a hysteresis analysis is required with cyclic loading in a quasi-static non-linear analysis. The global damage of the structure under any applied seismic loading can then be determined.

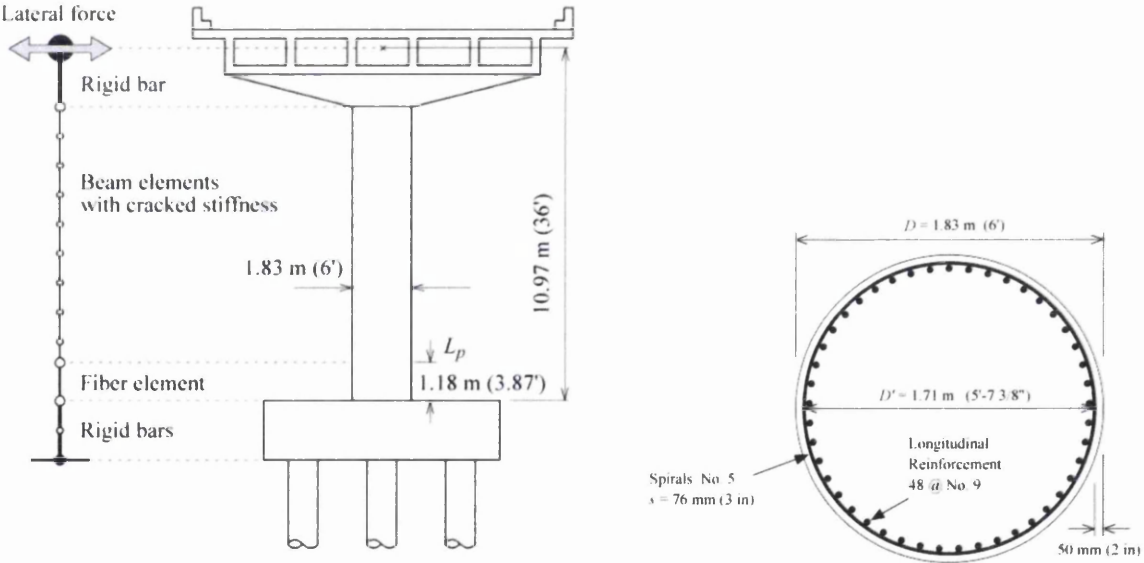


Figure 5.7 Designed RC bridge column [9]

The RC bridge columns are designed according to the Seismic Design Criteria SDC of the California Dept, of Transportations (Caltrans 2001) [9]. The SDC for a single-column bent is defined based on the demand/capacity principle, which assumes the displacement demand  $d_D$  is less than the displacement capacity  $d_C$ , or:

$$d_D < d_C \tag{5.13}$$

It should be noticed that the displacement capacity  $d_D$  is associated with the assumption of a plastic hinge of length  $L_p$  measured from the column base. The plastic displacement is:

$$d_p = \theta_p \left( h - \frac{L_p}{2} \right) \quad (5.14)$$

where,  $\theta_p$  is the plastic curvature capacity and  $h$  is the column height.  $L_p$  is calculated based on Priestly et al.(1996) [9], and equals 1.18 m for this column with aspect ratio = 6. For columns with aspect ratios 3 and 10,  $L_p$  is 0.74m and 1.76m respectively. The local damage spreads in a larger area as the aspect ratio increases but not necessarily being more intensive.

The RC bridge column structure has the following properties; aspect ratio  $h/D = 10.97\text{m}/1.83\text{m} = 6$ , natural period  $T_n$  of its 1<sup>st</sup> mode is 1.3 sec, where  $D$  is the column diameter and  $h$  is the height between the footing and the centre of gravity C.G. of the top mass. The column is subjected to an axial load of 4.5 MN, which is the dead load, and equivalent to 5% of its strength capacity. It has a longitudinal reinforcement ratio of 1.18% and a transverse reinforcement ratio of 0.61% [6].

**5.4.1 RC column Under quasi-static loading**

The RC column with aspect ratio 6 is subject to a quasi-static displacement cyclic loading that's imposed on the C.G. of the superstructure. The imposed displacement amplitudes in the first cycle  $d_{y1}$  and last (5<sup>th</sup>) cycle  $d_{y5}$  are 5 inches (0.127m) and 25 inches (0.635m), respectively.  $d_{y5}$  is estimated to be close to the ultimate lateral displacement of the column  $d_u = 0.58$  m (23 inches).

For the proposed problem, a good agreement with the published hysteretic loops by Sakai and Mahin [9] is obtained. However, some differences in the base-shear forces are found. This is due to the difference between the distributed-mass inelasticity method, implemented with Force-Based formulation with Plastic Hinge (FBPH) in the Seismostruct solver, and the variety of lumped-mass rigid elements, beam elements and fibre elements implemented in the analytical model by Sakai and Mahin [9], as previously shown in Figure 5.7.

Figure 5.8 shows the hysteresis for the RC column obtained by the Seismostruct. The capacity of the column is limited at the 5<sup>th</sup> hysteretic loop, and the column's degradation of strength and stiffness depends on the member's state of loading, geometry, properties and boundary context. The quasi-static analysis is important to determine the capacity of the column, its strength degradation and stiffness degradation.

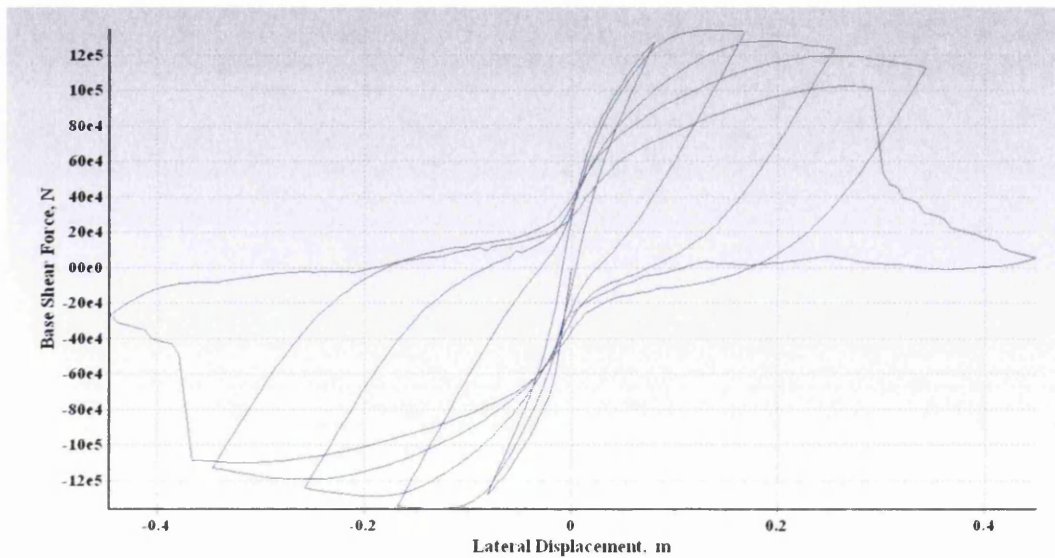


Figure 5.8 Hysteresis curve for R/C bridge column with aspect ratio 6.

There are many aspects of the column capacity that can be determined from the hysteretic behaviour. The most important aspects are shown in Table 5.1 [9].

	Aspect ratio $h/D$	Natural period $T_n$	Yield limit displacement & strength		Ultimate limit displacement & strength		Residual displacement by JRA		Ductility Demand < Capacity	
			$d_y$	$F_y$	$d_u$	$F_u$	$d_r$ with $\mu_d$	$d_r$ with $\mu_u$	$\mu_d$	$\mu_u$
SDC	6	1.26	0.112	1.3MN	0.58	1.3MN	-	-	4.15	5.19
JRA		1.26	0.112	1.3MN	0.58	1.3MN	0.21 (1.92%)	0.28 (2.56%)	4.15	5.19
Quasi-static Analysis		1.30	0.127 (5 in)	1.16MN	0.635 (25in)	1.44MN	-	0.434 (3.95%)	4.15	5.0

Table 5.1 Capacity limits for R/C column [9].

These capacity aspects obtained by the quasi-static analysis are found approximately in agreement with those calculated according to Caltrans Seismic Design Criteria (SDC), and those calculated according to the Japanese Road Association JRA. In addition, the accumulated energy dissipation throughout all the cycles is 3.52 MN.m, and the ratio of the post-yield stiffness to the initial stiffness is  $\kappa_{py}=3.9\%$ .

#### 5.4.1.1 Global Damage (Energy-Based Approach)

The quasi-static analysis is also used to obtain the global damage curve for the column, based on the principle of energy dissipation, by using the method adopted from the work of Kabir

Sadeghi [8]. In this method the work done for every time-step, also the dissipated energy  $E_{d,i}$ , which is calculated for each additional displacement in one oscillation side of the structure, and its accumulation is divided by the total work done, or the total dissipated energy  $E_{d,n}$ , at that side only. Recalling the global damage index:

$$D_i = \frac{\sum_i E_{d,i}}{\sum_n E_{d,n}} \tag{5.12}$$

Figure 5.9 shows the global damage curves for three R/C bridge columns, with aspect ratios of 3,6 and 10. For every displacement, the global damage increases as the aspect ratio decreases. This indicates that structural columns with higher aspect ratios  $h/D$  have lower ductility values  $\mu_u$ , which make them less vulnerable to high damage rates. As shown in Figure 5.9, less damage rates are experienced with structures having lower ductility values  $\mu_u$ , at higher aspect ratios.

As known from RC sections, ductility is inversely proportional to the longitudinal reinforcement ratio  $\rho_l$ , but in this case study, both geometry and reinforcement of the column section are held constant for all analyses, and the change in ductility is due to the change in the aspect ratio. Consequently, a higher damage rate is experienced as ductility increases in lower aspect ratios, which imposes shorter natural periods  $T_n$ , or;

Lower aspect ratio $\rightarrow$ Shorter $T_n$ $\rightarrow$ Higher ductility $\rightarrow$ Higher damage	(5.15)
---	--------

**5.4.1.2 Local Damage (Stress-Based Approach)**

In this analysis, Figure 5.10 shows large tensile strains in both cover and core selected concrete fibres with approximately zero fibre strength, indicating total theoretical fracture due to tensile forces. At compressive strains, cover fibre stresses start softening after passing the un-confined concrete stress  $\sigma_{ult} = -34.0$  MPa, and processing un-loading and re-loading cycles until fibre approaches total failure at approximately a strain of -0.05. In the core zone, fibres are less damaged at -0.05 strain, reaching -26.0 MPa after 4 hysteretic loops. Softening starts after the core fibres pass the ultimate strength of the confined concrete core  $\sigma_{ult} = -44.0$  MPa.

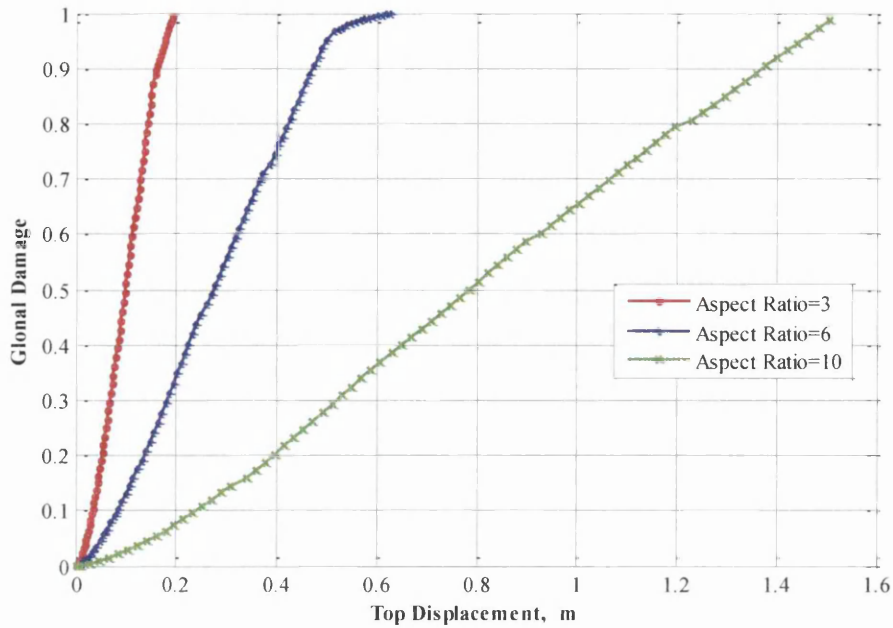


Figure 5.9 Global damage curves in R/C bridge columns, with 3,6 and 10 aspect ratios.

Local damage  $d_i$  needs to be determined independently for any required fibre point in the column section. Only the compressive damage can be calculated by using these fibre stress-strain curves, since that fibres under axial tensile stresses are, theoretically, fully damaged at very early time steps. It is important to know that tensile stresses can cause a great damage threat to the column core if the energy due to flexural failure is not sufficiently dissipated by the reinforcement longitudinal bars.

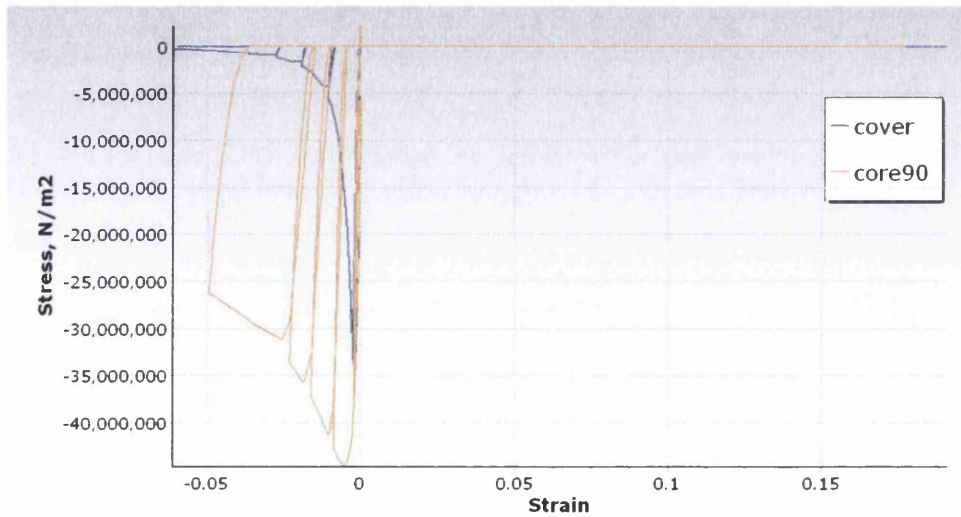


Figure 5.10 Stress-strain curves for selected fibres at cover and 90% of core radius, for a RC column with aspect ratio =6 under quasi-static analysis.

A Local compressive damage curve for concrete fibres is now introduced. This damage is based on the ratio between axial compressive stresses and the ultimate strength of concrete,



and can be obtained during the softening straining of the analysed fibres, as in the following equation:

$$d_i = 1 - \frac{\sigma_{i,fibre}}{\sigma_{ult}} \quad (5.16)$$

where  $i$  is the time-step or pseudo time in a hysteretic analysis of the column. When  $d_i$  equals 1, the fibre has lost its strength and is not capable of resisting any more axial compressive stresses, indicating a local totally damaged state under compression. Local damage curves are obtained using a MatLab programming code according to the local stress concept. The code is listed in Appendix [C].

Figure 5.11 shows the capacity of local compressive damage curves for selected fibres from the core and cover zones of the column section for a 6-aspect ratio column. The maximum local damage value, due to compressive stresses at 90% of the core radius, is about 0.28. At further inner core fibres, 80%, 70% and 60% of the core radius, much lower damage rates are found, indicating the local fracture state inside that column core section. On the peripheral zone of further inner core tips, there could be some fibres with no damage at all.

At the cover of the base zone, compressive stresses are very high, and its local damage reaches 0.9 at early stages in most cases. The local damage due to the axial tensile stresses of the fibres is not computed, since it theoretically, reaches unity at very early time steps, as previously mentioned.

#### 5.4.1.3 Damage Assessment

The previously determined global damage  $D_i$  curve is now plotted again in Figure 5.11 versus pseudo time, together with the local damage  $d_i$  curves for the same column analysis. It is obvious that the global damage curve is an intermediate between the two local damage curves of the cover and core fibres, representing the global behaviour for the whole structure. Cover fibres tend to damage severely in compression at relatively early time steps, while core fibres tend to have minor damages under compression. Being in the intermediate range of the damage curves, the global damage curve expresses the overall possible damage intensities in the core and cover due to both compressive and tensile stresses, which is accepted from a logical point of view.

Based on this index, global and local damage intensities can be determined for the same structure under any seismic loading, as will be shown in Figure 5.11. Such an approximation is useful for seismic assessment purposes, but more investigation is still needed concerning the initiation and growth of local damage in the section core.

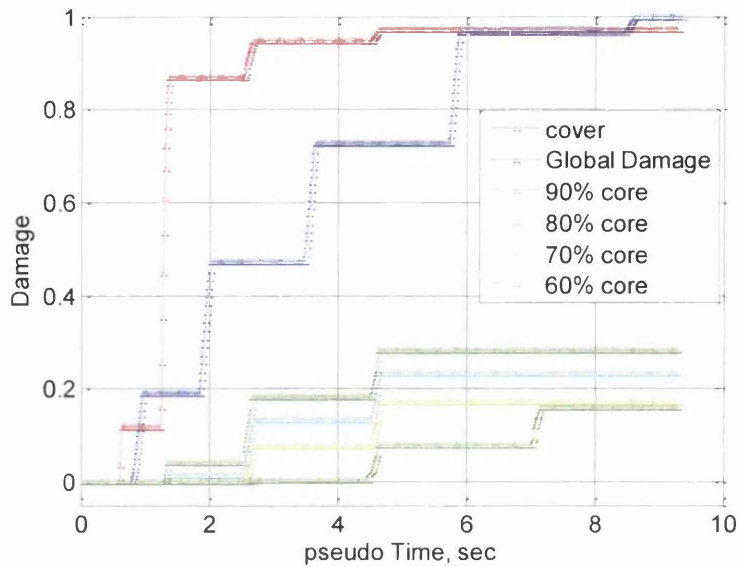


Figure 5.11 Capacity of local & global damage index vs. pseudo time for a quasi-static non-linear analysis of R/C bridge column with aspect ratio =6.

## 5.4.2 RC Column Under Dynamic Loading

Sakai and Stephen A. Mahin [9] conducted 80 seismic non-linear analysis runs, using lumped-mass frame elements, to determine the ultimate and residual responses for 8 single R/C bridge columns, with the aspect ratios 3,4,5,6,7,8,9 and 10, subjected to 10 different strong motion earthquakes.

For simplicity, only 3 non-linear analyses have been conducted using the SeismoStruct, to analyse the RC columns with the aspect ratios 3,6 and 10, being subjected to one single earthquake, which is the Loma Prieta earthquake in 1989, shown in Figure 5.12.a. The ground motion is a near fault Lexington Dam Record, with  $PGA = 6.73 \text{ m/sec}^2$ , Epicentral distance=6.3 and magnitude of 7.0.

The hysteretic curves of these analyses, performed by SeismoStruct, proved a reasonable agreement with the published curves. Dynamic hysteresis in Figure 5.12.c for the structure with aspect ratio 6, subjected to Lexington Dam Record showed a reasonable agreement with the analysed curve in Figure 5.12.b. It should be noted that the base shear forces are computed by dividing the base moment by the height,  $f_s = M/h$ , and displacements are obtained by multiplying curvature by the height,  $d = \theta \cdot h$ .



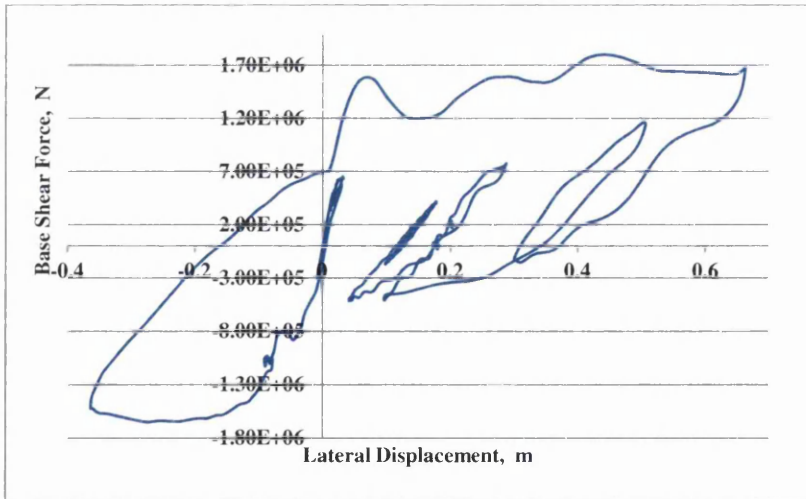
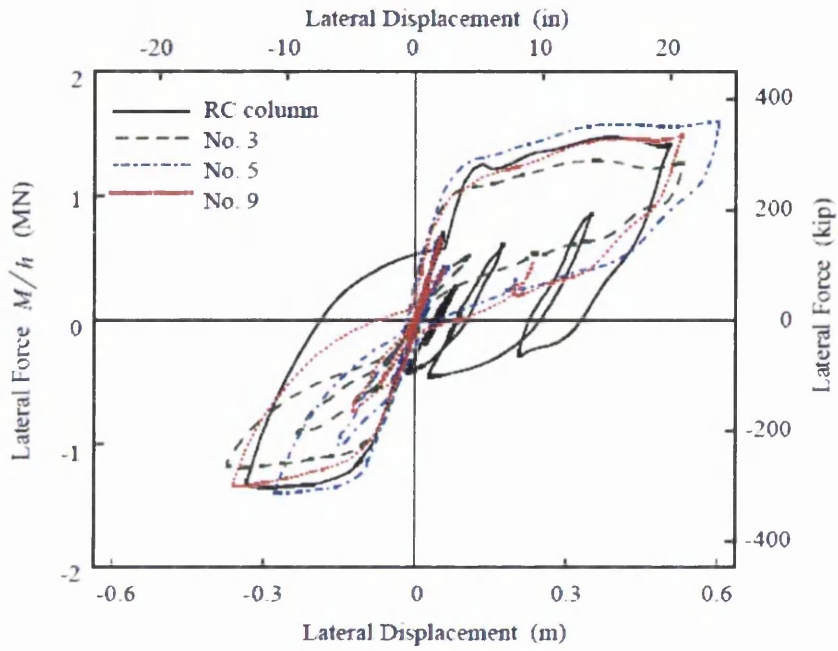
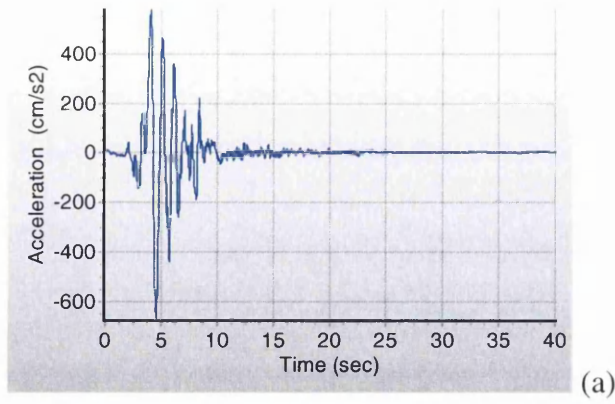


Figure 5.12 a) Lexington Dam record. b) Load-Deflection curve [9], c) Load-Deflection curve by Seismostruct

Table 5.2 shows some of the results obtained by the analytical models made by Sakai and Mahin [9] for the RC column with the aspect ratios 3,6 and 10, when subjected to 10 different strong motion seismic records.

Selected Strong motion Earthquake	Record	Magni-tude	Epic-entr-al Dist-ance (km)	PGA,g m/s <sup>2</sup>	Max & Min Ultimate Displacements $d_u$ (m)			Max & Min Residual Displacements $d_R$ (m)		
					AR= 3	AR=6	AR=10	AR= 3	AR=6	Aspect Ratio varies
					SDC Ultimate Capacities					
					0.173	0.58	1.485			
Tabas, Iran, 1978	Tabas	7.4	1.2	0.90g	0.07	0.32	0.70	0.002	0.004	0.035(AR=8)
Loma Prieta, USA, 1989	Los Gatos	7.0	3.5	0.72g	<u>0.15</u>	<u>0.60</u>	1.45	0.002	0.015	0.08(AR=9)
Loma Prieta, USA, 1989	Lexington Dam	7.0	6.3	0.68g	<u>0.20</u>	<u>0.53</u>	0.90	0.001	0.043	0.06 (AR=10)
Cape Mendocino, USA, 1992	Petrolia	7.1	8.5	0.64g	0.10	<u>0.47</u>	0.80	0.005	0.038	0.037(AR=6)
Erzincan, Turkey, 1992	Erzincan	6.7	2.0	0.43g	0.05	0.40	0.62	0.003	0.012	0.03(AR=4)
Landers, USA, 1992	Landers	7.3	1.1	0.71g	0.05	0.24	0.72	0.0	0.018	0.05(AR=7)
Northridge, USA, 1994	Renaldi	6.7	7.5	0.89g	<u>0.25</u>	0.44	0.53	0.0015	0.013	0.015(AR=6)
Northridge, USA, 1994	Olive View	6.7	6.4	0.73g	0.05	0.41	0.55	0.001	0.0175	0.03(AR=6)
Hyogo-ken Nanbu, Japan, 1995	JMA Kobe	6.9	3.4	1.08g	<u>0.25</u>	0.37	0.71	0.001	0.019	0.07(AR=9)
Hyogo-ken Nanbu, Japan, 1995	Takatori	6.9	4.3	0.78g	<u>0.20</u>	<u>0.66</u>	0.60	0.0	0.016	0.02(AR=5)

Table 5.2 Max & Min responses for the R/C column with aspect ratios 3,6 and 10, under 10 different strong motion seismic records [9].

The capacity of all columns was evaluated according to the SDC, and gave ultimate displacements of 0.173m, 0.58m and 1.485m for columns with 3, 6 and 10 aspect ratios respectively. Table 5.2 shows ultimate displacements under 10 seismic records loadings. The underlined values fall very close to the SDC capacity range or exceed it. This shows that the responses under strong motion records could affect the concrete core intensively, and plastic hinges would not be limited to spalling only but could get extensively damaged.

The residual displacements evaluated according to the Japanese Design Specifications for columns with AR between 3 and 10 are between 0.09m (1.58% drift ratio) and 0.71m(3.86% drift ratio) respectively. But all of the residual displacements obtained under the 10 seismic

records loadings have drift ratios much below 1%, which is the maximum allowable value for bridges according to the Japanese Design Specifications made by the JRA. In practice, this makes less need to improve the design for better residual displacements, and encourages more research to control the ultimate displacements.

Figure 5.13 shows the global damage curve for a RC column with AR=6 reaching high damage index when approaching its ultimate capacity. The seismic loads with low responses on this column, like Landres (0.71g, 0.24m) and Tabas (0.90g ,0.32m) cause medium global damages of 0.4 to 0.6 respectively. Seismic loads with severe responses on this column, like Lexington Dam (0.68g, 0.53m) and Takatori (0.78g, 0.66m), cause large global damages over 0.9. The rest of the records show global indices over 0.75. This indicates that most of the selected records cause a total collapse of the structure, leading to the fact that more investigations should be carried out, concerning the local damage due to both tensile and compressive stresses at the core zone of the column base.

Another important observation is that, records with relatively high PGA, like Tabas (0.90g) and Landres(0.71g) caused relatively small displacements; 0.32m and 0.24m respectively, whereas records with relatively low PGA, like Lexington Dam (0.68g) caused relatively larger displacements; 0.53m. This may be attributed to the phenomenon of acceleration pulse and acceleration spike, where long duration impulses and low frequency have the potential to cause displacement responses, more than those records having similar or even lower PGA's but with relatively short duration impulses and higher frequency.

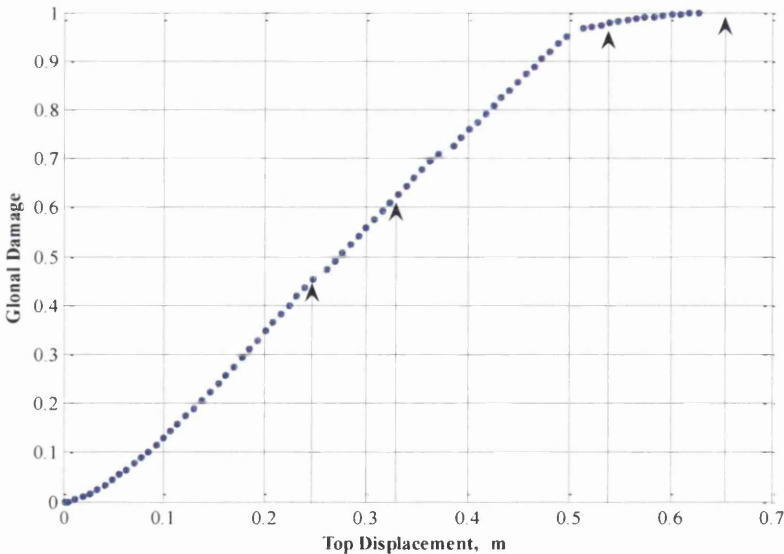


Figure 5.13 global damage intensities vs. displacement response of analysing R/C bridge column structure with AR=6, subject to Landres(0.24m), Tabas(0.32m), Lexington Dam(0.53m) and Takatori(0.66m).

## 5.5 CASE STUDY 2: SHAKING TABLE EXPERIMENT

As previously mentioned in section 5.1.2, this experimental test was conducted to investigate the effects of multi-directional seismic excitation on the dynamic response of RC bridge columns. Applied forces are the ground motions recorded near the Tsugaru Bridge during the 1983 Nihonkai Chubu earthquake in Japan.

The elastic limit capacity  $f_y$  was obtained for the RC circular column using a quasi-static analysis, and reached 100kN (0.1 MN) for this structure, which is also known as the flexural capacity of the structure [2].

In this test, the crack growth events have been observed on the column base in Figure 5.14, and carefully recorded in details in Table 5.3 [2].

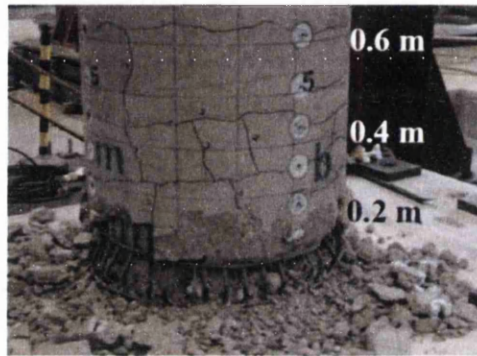


Figure 5.14 Damage at column base [2]

Points	Time (sec)	Distance	Disp. in X	Disp. in Y	Events observed at Xp and Xn faces
1p	7.500	0.050 m	0.046 m	0.019 m	Several cracks
1n	7.875	0.077 m	-0.065 m	-0.040 m	Several cracks
2p	8.635	0.034 m	0.034 m	0.004 m	Propagation of cracks
2n	9.125	0.090 m	-0.088 m	-0.014 m	Propagation of cracks
3p	9.630	0.091 m	0.084 m	-0.035 m	Propagation of cracks
3n	10.225	0.096 m	-0.093 m	0.022 m	Slight spalling at Xn face
4p	10.885	0.085 m	0.056 m	-0.063 m	
4n	11.425	0.090 m	-0.083 m	0.035 m	
5p	11.990	0.104 m	0.103 m	0.014 m	Slight spalling at Xp face
5n	12.520	0.123 m	-0.113 m	-0.048 m	
6p	13.195	0.108 m	0.108 m	0.012 m	Spalling at Xp face
6n	13.760	0.143 m	-0.139 m	-0.034 m	Spalling at Xn face
7p	14.410	0.150 m	0.147 m	-0.027 m	Buckling of rebar at Xp face
7n	15.120	0.154 m	-0.154 m	-0.008 m	Severe spalling at Xn face
8p	15.765	0.196 m	0.192 m	0.040 m	
8n	16.375	0.188 m	-0.188 m	0.005 m	Fracture of rebar at Xp face and buckling of rebar at Xn face

Table 5.3 Peak displacements and damage events in the x-direction [2].

From this table, the specimen experienced different damaging events as the lateral displacement response had increased. When the x-displacement response reached 0.147 m buckling of rebars started to occur, and at 0.188 m fracture of rebars started to occur. When



the displacement exceeded 0.20 m 22 of 40 longitudinal bars were fractured, and the core concrete was completely crushed at the bottom of the column [2]. These results are quite important for more understanding of the damage states of the core concrete and reinforcement bars under the seismic loading.

Figure 5.15 illustrates a hysteretic curve for the tested specimen in the x-direction, showing the peak displacements on the two sides of oscillation of the x-direction. The hysteretic loops are limited by the flexural capacity of the structure, 100kN, and by the maximum displacement, 0.192 m, which was reached at point 8p as shown.

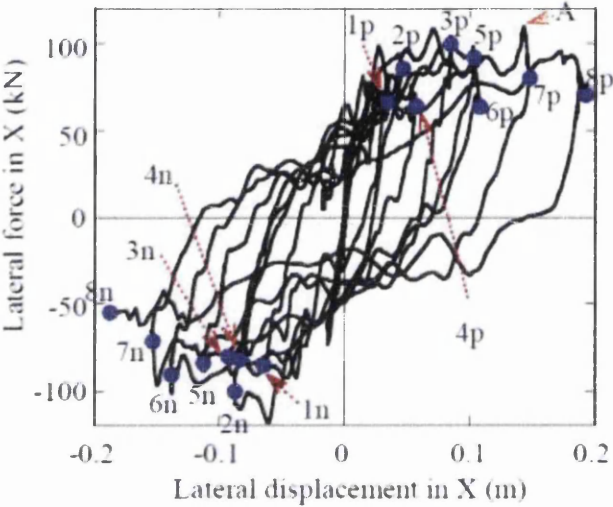


Figure 5.15 Hysteretic curve by the experiment [2]

A numerical analysis has been conducted using the SeismoStruct dynamic solver for this problem, and approximate results have been attained. The base shear in the hysteretic loops shown in Figure 5.16 is the base moment divided by the height,  $f_s = M/h$ , and the displacement is the curvature multiplied by the height,  $d = \theta \cdot h$ .

By drawing the energy curves, useful conclusions can also be attained concerning the behaviour of the hysteretic energy curve as crack growth increases.

**5.5.1 Accumulated Dissipating Yield Energy Curve**

As previously discussed, the hysteresis loops can express both dissipating and recovering energy during the loading and un-loading responses respectively. The difference between the two energy quantities is the absorbed energy. If the dissipating and recovering yield energy quantities are computed for one side of the column oscillating motion only, approximately half of the absorbed yield energy is attained.

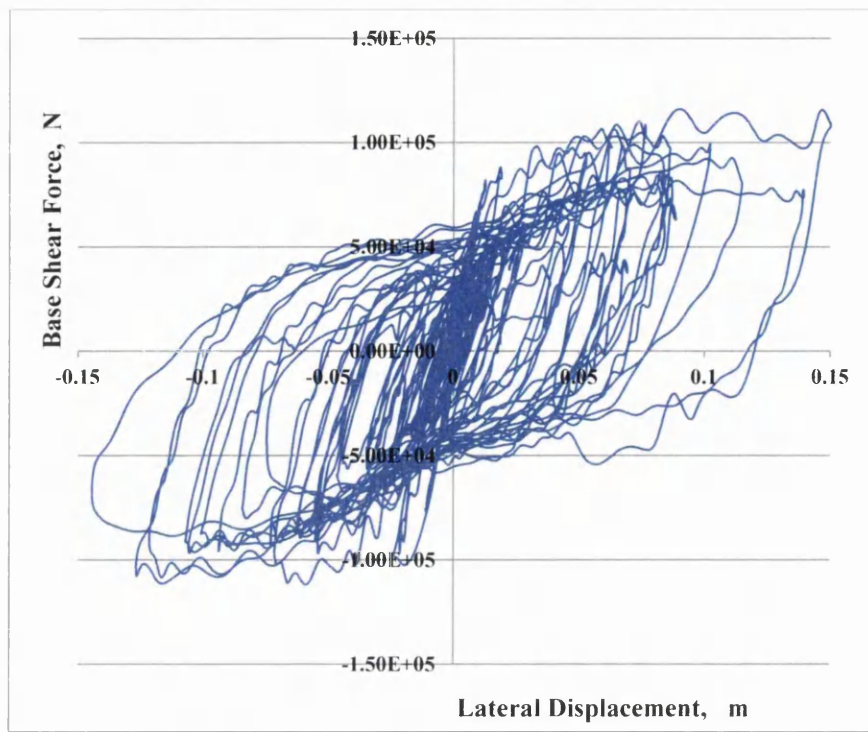


Figure 5.16 Hysteresis loops by SeismoStruct

If only the dissipated energy is computed for one side, this will express all stages of the stiffness resistance of the column, including the elastic, hardening and crushing behaviour, excluding the recovering consequences of the un-loading motion. Therefore, it is more proper to compute only the dissipating yield energy for one side in order to be able to differentiate between the different stages of damage, and also be able to define the yield energy domain that is responsible for the most severe damage. Definition of such an energy amount will give more understanding of the damaging behaviour, and therefore, more approximation of the capacity of a seismic isolation device might be determined to effectively mitigate the response of the substructure.

However, definition of the dissipating yield energy for this purpose will require computing the accumulating dissipated yield energy in an ascending-order basis, i.e. the dissipating yield energy values must be summed up in an order that is corresponding to an ascending order of the displacement values. This has been performed by processing the output data attained from the dynamic analysis for the column, and have them written in a MatLab program as listed in Appendix [D].

### 5.5.2 Yield Energy Curves and the Damage State in the Shaking Table Experiment

It is well known that the damage in the plastic hinge zones is the result of dissipation of the yield energy of the column. Therefore, useful conclusions can be attained concerning the behaviour of the hysteretic curves as crack growth increases.

From the global hysteresis curve obtained by the numerical analysis for this problem, the accumulated absorbed yield energy can be calculated as equal to the area enclosed within the hysteretic loops. As mentioned before, the absorbed energy is equal to the dissipated energy performed by the loading process minus the recovering energy which is performed by the unloading process of the column. The total accumulating absorbed yield energy which is performed along the x-axis reached  $2.30E05$  N.m at the end of the analysis.

The dissipated yield energy that has accumulated on one side of oscillation along the x-axis reached approximately  $1.0E05$  N.m at the end of the analysis. Another energy curve has also been processed for the one-side dissipated yield energy but with a different path of energy accumulation, that's corresponding to an ascending order of displacements on the same oscillation side, as shown in Figure 5.17.a. The same energy curves, with both normal order and re-ordered energy paths are also plotted but versus the displacement along the x-axis and for the same side of oscillation, as shown in Figure 5.17.b. These energy curves have been constructed by the MatLab program listed in Appendix [D] as mentioned. The one-side re-ordered dissipated energy curve can be useful to classify the different stages of damage experienced by the column on that side, and determine their corresponding scalar quantities of the dissipating yield energy that's computed on the same side.

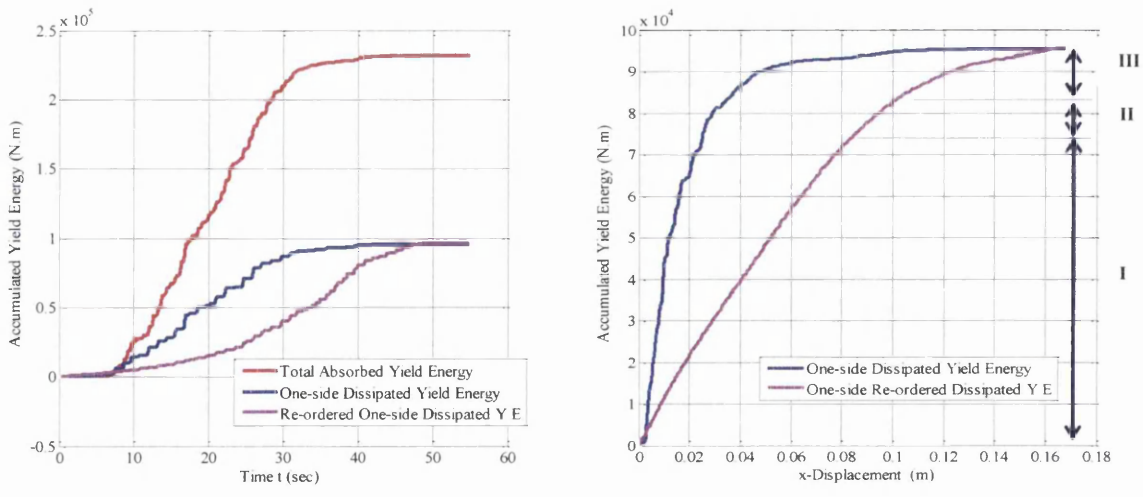


Figure 5.17.a & b Accumulating yield energy versus time and x-displacement.

From the previous Displacement-Damage Table 5.3, classification of damage states can be done by selecting the different damage limits that are denoted by the peak points on the “positive” side of the column, and expressed as “p”. The corresponding displacement values are used to classify the dissipated yield energy curve according to those damage limits. This should provide a reasonable approximation of the quantity and percentage of the dissipating energy that the column can have for different damage states. From the displacement of 0.0 to 0.084 m at peak point “3p” is the stage of “initiation and propagation of cracks”. From the displacement 0.084 m to 0.108 m at peak point “6p” is the stage of “slight spalling”. From 0.108 m to 0.192 at peak point “8p” is the stage of most of the severe damage states that includes “severe spalling, rebar buckling, severe spalling and fracture of rebars”.

One of the important conclusions that could be attained from the energy curve in Figure 5.17.b, is that the amount of dissipating energy corresponding to the last stage, state (III), described as “severe damage” reaches 1.00E04 N.m is approximately 10.5% of the total accumulating yield energy performed on this side. Therefore, if the damages are approximately symmetric on both sides of the column, this rate remains the same and would be responsible for such severe damages in the column, along the x-axis of the column oscillation motion.

The less damaging stage on the curve is state (II), which is the stage of “slight spalling” has shown a dissipating yield energy of approximately 1.20E04 N.m, which is about 12.5% of the total energy on one side of the column. Therefore, if the damages are approximately symmetric on both sides of the column, this rate remains the same and would be responsible for the “slight spalling” along the x-axis of the column oscillation motion. Consequently, the remaining 77% of the total dissipating yield energy, is therefore responsible for the least damaging stage, or state (I), along the x-axis of the column motion, which is the “initiation and propagation of cracks”. Table 5.4 summarises these conclusions. It should be noted that there are small differences between the numerically obtained results and the experimentally obtained results especially at large displacements in which experimental displacements reached 0.192 m, but numerical displacements reached only 0.165 m.

It should be also noted that the assumption of considering symmetric energy dissipation and damages on both sides of the RC column is an approximation due to the symmetry of the cyclic loading, since the damage may differ on each side due to the uncertainty of damage growth in concrete. However, very slight differences of energy dissipation can be observed on the two sides in the experimental test of Azizinamini et al [1], as was shown in Figure 5.1.b.



	Displacement Limits at x-Direction	Damage State	Dissipating energy on one side	Rate of dissipating energy on one side
State (I)	0 – 0.084 m	Initiation and propagation of cracks	7.3E04 N.m	77%
State (II)	0.084 – 0.102 m	Slight spalling	1.2E04 N.m	12.5%
State (III)	0.102 – 0.192 m	Severe spalling, rebar buckling, severe spalling and fracture of rebars	1.0E04 N.m	10.5%
Total			9.5E04 N.m	

Table 5.4 Damage states at different dissipating energy rates

### 5.5.3 Discussion of Results

The specimen suffered severe damage at state (III), which was concentrated in a zone starting from the column base to a height of 0.25 m. The bar buckling and fracture occurred in between the hoops at 0.075 and 0.150 m from the column base, respectively. A number of 22 out of 40 longitudinal reinforcing bars were fractured, which occurred mostly at the X faces, and the core concrete was completely crushed at the bottom of the column [2].

Based on the design specifications for the Japanese Road Association (JRA 2002), the yield and ultimate displacement of the specimen are 0.016 and 0.055 m, respectively. However, the displacement response exceeded the ultimate displacement at state (I), and exceeded twice the ultimate displacement at states (II) and (III). The designed column suffered internal crack growth at its core, and the plastic hinge was severely damaged as mentioned. This proves that the RC column design failed to sustain an appropriate resistance to the seismic loading to meet a performance-based seismic design.

## 5.6 SEISMIC ISOLATION BEARINGS (SIB)

### 5.6.1 Introduction

One of the most practical solutions to resist seismic responses in Bridge Engineering is the use of Seismic Isolation Bearings (SIB) or Base Seismic Isolation Bearings. Seismic isolation in RC bridges is used in RC bridges, since they can maintain serviceability of the bridge after

it is subjected to an earthquake. There is a large variety of seismic isolation systems but Lead Rubber Bearings (LRB's) are widely used in bridge structures. This is due to their simplicity and the combined isolation/energy dissipation function in a single compact unit [10]. In general, connections between the substructure and superstructure in a bridge have one of three alternatives:

- Rubber bearing systems, which have partial isolation of the substructure and the superstructure. They may either have low damping natural RB, high damping natural RB or Lead Rubber Bearings LRB.
- Fixed bearing systems, which have monolithic complete integrity of the substructure and the superstructure, and
- Roller bearing systems, which have complete isolation of the substructure and the superstructure. Also known as friction-based, or sliding-based systems, such as the Eradi-quake and friction pendulum systems (FPS) [11].

The isolation bearings are installed in the connection position between the superstructure and the substructure. A large part of the seismic energy would dissipate throughout the isolation bearings, and a substantial amount of input energy is mitigated, with relatively smaller amount of energy taken by the sub-structure's stiffness and damping resisting forces. The performances of seismic isolation bearings in several application cases have shown success in reducing earthquake response on the structure [12].

One of the most important practical aspects of installing SIB fittings into existing bridges is that its cost is 30% of the cost of retrofitting [11]. Conventional retrofitting methods are based on strengthening and enhancing ductility of the existing substructures and are quite expensive and difficult to implement [11], but replacement of the vulnerable existing bearings by SIB is much more practical.

As shown in Figure 5.18, a LRB isolation device consists of two parts; the first part is an isolator, i.e. the rubber part, which works as a flexibility inducer that increases the natural vibration period of the structure away from the high-energy periods of the earthquake. The second part is the damper, or the lead plug, which functions as an energy absorber, or shock absorber, that retains energy and residual forces when unloaded. This device of combined materials reduces the applied seismic forces effectively [13], and is to be mounted on top of the column as a seismic isolator between the sub-structure and super-structure, as shown in Figure 5.18.

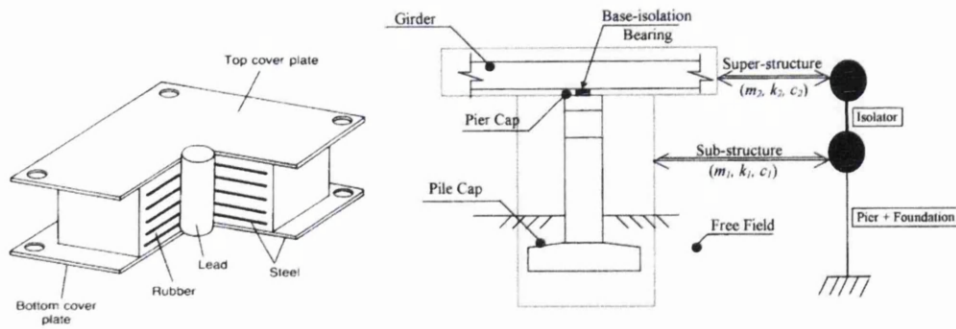


Figure 5.18 Elastomeric isolation LRB and position of installation

In general, LRB's allow for longitudinal and transverse movements, but in terms of design this movement is limited. There are two types of seismic isolation in terms of seismic restraints; bi-directional seismic isolation (BDSI) and partially restrained seismic isolation (PRSI), in which both ends of the superstructure are usually restrained in the transverse direction [14]. To restrict the transverse movement for the PRSI bridges, shear-rod stoppers are often used [14].

Another aspect of design in Bridge Engineering is limiting the superstructure movement to some allowable displacement limit in the transverse direction. Such a limit is necessary for the functionality of the bridge after the earthquake event, and is dictated by the building codes for seismic design. This is performed by installing lateral side stoppers [14], which would stop excessive lateral movements of the superstructure, and eventually, transfer more dissipative energy to the sub-structure.

To mitigate the earthquake response, rubber bearings have been used in railway and highway bridges [15], and it has been a task of controlling the mechanical properties of rubber and lead bars to successfully design the rubber bearings RB or lead-rubber bearings LRB, in order to sustain the vertical loading as well as to provide sufficient displacements to the superstructure, or provide sufficient damping [15]. Accordingly, the mechanical properties of the presumed isolation bearing can be summarized as vertical stiffness  $K_v$  and yield stiffness  $K_d$  which are represented by:

$$K_v = \alpha \frac{E_{cb}G}{A}, \quad K_d = \alpha \frac{K_{eq} - Q_d}{\delta} \quad (5.17)$$

where,  $\alpha$  effective,  $E_{cb}$  elastic modulus,  $G$  shear modulus respectively,  $A$  cross section area,  $K_{eq}$  equivalent stiffness,  $Q_d$  yield load,  $\delta$  shear horizontal deformation [15].

In numerical analysis using the Seismostruct package, the representation of such seismic isolation bearings is controlled by a linkage element that's installed between the sub-

structure and the super-structure, and given the mechanical properties of the rubber bearing RB or the lead rubber bearing LRB [16]. The mechanical behaviour of the linkage element in 3D representation should be assigned for the six degrees of freedoms DOF's of one node in relative to the other node of the linking element. These 6 DOF's are the bearing's forces and moments;  $F_1, F_2, F_3, M_1, M_2, M_3$ , for the principal coordinate directions 1,2 and 3 [16].

Each degree of freedom DOF is to be given the stiffness coefficient  $K$  that governs its motion in relation to the other node of the linking element.  $K$  is represented by a force-deflection curve or a moment rotation curve of the material behaviour. However, different stiffness coefficients are required to represent different material behaviour, such as linear and non-linear behaviour of the RB or LRB bearings. The stiffness of seismic isolation bearings and dampers in Seismostruct can take different model shapes, and they are mainly characterized by: Elasto-plastic / rigid-plastic, Bi-Linear and Tri-Linear curve shapes, in addition to the symmetry and asymmetry of the curve shape.

SeismoStuct [16] provides 14 different curves that represent 16 different governing models for the linking element representation. The model should be able to represent the linear and non-linear behaviour of the linkage element in the loading, un-loading and re-loading process. However, the hysteresis property of the model depends on the formulation of the model itself. Consequently, more complex models contain more parameters. For example, the Seismostruct provides the Multi-Linear curve, which has 16 parameters that need to be fully characterised, and the Smooth curve, which contains 22 parameters that also need to be fully characterised. Other models, such as the Simplified Bilinear Takeda curve has only 4 parameters, and the Ramberg-Osgood curve has also 4 parameters. Both are also applicable for linkage-element modelling [16].

**5.6.1.1 Future research point**

The modelling of a SIB depends on the parameters which formulate the load-deflection non-linear curve of the isolation material compound. However, it cannot be guaranteed that the same hysteresis behaviour would remain unchanged after strong seismic excitements being applied in a multi-directional manner. If a specimen has been tested under cyclic loading, acting in three different directions to determine its hysteresis behaviour for each direction independently, the multi-directional combined manner of loading would produce different capacity limits in each direction. This point is worth being investigated in future research work.

A similar argument can also be extended to the stiffness behaviour of a SIB specimen during different normal and shear strains as the specimen is subjected to a dynamic loading. It has been found by a group of researchers [15] that the mechanical characteristics, such as the horizontal stiffness, of different SIB specimens are not stable when shear straining is small, but become more stable as shear strains become larger than 100%, as can be observed from Figure 5.19.

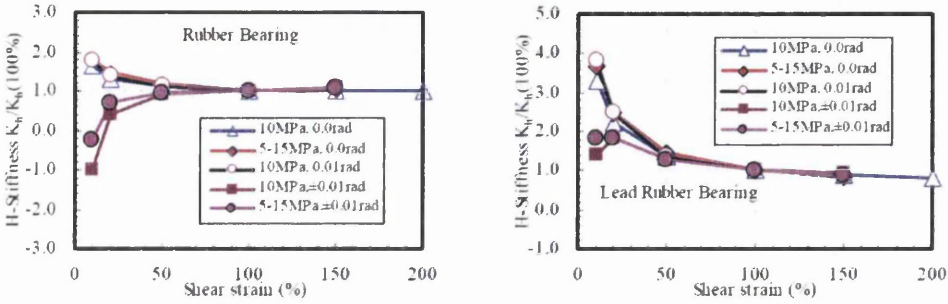


Figure 5.19 Variation of mechanical characteristics of RB and LRB under dynamic loading [15]

### 5.6.2 Damage in the Isolated and Non-Isolated Systems

When a relatively large amount of energy is dissipated by the bearings in an isolated system, this implies that the isolation system is offering an effective resistance against earthquake damage responses. However, movable bearings such as steel rollers with limited displacement movement are also providing effective energy dissipation corresponding to the earthquake response, but they could cause a great damage since they are non-absorptive devices and must be limited by displacement stoppers, which will lead to a sudden transfer of the energy to the substructure. When a part of the seismic energy is not absorbed by the bearings, it will certainly be transferred to members of the substructure, which will dissipate it in the form of structural damage. Due to this energy mechanism both fixed and roller bearings exhibit unsafe seismic resistance to earthquake strikes in single RC columns supporting box-girder bridges. It can be stated that *“for less energy absorption by the isolators more damage potential is exhibited on the structure”*. Figure 5.20.a&b shows two extreme examples of the mechanical behaviour of two different isolators; low absorptive and highly absorptive. The former exhibits less ductility than the latter, and thus more damage potential is transferred in the low absorptive model to the substructure.

RB and LRB isolation devices exhibit energy dissipation in the form of lateral displacements. They are absorptive systems since they sustain residual deformation when unloaded.



However, they must also be limited by displacement stoppers according to the seismic code regulations, but their capability to absorb some of the energy offers appreciated benefits to mitigate the expected damage to the substructure members. Therefore, it is a criterion of seismic design to select the material properties for RB and LRB devices that are most appropriate for the loaded structure. This implies that appropriate mechanical properties of the seismic isolators should be able to mitigate the earthquake response by the bridge structure, and thus resulting in less damage.

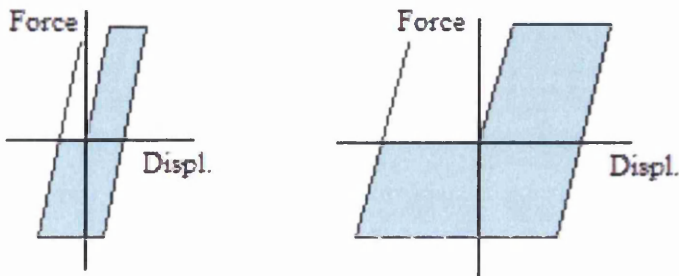


Figure 5.20.a&b Low and highly absorptive isolators models

Carlos Mendez Galindo and others [17] found that the best use of LRB to provide maximum seismic energy dissipation capacity as well as limited maximum deck displacement is by using LRB devices designed for an optimum ratio of yield force level to superstructure weight ( $F_y/W = 0.1$ ) and optimum pre-yield to post-yield stiffness ratio  $\frac{K1}{K2} = 10$ . It is also considered in design that this ratio is acceptable with  $3 < \frac{K1}{K2} < 50$  [13].

The ratio  $K1/K2$  of LRB also provides a moderate period shift, as recommended by Japan’s Highway Bridges Specifications [17]. In their steel bridge seismic analysis, Carlos Mendez Galindo and others [17] designed LRB isolators with dynamic characteristics to obtain fundamental natural periods of 1.3 seconds for the isolated bridge model, which are slightly larger than twice the fundamental period of the non-isolated bridge model (0.6 seconds). Carlos Mendez Galindo and others [17] consider that this is a moderate period shift as recommended by Japan’s Highway Bridges Specifications. Meng-Hoa Tsai [14] also used values for the fundamental natural periods close to what has been mentioned.

However, maximum seismic energy dissipation capacity attained by selecting a moderate period shift for the isolated system, does not guarantee low damage results in all cases since isolated systems with moderate period shifts could exhibit less absorption energy in some cases [17].

Another important factor that controls the performance of a LRB is the lead plug size in the isolator. Larger size of a lead plug increases its stiffness, and smaller size would decrease its stiffness. The efficiency of isolators depend on the size of the plug, since relatively large or small lead plug sizes may cause significant damage to the pier structure [17]. Therefore design for seismic isolators may be preceded by detailed dynamic analysis of a parametric study for the mechanical properties of the isolation devices installed in the structural system.

### **5.6.3 A Low Fidelity Model Representing an Ideal Seismic Isolation System**

The optimum seismic energy dissipation capacity for a seismic isolation device is related to two principal aspects; firstly; the PGA magnitude and the acceleration pulse of the ground motion, and secondly; the stiffness of the substructure system.

The previously mentioned statement: *“for less energy absorption by the isolators more damage potential is exhibited on the structure”* implies that an optimum seismic device should have optimum absorptive and dissipative energy in order to help the substructure resisting earthquake responses with the lowest damage consequences.

From previous sections 5.5.2 and 5.6.2, it can be concluded that the amount of dissipative energy that’s accounted for crushing of the column core is the one that needs to be absorbed the most by the seismic isolators. Meanwhile, both SIB and the substructure should together dissipate an energy amount that would not be causing over limited displacements.

Similar to the energy curves in section 5.5.2, such dissipative energy amount can be determined by energy curves obtained by either experimental tests or liable fracture analysis models.

Out of searching, there was no method specifically found in the literature in relevance to seismic isolation, which assigns applying a certain amount of energy to an ideal seismic isolator, but it might be ideally acceptable to build a numerical model that can apply such energy dissipation for an ideal isolator. A low fidelity model, using Newmark’s method to solve for elastoplastic beam-column elements, can handle the simulation of a MDOF column structure with an ideal stiffness isolator, subjected to a dynamic or seismic lateral loading. From searching the literature, one of the most suitable models to perform energy dissipation based on damage assessment for the RC column is the simplified moment-curvature damage model for bridges subject to seismic loads by S. Oller and A. Barbat [18], which will be briefly explained in the following section, and is very much recommended for future work as will be discussed in Chapter 8 later on.

### 5.6.3.1 A simplified moment-curvature damage model for bridges subject to seismic loads

This numerical model [18,19] is significantly useful since it applies a simple and reliable non-linear analysis based on damage detection and evaluation. It combines both utilizing the moment-curvature model which is a highly practical approach for time-stepping (iterative) methods in the non-linear analysis, and the continuum damage model which is based on the constitutive damage law in a cross section for a loaded member. In addition to providing the stiffness of a combined RC section to the analysed element for the column, linkage-type elements could also be provided to consider the seismic isolation bearing (SIB) at the column's top, and the soil-structure interaction (SSI) at the column's base, which is shown in Figure 5.21.

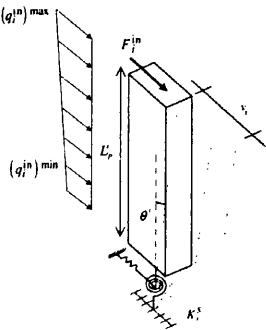


Figure 5.21 Pier displacement considering soil-structure effect [18]

Even though energy quantities are not measured parameters in this model, the process of verification of the equilibrium equation, (as shown below in step 4.c), on the plastically hinged cross section should work in conjunction with the SIB isolators to give an ideal performance of the substructure. Such an analysis is based on the balance of controlled energy dissipation by the isolators and controlled minor damage in the RC columns.

Other characteristics can also be provided for this model such as the possibility of including the fatigue behaviour, the effect of shear stress, local and global stability, and the debonding effect between steel and concrete [18]. Such characteristics made the model eligible for analysing existing bridges for seismic assessment projects held by many European governmental firms [18]. However, B. Richard et al. [20] concluded in their investigation that the use of continuum damage mechanics fails in evaluating cracks opening and spacing even if the global behaviour of the structure is correctly predicted.

#### Explanation of the model:

According to the damage theory, the presence of small cracks and voids degrades the material properties. This phenomenon is expressed by means of continuum damage mechanics, and



the level of degradation is measured by the damage factor  $d$  which is based on the effective stress  $\sigma_{eff}$  after the damage and Cauchy stress  $\sigma$  before the damage as follows:

$$\sigma_{eff} = \frac{\sigma}{1-d} \quad 5.18$$

where the damage factor represents the loss of stiffness level in the member, and is limited between 0, where no damage exists, and 1, where damage is maximum.

In this model, numerical computations are divided into three parts; Newmark's method at steps 1,2 and 3, computation of the residual forces  $\Delta\hat{\sigma}(x_3)$  for the critical section  $x_3$  (will be shown at step 4 below), and computation of the damage constitutive equation (at step 4.(e) below). In general, the model is explained in the following:

1. Using Newmark's method, top displacement and velocity are first predicted then the incremental displacement  $\Delta\mathbf{U}^{t+\Delta t}$  is determined starting from applying the linearized equilibrium equation until correcting the predicted displacement, velocity and acceleration vectors.
2. Due to the material degradation, the reduction in properties of the plastic hinge section,  $x_3$ , is computed for the moment of inertia  $I(x_3)$  and cross section area  $A(x_3)$ , and is formulated in the Jacobian matrix  $J(x_3)$  as shown below in step 4.(e). This reduction is used to update the internal generalized stress  $\hat{\sigma}^{int}(x_3)$  sustained by the damaged section, as shown below in step 4.(e). The difference between the updated internal generalized stress and initial generalized stress  $\hat{\sigma}^0(x_3)$  is the residual unbalanced forces  $\Delta\hat{\sigma}(x_3)$  which must come to a small tolerance number to verify the balance of the equation of equilibrium.
3. The parameters of the Jacobian matrix are computed according to the damage constitutive law, in which the local damage variable  $f(x_1, x_2, x_3)$  at all points of the cross section  $x_3$  is calculated by the damage constitutive equation:

$$f(x_1, x_2, x_3) = 1 - d(x_1, x_2, x_3) = \frac{\tau^{max}}{\tau} e^{a(1 - \frac{\tau(d)}{\tau^{max}})} \quad 5.19$$

where  $0 \leq \tau^{max} \leq \tau$ ,  $\tau^{max}$  and  $\tau$  are the maximum and current tension strength at each point, respectively.  $a$  is dependant on the fracture energy, and  $d(x_1, x_2, x_3)$  is the damage factor at all sections. The Jacobian parameters are determined according to  $f(x_1, x_2, x_3)$  for the sub-section b, as follows:

$$A(x_3)_b = \int_A f(x_1, x_2, x_3). dA \text{ damaged area of the sub-section b.}$$

$$m_i(x_3)_c = \int_A f(x_1, x_2, x_3). x_j. dA \text{ damaged first moment of the sub-section c.}$$

$I_{ii}(x_3)_a = \int_A f(x_1, x_2, x_3). x_j^2. dA$  damaged moment of inertia of the sub-section a.

$I_{ij}(x_3)_d = \int_A f(x_1, x_2, x_3). x_j. x_i. dA$  damaged product of inertia of the sub-section d.

The integration is performed numerically by the use of numerical weight coefficients for all the sub-sections of the targeted cross section  $x_3$ .

The following steps are a summarized explanation of the moment-curvature damage model:

1. Prediction of Displacement and Velocity at top of column:

$$\begin{aligned}\dot{\mathbf{U}}^{t+\Delta t} &= \dot{\mathbf{U}}^t + (1 - \gamma)\ddot{\mathbf{U}}^t. \Delta t \\ \mathbf{U}^{t+\Delta t} &= \mathbf{U}^t. \Delta t + \dot{\mathbf{U}}^t \left(\frac{1}{2} - \beta\right) \ddot{\mathbf{U}}^t. \Delta t^2\end{aligned}$$

$\gamma = 0.5$ ,  $\beta = 0.25$ , and  $\ddot{\mathbf{U}}^t, \dot{\mathbf{U}}^t, \mathbf{U}^t$  are given from last time instant.

2. Compute displacement increment  $\Delta \mathbf{U}^{t+\Delta t}$  starting from the linearized equilibrium equation:

$$\Delta \mathbf{f}^{t+\Delta t} = \Delta \mathbf{J}^{t+\Delta t}. \Delta \ddot{\mathbf{U}}^{t+\Delta t}$$

Given  $\Delta \mathbf{f}^{t+\Delta t}$  and  $\Delta \mathbf{J}^{t+\Delta t} = \mathbf{M} \frac{1}{\beta \Delta t^2} + \mathbf{K}$ , where,  $\mathbf{M}$  and  $\mathbf{K}$  are the mass, stiffness matrices,  $\Delta \mathbf{f}$  is the increment of inertia force.

3. Correction of Displacement and Velocity for the same time instant, using Newton-Raphson's trials for nonlinear conversions.
4. Computation of the residual forces using the continuum damage model:

- 4.(a) Computation of elastic generalized initial stress, (the Predictor), using top displacement  $\mathbf{U}^{t+\Delta t}(0)$ :

$$\hat{\boldsymbol{\sigma}}^0(x_3) = \begin{bmatrix} N^0(x_3) \\ M_1^0(x_3) \\ M_2^0(x_3) \end{bmatrix}, M_1^0(x_3) = \frac{(L-x_3)}{L^2 \frac{L^3}{K^s + 3E^0 I_{11}}} v_2 L^{t+\Delta t}, M_2^0(x_3) = \frac{(L-x_3)}{L^2 \frac{L^3}{K^s + 3E^0 I_{22}}} v_1 L^{t+\Delta t}$$

where,  $K^s$  is the rotational stiffness,  $L$  length of the pier,  $v_1, v_2$  rotations at pier top.

- 4.(b) Computation of residual generalized stress,(the Residual). The unbalanced equilibrium equation is:

The Residual= elastic generalized initial stress – generalized internal stress

$$\Delta \hat{\boldsymbol{\sigma}}(x_3) = \hat{\boldsymbol{\sigma}}^0(x_3) - \hat{\boldsymbol{\sigma}}^{\text{int}}(x_3)$$

- 4.(c) Verify the equilibrium equation if  $\Delta \hat{\boldsymbol{\sigma}}^{\text{int}}(x_3) \begin{cases} = 0, (\text{verified}) \text{ Go to step 6} \\ \neq 0, (\text{not verified}) \text{ Continue} \end{cases}$

- 4.(d) Computation of incremental generalized strains, using the Newton-Raphson iterations:

$$\begin{aligned}\Delta \boldsymbol{\varepsilon}^{t+\Delta t}(x_3) &= -[J(x_3)]^{-1}. \Delta \hat{\boldsymbol{\sigma}}(x_3) \\ \boldsymbol{\varepsilon}^{t+\Delta t}(x_3) &= \boldsymbol{\varepsilon}^{t+\Delta t}(x_3)^{\text{last}} + \Delta \boldsymbol{\varepsilon}^{t+\Delta t}(x_3)\end{aligned}$$

4.(e) Computation of section properties  $J(x_3)$  and generalised internal stress  $\hat{\sigma}^{\text{int}}(x_3)$  using the continuum damage model

$$J(x_3) = \begin{bmatrix} A(x_3) & m_1(x_3) & m_2(x_3) \\ m_1(x_3) & I_{11}(x_3) & I_{12}(x_3) \\ m_2(x_3) & I_{21}(x_3) & I_{22}(x_3) \end{bmatrix}$$

$$\hat{\sigma}^{\text{int}}(x_3) = E^o J(x_3) \cdot \boldsymbol{\epsilon}^{t+\Delta t}(x_3) = \begin{bmatrix} N(x_3) \\ M_1(x_3) \\ M_2(x_3) \end{bmatrix}$$

- 5. Go back to step 4.(b)
- 6. Computation of displacement at  $x_3$ :

$$\mathbf{U}^{t+\Delta t}(x_3) = \begin{bmatrix} u(x_3) \\ v_1(x_3) \\ v_2(x_3) \end{bmatrix}^{t+\Delta t}$$

- 7. Back to step 1 for a new time increment and dynamic load increment  $\Delta \mathbf{f}^{t+\Delta t}$

In addition to the inclusion of rotational stiffness  $K^s$  of the soil-structure interaction behaviour, the stiffness for seismic isolation bearing SIB can also be included in the global stiffness matrix, and thus the effect of both damaged section properties and seismic isolation can be controlled.

### 5.6.4 A Numerical Example

It is useful to describe the behaviour of a seismic isolated-bearing system throughout two numerical examples; the first is the RC bridge column subjected to a multi-directional seismic excitation [2], and the second is a group of single RC columns supporting a single-cell box-girder bridge. Both examples are to be supplemented with a SIB system, and subjected to an earthquake loading.

#### 5.6.4.1 Single RC Column with a Seismic Isolated Bearing System

From the previous investigation in section 5.5.2, most of the severe damage in the RC bridge column subjected to the 1983 Nihonkai Chubu earthquake [2] occurs when the structure reaches the defined state (III). The seismic energy dissipated at this stage needs to be alleviated and alternatively dissipated by the isolation device. Using the Seismostruct dynamic solver, a lead-rubber bearing device is numerically simulated by a linkage element, and installed between the column (substructure) top node and the bridge deck (superstructure) bottom node. The linkage element is idealised by an elastic-plastic model of bi-linear symmetric curve, as shown in Figure 5.22. It should be noted that a kinematic-hardening

property is selected to suit the mechanical non-linear behaviour of the rubber, while other materials may follow an isotropic-hardening rule in the non-linear mechanical behaviour [16]. The model is governed by 3 parameters as follows; the initial stiffness  $K_0$ , the yield force  $F_y$  and the post-yield hardening ratio  $r$  which is given the default 0.005.

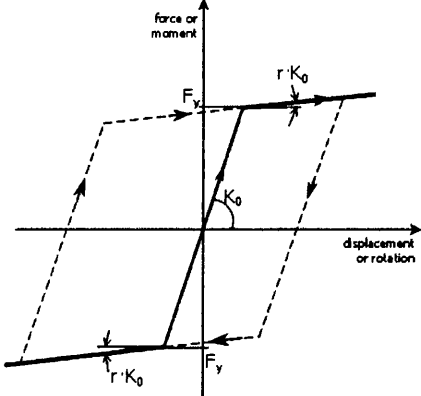


Figure 5.22 the Bi-Linear Kinematic Curve for a LRB modelling of a linkage-element[16]

There are three important modelling steps to build a linkage-element model in the Seismostruct, and are summarized in the following:

- Creating the super-structure/linkage-element node with coordinates fully coincident with the sub-structure/linkage-element node.
- Giving the above parameters to the linkage-element in all of its 6 forces and moments as follows:  $F_1 = F_2 = F_3 = F_y$ ,  $M_1 = M_2 = M_3 \cong 0$ .
- Providing the nodes connectivity between the linkage-element nodes and the nodes of the structure.

Given that over isolated structures may cause large displacements in the bridge deck during a severe earthquake, they are, practically, restrained by special stoppers to prevent such displacements. However, stoppers will enforce additional columns' resistance to the seismic load, leading to more damages in the column. Therefore, an adequate isolation system is required to act together with the columns stiffness in order to mitigate the expected damage effectively and, simultaneously, minimize the lateral displacements. This depends on the properties of the isolation devices. Thus, a parametric study was carried out on this isolation device model for the same structure and same loading, to obtain a column performance that is not engaged within state (III) of severe damage. As can be seen from Figure 5.23, the isolated column reaches state (II) with displacements between 0.084 and 0.102 m, in much less dissipated yield energy of 45 kN.m. The rest of the seismic energy was alleviated, and dissipated by the isolation device. The 'convergence' of the curve occurs when it starts to

become more horizontal as the contribution of the dissipating energy starts to reduce. Therefore, the structure needed a large amount of energy to be alleviated by the isolators in order to converge at such low displacement value to avoid engagement with state (III).

As minimum column's damage can be attained at a range of isolation between highly isolated and fully fixed cases, the intermediate properties for such minimum damage for this structure were found to be as follows: initial stiffness  $K_o$  or  $K1= 55.1E06$  N/m, yield force  $F_y=551.E03$  N and hardening ratio  $r = 0.005$ . It is important to know that such properties are considered as medium range between other LRB strength extremes [17], and that the PGA's for the x, y and z components applied on this structure are scaled up by 400%, and are as high as  $11.12$   $m/s^2$ ,  $9.52$   $m/s^2$  and  $8.2$   $m/s^2$ , respectively [2].

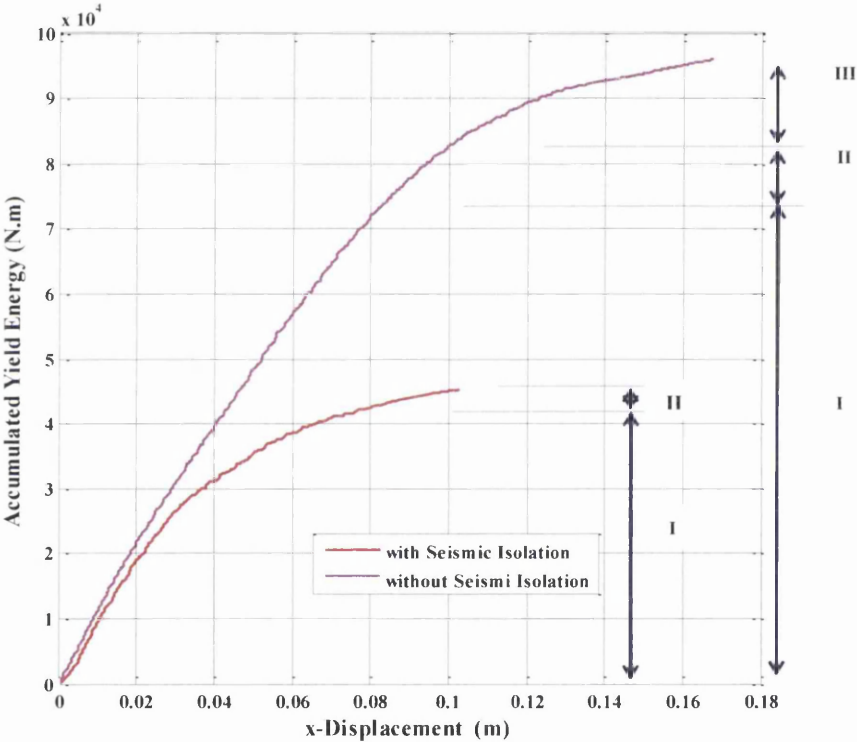


Figure 5.23 Dissipated yield energy in RC column with and without seismic isolation

Figure 5.24 shows the comparison in the structure's curvatures between isolated and non-isolated RC columns. The isolation is successful in eliminating the rotational motion with very limited residuals. Figure 5.25 shows that the velocities of the substructure and superstructure are not in phase. In fact they differ enormously in frequency, and the elastoplastic property of stiffness for the LRB model enables the higher mass superstructure to respond with much less frequency than the response of the lower mass substructure.

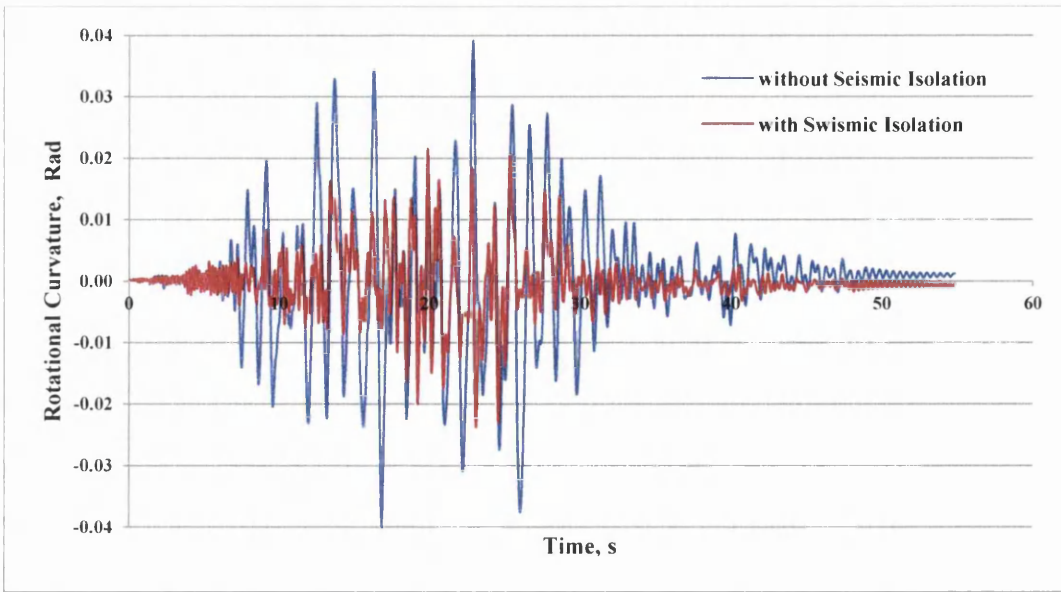


Figure 5.24 Time history of relative rotational response in RC column with and without seismic isolation

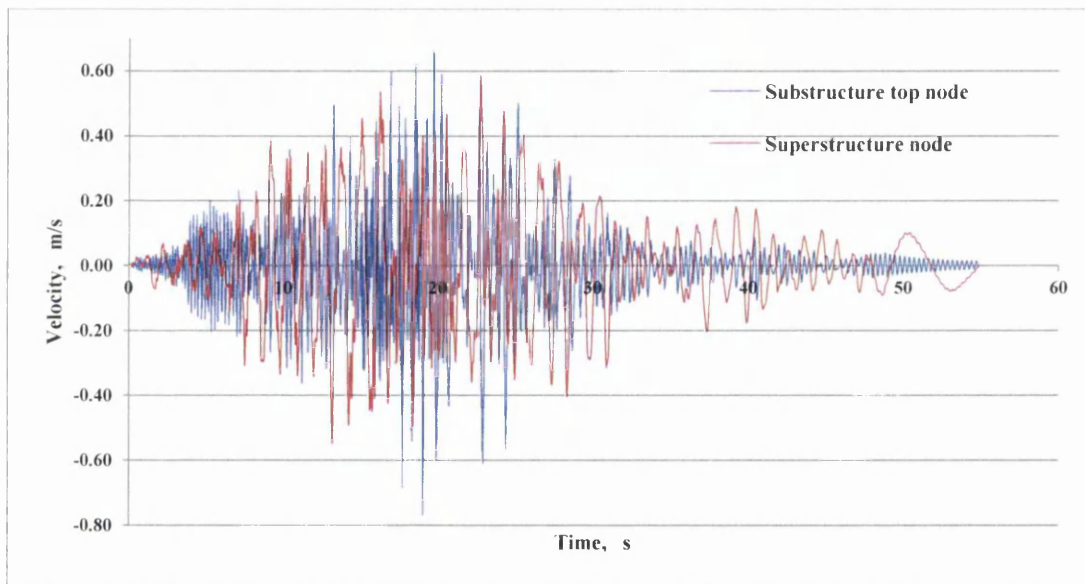
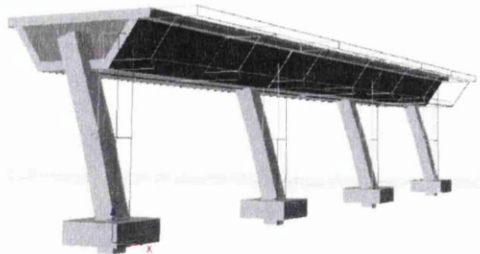


Figure 5.25 Nodal relative velocities in the isolated substructure and superstructure

#### 5.6.4.2 Single RC Columns with a Seismic Isolated Bearings System

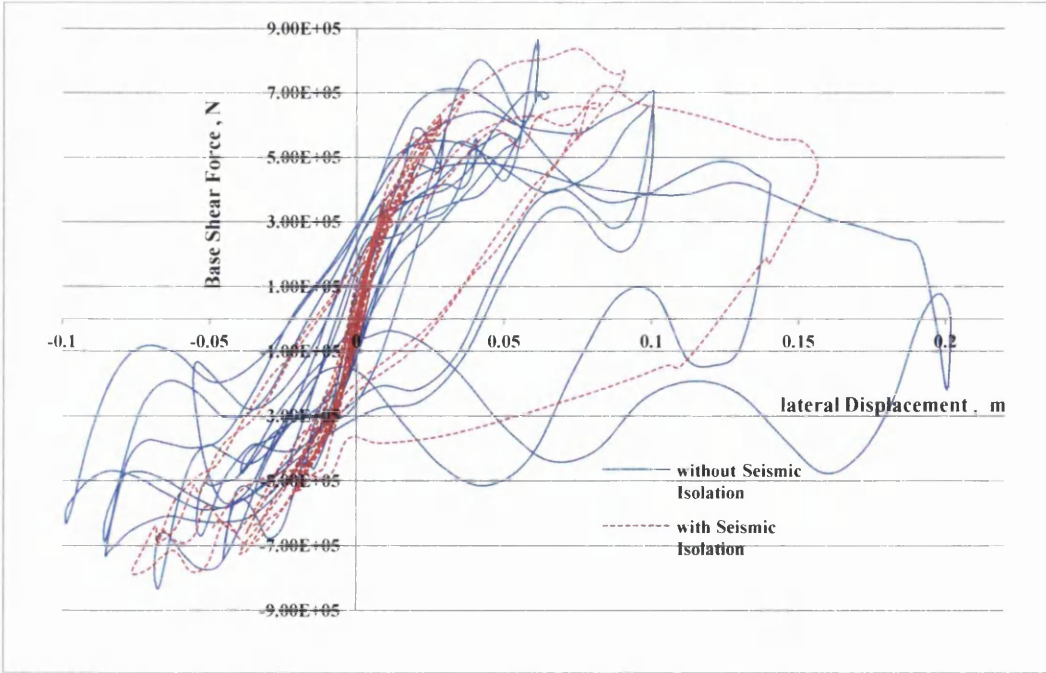
The proposed structure, Figure 5.26, is subjected to a seismic loading with  $PGA=0.25g$  only, applied in the transverse direction of the bridge, and solved numerically by SeismoStruct. The seismic isolation system is modelled similarly to what was explained in the previous section. A parametric study was carried out to minimize the columns damage, which can be attained at a range of isolation between highly isolated and fully fixed cases. The intermediate properties for such a minimum damage for this structure were found to be as

follows: initial stiffness  $K_0$  or  $K1= 20.E08$  N/m, yield force  $F_y=700.E04$  N and hardening ratio  $r = 0.005$ .



**Figure 5.26 Bridge structure**

The difference in performance between the adequately isolated and non-isolated fully fixed structures can be clearly seen in the following load-deflection hysteresis curve and the stress-strain plot. The isolation process mitigated the structural response of the substructure, and decreased its top displacement response by approximately 25%. The maximum top displacement of the columns dropped from 0.2 to 0.15 m, and the overall hysteresis loops shrunk towards a more elastic response, as can be seen in Figure 5.27. However, on the cover of the column base, the stress-strain plots in Figure 5.28 show less damage in the stressed fibres of the isolated structure, and higher damage in the non-isolated structure. The softening compressive maximum stresses reached by the non-isolated and isolated structures were  $2.9E07$  and  $1.2E07$  Pa respectively. The corresponding maximum strains reached by the non-isolated and isolated structures were  $-0.0032$  and  $-0.0058$  respectively.



**Figure 5.27 Hysteresis curves for different analyses of the bridge columns**



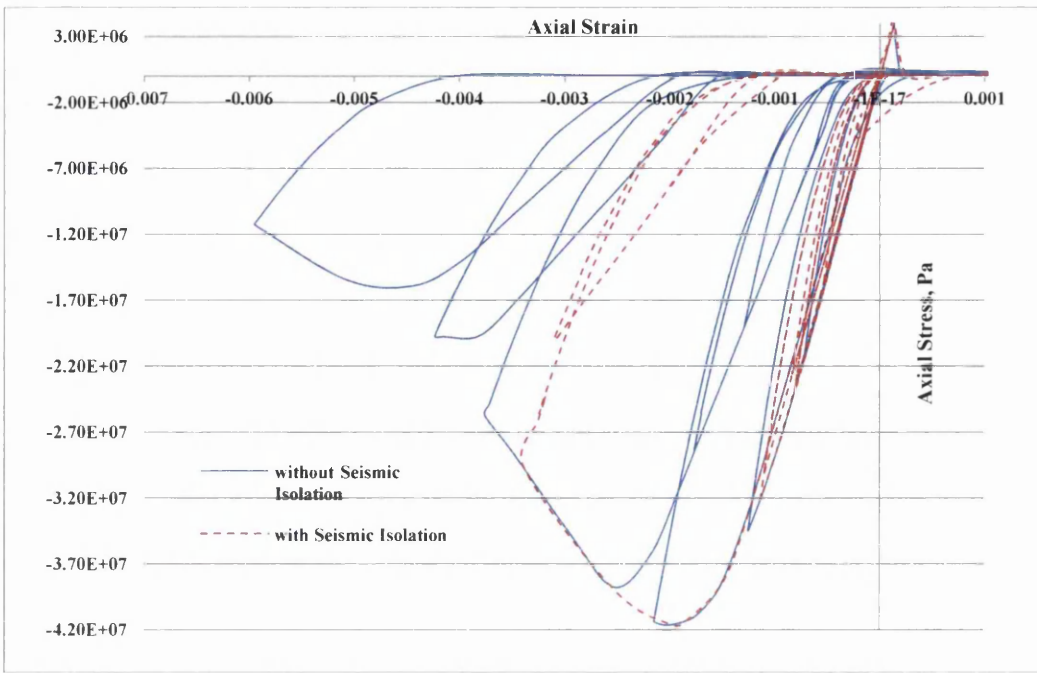


Figure 5.28 Stress-strain curves for a point on the RC column cover at PH section

### 5.6.4.3 Discussion of Results

Theoretically, the seismic energy is partially dissipated by isolators set up at this transitional zone between the substructure and the superstructure, and thus, the column damage is minimized significantly. However, an effective isolation device with adequate mechanical properties needs to be carefully designed for the structural system to create the balance between relatively large isolation with large displacement of the super-structure, and little isolation with a high damage rate in the sub-structure. Assessment of the isolation performance can be done using the following methodology:

1- Comparison between the isolated/non-isolated performances for the sub-structure part only. This can be done by evaluating:

1. Global damage; using the Energy-displacement relation to evaluate the different states of global damage.
2. Local damage; by using the stress/strain relation to evaluate the local damage at the base.
3. Over-all performance; by using the hysteresis, displacement and rotational time histories.



2- Comparison between the sub-structure/super-structure performances for the isolated structure only. This can be done by evaluating the frequency performance; by using velocity and displacement time-histories, to test the elastoplastic property of the LRB model that enables dominance of the higher-mass superstructure frequency over the lower-mass substructure frequency.

From the above methodology, both damage and ultimate lateral displacement response can be used as analytical constraints to determine some of the mechanical properties for the rubber bearing seismic isolation device that's most adequate for the structure.

As a simple evaluation process for the multi-column bridge example, the *local* damage at a point on the cover fibre can also be approximated from the ratio between the softened stiffness and initial stiffness  $E$  in the previously obtained stress-strain curve in Figure 5.28. The local damage is approximated for the fibres of the non-isolated (monolithic) and isolated structures as follows [21]:

$$D_{mono} = 1 - \frac{E^{softened}}{E^{initial}} = 1 - \frac{852.9e7}{2450e7} = 0.915$$

$$D_{iso} = 1 - \frac{E^{softened}}{E^{initial}} = 1 - \frac{206.8e7}{2450e7} = 0.651$$

The difference in the two damage estimations is 26%, and it is the largest difference found between the performances of the two structures. Values having small differences are found for other fibres on the core of the column, where damage is minimum. *Global* damage can also be numerically determined for this structure using the previously mentioned methods, however, irregularity of the hysteretic curve due to the dynamic motion does not express the global damage measure accurately. Rather, it may be possible to define the global damage for the whole structure by statistically defining the local updated stresses for all of the critical fibres in the column [21].

## 5.7 CONCLUSION & RECOMMENDATIONS

Damage analysis in dynamic problems under seismic loading could lead to major conclusions, which can be considered useful for performance-based seismic engineering PBSE and design PBSB in RC bridge columns. From the previous study the following conclusions are found:

- The intensity of local damage in a plastic hinge (PH) is critically significant, and the damage growth in the PH zone inside the concrete core could easily lead to a total

collapse, or more often, excessive residual displacements. This occurs when large parts of the longitudinal bars lose their bond effect as the concrete core is damaging.

- Global damage curves obtained in this chapter are based on the energy dissipation in the hysteresis performance of the structure, indicating a fairly representative global damage index measure for the whole structure in general. However, the corresponding global state is usually based on experimental and site observations, but not necessarily reflecting the inner core damage state for the members.
- Local damage curves obtained in this chapter are based on fibrous damage due to the performance of the compressive axial stresses only, while the concrete fibres under tensile axial stresses are not represented in these curves, since they are considered fully damaged at very early stages.
- Based on the Demand/Capacity principle  $d_D < d_C$ , the Seismic Design Criteria (SDC) for RC bridge columns is also assuming the initiation of a plastic hinge, which dissipates seismic energy. But the cracking growth nature of the fracturing mechanism cannot be estimated in this manner, or assured not to reach severe damage rates, even if the Demand/Capacity principle is adopted.
- Seismic isolation is an efficient method to control both the damage in RC members and consequently, the large displacements exceeding allowable movement limits of the superstructure, in addition to its efficiency in reducing the residual deformations.
- Evaluation of the isolated structure can be done by modelling the isolation devices numerically, and thus comparing the seismic performance of the isolated and non-isolated sub-structure, using evaluation methods for global damage, local damage, energy curves, hysteresis curves and time-histories. Another useful seismic evaluation method is the performance of the isolated sub-structure/super-structure zones based on the formation of yield energy curves. Such evaluation methods help to design the mechanical properties of the isolation devices.
- The moment-curvature damage evolution model can be applied to perform seismic non-linear analysis with controlled damage and controlled seismic isolation. It is significantly practical and reliable since it combines both continuum damage mechanics and structural mechanics in a simplified formulation capable of analysing MDOF global structures under seismic loading.
- The Seismostruct dynamic solver is capable of performing and evaluating seismic response of RC frame structures efficiently with and without seismic isolation.

## 5.8 REFERENCES

- [1] E. Erduran, A. Yakut, Component damage functions for reinforced concrete frame structures. *Engineering Structures*, 2007. 29(9): p. 2242-2253.
- [2] J. Sakai, S. Unjoh. Earthquake simulation test of circular reinforced concrete bridge column under multidirectional seismic excitation. *Earthquake Engineering and Engineering Vibration*, 2006. Vol. 5, No. 1.
- [3] A.K. Chopra, *Dynamics of Structures*, Pearson Education, Inc., third edition, 2007.
- [4] R.W. Clough, J. Penzien. *Dynamics of structures*. McGraw-Hill, Inc., international edition, 1993.
- [5] E.S. Neto, D. Perić, D. Owens, *Computational methods for plasticity: theory and applications*. 2008, Chichester: Wiley.
- [6] K. Antoniadis, T. Salonikios, A. J. Kappos. Evaluation of hysteretic response and strength of repaired R/C walls strengthened with FRPs. *Engineering Structures* 29 (2007) 2158–2171.
- [7] W. F. Chen, A. F. Saleeb. *Constitutive Equations for Engineering Materials*. John Wiley & Sons. Inc., 1982.
- [8] K. Sadeghi, Energy based structural damage index based on nonlinear numerical simulation of structures subjected to oriented lateral cyclic loading. *International Journal of Civil Engineering*, 2011. 9(3): p. 155-164.
- [9] J. Sakai, S. Mahin., *Analytical Investigations of New Methods for Reducing Residual Displacements of Reinforced Concrete Bridge Columns*, 2004, Pacific Earthquake Engineering Research Center(PEER).
- [10] W.H. Robinson, Lead-rubber hysteretic bearings suitable for protecting structures during earthquakes. *Earthquake Engng. & Struct. Dyn.*, 1982. 10(4, Jul.-Aug. 1982).
- [11] M. Dicleli, M.Y. Mansour, M.C. Constantinou. Efficiency of seismic isolation for seismic retrofitting of heavy sub-structured bridges. *JBE Journal of bridge engineering* vol.10 No.4 July/Aug 2005.
- [12] J. Stewart, J. Conte, I. Aiken, Observed behavior of seismically isolated buildings. *Journal of Structural Engineering*, 1999. 125(9): p. 955-964.
- [13] P. Kumar, D.K. Paul. Force-deformation behaviour of isolation bearings. *JBE Journal of bridge engineering* vol.12 No.4, 2007.
- [14] M.H. Tsai. Transverse earthquake response analysis of a seismically isolated regular bridge with partial restraint. *Engineering Structures*, 2008. 30(2): p. 393-403.

[15] W. Liu, F. Zhou., F. Sun, D. Huo, W. Yan, Product Specification and Mechanical Properties of Chinese Rubber Bearings. Transactions, SMiRT 16, Washington DC, 2001.

[16] Bibliography of SeismoStruct Earthquake engineering Software, SeismoStruct v5.2.2 Official release of 22/08/2011.

[17] C. Galindo, J. Belda, T. Hayashikawa. Non-linear seismic dynamic response of curved steel bridges equipped with LRB supports. Steel Construction, 2010. 3(1): p. 34-41.

[18] S. Oller, A. Barbat. Moment–curvature damage model for bridges subjected to seismic loads. Computer Methods in Applied Mechanics and Engineering, 195 (2006) 4490–4511.

[19] J. Faleiro, S. Oller, A.H. Barbat. Plastic–damage seismic model for reinforced concrete frames. Computers and Structures 86 (2008) 581–597.

[20] B. Richard, F. Ragueneau, C. Cremona, L. Adelaide. Isotropic continuum damage mechanics for concrete under cyclic loading: Stiffness recovery, inelastic strains and frictional sliding. Engineering Fracture Mechanics 77 (2010) 1203–1223.

[21] M.O. Benamer, Y. Feng. Energy-based assessment for reinforced concrete bridge columns with fixed connexions and isolated bearings. Proceedings of the 20<sup>th</sup> UK conference of the association for computational mechanics in engineering, 2012, Manchester University.

# Chapter 6

---

## Combined DE/FE Nonlinear Analysis

---

### Contents

6.0	INTRODUCTION .....	186
6.1	THE EXPLICIT-ELFEN MODEL .....	187
6.1.1	Elements .....	187
6.1.2	Time-step and the Explicit approach .....	188
6.1.3	Building the model in the Elfen environment .....	189
6.1.4	Pre-fracture properties .....	189
6.1.5	Post-fracture properties.....	190
6.1.6	Changes in the Elfen Defaults.....	192
6.1.7	Damping for explicit dynamic analysis.....	192
6.2	MATERIAL MODELLING .....	193
6.2.1	Elasticity and plasticity.....	194
6.3	MODELLING OF QUASI-BRITTLE MATERIALS.....	195
6.3.1	The Continuum Approach .....	195
6.3.1.1	Fracture Energy .....	196
6.3.1.2	The Smeared Crack Model.....	198
6.3.2	The Discrete Approach (Discrete Fracture Modelling).....	198
6.3.2.1	Rotating Crack Model .....	198
6.3.2.2	Fixed and Rotating Crack models .....	198
6.4	MODELLING OF QUASI-BRITTLE MATERIALS IN ELFEN .....	200
6.4.1	Rankine Failure Criterion with Fracture (Model 08).....	201
6.4.2	Mohr-Coulomb Failure Criterion Combined with Rankine (Model 19).....	202

6.4.3	Non-associative Flow Rule in M-C Compressive Strains (Strains Dilation) .....	203
6.4.4	Definition of pre-failure, post-failure and post-softening stages.....	205
6.5	MODELLING OF REINFORCEMENT BARS IN ELFEN .....	206
6.5.1	Von-Mises model .....	207
6.6	ASSUMPTIONS IN THE DE/FE MODELLING .....	208
6.6.1	Methods of Applied Loading.....	208
6.6.1.1	The Ground Acceleration Loading.....	208
6.6.1.2	The Equivalent-Force Loading.....	209
6.6.1.3	The Displacement-Based Loading .....	209
6.6.2	Axial Loading.....	210
6.6.3	Geometric Modelling.....	211
6.6.3.1	Geometric and Loading Symmetry .....	211
6.7	DIFFICULTIES IN ACTIVATING THE CRACKING PROCESS IN THE EXPLICIT-ELFEN FRACTURE MODEL .....	211
6.7.1	Effect of Mass Density on this Problem.....	213
6.7.2	Modelling of Reinforcement Bars .....	213
6.7.3	Modelling of Reinforcement Stirrups.....	214
6.7.4	Computational Size of the Analyzed Problem .....	215
6.8	PROBLEM SET-UP FOR DE/FE ANALYSIS .....	216
6.7	RESULTS AND DISCUSSION .....	218
6.7.1	Comparison of Collapse Performance Between Mohr-Coulomb and Rankine...	224
6.7.2	Fracture and axial plastic strains .....	225
6.8	CONCLUSION.....	227
6.9	REFERENCES .....	229

## 6.0 INTRODUCTION

In many research papers the damage assessment for similar RC columns has been defined using damage index curves, which indicate the expected *Global Damage*, that's approximated for the whole structure. However, more investigation should be conducted to explore the *Local Damage* state at the plastic hinge zone itself. It is obvious that the column cover, core and reinforcement bars would have different damage states at different time-step loading, and they should be investigated independently in order to obtain an overall damage assessment that's more specific than the typical *Global Damage* approximations.

The combined DE/FE Discrete Element/Finite Element analyses are applied by using the Elfen-Explicit application to solve the RC column under dynamic loading, and investigate the non-linear behaviour of the structure, associated with the expected damage in the concrete. This requires defining the analysed elements with the discrete properties as well as the plastic properties for the material assigned to the finite elements. The algorithm associated with the discrete properties of the elements is functioning within so many restrictions concerning the processes of failure, fracturing and post-fracturing of the elements.

The algorithm will not function properly, i.e. will be producing numerical and geometric errors, when these processes are not functioned as designed. The workability of the combined DE/FE analyses is a matter of a case-by-case task, in which many modelling testing trials must precede obtaining the expected simulation for every analysed problem independently. In addition to testing the functionality of the elements discrete properties, such trials also include the geometry of the structure, mesh refinement, plastic properties, time-step restrictions and loading magnitudes and rates. A relatively large effort and time consuming task is spent to obtain DE/FE simulations for each independent engineering problem, especially when a parametric study is required to obtain useful conclusions.

There are three important subjects that are discussed in this chapter, which encompass the main parameters of the DE/FE simulation. Figure 6.1 shows the material properties, failure criterion and the DE/FE algorithm are all inter-dependant and act together to perform the analysis. In this way, many computer error messages given by the Elfen seemed irrelevant to the real cause of the problem. In general, in this chapter the properties and input data of the proposed problem are explained, in addition to discussing the techniques followed to build the problem model, and difficulties that faced the execution of those models during their computer runs.

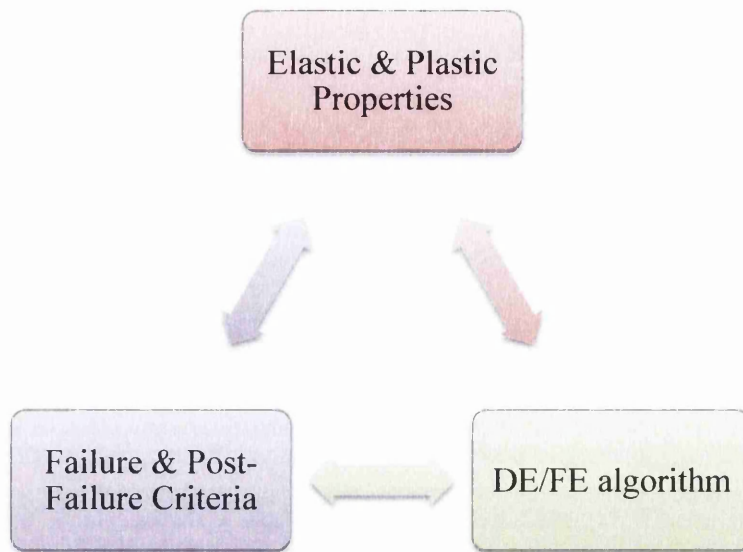


Figure 6.1 Interaction between failure & post-failure criteria, DE/FE algorithm and the elastic & plastic properties of the material

## 6.1 THE EXPLICIT-ELFEN MODEL

### 6.1.1 Elements

The Elfen application has five families of elements. Two types of finite elements are used in this analysis. For a 3D concrete continuum, the 4-noded solid tetrahedral elements are used, also known as 4-nodes Strain Stabilisation Tetrahedral Elements, or SSET\_4, as shown in Figure 6.2. For 3D Bars, the 3D 2-noded pin jointed bar elements are used, also known as 2-nodes Strain Bar Elements SBE3\_2.

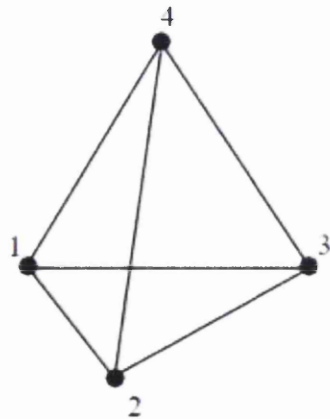


Figure 6.2 The tetrahedral element



The algorithmic formulation of the finite elements is based on the standard iso-parametric approach, in which the same shape function is used to interpolate both the displacement and geometry formulations. The strain-displacement relationship is formulated using a velocity strain measure, from which the incremental strains are evaluated. SSET\_4 elements are known between users to be more reliable for fracture simulation in 3-D continuums.

### 6.1.2 Time-step and the Explicit approach

Time step is the time interval that's used by time-stepping methods to calculate the incremental values numerically. As generally known, a time-step is lowered to avoid numerical divergence and instability, and approach the numerical convergence required to solve the problem. In addition, a lower-value time-step gives more accuracy to the output results and smoother output curves. However, this costs more expensive computational efforts especially in nonlinear problems and problems with fracture mechanism.

It should be noted that the combined DE/FE analyses algorithm for solving dynamic non-linear problems with fracture in Elfen is solved by using the explicit scheme only. The time-step in the explicit central difference solution algorithm is relatively smaller than that in the implicit approach, and the explicit approach requires a very large number of time steps to maintain stability. This highlights how computationally expensive the explicit central difference time integration scheme can be, especially for problems that require a large overall time period such as earthquake problems. The critical time step  $\Delta t_{cr}$  is given by:

$$\Delta t_{cr} = \frac{l}{\tilde{c}} \tag{6.1}$$

where,  $\tilde{c} = \sqrt{\frac{E}{\rho}}$ ,  $l$  is the characteristic length of the smallest element in (mm),  $\tilde{c}$  is the wave speed in (mm/s),  $E$  is Young's Modulus in (N/mm<sup>2</sup>) and  $\rho$  is the density in (N.s<sup>2</sup>/mm<sup>4</sup>). Initially, the first time step should be given by any estimation, then it is corrected according to the previous equation. However, a modified version of this formula is used in Elfen, to ensure stability when dealing with different shape elements, especially when geometrically distorted. Using the Elfen-Explicit Dynamic selection, the following time step control data are defined:

- Factor of Critical Step: which factorises the size of the time-step when smaller values are needed, especially in problems with expected fracturing elements.
- Termination Data: is the maximum number of time-steps that could be reached by the computational process.

- Termination Time in seconds: usually equals or less than the loading time. Obviously, it has nothing to do with the computing time of the machine.

### 6.1.3 Building the model in the Elfen environment

The structure of a finite element in the Elfen is made of entities. Entities are either nodes, lines, surfaces or volumes. They are divided into 2 categories;

- Dependant entities, which form upper level entities such as lines forming surfaces and surfaces forming volumes.
- Top-level entities, which do not form other upper entities.

These two types are important for the entity size inheritance from the upper level entity size to the lower level entity size. It is also important to be defined for the proposed RC model, since the reinforcement bar elements must be top-level entities in order to be meshed, sized and assigned their material properties to function independently.

### 6.1.4 Pre-fracture properties

The following Table 6.1 shows the material properties used for the proposed problem, which are used to perform the linear and non-linear pre-fracture process.

For the non-linear computations, the following parameters are required for Rankine (model 08) and M-C with Rotating crack (model 19):

Tensile strength  $\sigma_T = 0.5\sqrt{27.58} = 2.625 \text{ E06 N/m}^2$ , since the tensile stress of concrete  $= 0.5\sqrt{f'_c} \approx 0.1 f'_c$ , where  $f'_c$  is in  $\text{N/mm}^2$ . The Fracture Energy  $G_f$  for concrete is estimated as 100 to 200N/m.

Elastic Modulus $E$	Shear Modulus $G$	Compressive Yield stress $f'_c$	Tensile stress* $\sigma_T$	Cohesion or Shear Strength $c_u$	Density $\rho$	Poisson's ratio $\nu$
2.485E10 N/m <sup>2</sup>	1.035E10 N/m <sup>2</sup>	2.7579E07 N/m <sup>2</sup>	2.7579E06 N/m <sup>2</sup>	13.7x10 <sup>6</sup> N/m <sup>2</sup>	2356.0 N.s <sup>2</sup> /m <sup>4</sup>	0.2
$E$	$G \approx 0.4E$	$f'_c \approx 10^{-3}E$	$\sigma_T \approx e^{-4} E$ $\sigma_T \approx e^{-1} f'_c$ $\sigma_T \approx .5\sqrt{f'_c}$	$c_u \approx 5e^{-4} E$ $c_u \approx 0.5 f'_c$ $c_u \approx 5 \sigma_T$	$\rho \equiv 10^{-7} E$ $\rho \equiv 10^{-4} f'_c$ $\rho \equiv 10^{-3} \sigma_T$	-

\*also known as Uniaxial Yield stress in Rankine criterion, or Hydrostatic Tension Cut off stress in Drucker Prager criterion.

**Table 6.1 Mechanical properties of concrete and useful relations**

## 6.1.5 Post-fracture properties

This stage is concerned with Contact Mechanics of the discrete elements (DE) after fracture has occurred, and the assigned properties serve this stage in particular, which is not significantly useful to the field of seismic engineering. However, the post-fracture parameters are still important for the continuation of the dynamic analysis even if they have no significance to the seismic problem.

The physics of post-fractural discrete elements prohibits the partial interaction, or known as penetration, of two discrete elements in the same space simultaneously. But to obtain the simulation such penetration is allowed between the ‘impactor’ and the ‘targetter’ but with very large stress values, or known as penalty values, in the normal and tangential planes coordinate.

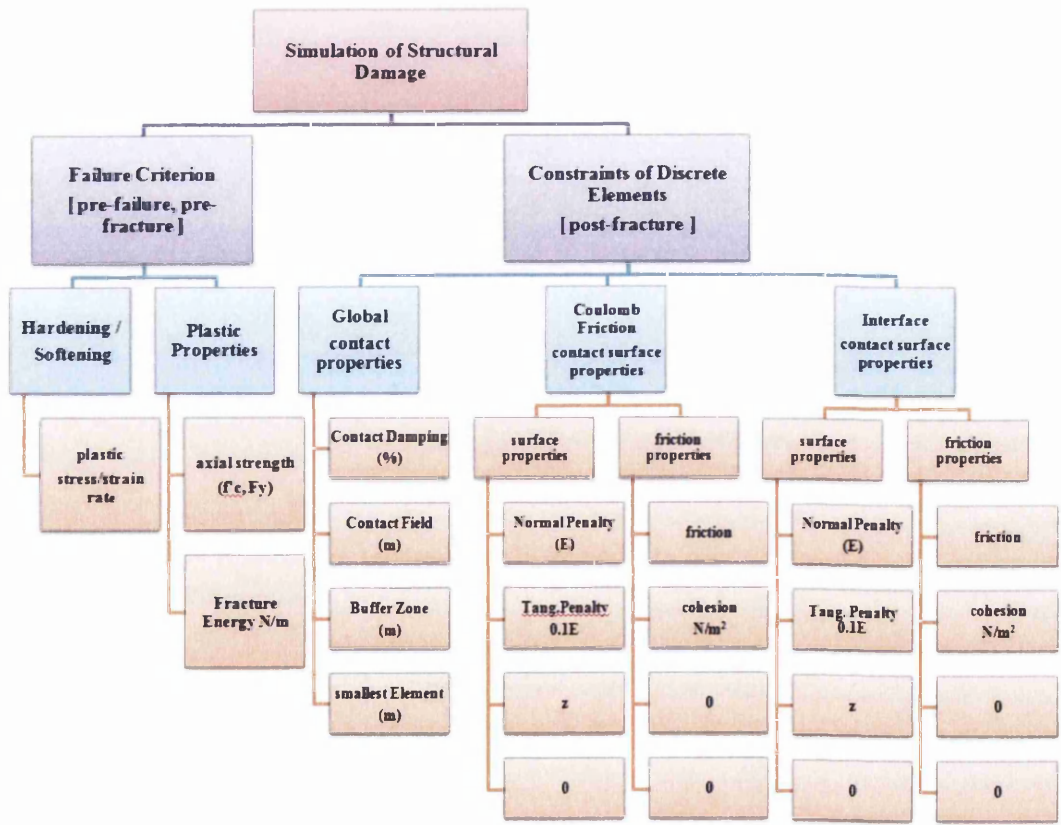
To avoid numerical instability caused by such large penalty values, a ‘relaxed’ situation is provided by allowing the penetration of an element node to the element edge or element surface, for a permissible penetration domain controlled by a ‘contact damping field’.

The following are the post-fracture parameters that are given in the Elfen code to activate the discrete element mode:

- **Contact Damping:** defines the damping factor which is used to modify the contact penalty force which in turn may be increased or decreased depending on the velocities of the contacting bodies. For fracture, values in the range 10%-50% are recommended. A Damping ratio of 200% is given for contacting surfaces that are moving apart. Given 30%.
- **Contact Field:** is the maximum permissible penetration as a function of the length of the element size. It is normally set at 10% to 20% of the smallest element size in the mesh. It was found in this research that if the contact field is too small (less than 10%), it causes excessive penetration of the node towards the element. However, it has also been found that if the contact field is too large (more than 20%), there is no effect on the node-edge algorithm but it has a negative effect on the edge-edge algorithm. Given 0.01 m.
- **Normal Penalty:** the normal penalty value  $P_n$  for the evaluation of the contact force. The value is typically in the range  $0.5E < P_n < 2.0E$  where  $E$  is the Young’s Modulus. Given  $2.76E10 \text{ N/m}^2$ .
- **Tangential Penalty:** the tangential penalty value  $P_t$  for the evaluation of the tangential contact force. The value is typically an order of magnitude less than  $P_n$ .  $P_t \approx P_n/10$ . Given  $2.76E09 \text{ N/m}^2$ .

- Buffer zone: the domain where local nodes of contact are searched in the contact algorithm. It is given an average size of side length of the finite element. Generally this is set as the average side length of the mesh. Given 0.06 m.
- Smallest element: the minimum size of element after fracture occurs. If it is given a size larger than the size of a fracturing element, fracture would occur in between the adjacent elements and not through the element, and it will not be allowed to fracture further. Given 0.05 m.
- Contact Damping types are: No Damping, Rigid Body Defender Node, Node-Edge Velocity Momentum, Velocity/Momentum and Viscous type. The “Velocity/Momentum” contact damping type is recommended for modelling general mechanical interactions.
- Contact Type: Edge-Edge or Node-Edge. Selected the Node-Edge contact type.
- Friction between contacting surfaces is given 0.0.
- Cohesion between contacting surfaces is given 0.0.

Figure 6.3 shows a diagram of the material properties required for pre-fracture and post-fracture processes as related to different categories.



z = -10E-10 = minimum tensile cut-off contact stress, 0 = initial tension cut-off contact stress.

Figure 6.3 Material properties for failure criterion & discrete elements

### 6.1.6 Changes in the Elfen Defaults

In Elfen there are three categories of parameters that have been set at default, and are accessible for amendments according to requirements of the problem. They are; Element Options, Global Options and System Variables. In this proposed problem two parameters in the System Variables category are amended. They are; "RFRACT", or the reserved fraction for discrete element fracturing, which has been changed from 2 to 10, and "MAXDEG" , or the maximum number of edge connections for each node, which has been changed from 40 to 80 or 100 in some runs. Both are associated with the algorithm capacity of the fracturing mechanism for the analysed problem.

Another important default value, which is associated with the time-step control data, and also needs to be amended, is the factor of critical time step, which is 0.9 as a default and changed into a value less than 0.6 for fracturing purposes. In this problem the time-step needed to be reduced by 0.2 and 0.4 to obtain the fracture analysis.

### 6.1.7 Damping for explicit dynamic analysis

In addition to the energy dissipated by the nonlinear yield response of the excited structure, there are other dissipative forces that resist the loading effect, and dissipate some portion of the input energy. These forces are the damping forces. In General, the damping forces are classified according to the following groups:

- *Viscous damping*: most widely used model that was found to be a good approximation for the friction effect on an oscillator in oil or air. The viscous damper (also known as dashpot) dissipates the vibrational energy of the system.
- *Structural damping*: which is due to the internal material damping and friction of joints,
- *Dry friction or Coulomb damping*: describes the motion of a body on a dry surface [1].

Damping forces are assumed proportional to the velocity response of the structure by a proportionality factor  $c$ , which is assumed to be a constant damping matrix, and can be either measured experimentally or estimated [1]. Because of difficulty in determining the damping constant  $c$  for the structural damping type, the viscous model is used as an equivalent to represent damping in RC structures. The equivalent viscous damping contributes in dissipating the energy absorbed by the system.

In an Elfen-Explicit algorithm Point Damping is applied. Point damping applies velocity proportional damping to the nodes created on entities to which it is assigned, i.e. every selected node in the problem will be subjected to point damping. The value of damping prescribed is defined relative to the automatically estimated lowest frequency of vibration for the application and the damping may be prescribed differently for each freedom of the node. For the proposed problem, a damping ratio of 5% is given to the column surfaces to approximate the damping effect for such structures under such low frequency vibrations. For very high frequency vibrations, the Elfen-Explicit is provided with an artificial bulk viscosity for all of the mesh elements to smooth shock discontinuities that may occur in impact problems [2].

## 6.2 MATERIAL MODELLING

For reinforced concrete structures, the material modelling in Elfen encompasses the following materials:

- 1) Isotropic Elastic materials.
- 2) Incompressible Elasto-plastic and Metal Plasticity materials.

Generally, those materials that do not show any volume change when compressed (or tensioned), i.e. incompressible materials have theoretically no volume change, i.e.  $\Delta V = 0$ , and the rate of volume change is the volume change divided by the initial volume:

$$e = \frac{\Delta V}{V_o} = \varepsilon_x + \varepsilon_y + \varepsilon_z = 0 \tag{6.1}$$

where,  $V_o$  is the original volume and  $\varepsilon_i$   $i = 1,2,3$  are the strains in the  $i$ -direction. From Mechanics of Solids, the rate of volume change for isotropic materials is:

$$e = \frac{\sigma_x}{E} (1 - \nu - \nu) \tag{6.2}$$

For incompressible isotropic material, Poisson’s ratio will be  $\nu = 0.5$ , and for incompressible orthotropic materials lower Poisson’s ratios are given, i.e.  $\nu < 0.5$ .

Steel reinforcement bars are Von-Mises elasto-plastic material that may be related to failure, hardening and softening. The constitutive stress-strain relationship exhibits 3 stages defined in Elfen as follows:

- Definition of failure initiation: a yield point where the initiation of failure occurs.
- Definition of material hardening

- Definition of failure softening : at which the stress reduces either immediately or gradually until complete failure is reached where stresses vanish.

### 3) Compressible Elasto-plastic Materials.

Concrete is modelled as an isotropic compressible elastic plastic quasi-brittle material. This is explained as follows:

#### *Isotropy*

Concrete is modelled in most cases having the same elastic properties, namely; Young’s modulus  $E$ , Bulk modulus  $G$  and Poisson’s ratio  $\nu$ , in any uni-axial direction of a specimen.

#### *Compressibility*

As a brittle material, concrete is vulnerable to certain volume change  $\Delta V$  when compressed and damaged. The rate of change in volume for a unit element is:

$$e = \frac{\Delta V}{V_0} = \epsilon_x + \epsilon_y + \epsilon_z \neq 0 \tag{6.1'}$$

When a specimen is compressed in the x-direction all strain components can be found according to the character of compressibility at which the Poisson’s ratio  $\nu$  is larger than zero and less than 0.5. For an isotropic compressible material:

$$e = \frac{\Delta V}{V_0} = \epsilon_x (1 - \nu - \nu) > 0 \tag{6.2'}$$

$\nu$  is given between 0.2 and 0.3 for concrete.

## 6.2.1 Elasticity and plasticity

The uniaxial stress-strain constitutive relation for concrete is assumed linearly-elastic with plastic softening in the tensile stress field. This assumption simplifies the computational effort and in the same time represents the mechanical behaviour successfully. When compared with a typical uni-axial stress-strain curve for concrete, shown in Figure 6.4, the adopted linearized curve makes a reasonable simulation with the reality.

In contrast to the tensile constitutive curve, the compressive uniaxial stress-strain constitutive relation for concrete is approximately 10 times larger in size, and has a hardening part before reaching the failure point, as shown in Figure 6.5. These characteristics are also incorporated within the material properties section of the Elfen. The Elfen code utilizes this relationship in the principal planes and in the 3D configuration in order to control the elastic and plastic behaviour of the loaded material.

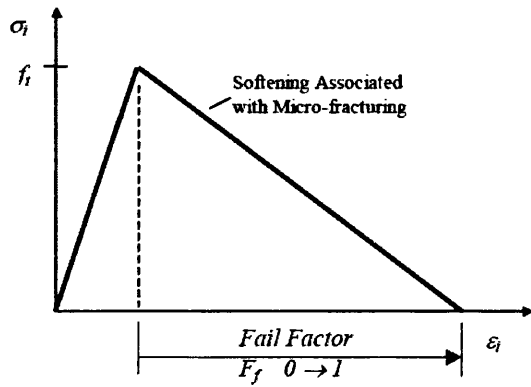


Figure 6.4 Linearized constitutive model[2]

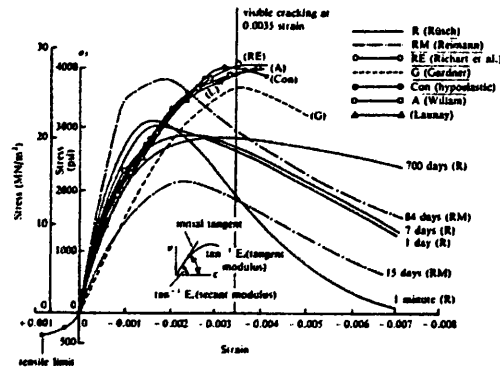


Figure 6.5 Typical uni-axial test [3]

### 6.3 MODELLING OF QUASI-BRITTLE MATERIALS

From a general literature preview on material modelling by the FEM, the post-failure modelling of brittle materials has usually taken one of the following routes:

- Continuum-based approach which adopts the idea of “smeared crack models”
- Discrete-based approach which physically models the fracture paths and its growth.

#### 6.3.1 The Continuum Approach

In the continuum approach the total strain rate is additively decomposed into two components:

- 1- Elastic strain rate: in which the constitutive law defines the relationship between elastic strain rate and stress rate through the *Elasticity Matrix*, and
  - 2- Failure strain rate, which will be, according to associated flow theory of plasticity, analogous to softening plasticity, and dependent on the constitutive law of the failure model.
- The failure model is a function of stress, strain and internal variables.

To model the softening response, experimental data are utilised to obtain a *global* tangent softening modulus  $E^t$  for the material. As shown in Figure 6.6, the experimental data are for a concrete bar under tension, in which a *global* load-displacement curve is obtained. However, the softening modulus has no length scale to ensure mesh independent solutions.



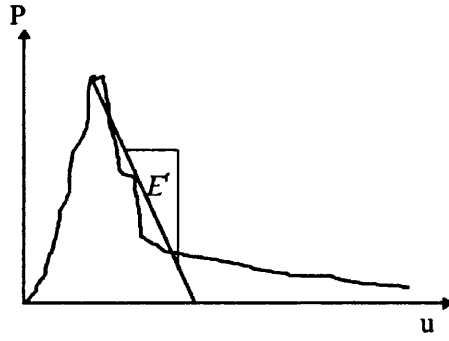


Figure 6.6 Global load-displacement curve of concrete bar under tension

### 6.3.1.1 Fracture Energy

The Fracture Energy  $G_f$  is an appropriate material constant that controls the softening process at some controlled volume, and determines the instantaneous tangent softening modulus  $E^t$  for that volume, i.e., a *local* softening modulus. The fracture energy is defined as the amount of energy needed to create a continuous crack on a unit area, and it is the equivalent alternative to the softening law. The fracture energy for a controlled volume, often chosen to be the finite element, is the area under the softening curve, as shown in Figure 6.7. Modelling wise, if the stresses have not dropped to zero, the area under the softening curve is less than the assigned fracture energy  $G_f$ , and the material is partially damaged, i.e. the Failure Factor is assigned between 0 and 1, and the controlled volume is under micro-cracks but no cracks are initiated yet. If this area is equal to the fracture energy, the material is totally damaged, i.e. Failure Factor=1, and cracks start to initiate.

The release of the fracture energy rate  $\partial G_f$  is dependent on the degree of damage caused during the softening stage, which is defined as:

$$\partial G_f = \sigma \cdot du \quad (6.3)$$

$$G_f = \int \sigma \cdot du = \int \sigma \cdot \varepsilon(s) \cdot ds \quad (6.4)$$

where  $\varepsilon(s) = \frac{du}{ds}$  is the softening strain in the direction of the principal plane. Integrating over a localization band with  $l_c$  for a constant slope softening model, this gives:

$$E^t = \frac{\partial \sigma}{\partial \varepsilon} = -\frac{f_t^2 l_c}{2G_f} \quad (6.5)$$

where,  $l_c$  is a function of an element area, and the negative sign is for the modulus slope. The fracture energy is used to define the softening curve  $E^t$ , and the resulting area under the curve is either larger or less than the energy fracture  $G_f$ .

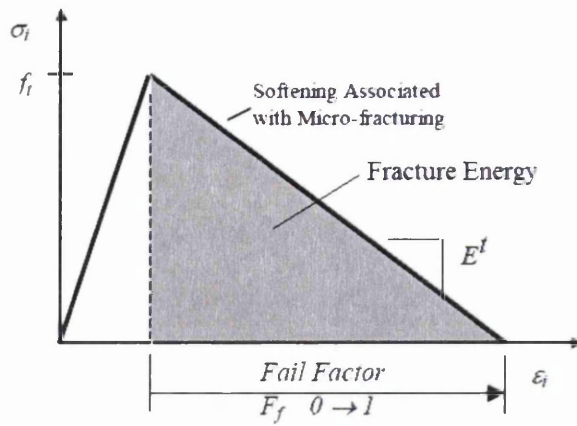


Figure 6.7 Fracture energy under softening curve

Once the plastic stresses drop, the resulting area under the curve is either less than or equal to the fracture energy  $G_f$ . When the area under the curve reaches  $G_f$ , the fracture energy of that point is said to be released, i.e. work of “softening strains” is completed during the softening stage at that plastic zone, and a crack initiates.

As a conclusion, the reason that softening strains occur is that softening is associated with “micro cracks”, which permit such an energy to be released after that Gauss points had gained high stresses at the failure initiation point.

During the Micro-fracture process, an opening of micro-cracks and closing of micro-cracks occur in a brittle material such as concrete, therefore, an unloading of the stress may occur at any stage of Micro-damage before the softening is completely finished, as shown in Figure 6.8. In this case, new strain values are to be calculated for the unloading. The stress-strain slope at that damage is:

$$E^d = (1 - w)E \tag{6.6}$$

where  $w$  is the damage parameter that is dependent on the fracture energy  $G_f$ .

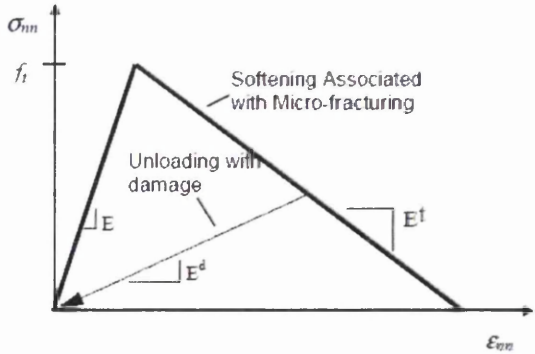


Figure 6.8 Constitutive relation for plastic softening and unloading [2]

### 6.3.1.2 The Smearred Crack Model

The *Smearred Crack* model is a plastic softening model based on the continuum approach. The idea of this model is introduced to rationalise the relationship between  $E^t$  and  $G_f$ . It replaces the physical discrete crack in a controlled volume with continuous micro-cracks evenly distributed across the whole volume, such that the energy dissipated in the discrete and smeared failure process are equivalent. Plastic stresses and softening strains produce the softening work which is equivalent to the resultant micro cracks, as according to the *Smearred Crack* principle. Therefore, visible cracks are assumed to appear directly after the end of this stage.

## 6.3.2 The Discrete Approach (Discrete Fracture Modelling)

Continuum approaches are unable to express post failure interactions since they alternatively exhibit regions of zero strength only. However, the finite/discrete formulation is able to undergo large deformation in quasi-brittle materials.

### 6.3.2.1 Rotating Crack Model

The *Rotating Crack* model is a discrete-based approach. It is neither a plastic softening model nor a pure damage model, and may be seen as a combination of both approaches. The modelling of material failure by the *Rotating Crack* theory is very much an engineering approach.

The *Rotating Crack* model assumes that the direction of a smeared crack rotates, following the maximum principal stress direction during the failure process. From a micro-mechanics point of view if failure occurs in one direction, a system of micro-cracks is activated parallel to the failure direction, and they begin to grow. However, if the maximum principal stress direction progressively rotates, these micro-cracks partially close, and the micro-cracks parallel to the new failure direction are activated, i.e. they open up, and dominate a further crack growth.

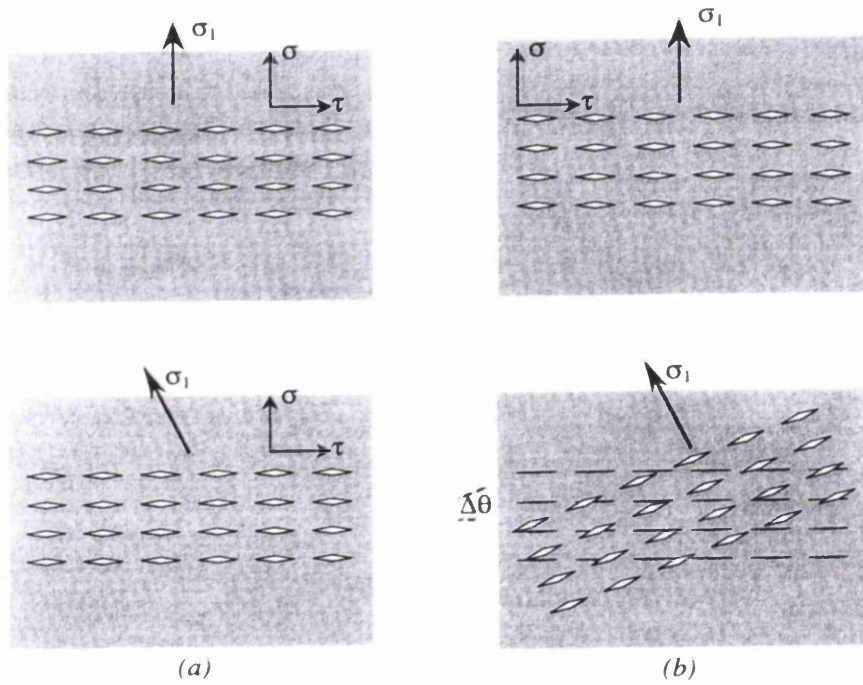
### 6.3.2.2 Fixed and Rotating Crack models

The rotation of any of the principal stresses  $\sigma_1, \sigma_2, \sigma_3$  by a small angle  $\Delta\theta$  is due to the dynamic nature of the internal forces during the loading process. In a *Fixed Crack* model, the

degraded elastic modulus  $E_n^d$  for the failure plane  $n$  remains the same when rotated into plane  $nn$  in the new time-step. This is known as the characteristic of isotropic softening at the *Fixed Crack* model, and thus;  $E_n^d = E_{nn}^d$ .

However, in a *Rotating Crack* model, the degraded elastic modulus  $E_n^d$  for the failure plane  $n$  becomes different when rotated into plane  $nn$  in the new time-step. This is known as the characteristic of anisotropic softening at the *Rotating Crack* model, and thus;  $E_n^d \neq E_{nn}^d$ . The degraded elastic modulus  $E_{nn}^d$  in the rotated failure plane  $nn$  was shown in Figure 6.8.

Moreover, the strength on plane  $n$  in the new time-step returns to its original strength, with modulus of  $E_n$ , and is not degraded since the micro-crack openings are considered 'closed' at that time-step. Thus;  $E_n^d \neq E_{nn}^d \neq E_n$ . The physical difference between the fixed and rotated crack models can be illustrated in Figures 6.9.a and 6.9.b.



**Figure 6.9. a) Fixed crack model b) Rotating crack model**

In post yield, the Rotating Crack represents the damage evolution using the degraded elastic modulus  $E^d$ , and the direction of the principal plastic strains  $\varepsilon_i$  is associated with the principal plastic stresses  $\sigma_i$ , which determine the direction of cracks. This is represented as follows:

$$\sigma_{nn} = E_{nn}^d \varepsilon_{nn} \quad (6.7)$$

where  $nn$  is the local coordinate system of a rotated plane.

## 6.4 MODELLING OF QUASI-BRITTLE MATERIALS IN ELFEN

Concrete is a quasi-brittle material characterised by heterogeneous microstructures, which are known in *linear elastic fracture mechanics* LEFM as *flaws* [7,8]. Flaws constitute in random distribution to concentrate local tensile strains and initiate fracture in the zones of compressive and tensile stresses. *Non-linear fracture mechanics* NLFM is an extension of the LEFM, and has been developed by researchers to account for non-linear effects during fracture. Several models utilize NLFM principals either combined or individualized in order to be capable of simulating the quasi-brittle material. The post-failure models used by the Elfen-Explicit application are listed below:

- Rankine plasticity with softening governed by fracture energy, which is an isotropic plasticity model with failure governed by the tensile strength and isotropic softening. Model 08.
- Rotating crack model with softening governed by fracture energy, which is an anisotropic damage model with failure governed by the tensile strength and anisotropic softening. Model 14.
- Rate dependent rotating crack model, an extension of the standard formulation by inclusion of a rate dependent tensile strength and softening governed by a combination of fracture energy and material viscosity.
- Non-Associated Mohr-Coulomb model with softening, which is a pressure dependent yield function allowing yielding in shear.
- Drucker-Prager Cap model, which is a pressure dependent yield function that allows yielding in shear and compaction in compression.
- Non-Associated Mohr-Coulomb model with tensile strain softening model, which is a pressure dependent yield function allowing yielding in shear, combined with a rotating crack strain softening model for tensile stress states. Model 19.

Two models have been selected in this research to represent the concrete material using Elfen. Both models simulate the quasi-brittle material in 3D formulation under strain-rate independent loading. They are:

- 1- Rankine failure criterion associated with micro-fracturing isotropic plastic softening model, known as Smearred Crack model, and also supplemented with optional fracture mechanism, known as Model 08.

2- The isotropic Mohr-Coulomb failure criterion with tension cut-off, associated with anisotropic damaging model, known as Rotating Crack model. Known as Model 19.

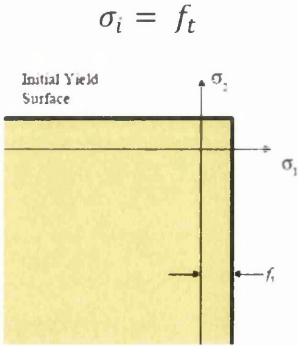
### 6.4.1 Rankine Failure Criterion with Fracture (Model 08)

The Rankine failure, or yield, criterion is based on the critical value of tensile stress of the modelled material. Once the critical tensile strength of the quasi-brittle material is exceeded the resulting strains enter the plastic softening stage, hence the Rankine model is a softening plasticity model.

The Rankine tensile corner introduces an additional yield criterion defined by:

$$\sigma_i - f_t = 0 \tag{6.8}$$

where  $\sigma_i$  are the principal stress invariants ( $\sigma_{1,2,3}$ ) and  $f_t$  is the tensile strength of the material. Both Rankine & Rotating Crack criteria model the tensile failure of a brittle material for Mode (I) fractures according to the criterion shown in the Figure 6.10, and expressed as:



**Figure 6.10 Yield surface for both rotating crack and rankine models**

As the softening strains increase between the failure initiation point and the zero failure stress, the failure energy is built up and fracture begins in this direction, as previously shown in the Figure 6.7. If stress is unloaded before reaching total failure, as previously shown in the Figure 6.8, it is reloaded without damage, i.e. the stress-strain curve in this direction is still isotropic. This means that no damage is considered unless total failure is reached.

Rankine failure is a tensile fracture type, which has the fracture Mode (I). However, when the principal stresses are compressive, no failure is detected by Rankine, and consequently no fracture applies. It should be known that Rankine’s flexural failure is restricted to tensile principal stresses only, and no failure takes place due to compressive principal stresses.

Quasi-brittle materials such as concrete have an anisotropic softening response [2] since the resulting fracture is generally an anisotropic phenomenon. However, the Rankine model is an isotropic plasticity model which considers equivalent strength degradation in all directions. This could be a major shortcoming in the Rankine model [2], nevertheless the application of the Rankine model to concrete systems can be very successful for the restrictive case of Mode (I) failure, where failure is due to tension only.

### 6.4.2 Mohr-Coulomb Failure Criterion Combined with Rankine (Model 19)

In order to simulate a brittle material such as concrete, the M-C failure criterion is slightly modified by having its conic envelope at the tensile stresses cut off, to conjugate with the tensile strength of the concrete. In this case the tensile failure in this modified M-C criterion would be as similar to that in Rankine, as can be seen in Figures 6.11 and 6.12.

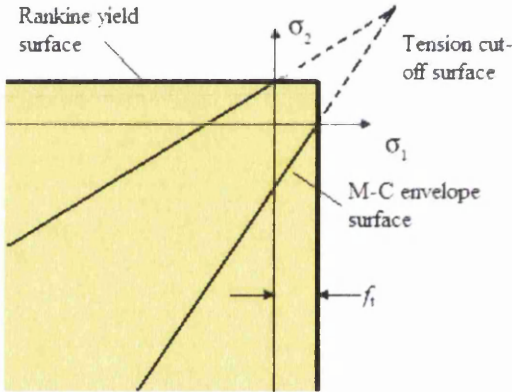


Figure 6.11 Rankine and M-C yield surfaces in 2D space

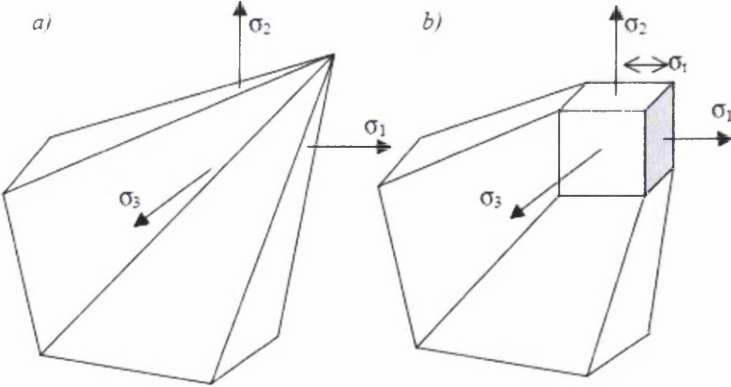


Figure 6.12 Rankine and M-C yield surfaces in principal stress space

The tension cut-off surface boundaries are to be defined by an additional yield criterion such as:

$$\sigma_i - \sigma_t = 0 \quad \text{for } i = 1, 2 \text{ and } 3 \quad (6.9)$$

where,  $\sigma_i$  = principal stresses  $\sigma_t$  = tensile strength of the concrete. The M-C criterion is a generalization of the Coulomb friction failure law and is defined by:

$$\tau = c - \sigma_n \tan \phi \quad (6.10)$$

where  $\tau$  is the magnitude of the shear stress,  $\sigma_n$  is the normal stress on the internal plane,  $c$  is the cohesion and  $\phi$  is the friction angle.

When the compressive principal stresses are combined in certain magnitudes a deviatoric stress,  $\sigma_d = \sigma_1 - \sigma_2$ , initiates, leading the principal stresses coordination point to approach towards the M-C failure envelope. When the M-C envelope is violated, a failure shear stress  $\tau_f$  generates on the internal failure plane of the specimen. However, a shear mode failure, Mode (II), is activated by reaching the M-C envelope, but no consequent fracture is allowed in this modelling algorithm. In this case the finite elements fail in strength but do not fracture since Mode (I) tensile fracture is the only fracture mode that is assigned in this modelling algorithm.

### 6.4.3 Non-associative Flow Rule in M-C Compressive Strains (Strains Dilation)

As being different from Rankine, the M-C is associated with shear stress in the internal failure plane. It is not a softening model since it doesn't consider softening in the compressive field. However, M-C is conjugated with the *Flow Rule*, which controls the direction of the principal strains. Principal strains are responsible for the volume change in concrete, which is known as *Dilation*.

Plastic principal strains  $\Delta\varepsilon$  can consist of two parts; deviatoric strains  $\Delta\varepsilon_q$  and volumetric strains  $\Delta\varepsilon_v$ . Concrete can dilate when the volumetric strains  $\Delta\varepsilon_v$  exist, leading to a possible tensile fracture. However, concrete will not dilate when the plastic strains have no contribution of volumetric strains, i.e. they consist of deviatoric strains  $\Delta\varepsilon_q$  only. In this case they are known as *non-associative* strains since they do not follow the same directions of the plastic principal stresses  $\Delta\sigma$ , i.e. they are not associated with their direction.

Therefore, when dilation exists, the plastic strains envelope, known as the *Plastic Potential Surface (Q)*, creates an angle with the M-C envelope, which is known as the *Yield Surface*



( $F$ ). This angle is known as the *angle of Dilation*,  $\varphi$ , as illustrated in Figure 6.13. When this angle equals the angle of friction  $\phi$ , the plastic potential is fully associated with the yield surface, otherwise it is either partially associated or a non-associative case.

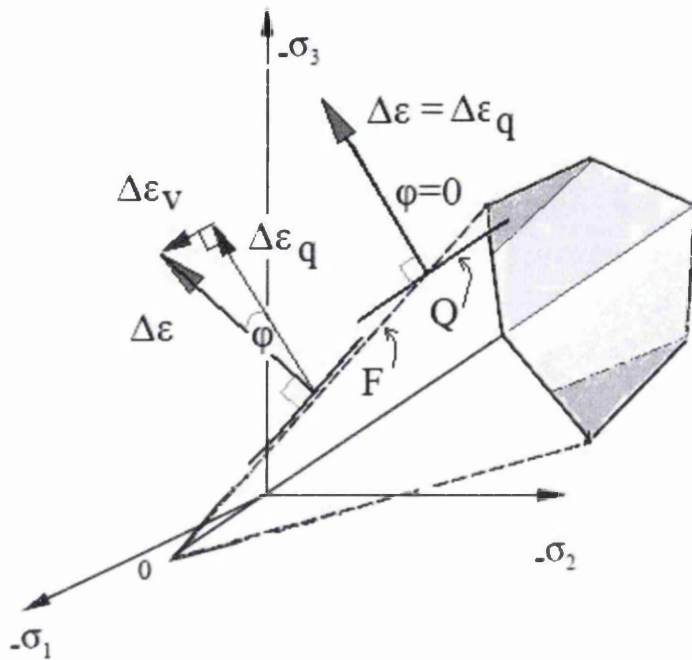


Figure 6.13 M-C yield surface ( $F$ ) and plastic potential surface ( $Q$ ), with associated and non-associated flow rule cases [4]

The angles of dilation decrease as hardening strains increase. In this problem, concrete hardening strains are increased from 0, 0.03 up to 1.0, and in correspondence, the angles of dilation  $\varphi$  are decreased from 15, 5 to 0, respectively. All strains in the softening stage are calculated according to the *Flow Rule* that's associated with the plastic theory of the applied softening model. However, when reaching a non-dilation angle, the *Plastic Potential Surface* ( $Q$ ) which is normal to the plastic strains is not associated with the *Yield Surface* ( $F$ ), which implies that the compressed material becomes a non-dilatent material and the flow of the plastic strains will be deviatoric only; i.e. not straining in the direction of the applied stresses.

In concern with the proposed problem, it was concluded that this phenomenon has a relatively small effect on the overall fracture behaviour of the concrete column. It is believed that the influence of dilatency is little in unconfined problems, and such phenomenon is more significant in problems with structures that have relatively thick geometry and in soil continuum problems [4].

## 6.4.4 Definition of pre-failure, post-failure and post-softening stages

The simulation of concrete in a 3D problem is based on defining the different mechanical stages of the problem, by updating the stresses at the level of an element for every iterative loading process. This is summarized in the following:

- a) Definition of the linearly elastic behaviour by applying the Hook's law for the elastic properties of the material.
- b) Definition of the pre-failure behaviour to consider plasticity as a non-failure process. For concrete this occurs in the compressive stresses field, with hardening stresses preceding the yield point.
- c) Definition of the failure initiation point which occurs due to either compressive or tensile overloading. Once the element stresses are updated and reach the plastic surface, the material is said to have entered the softening stage.
- d) Definition of the post-failure stage, where failure softening process initiate micro cracks to occur in association with the softening strains. When strains reach their maximum value all stresses drop to zero and all of the fracture energy is totally released. At this stage visible cracks should initiate, and the discrete algorithm is put into function.
- e) Definition of a post-softening.

This stage is a response after the softening stage has been completed. When the strain energy is totally released, i.e. it reaches the proposed fracture energy  $G_f$ , which is usually 100 to 150 N/m for concrete, a discrete fracture is formed, which is equivalent to all micro-fracturing that has been associated with the stress softening stage.

Fracture is now introduced using an algorithm that updates the topology of the mesh through insertion of discrete fractures in the "failed" regions. A visible crack is now allowed to initiate, and also propagate, after all fracture energy is released as mentioned before. It is important to know that the Elfen code is applying fracture for the first mode of fracturing, Mode (I), which is the tensile fracture. The Elfen algorithm of fracture is explained as the following:

- 1- The level of damage is calculated in the softening stage for every Gauss point of each element as according to the stress update algorithm of the material model.
- 2- Such failure information for the brittle material is known as the *failure factor*  $F_f$ , which is the percentage of tensile softening in the principal strain.

3- The *Failure Prediction Algorithm* then constructs a *failure map* for the whole domain, based on the previously defined failure information, or the level of damage, which was calculated at every Gauss point for each element.

4- The maximum failure factor  $F_f$  and the average failure factor are calculated from the *failure map* for the whole domain.

5- A searching loop process is activated to determine the highest *average failure factor*  $F_f$ .

6- The corresponding average direction is also determined and a crack is inserted in that point to form a crack initiation by inserting new nodes in the critical elements, as in Figure 6.14.b, or inserting a new edge between two adjacent elements, as in Figure 6.14.c.

7- A crack propagation is also performed in the same procedure for the same elements by inserting new nodes then new edges, and so forth.

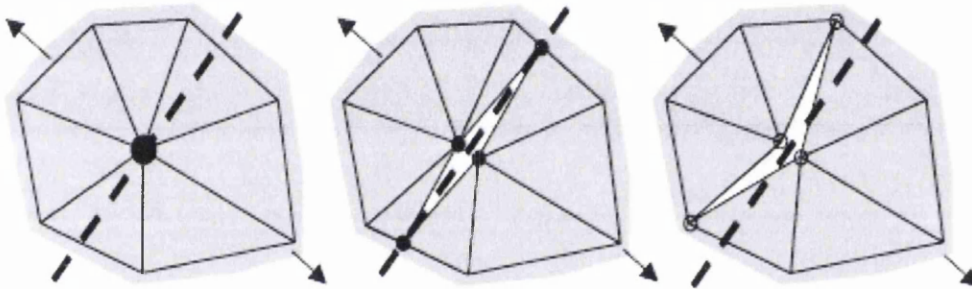


Figure 6.14 Crack insertion procedure; a) Initial state, b) New nodes through element, Or c) New edge along element boundary [5].

## 6.5 MODELLING OF REINFORCEMENT BARS IN ELFEN

The constitutive model of reinforcement steel bar elements subjected to seismic loading can be modelled using a rate independent plastic model, with an isotropic Von-Mises failure criterion. This model is utilised by *Backward Euler* stress update algorithms, with the Von-Mises model being implemented in a nonlinear isotropic hardening form, (which is the plasticity model 07 in Elfen library). However, piecewise linear hardening data are specified using the hardening properties of steel. This is because the linear hardening form is more efficient as the stress update is performed in a closed form, whilst the nonlinear hardening model requires an iterative update procedure [2, page 36 ].

At post hardening, the material suffers softening, where the material strength starts to deteriorate as it strains until fracture occurs, where the topology of the mesh is updated by insertion of a discrete fracture in failed regions. However, the stress-strain constitutive curve for the steel reinforcement bars does not contain the softening nature which probably exist in other Von-Mises materials. Therefore, its fracturing behaviour is sudden and occurs after relatively high ductility behaviour takes place. On the other hand, the Elfen Explicit 3.7 is capable of inserting a discrete fracture in the failed regions, but only for 2D stress states. For these reasons fracture is not modelled in the proposed 3D problem, which is considered as one of the defects in this computational process. Figure 6.15 shows an idealized elasto-plastic constitutive steel curve with hardening.

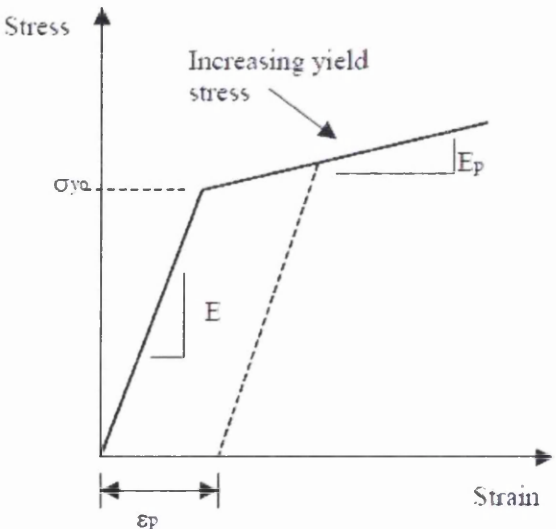


Figure 6.15 Uniaxial steel stress-strain curve with hardening

### 6.5.1 Von-Mises model

The Von Mises failure criterion takes the form of a right cylinder symmetrical around the space diagonal. The only significant invariant is the second deviator stress invariant  $\bar{\sigma}$ , which determines whether a stress state has reached the limit of an elastic behaviour. The other two invariants, namely;  $\sigma_m$  mean stress and  $\theta$  measure of the angular position of the stress point on the  $\pi$ -plane, are not functions of this criterion. The Von Mises, therefore, can be expressed in terms of the 2D stress invariants ( $\sigma_m, \bar{\sigma}$ ) in the plane strain. For the plane  $n$  the Von Mises criterion is shown in Figure 6.16, and given by its strength as:

$$F = \bar{\sigma} - 2 c_u = 0 \tag{6.11}$$

where,  $c_u = \frac{\sigma_1 - \sigma_2}{2}$  is the shear strength, or cohesion, of the material.

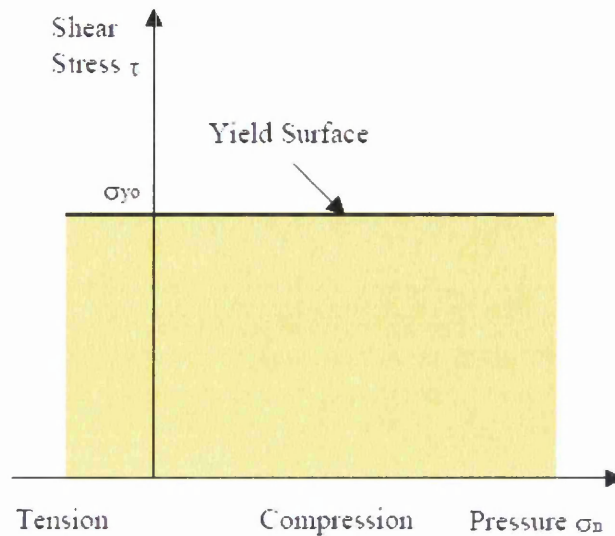


Figure 6.16 yield function for Von Mises model

## 6.6 ASSUMPTIONS IN THE DE/FE MODELLING

Modelling assumptions have been made to mainly suit the requirements of the dynamic analysis and, at the same time, reduce the computational effort as much as possible.

### 6.6.1 Methods of Applied Loading

There are different ways for loading this problem. Either of the following methods can possibly be used, but might result in differing performance due to the different engineering assumptions. The following are the different possible loading methods:

#### 6.6.1.1 The Ground Acceleration Loading

Acceleration load is applied directly to the base of the structure. This is the ideal loading method which represents the realistic response under a full record of ground acceleration loading. It will however, consume a large computational time since the displacement response will have a time delay shift from its corresponding acceleration loading.

If a part of the ground acceleration record is applied, a better response is obtained if at least a record of one peak acceleration between two zero accelerations is applied, so that to include paths of opposite directions of loading. This is important since the change of direction in the

acceleration loading will give more analysis time to allow the top free-moving mass to respond to the peak acceleration loading.

It is important to know that it is not possible to calculate the resulting base-shear if the ground acceleration loading was used. This is because the entire structure would be moving in absolute motion, with no fixities providing the required base-shear force at the base of the structure.

### **6.6.1.2 The Equivalent-Force Loading**

Equivalent load is applied at the C.G of the structure, representing the motion intensity and direction of the virtual force that's equivalent to the ground acceleration effect. This force may be applied to the column top side surface of the top mass.

This force could be approximated by either multiplying the mass of the structure by the ground acceleration according to Newton's 2ed law, or applying the base-shear forces, which is extracted from "another" external analysis, as an equivalent-force loading. Either loading method should have the same effect in a theoretically elastic static analysis. However, in elastic-plastic dynamic analysis the equivalent loading due to base-shear forces and ground forces is different. This is due to the dynamic effect and strength degradation of the structure. However, as an approximated method of loading for the peak loading value for the DE/FE analysis, the peak base-shear forces are selected as equivalent loading, since that the load is applied at the top mass, and its rate of loading should be similar to the rate of base-shear forces.

In Elfen, there are different loading methods for applying such a force-based loading. They are namely; surface loading assigned in  $N/m^2$ , body loading assigned in  $N/m^3$  and point loading assigned in N. As an equivalent-force loading for this modelled problem in particular, the point loading method should be avoided since it causes unrealistic effects on the elements adjacent to the point of application, especially during the non-linear stage of the analysis. Moreover, point loading requires special arrangements, recommended by the Elfen Help manual, concerning special changes to be done in the *Neutral* file. In this research surface loading is applied as an equivalent-force loading.

### **6.6.1.3 The Displacement-Based Loading**

In this type of loading, displacement response of the C.G. of the structure is obtained from "another" external analysis first then applied into this FE analysis. This method will restrain

the displacement according to the previously obtained responses for each time-step, and thus, it will cancel out the mass inertia dynamic effect. Accordingly, this makes the analysis appear to be more like a quasi-static problem, but without excluding the possible damping effect. This loading method must be taken with care, since there are two different movement choices of the top mass:

- a) Movement in the longitudinal z-direction of the bridge structure, where the top-element's movement is vertically restrained due to relatively large moment of inertia of the bridge deck, and the horizontal movement of the top part of the structure is a straight path displacement in the z-direction.
- b) Movement in the transverse x-direction of the bridge structure, where the top mass follows a curved path movement of the C.G. point, and thus, requires more than one component of displacement at a time; the lateral x-component and the vertical y-component. In the x-y plane, both x & y components of the displacement time-history loading must be applied having the same time-steps. However, this choice did not give the correct response since the controlled vertical motion of the loaded surface, or loaded volume, at the y-direction will apply overstressed zones in the column elements, resulting in a topology error in the mesh. On the other hand, the x-displacement cannot be applied alone since it will result in unrealistic straight path movements for the top part of the structure. Such a straight path will enforce a different mode of the column deformation response, and thus, causes unrealistic stressed zones especially in the non-linear stage.

Another problem involved with this choice is the difficult procedures of loading if applying a multi-directional loading on the bridge column problem. Such a problem will need two more displacement components to be assigned in each of the x and z directions in addition to the vertical y-direction.

## 6.6.2 Axial Loading

The R/C bridge column is bearing a permanent static loading representing the dead load of the bridge. This can be represented in the Explicit-Elfen model by either one of the following:

- a. Having an artificial mass structure with density and volume producing an equivalent loading effect.

- b. Applying a permanent face-load value on the column's top surface.
- c. Or, applying pre-stressed values in all of the column elements, to represent the axial load effect.

In this analysis an artificial mass structure is built on the top of the analysed column, and the global gravity loading is activated to produce the dead load effect.

### **6.6.3 Geometric Modelling**

To lower the computational effort, the model body is reduced to half since the loading is applied in one direction only. All parts of the analysed column core, cover and reinforcement bars are analysed for the non-linear behaviour with fractural representation. However, the top mass of the model is analysed linearly and the footing is nonlinearly analysed but without fracturing. This choice was selected to save more computational efforts since the top and footing's contribution to the overall analysis is less important.

#### **6.6.3.1 Geometric and Loading Symmetry**

The geometric and loading symmetry of the proposed problem enabled to run the dynamic analysis for half of the problem only to save the computational effort substantially. Another benefit is to be able to explore the contour results along the core cross section and reinforcement bars directly and more clearly, without the need to work out more post-analysis requirements.

With regard to obtaining fracture representation in a half symmetric structure, it was reported by one user of the Explicit-Elfen code that a better fracture can be obtained by analysing the full geometry and loading in the 3D structure, rather than analysing half volume of the symmetric problem [5]. However, this might not be true for the case of strain-independent problems such as earthquake problems.

## **6.7 DIFFICULTIES IN ACTIVATING THE CRACKING PROCESS IN THE EXPLICIT-ELFEN FRACTURE MODEL**

The fracturing process is activated post to the completion of the softening process. The characteristics of cracks, however, are sensitive to both pre-fracturing and post-fracturing



parameters. However, the scope of this problem is more towards the pre-fracturing parameters, which are the elastic and plastic parameters of the material, since they determine the intensity and rate of initiation and growth of the cracks, whilst post-fracturing parameters govern the motion of the discrete elements after fracture is produced.

The main target in analysing this problem was to attain an active fracturing process that falls between ‘explosive, or progressive’ fracturing and ‘lack of’ fracturing. So many trials of computational runs have been conducted under a variety of parameters in order to reach the targeted fracture. This took a longer time than expected, and can be considered as the major difficulty in analysing fracturing problems using the Elfen program.

Two important parameters of the FE analysis; the time step and the element size, affect the fracturing process significantly. If the time step is too big, quite a few elements would satisfy the fracture criterion within a few analytical time steps, but the process ends up with an explosive type of fracture, which is not realistic. Also if the applied mesh is too coarse at the critical zones, elements cannot express the stress concentration around the fracture tip and therefore, an error of element topology would be prompted.

Therefore, it is more effective to have time step that is as small as possible, and create as finer mesh over the expected fracture plane. The difficulty in setting up such problem parameters is to reach a suitable time step size and mesh size for every different analysed problem, and with every different loading rate.

The explicit algorithm in Elfen computes the size of the time-step automatically, by computing the wave speed,  $c = \sqrt{\frac{\text{Elastic Modulus}}{\text{density}}}$ , which is inversely proportional to the critical time-step,  $\Delta t_{cr} = \frac{1}{c}$ . Therefore, the time step can be controlled by changing the density. Thus if the density is increased by 100 times, the time step will increase by 10 times, and the time of analysis will consequently reduce substantially.

Another way of controlling, or decreasing, the time step is that the time-step is factorised by the *factor of critical time step*  $f_{cr}$  that is set through the control section of the Explicit-Elfen. This factor is multiplied by the critical time step to reduce the actual time step. As a default this factor is set to 0.9, but it has been recommended by one of the local users to use less than 0.6 for fracture propagation projects.

## 6.7.1 Effect of Mass Density on this Problem

Mass density has a major influence on the analysis of dynamic problems since mass inertia is one of the resisting forces against the external applied force. However, when the applied load is chosen to be a displacement-based loading, the mass inertia will not be effective in the analysis, and therefore mass density of that controlled part of the structure can be assigned to any required value without being affected.

However, if the structure is loaded by an external force loading, mass density would be very effective, and only the densities of elements that can be changed are those that do not constitute the top mass. This technique can be used without affecting the main dynamic parameter of mass inertia.

## 6.7.2 Modelling of Reinforcement Bars

The greatest difficulty that was encountered in this research was the time consuming analysis runs when using the Explicit-Elfen on a PC system. Modelling and running the beam elements, or bar elements, as reinforcement bars within the concrete continuum of tetrahedral elements for this dynamic non-linear problem subject to a seismic record of about 1 second only would take about one week to solve the problem. This shows that engineering assumptions must be taken to reduce many modelling parameters, size and geometry. The most time consuming among all other parameters is the analysis of reinforcement bar elements within the concrete continuum elements.

In this problem, two reinforcement types are modelled; longitudinal bars and transverse stirrups. Elfen allows analysing bar elements, or beam elements, together with the tetrahedral elements, with the condition of placing every bar element at the line edge of the modelled volume of a tetrahedral element. This condition assumes orthogonal placements of the reinforcements only, which is not representing the spiral reinforcements for columns, and assuming horizontal typical stirrups, or hoops.

Moreover, no bond effect between concrete and reinforcement is modelled. Elfen assumes full bond between the two different elements, which means that the possible friction effect between the concrete and the longitudinal bars during the dynamic motion is not included. Therefore, the main function of the modelled longitudinal bars is to simulate the overall stiffness of the R/C column member, and the main function of the modelled transverse bars is to simulate the confinement effect of the stirrups.

The non-linearity of the beam elements is controlled by the Von-Mises failure criterion with tensile strength = 475MPa, ultimate strength= 655 MPa and hardening rates of strain-stress couples as follows: (0, 475MPa), (0.0125, 475MPa), (0.07, 655MPa) and (0.12, 655MPa).

### 6.7.3 Modelling of Reinforcement Stirrups

The transverse reinforcement, or stirrups, are modelled as beam elements between the cover and the core of the concrete column, and placed at the edge of the tetrahedral elements as required by Elfen's method for modelling beam elements and tetrahedral elements. For a lower number of nodes, the beam elements are modelled as straight element segments and not circular bar element segments. The latter type requires 3 nodes to be built for each element segment. The horizontal distance between two adjacent longitudinal bars is small, and no effect is caused by this assumption.

The stirrups apply confinement forces on the concrete core of the member, and thus, increase its compressive strength. Seiesmo-Struct uses equivalent confinement parameters to approximate the expected strength of a confined section. This approximation depends on many parameters such as spacing, number of stirrups and others. In the proposed column problem, stirrups are supposed to produce this confinement effect, but no evidence is known about the validity of this assumption in Elfen models.

The expected non-linearity of the stirrups beam elements is controlled by the Von-Mises failure criterion, with tensile strength = 475MPa, ultimate strength= 655 MPa and hardening rates of strain-stress couples as follows: (0, 475MPa), (0.0125, 475MPa), (0.07, 655MPa) and (0.12, 655MPa).

From the Explicit-Elfen analysis for the proposed R/C column problem, results for the xx-In-plane Forces (local axial forces) of the stirrups elements showed very small values at most of the analysed time-steps.

This concludes that there is approximately no effect of transverse reinforcement stirrups found in the proposed problem. The low confinement action found in this problem is attributed to the low gravity load that's applied by the top mass of the structure. Consequently, for larger top mass problems, larger gravity dead load is applied and thus larger confinement will be found.

Other xy & zx Inplane forces (local shear forces), yy & zz Inplane moments (local moments) and torque forces, also showed very small magnitudes at most of the analyzed time-steps.

This showed that stirrups actions, including confinement, shear and torque, in this particular problem analysis did not affect the global flexural mode of failure that the structure is accounted for, and had no other effect either in the elastic or the inelastic stages of response.

This encouraged modelling the RC column member without including transverse beam elements for this particular problem, yet still obtaining similar elastic and non-linear responses. This cuts down the analysis time to a great extent. As a comparison between a RC column model with stirrups and a RC column model free of stirrups, the computer running time ratio was 3:1 respectively.

It should be noted that the stirrups are modelled along the estimated length of the plastic hinge PH for this problem, which is 1.18 meters. It should also be noted that the structure is considered as a generalized SDOF structure that vibrates in the 1st mode of the structural motion, and thus, the only generated plastic hinge is near to the column base. Therefore, the only stirrups needed are along the PH near to the column base only, and there is no need to model stirrups at other parts of the column since no PH is expected. Moreover, it will not be practical to conduct the analysis in terms of computer running time if stirrups are modelled along the entire length of the column.

#### **6.7.4 Computational Size of the Analyzed Problem**

The proposed problem has only 5164 finite elements, (3D tetrahedral & 2D bar elements). The calculated critical time-step size is 0.316625E-06 seconds, which is factorized by the time-step factor that's chosen for this problem as 0.2, and the applied time-step size becomes 0.6332E-07 seconds. It should be noted that the applied time-step is important for the performance of the fracture mechanism in the Explicit-Elfen, and it is crucial to adjust its value independently in order to avoid both 'lack of' fracturing and 'progressive or explosive' fracturing. Definition of the most accurate time-step factor is unique for each analysis independently, since it depends on the loading rate and size of the problem.

The number of numerical steps performed for the first 0.30 second of analysis for this problem was about 2,000,000 steps, which lasted for about 24 hours of running time. This rate is not consistent for successive numerical steps since other stages of non-linear analysis with an implemented fracturing mechanism may take much more running time than this rate. It is worthy to mention that the running analysis for approximately 1 second of analytical time took about 13 days, using a 3 GHz PC machine with Intel Core 2 Duo CPU E8400. The

analysis consumed 17,183,404 time-steps which occupied a space of 30GB, to give the solution for a problem with only 5164 finite elements and time step size of  $0.6332e-07$  seconds.

The total mass of this problem is 294,118 kg which is applied in any direction. The mass centre for the structure is calculated for every time-step. At time 0.30 seconds the mass centre is located at  $x=0.709242E-01m$ ,  $y=10.2045m$  and  $z=0.999004m$ . It should be noted that  $y$  and  $z$  co-ordinations are approximately stable but  $x$ -coordination changes versus time since the applied loading is in the  $x$ -direction.

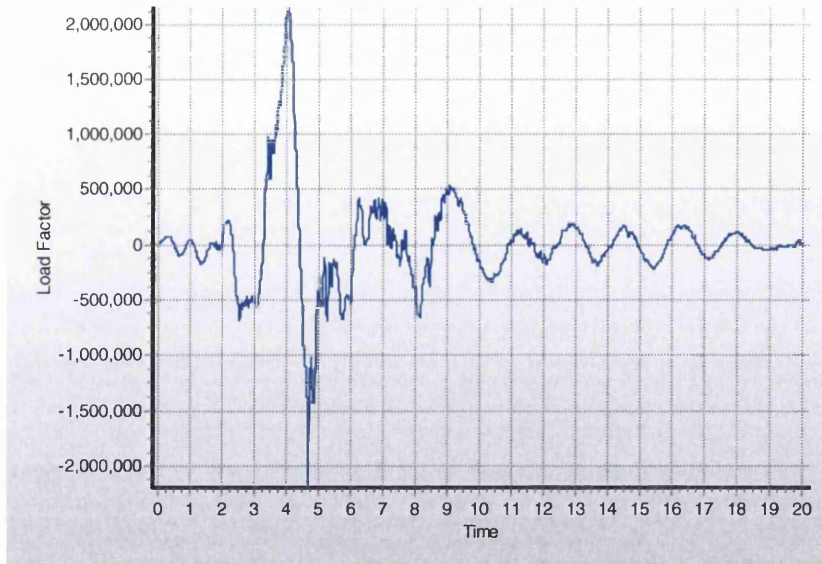
## 6.8 PROBLEM SET-UP FOR DE/FE ANALYSIS

This is the same case study that was adopted in chapter 5. A summary description for the analysed problem is repeated in this section for convenience. The RC bridge column structure has the following properties; aspect ratio  $h/D=10.97m/1.83m=6$ , natural period  $T_n$  of its first mode is 1.3 sec, where  $D$  is the column diameter and  $h$  is the height between the footing and the centre of gravity C.G. of the top mass. The column is subjected to an axial load of 4.5 MN, which is the dead load of the single-cell box-girder bridge, and is equivalent to 5% of the RC column's strength capacity. The RC column has a longitudinal reinforcement ratio of 1.18% and transverse reinforcement ratio of 0.61% [5].

The structure is given a 5% damping ratio, using the Point Damping of the Explicit-Elfen algorithm.

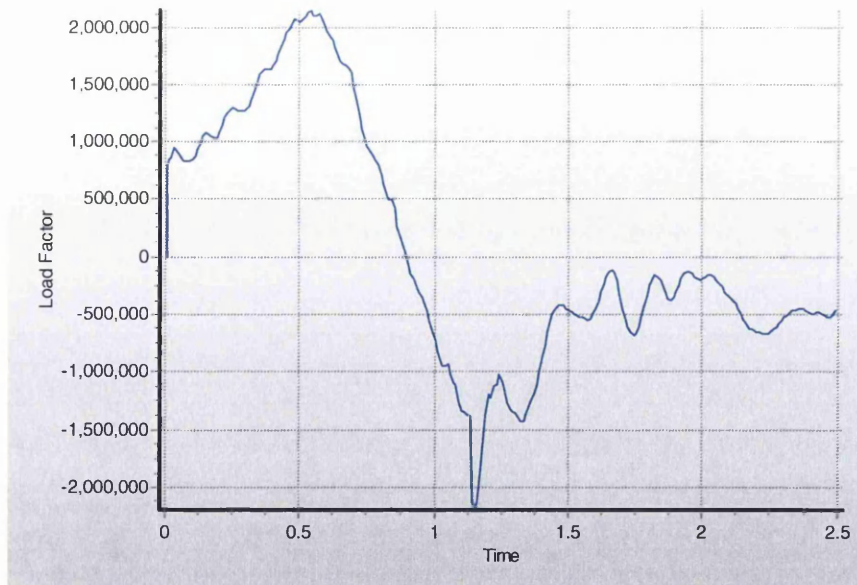
The structure is subjected to the Lexington Dam record, from the Loma Prieta earthquake 1989 [6], as previously mentioned. As equivalent to the peak ground acceleration PGA of this ground motion, an equivalent force is applied on the centre of gravity C.G. of the top mass. This equivalent force is extracted from the base shear analysis for the structure under this ground motion. The structural analysis is performed by the SeismoStruct dynamic solver, and the base shear forces for the whole analysis are shown in Figure 6.17.

The required axial loading is due to the dead load which is modelled by having an artificial mass structure with density and volume producing an equivalent loading effect. For less computation efforts in the analysis, the following procedures have been taken:



**Figure 6.17 Base-shear force response of the Lexington ground motion as load factors (N)**

1. Applying only half a structure since both geometry and loading are symmetric about the xy vertical plane.
2. Excluding modelling of reinforcement stirrups apart from the PH zone, since the confinement of concrete core is more important in that zone.
3. Out of the total record time of 40 seconds, only the peak loading values are selected from the base shear analysis. The maximum lateral force loading is approximately  $2.2 \times 10^6$  N, and the corresponding time is from 3.48 seconds up to 5.98 seconds, lasting for 2.5 seconds only, as shown in Figure 6.18.



**Figure 6.18 Selected peaks of the base-shear forces as load factors (N)**

# 6.7 RESULTS AND DISCUSSION

By using the equivalent-force method of loading, it is possible to obtain the base-shear forces from the DE/FE analysis. This analysis was performed for the proposed problem, using the previously described modelling assumptions, and Mohr-Coulomb failure criterion with the Rotating Crack model, or model (19) in the Elfen code.

The curve of base-shear versus lateral displacement is plotted as shown in Figure 6.19, together with the hysteretic quasi-static curve and the non-linear dynamic hysteresis curve previously obtained by the SeismoStruct analysis for the same structure.

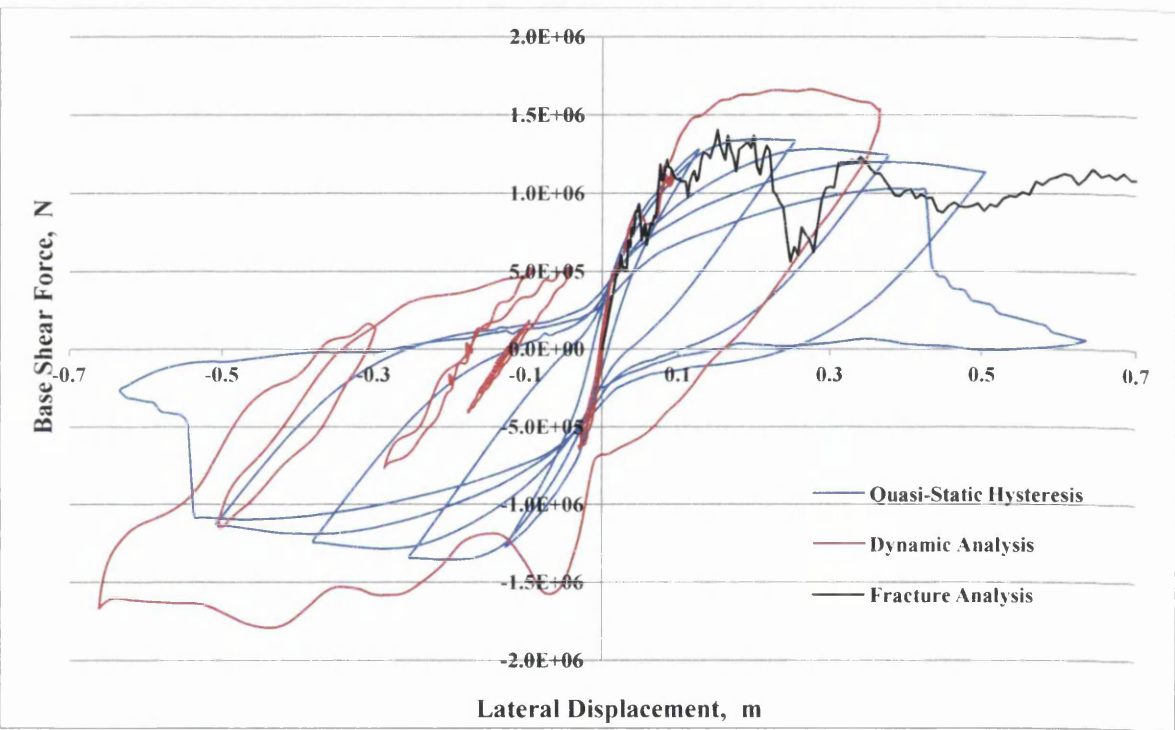


Figure 6.19 Load-deflection curves by quasi-static, dynamic and fracture analyses for the RC column structure under Loma Prieta earthquake

Comparing between the SeismoStruct analyses in Figure 6.19, the difference between quasi-static and dynamic analyses is due to the difference between the cyclic loading effect and dynamic loading applied by the fibre element analysis, where more energy is dissipated by the cyclic effect, producing the hysteresis loops with more strength degradation.

Comparing between the SeismoStruct and fracture analyses in Figure 6.19, the linear stiffness of both quasi-static and dynamic analyses curves have good agreement with the fracture



analysis by Elfen. However, degradation of strength is noticed before reaching the maximum loading, and base-shear force remains approximately at 1.0MN during the rest of the analysis until total collapse occurs. Due to severity of damage, the structure is deflecting towards an unstable position as the plastic hinge PH becomes severely fractured.

Table 6.2 shows the structural response at selected times of the analysis. The responses are: lateral displacements at the c.g. of the top mass and stresses of the longitudinal bars at the plastic hinge zone, base-shear forces, bars stresses at mid level of the plastic hinge PH zone and evaluation of damage occurred at the plastic hinge.

<b>Time (s)</b>	<b>Applied Lateral Load (MN)</b>	<b>Lateral Displacement (m)</b>	<b>Base-Shear Forces (MN)</b>	<b>Bar Tensile Stress at PH, MPa</b>	<b>Bar Compressive Stress at PH, MPa</b>	<b>Evaluation of Damage at PH</b>
<b>0.1</b>	0.838	0.0205	0.60	154.6	-77.3	Few cracks
<b>0.2</b>	1.0753	0.0844	1.15	464.0	-309.3	Propagation of cracks
<b>0.3</b>	1.273	0.196	1.35	477.8	-77.3	Core cracks and slight spalling of cover
<b>0.4</b>	1.661	0.367	1.2	525.0	-61.8	Core cracks and cover spalling and One bar tend to buckle
<b>0.5</b>	2.039	0.618	1.0	572.0	-61.8	Severe core cracks and severe cover spalling
<b>0.6</b>	1.964	0.961	1.0	618.6	-32.4	Severe cracking and buckling of Two bars
<b>0.7</b>	1.490	1.388	1.0	626.3	-46.4	Collapsing and buckling of Five bars
<b>0.8</b>	0.717	1.873	0	626.3	-46.4	Total collapse
<b>0.9</b>	-0.081	2.358	0	626.3	-46.4	Total collapse
<b>1.0</b>	-0.648	2.771	0	626.3	-30.9	Total collapse

**Table 6.2 Fracture Analysis Responses of The RC Column Structure Under Loma Prieta Earthquake**

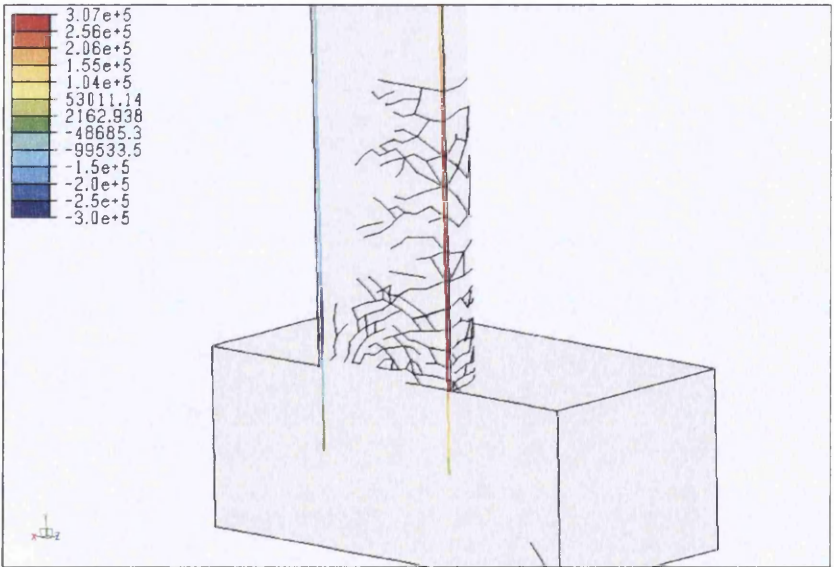
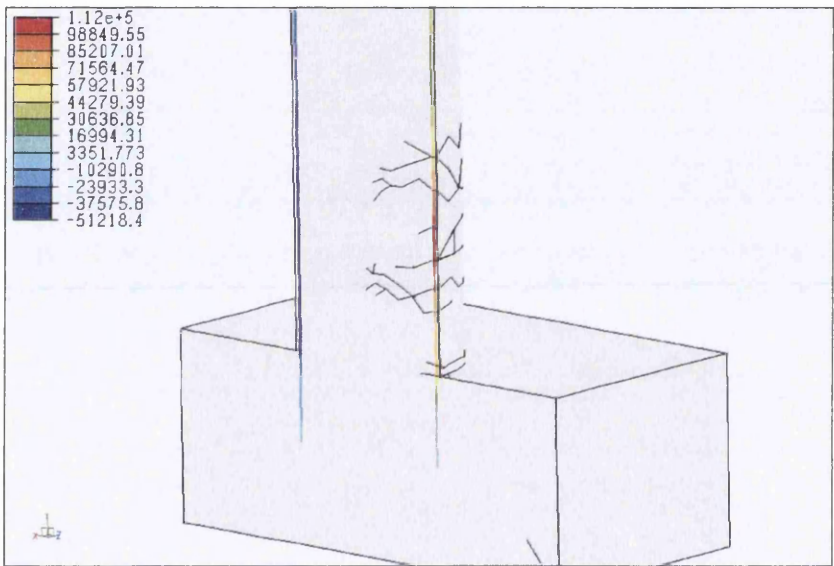
The base-shear values are approximated in Table 6.2 because of the fluctuation of values, as appearing clearly in the load-deflection curve in Figure 6.19. The base shear tends to decrease at time 0.4 seconds when one bar tends to buckle. The base-shear remains at 1.0MN when severe core cracking occurs at times 0.5, 0.6 and 0.7 seconds. At times 0.8, 0.9 and 1.0

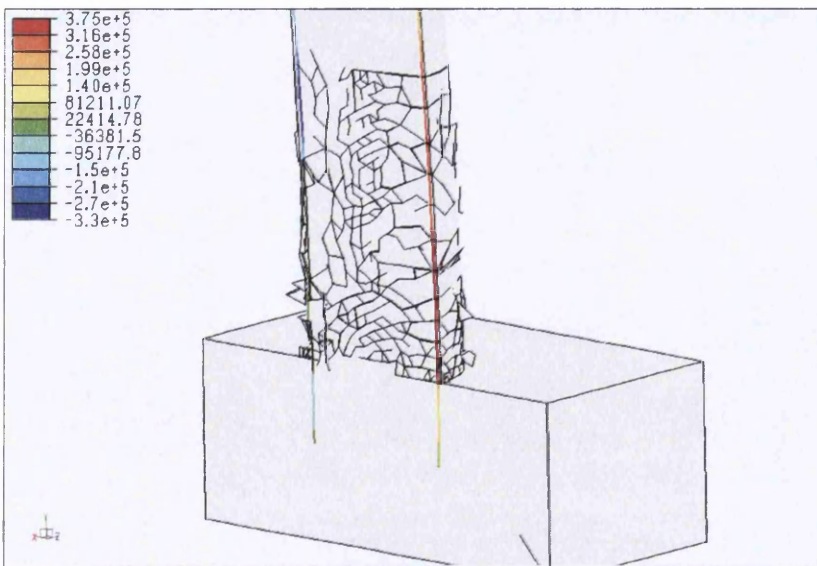
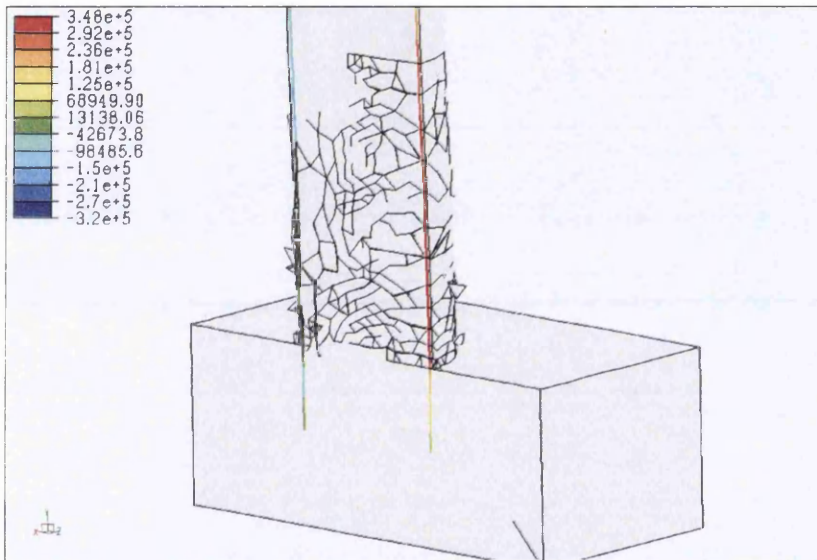
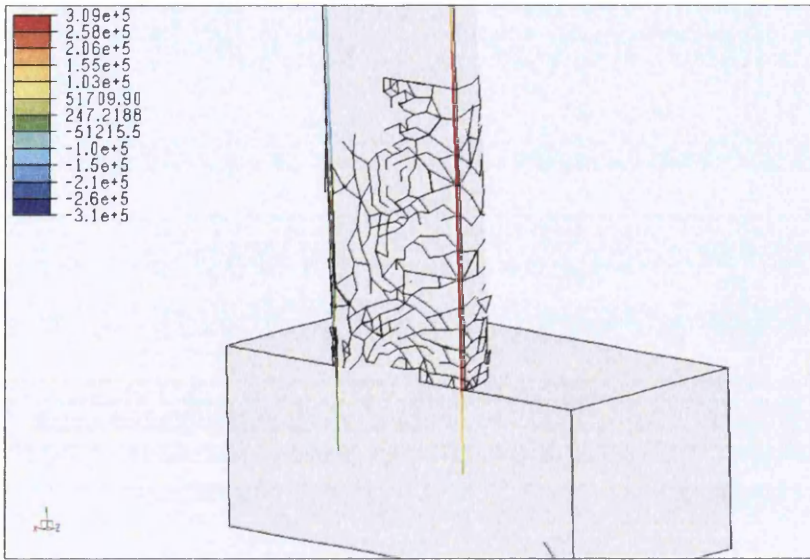


seconds, the structure does not respond to the applied load since no base shear is found, but rather moving laterally in the same x-direction towards total collapse.

In respect to bar tensile stresses, the yield strength and ultimate strength of the longitudinal reinforcement bars are 475.0MPa and 655.0MPa respectively. Bars tend to yield between 0.20 and 0.30 seconds of the analysis time, as can be seen in Table 6.2. Then, they start hardening until reaching their ultimate strength at 0.70 seconds of the analysis time. Then, they don't exceed 626.3MPa during the stage of total collapse.

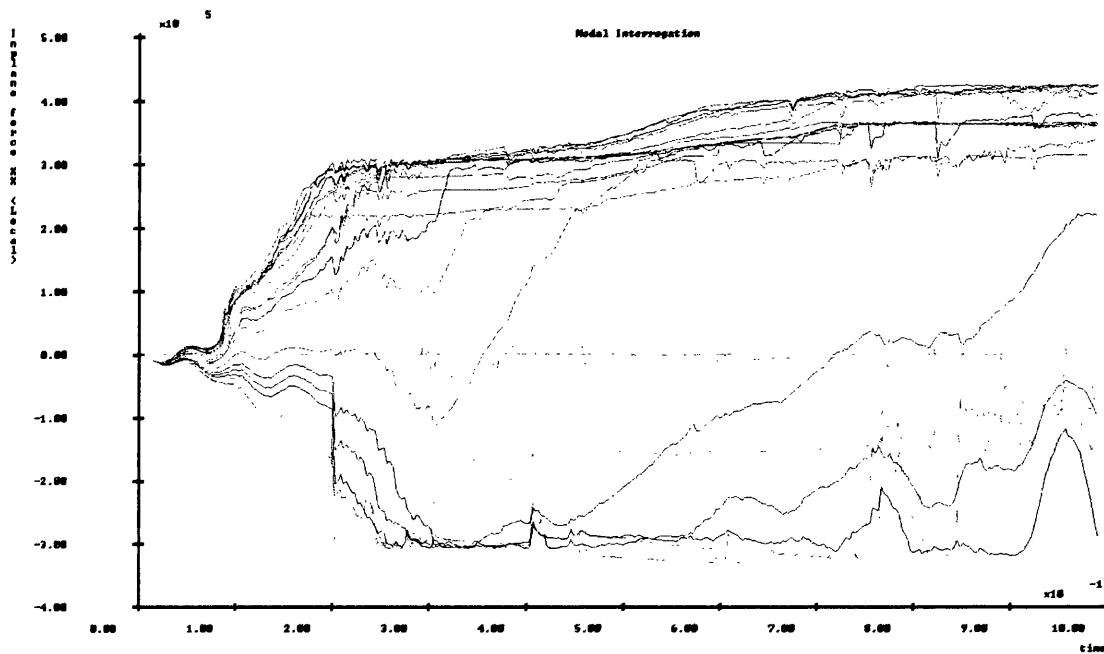
The following Figures 6.20, 6.21, 6.22, 6.23 and 6.24 show the fracture in concrete and axial forces in the reinforcement bars at the analysis times of 0.1, 0.2, 0.3 0.4 and 0.5 seconds respectively. The pictures show the plastic hinge zone of the RC column.





Figures 6.20, 6.21, 6.22, 6.23 and 6.24 Fracture in concrete and axial forces in the reinforcement bars at 0.1, 0.2, 0.3 0.4 And 0.5 seconds, respectively

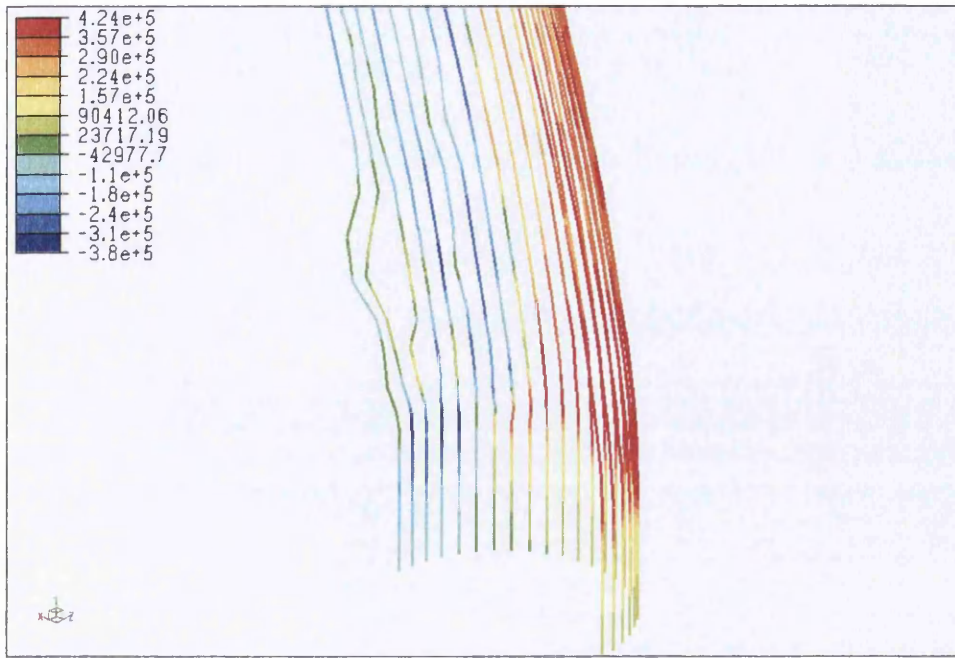
Figure 6.25 shows the time history of axial forces of the reinforcement bars at some level in the plastic hinge zone. Bars of tension stresses reach 626.3MPa during the collapse stage, which is close to the ultimate strength (655.0MPa) of the steel bars. Some bars alternate from compression to tension and lose their efficiency in compression, since they lose the assumed full bond effect when concrete fractures at the plastic hinge. Figure 6.25 shows that when exceeding 0.3, 0.4, 0.5 and 0.6 seconds some bars under compression tend to lose compression stresses because of buckling. This is also shown in Table 6.2, in which many bars lose their compression stresses from -309.3MPa to become as low as -61.8MPa and -32.4 MPa.



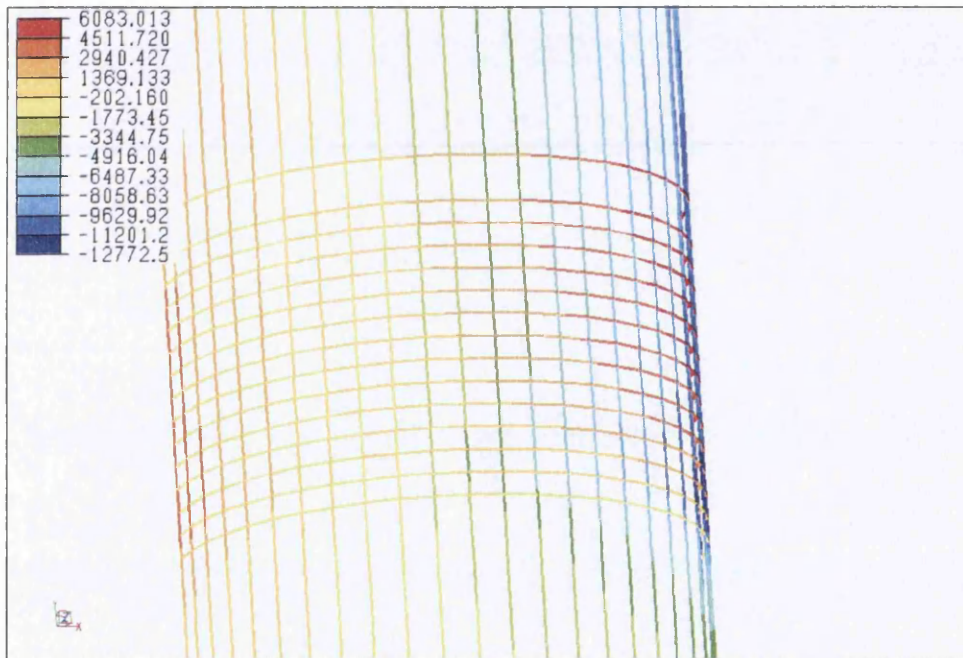
**Figure 6.25 Axial tensile & compressive forces (N) on longitudinal bars at plastic hinge zone**

Figure 6.26 shows a picture of longitudinal reinforcement bars only, buckling in the compressive stress bars, with tensile stress of 626.3MPa in the tensile stress bars. As the analysis is running and more cracks are growing, the structure loses its stability, causing fully damaged core elements. This indicates a severe damage state in the PH zone with total failure, as the longitudinal reinforcement bars are completely or partially destroyed.

However, in cases where bars are not totally exposed and not severely deformed, they tend to prevent the structure from totally collapsing, even though residual displacements still exist. Elfen does not model fracture in reinforcement bar elements, but is rather able to show their elastic and plastic axial stresses, in addition to their deformation due to both tensile and compressive actions.



**Figure 6.26 Buckling of some bars causing instability at 626.3MPa of bar tensile stresses**



**Figure 6.27 Confinement of stirrups reaching only 4.5% of ultimate steel tensile stress**

Figure 6.27 shows that in this proposed example very low confinement around the concrete core is achieved, since the tensile stress in the stirrups reached only 6.5% of the tensile stress of steel (475.0MPa). This is because the axial dead load is very low in this example, reaching only 5% of the capacity of the RC column as previously mentioned. This amount of stirrups confinement does not contribute much to the integrity of the confined core, and thus, cracks grow and spread densely, leading to total collapse.

## 6.7.1 Comparison of Collapse Performance Between Mohr-Coulomb and Rankine

Figure 6.28 shows a comparison of base-shear/deflection curves between two fracture analyses, using two failure criteria; Rankine failure criterion and Mohr Coulomb failure criterion with tension cut-off surface. Both analyses are supplemented with fracture models, but differences exist in the two responses.

In the beginning of the plastic range, the Mohr-Coulomb response curve is more conservative than the Rankine response curve. This is because Model (19) in Explicit-Elfen is utilizing the M-C criterion together with the dilation-hardening properties, whilst the Rankine criterion is not associated with the dilation-hardening properties. In Model (19), concrete is assigned a pre-failure plastic behaviour in the compressive stresses field, with hardening stresses preceding the failure point.

The angles of dilation decrease as hardening strains increase. As mentioned before, concrete hardening strains in this problem are increased from 0, 0.03 up to 1.0, and in correspondence, the angles of dilation  $\varphi$  are decreased from 15, 5 to 0, respectively. All strains in the softening stage are calculated according to the Flow Rule that's associated with the plastic theory of the applied softening model.

However, once the failure point is exceeded for the majority of elements in the PH, fracture is processed as soon as the fracture energy value is reached. In this sense, the Rankine criterion is less conservative than the M-C criterion, since its failure surface is wider than Mohr Coulomb's surface, as can be noticed from both failure surfaces in Figure 6.11. As a rule of thumb, the Rankine failure criterion accounts for tension failure mode only, while the M-C failure criterion accounts for both tension and shear failure. This is the reason why the base-shear/displacement curve with the Rankine response is less conservative than the M-C response curve during the fracture and collapse stages of the majority of elements in the analysis, as clearly seen in Figure 6.28.



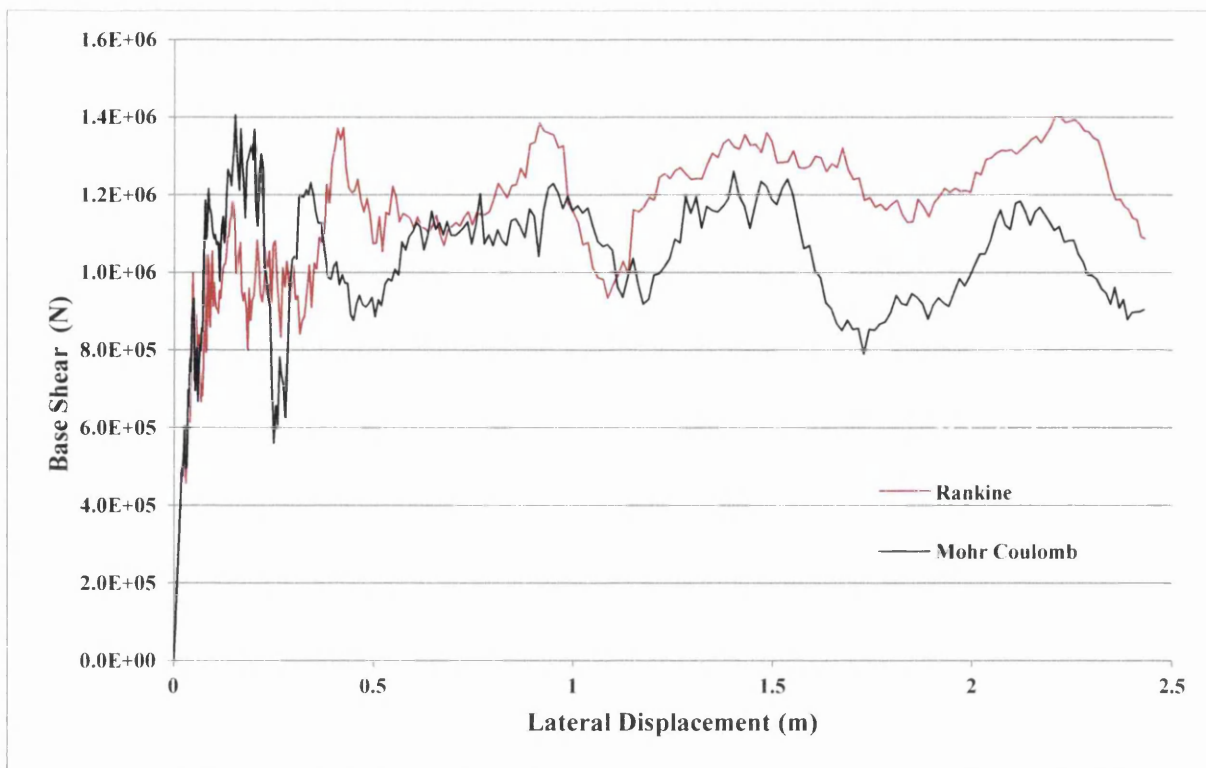
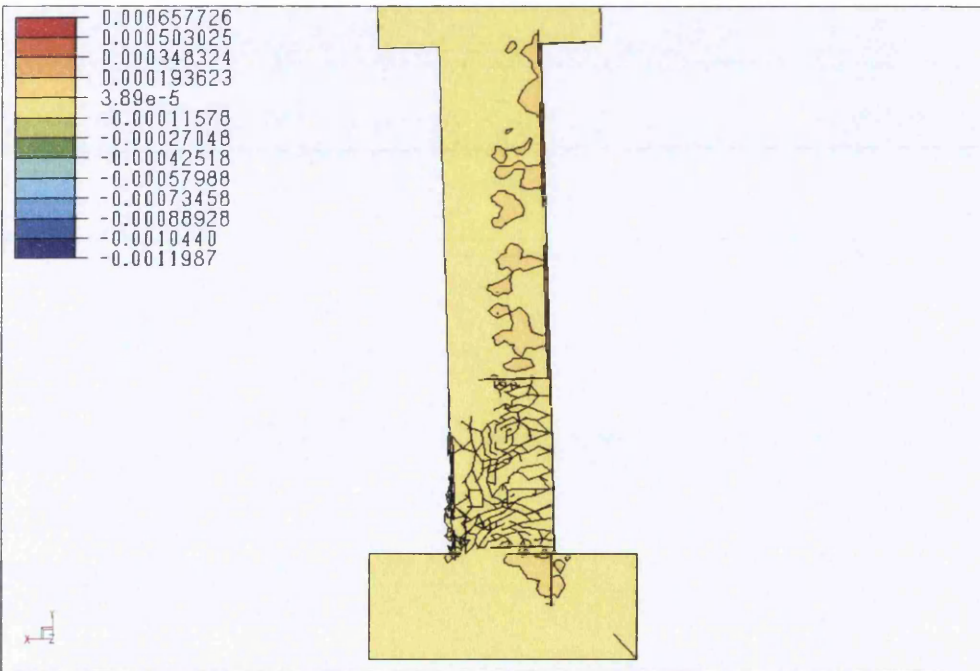
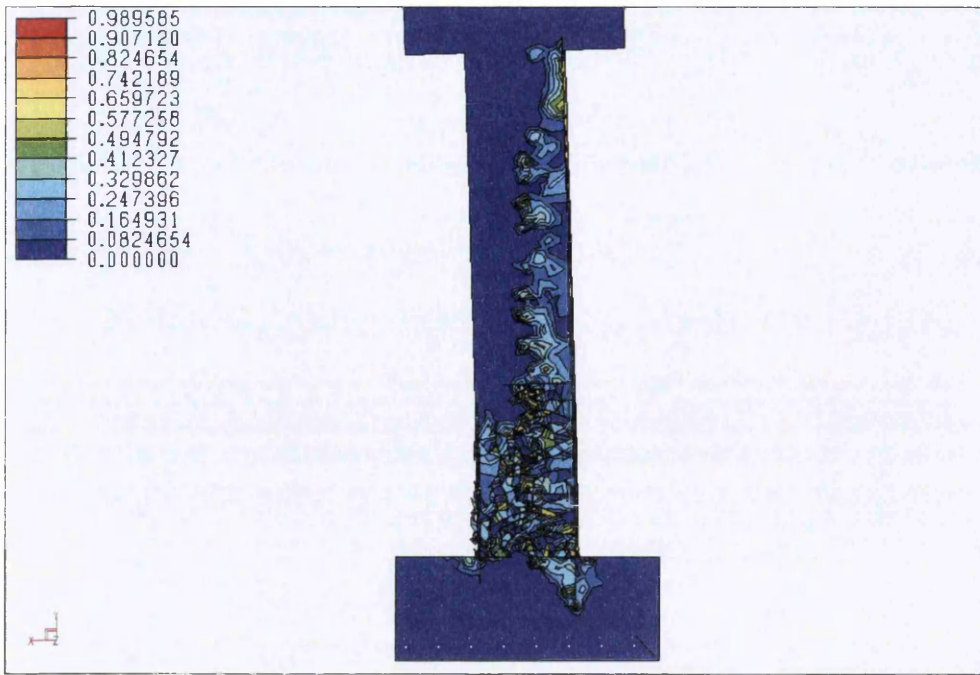


Figure 6.28 Base-shear versus displacement curves of collapse under different failure criteria

## 6.7.2 Fracture and axial plastic strains

The Explicit-Elfen can indicate the fracture state of the modelled problem by using a range of damage between 0 and 1, as shown in Figure 6.29 for the model when subjected to 1.619MN lateral loading. The coloured zones on the tension side of the column are not necessarily fractured. However, when they are below 1.0 they are still within the softening stage, as shown in the upper part of the column, and they fracture when they exceed 1.0. Figure 6.30 indicates a few plastic zones with axial strains in the y-direction, or vertical direction, at the upper part of the column and the footing part, while the fractured zone does not indicate any plastic strains since it is a post-softening zone.



**Figure 6.29 & 6.30 Fracture state indicator and axial plastic Y-strains under 1.619MN lateral load.**

The rest of the structure elements show zero or very small compressive and tensile axial strains in the y-direction. It should be noted that the crack model in this analyser is applied with tension mode (I) only, and therefore, all fractures on the tensile parts of the column crack perpendicular to the axial strains in the y-direction, and all cracks on the compression parts are perpendicular to the axial strains in the x-direction, as can be clearly noticed in Figure 6.30.

## 6.8 CONCLUSION

- The combined DE/FE analysis using the Elfen-Explicit application is a successful tool to solve RC column structures under dynamic loading, investigate the non-linear behaviour and determine the expected local damage state.
- The time-step size in the explicit central difference solution algorithm is relatively smaller than that in the implicit approach. This requires a very large number of time steps to maintain stability. The explicit central difference time integration scheme is computationally expensive, especially for combined DE/FE analysis problems that require a large overall time history such as in earthquake problems.
- The combined Discrete/Finite Elements DE/FE method performs the analysis for both pre-fracture and post-fracture behaviour. The post-fracture properties are not significantly useful to the field of seismic engineering, but it is necessary to run the problem analysis. However, the pre-fracture process is essential to define the expected local damage for the structure.
- Two models for solving the RC structure are used under the principles of *Non-linear fracture mechanics* NLFM principals to simulate the quasi-brittle material in 3D formulation and under strain-rate independent dynamic loading. They are; 1) Rankine failure criterion associated with micro-fracturing isotropic plastic softening model, known as Smearred Crack model, and also supplemented with optional fracture mechanism, Model 08 in Elfen. 2) The isotropic Mohr-Coulomb failure criterion with tension cut-off, associated with anisotropic damaging model, known as Rotating Crack model, Model 19 in Elfen. The Differences between the two models lead to slight differences in the load-deflection curves during the plastic pre-failure stage of the analysis and during the post-fracture stage. Model 19 is more suitable to simulate quasi-brittle 3D structures since it contains more detailed properties of the material such as hardening, dilation and both tension and shear failure modes. It is also provided with the Rotating Crack Model which is more sophisticated than the Fixed Crack Model.
- Reducing the computational effort and time of the analysis requires that engineering assumptions must be taken to reduce many modelling parameters, size and geometry. In contrast, the computational size of the problem needed to be increased by decreasing the time step by 0.4 or 0.2, since it is strongly recommended that the time-step must be factorised by less than 0.6 to obtain fracture propagation. Therefore, practical judgements must be taken to run such problems on PC systems. The most time consuming among all



other parameters was the analysis of reinforcement bar elements within the concrete continuum elements.

- The Explicit-Elfen algorithm is not capable of modelling realistic bond effect between concrete and reinforcement. Explicit-Elfen assumes full bond between the two different elements, which means that no possible frictional effect between the concrete and the steel bars could exist during the dynamic motion. However, a damping ratio of 5% was implemented in the analysis to account for possible viscous damping due to resisting factors such as friction between elements.
- No fracture is simulated for the reinforcement 2D bar elements in the Explicit-Elfen algorithm, but rather elastic and plastic axial stresses are processed together with consequent strains.
- When concrete fractures at the plastic hinge zone, longitudinal bars lose some of their efficiency in tension and compression, since they lose the assumed full bond effect. This causes buckling of bars, and at advanced loading, some bars under compression tend to lose compression stresses because of buckling. The structure loses its stability as more cracks are growing, causing a fully damaged core zone and largely deformed bar elements.
- High confinement action can prevent much of crack penetration inside the concrete column core, however, the formation of confinement stresses around the core is a function of the axial load on the section, and it produces the balance between outward strains of the concrete core and inward stresses of the steel hoops. If the axial loads are not sufficient, very low confinement is produced, and therefore, more cracks may penetrate inside the column core.
- Very low confinement around the concrete core is achieved in this example, since the tensile stress in the stirrups achieved only 6.5% of the tensile stress of steel (475.0MPa). This is because the axial dead load is very low, reaching only 5% of the column capacity. Such confinement does not contribute much to the integrity of the confined core, and thus, cracks grow and spread densely, leading to a total collapse.
- The crack model simulates fracture according to the tension mode (I) only. Consequently, all cracks on the tensile stresses zone of the column are perpendicular to the axial strains in the y-direction (vertical direction), and all cracks on the compressive stresses zone of the column are perpendicular to the axial strains in the x-direction (horizontal direction).

- The SDC seismic design criterion that's used by many building codes is based on the principle of seismic demand/seismic capacity balance. This principle functions effectively to achieve Performance-Based Seismic Design, but requires an effective ductility of the members to function properly during the non-linear stage. However, in RC sections this principle lacks to sufficient members ductility, since that ductility is disrupted by concrete cracks which cause less concrete/steel bond, and thus, the steel bars become vulnerable to large deformation or buckling. Therefore, the seismic demand/capacity principle is not sufficiently fulfilled.
- Single RC columns supporting single or multiple-cell box-girder bridges are vulnerable to high risk damage at their plastic-hinge zones, since they have less confinement action failing in the flexural mode and are subjected to strong ground motion or long duration ground acceleration.

## 6.9 REFERENCES

- [1] H.P. Mlejnek, J. H. Argyris, Dynamics of structures (Texts on Computational Mechanics), V5, Elsevier Science & Technology, 1991.
- [2] Swansea University, ELFEN-Explicit User Manual, Version 3.8, Rockfield Software Ltd 2006.
- [3] Y. Bozorgnia, V.V. Bertero. Earthquake Engineering: From Engineering Seismology to Performance-Based Engineering. 2004, CRC Press.
- [4] M. O. Ben Amer, Effect of Pile loading on a rock layer of finite thickness (Numerical Investigation), M.Sc. Thesis, May 1996, Benghazi.
- [5] Z. B. Jaini. Computational multi-scale modelling of ceramic composite layer and reinforced concrete slabs subjected to blast loading. PhD Thesis, University of Wales, Swansea, 2012.
- [6] Junichi Sakai, Stephen A. Mahin, Analytical investigations of new methods for reducing residual displacements of reinforced concrete bridge columns, Pacific Earthquake Engineering Research Centre, PEER Report 2004/02.
- [7] TA. T. Bere. Computational modelling of large-scale reinforced concrete structures subjected to dynamic loads. *PhD Thesis*, University of Wales, Swansea, 2004.
- [8] P. A. Klerck. The finite element modelling of discrete fracture in quasi-brittle materials. *PhD Thesis*, University Of Wales, Swansea, 2000.
- [9] M. Janssen, J. Zuidema, R. Wanhill, FractureMechanics, Spon Press, 3ed edition 2004.

# Chapter 7

---

## Effect of Loading Rate on the Fracture of RC Columns

### Multi-scale analysis

---

#### Contents

7.0	INTRODUCTION .....	231
	(PART ONE) .....	231
7.1	CLASSIFICATION OF LOADING RATES .....	231
7.1.1	Strain-Rate Dependent Problems .....	231
7.1.2	Acceleration Pulse .....	233
7.2	DAMAGE APPROACH.....	235
7.2.1	Stress-Based Damage .....	235
7.2.2	Fracture-Based Damage .....	238
7.2.2.1	Problem Set-up for the FE Analysis .....	239
7.2.2.2	Results and Discussion .....	240
7.2.2.3	Conclusion.....	243
	(PART TWO).....	244
7.3	MULTI-SCALE SEISMIC ANALYSIS .....	244
7.3.1	Relative Response Technique RRT .....	245
7.3.2	Set-up of Problem Modelling .....	246
7.3.3	Discussion of Results.....	249
7.3.4	Conclusion.....	250
7.4	REFERENCES .....	251

## 7.0 INTRODUCTION

In this chapter, two important applications of fracture-based analysis are introduced. The first is concerned with the effect of loading rates on the RC column of a bridge structure in terms of its vulnerability to damage.

The second part is concerned with re-modelling of loading and boundary conditions of a structural problem, to reduce its computational capacity from a large-scale model to a small-scale model, by introducing a transformation technique for multi-scale problems, and named herein as the Relative Response Technique RRT.

### (PART ONE)

## 7.1 CLASSIFICATION OF LOADING RATES

Different loading rates can have significant effects on the performance of a RC structure. The uncertainty of intensity and rate of earthquake loading increases the challenge to predict responses of high risk excitements. In general, there are two important methods to classify the rate of loading on structures; the first deals with loads classified by the strain rate response of the structure. The second deals with seismic loads in specific, which are classified by the ground acceleration rate, or shortly, its loading rate.

### 7.1.1 Strain-Rate Dependent Problems

The mechanical behaviour of structures varies according to the different loading rates, leading to different strain rates responses. Approximate ranges of the expected strain rates for different loading conditions are shown in Figure 7.1, which contains most types of loading; quasi-static, earthquake, impact and blast loading types. A high loading rate such as impact loading, causes a response of high strain rates of  $10 \text{ s}^{-1}$ , and thus, altering the dynamic mechanical properties of the structure. This has a significant effect on the fracture mechanism of various structural elements. In general, higher strain rates would increase the material strength of the structure, and thus, it is said that the structural problem is a strain-rate dependent problem when subjected to a higher rate loading type.

A strain-rate dependent problem will have a varying constitutive relation to its materials, due to the change in the yield strength and the change in the softening slope. This is due to the effects of inertia on the micromechanical response [1]. As a result, the area under the softening curve is no longer equal to the fracture energy  $G_f$  of the material, and thus minimizing the expected damage in the structure, as shown in Figure 7.2.

Key features of dynamic fracture propagation at a high strain rate identified from the experimental tests are [1]:

- Low strain rates ( $10^0$ ) - Fracture propagation is independent of time or strain rate
- Medium strain rates ( $10^3$ ) - The stress sustained prior to fracture increases and fracture propagation occurs at a higher velocity
- High strain rates ( $10^6$ ) - The microstructure deformation mechanisms require a finite time to propagate a crack [1].

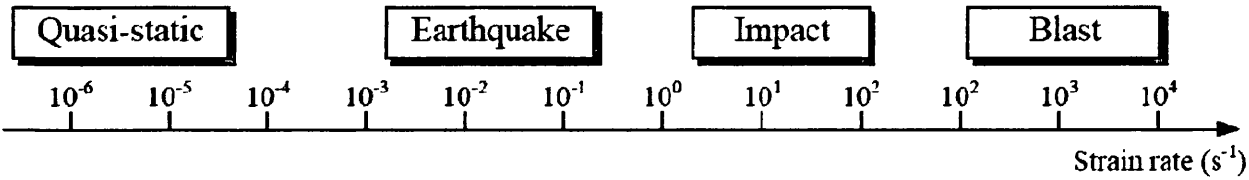


Figure 7.1 Strain rate associated with different types of loading [2]

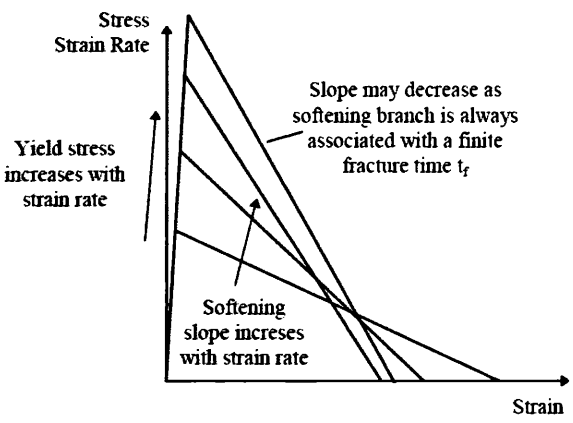


Figure 7.2 Softening slope as a function of strain rate [1]

As can be seen from the strain-rate range diagram, Figure 7.1, structural problems subject to earthquake loading produce low strain rate responses, ranging from  $10^{-3} \text{ s}^{-1}$  to  $10^{-1} \text{ s}^{-1}$ ,

and thus, are considered below low strain-rate problems, or strain-rate independent problems, which have no effect on the constitutive initial model of the material, and thus no change on the expected fracture mechanism.

### 7.1.2 Acceleration Pulse

The PGA peak ground acceleration is most often associated with the severity of ground motion, since inertial forces are proportionally related to acceleration according to the second law of Newton. PGA is a major intensity measure of earthquakes, and its applications are widely used in Earthquake Engineering.

There are two useful classifications of the ground acceleration records that are relevant to the expected damage in the structures. The first is the phenomenon of long duration impulses with low frequency in ground acceleration records, known as the Acceleration Pulse, or Fling [3]. The second is the acceleration peak associated with short duration impulses of high frequency, known as an Acceleration Spike [3]. It has been found that an Acceleration Spike is not as severely damaging to the RC bridge columns as an Acceleration Pulse [3]. The Acceleration Pulse increases the seismic hazard and brings more challenges to performance-based seismic engineering PBSE in the field of RC bridges design and assessment.

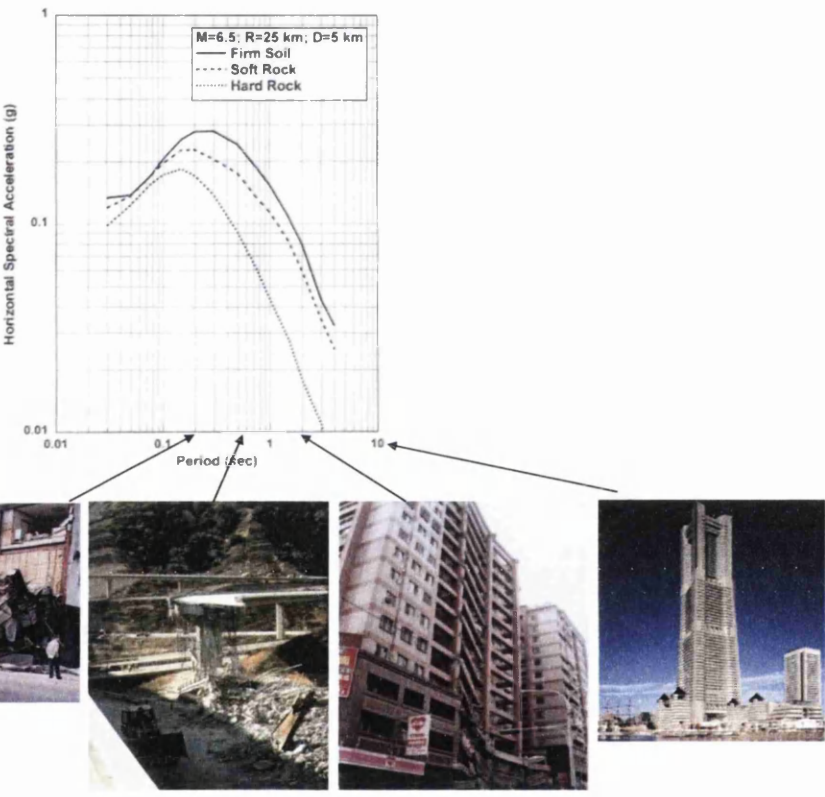
The reason behind having such a high potential damage in a long duration impulse is that it allows for a high velocity, and thus, high displacement responses. However, short duration impulses in a record of high frequencies, i.e. acceleration spikes, can also be very damaging if their high frequencies are within the range of the structure's natural frequencies. However, PGA's of high frequencies, (short periods), can seldom initiate resonance or produce large scale damage, since most structures are not within the range of high frequencies records [4]. Therefore, large PGA alone can seldom initiate resonance or produce large scale damage.

According to Newmark-Hall spectral representation, vibration periods are divided into: very low (from 0.0 to 0.25 seconds), low (from 0.25 to 0.7 seconds), medium (from 0.7 to 1.5 seconds) and long periods (from 1.5 to 3 seconds or more) [5].

In general, the typical range of fundamental periods  $T_n$  of the majority of bridges is as follows:  $0.2 < T_n < 1.0$  seconds [6, pg1650], which are apart from very short periods, and therefore, resonance does not occur. However, other bridge structures can have even longer fundamental periods. As mentioned in the analytical investigation for a variety of RC columns [9], a range of single-cell box-girder RC structures have fundamental periods ranging between 0.44 and 2.71 seconds.

To have a wider view, Figure 7.3 shows different fundamental periods for different structures. Most of these periods of structures are longer than periods of peak ground accelerations. In this figure, a period of approximately 0.5 seconds is the fundamental period for the shown single-cell box-girder bridge which is supported by single RC columns.

The damaged single-cell box-girder bridge is due to the Northridge earthquake in 1994 January 17, located 35 km northwest of Los Angeles city. It caused the death of 55 people, injury of more than 7000 people and direct economic losses of \$ 20 billion, which is classified as the loss of the worst loss caused by an earthquake in the history of the United States.



**Figure 7.3 Different fundamental periods for different structures**

With respect to Acceleration pulse, Singh [3] explained the effect of frequency in two different earthquake events with different frequencies of ground acceleration in the following two examples:

The first is the Parkfield earthquake, California in June 1966, with  $PGA= 50\%g$ , only 200 feet from the fault trace and maximum Incremental Velocity  $IV = 35$  inches/sec.

The second is the Bucharest earthquake, Romania in March 1977, with  $PGA= 20\%g$ , a large distance from the epicentre and maximum  $IV = 50$  inches/sec.

The first example has less IV than the second one even though it has got a higher PGA, and is very close to the fault trace. The Bucharest earthquake had a large damage impact and caused severe destruction. However, the Parkfield earthquake had a very low effect and received limited attention [3].

Many researchers have shown that the frequency, pulse duration, incremental velocity and incremental displacement can have profound effects on the structural response more than the effect of the PGA alone, especially in the inelastic range [4]. Cosenza and Manfredi stated that the PGA is a basic measure of earthquake potential but is not totally reliable [5]. Examinations of recorded seismic events have shown that earthquakes with a very large PGA could not produce appreciable structural damage, while earthquakes with a very low PGA produced an unexpectedly high level of destruction [5]. Instead, the PGV seems to be a more representative measure of earthquake intensity, since it is directly connected with energy demand [7]. Singh [3] considers PGA as an Intensity Measure, IM, is a poor parameter for evaluating the damage potential.

## 7.2 DAMAGE APPROACH

### 7.2.1 Stress-Based Damage

Damage can be estimated by measuring the loss of stresses at the critical zones in a plastic hinge. In inverted pendulum problems, such as bridge column problems, most of the damage is due to excessive axial compressive and tensile strains. Thus, classified as flexural damage. However, a very limited portion of the damage is caused by shear failure in these problems, especially in relatively small diameter members, therefore, no shear failure is expected.

The elasto-plastic constitutive relationship for a selected element can be used to approximately indicate the damage state at that zone. The local compressive damage index for concrete fibres is based on the ratio between axial compressive stresses  $\sigma_{i,fibre}$  and the ultimate strength of concrete  $\sigma_{ult}$ , and can be obtained during the strain softening of the analysed fibres, as in the following equation:

$$D_i = 1 - \frac{\sigma_{i,fibre}}{\sigma_{ult}} \quad (7.1)$$

where  $i$  is the time-step, or pseudo time in case of quasi-static analysis. When  $D_i$  equals 1, the fibre has lost its strength and is not capable of resisting any more axial compressive stresses, indicating a local totally damaged state under compression.



This index is sufficiently expressive, but it is mostly used for elements under compressive stresses only since that concrete elements with tensile stresses are considered fully damaged due to their very limited strength to resist tension.

Using the Fibre Element Method, the non-linear analysis for the RC columns is performed, by using the SeismoStruct dynamic solver [8], which is capable of plotting the constitutive curves of the stressed fibre elements. The fibre elements are designed to compute the non-linear axial forces with the flexible failure mode. However, shear forces are also obtained from the coupled stiffness matrix, but their corresponding shear stresses are not calculated since the shear failure mode in these problems is not dominant.

The following example of RC single-cell box-girder bridge columns, shown in Figure 7.4, has a damping ratio of 5% and subjected to artificial ground accelerations applied at the base of the structure. The relative change in the duration of acceleration pulses of ground acceleration is conducted in 3 different slope rates; 1.414 g/s, 1.880 g/s and 2.801 g/s, where g is the gravity constant, as shown in Figure 7.5. These loading rates have been taken based on the PGA of Lexington Dam record from the Loma Prieta earthquake 1989, which reaches approximately 6.0 m/s<sup>2</sup>.

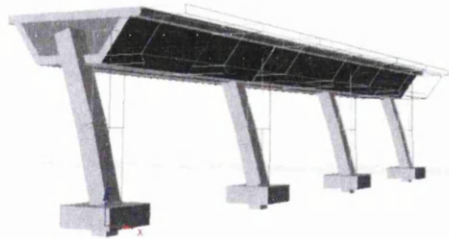


Figure 7.4 Displacement in RC bridge columns

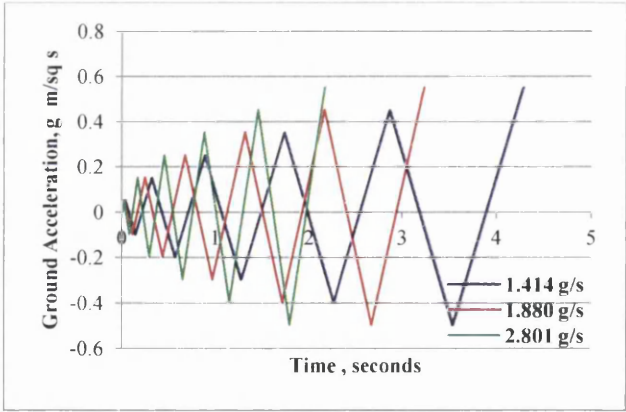
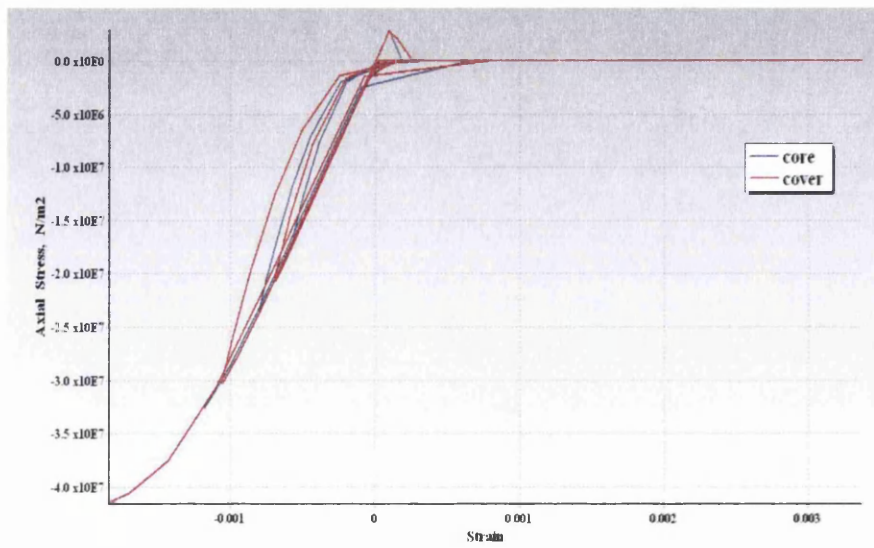
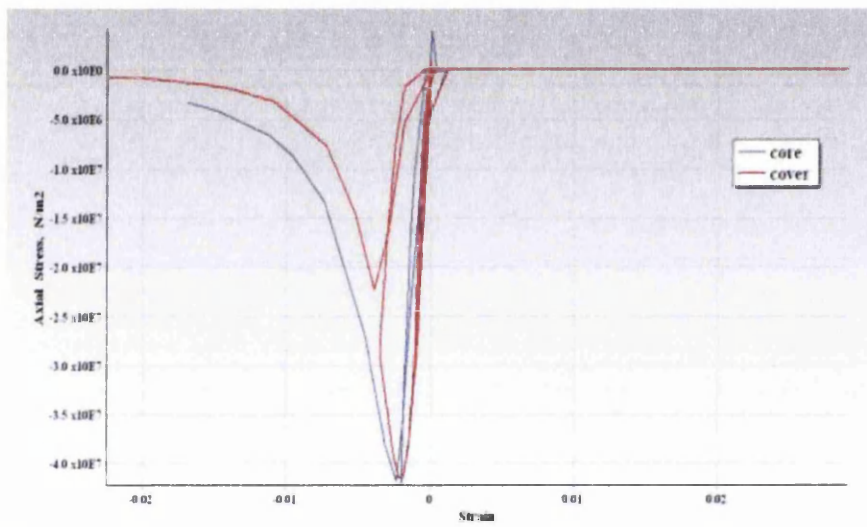
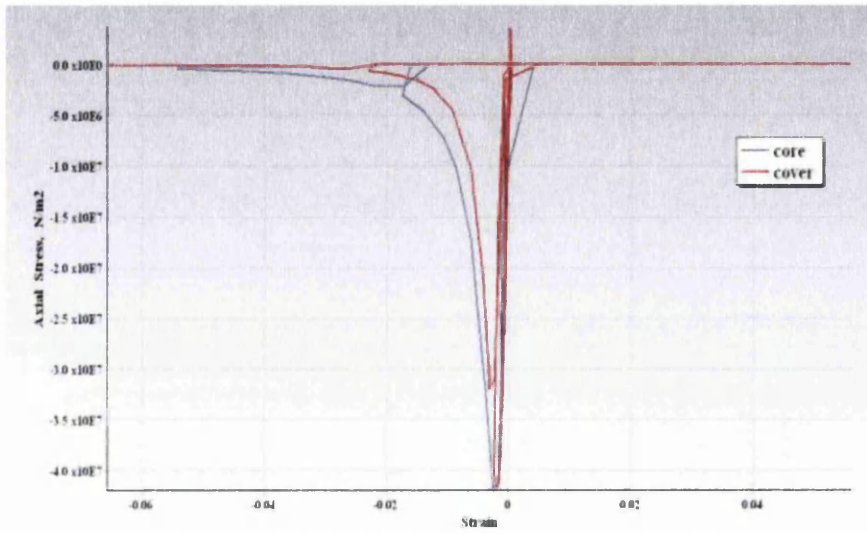


Figure 7.5 Loading rates

As a nonlinear response to the effect of different loading rates, the constitutive curves shown in Figures 7.6, 7.7 and 7.8 show that for longer durations of an acceleration pulse the response tends to have more plastic stresses, and for shorter durations the response tends to have less plastic stresses. The corresponding damage can then be determined for the stressed fibres at selected points on the cover and core of the column's section, using equation (1). The loading rate of 1.414 g/s, (longer duration loading), showed an extended constitutive curve with large plastic strains and degraded strength on the core and cover in Figure 7.6.



Figures 7.6, 7.7 and 7.8 Stress-strain curves at 1.414 g/s, 1.88 g/s and 2.801 g/s loading rates, respectively

In Figure 7.7 less plasticity is expressed on the core and cover with 1.880 g/s loading rate, and almost linear constitutive curves are found with 2.801 g/s loading rate, (shorter duration loading). This indicates that much less damage occurs with larger loading rates, and more damage occurs as the loading rate decreases.

In the methodology of SeismoStruct software, it should be noticed that fibres that fail to resist tensile stresses on the opposite side of the column section at some time step are still valid to resist compressive stresses at successive time steps. Only those fibres that lose strength under excessive compressive stresses are not utilised in the proceeding loading operations.

## 7.2.2 Fracture-Based Damage

This method is based on modelling the fractured elements of the model by using a DE/FE Explicit Dynamic solver. The Explicit-Elfen code is used to perform the non-linear dynamic analysis for a limited time of applied loading, since fracture analysis takes a relatively long computational time to attain the analysis of a few seconds of loading.

The non-linear dynamic analysis in this approach is governed by Mohr-Coulomb/Rankin with the tension cut-off model, covering both tensile and shear failure modes, Mode (I) and Mode (II), respectively. The failure model is characterised by shear strength, angle of friction, angle of dilation and tensile strength. The fracture model is characterized by tensile strength and fracture energy, to simulate the tensile cracking mode Mode(I) only, and is known as the Rotating Crack model. Mode (I) is suitable for representing the cracks in the column's dynamic oscillation motion, since the fracture in the column base is mostly due to tensile cracking mode.

The applied dead load in the proposed example is 4.5MN, which is only 5% of the column's capacity for axial load, and thus, the confinement reached by the transverse reinforcement stirrups is found to be only 4.5% of the steel yield stress  $f_y$ . This leads to less confinement, and thus, the principal stresses of the concrete become closer to the failure envelope, and concrete is more vulnerable to fail.

In this FE analysis the bond effect is not simulated since 2D steel bar elements are fully conjugated with the edges of the tetrahedral 3D concrete elements. In general, bond friction could have some effect on the fracture mechanism and crack growth, but its existence could also increase the computational effort significantly.

### 7.2.2.1 Problem Set-up for the FE Analysis

The analysed structure is the single RC column with an aspect ratio of 6 that has been previously described, and subjected to the Lexington Dam record, from the Loma Prieta earthquake 1989 [5], as previously mentioned.

A force equivalent to the peak ground acceleration PGA of this ground motion is applied to the centre of gravity C.G. of the top mass. This equivalent force is extracted from the base shear analysis for the structure under this ground motion, by using the SeismoStruct dynamic solver as previously explained. The required axial loading is due to the dead load which is modelled by having an artificial mass structure with density and volume producing an equivalent loading effect.

Out of the total record time of 40 seconds, only partial loading with the PGA value is selected from the Lexington Dam record of the Loma Prieta earthquake 1989. The maximum loading lateral force is approximately  $2.2 \times 10^6$  N, and the corresponding time is from 3.48 seconds up to 5.48 seconds, lasting for 2.0 seconds only. This applied peak forces vary in rate, from 0.70 to 2.0g per second, as shown in Figure 7.9.

Another dynamic loading rate is applied, with a loading rate of 2.27g per second on the same example, to compare its analysis with the previous one, and discover the influence of rate change.

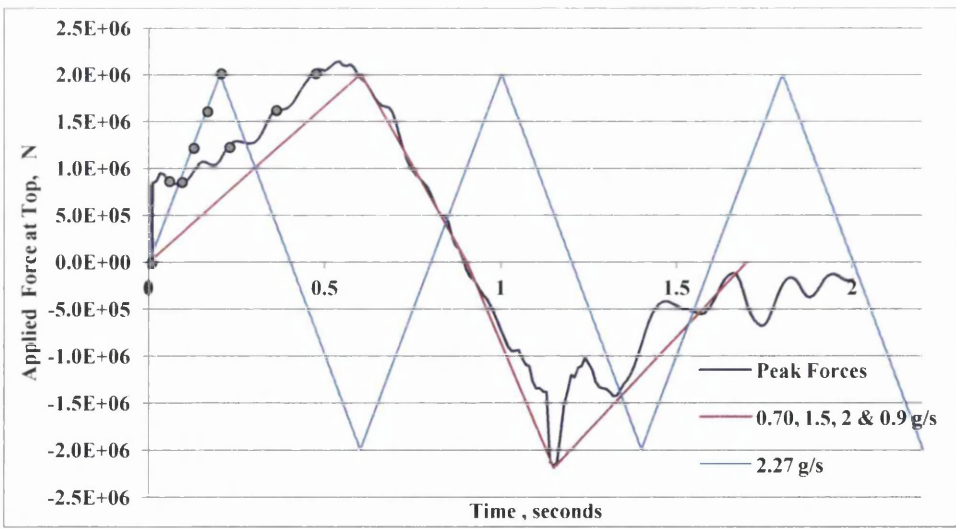


Figure 7.9 Different Rates of Applied Forces at Top of Structure

### 7.2.2.2 Results and Discussion

Comparing the responses of these two different loading rates, Figure 7.10 shows the load-deflection curves by DE/FE fracture analysis for the RC column with an aspect ratio of 6. It also shows the load-deflection curves obtained by the SeismoStruct analysis which were previously illustrated.

Under different rates of loading, different responses have been obtained for the same magnitudes of lateral loads, as shown in Figure 7.10. The figure shows that the base shear curve is more resisting when a higher loading rate, 2.27g/s, is applied, and less resisting when a lower loading rate, 0.7g/s, is applied. This indicates that less damage is obtained with a higher rate of loading, and more damage is obtained with a lower rate of loading. Due to the severity of damage in both cases, the structure top mass is deflecting towards an unstable position as the plastic hinge PH becomes severely fractured, but with different rates, leading to total collapse.

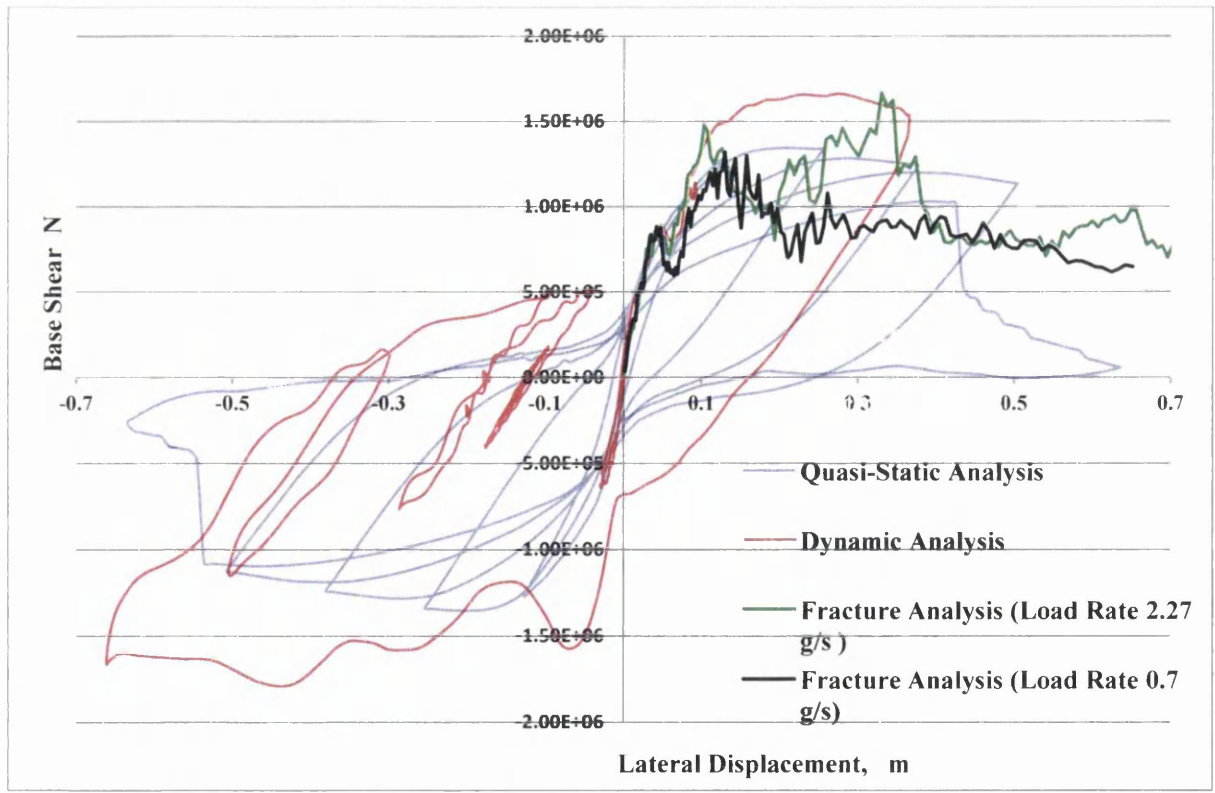


Figure 7.10 Load-Deflection curves by different analyses for the structure under Loma Prieta earthquake



Table 7.1 shows the responses of time, displacements, degree of damage and bar tensile stresses for both long and short duration lateral loads. The table shows 8 selected responses for the two cases of loading, 4 of them are responses of the 4 applied loads of: 0.821, 1.208, 1.619 and 2.03 MN, which were previously indicated in Figure 7.9 as marked black dots for the two curves of proposed loading rates.

Applied Lateral Load (MN)	Case (A): Long Duration, Low Frequency Acceleration Pulse, 0.70g per second.			Case (B): Short Duration, High Frequency Acceleration Spike, 2.27g per second.		
	Time (s)	Lateral Displacement (m)	Bar Tensile Stress at PH, MPa	Time (s)	Lateral Displacement (m)	Bar Tensile Stress at PH, MPa
0.76	0.01	0.0163	9.92(comp.)	0.076	0.002	1.9
0.821	0.09	0.04093	98.7	0.082	0.007	11.5
1.04	0.14	0.10242	269.0	0.104	0.0141	94.7
1.208	0.22	0.24028	474.8	0.121	0.022	121.9
1.44	0.33	0.29027	491.8	0.144	0.0365	221.1
1.619	0.36	0.43260	524.3	0.162	0.0517	399.0
1.83	0.43	0.43260	524.3	0.183	0.074	475.0
2.03	0.47	0.53106	550.6	0.2	0.095	475.0

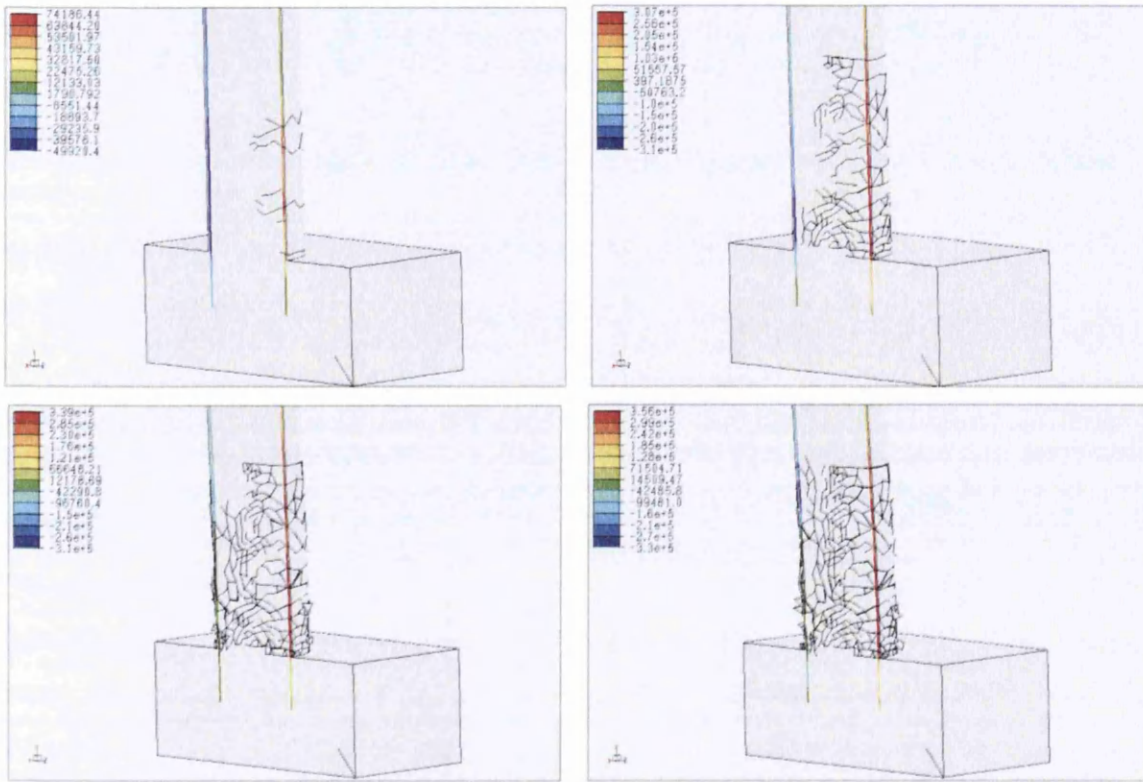
**Table 7.1 Responses of RC column under long and short duration applied lateral loads**

For these 4 selected applied loads, 4 damage pictures are captured in Figures 7.11, 7.12, 7.13 and 7.14, which correspond to the 4 responses of case (A) respectively.

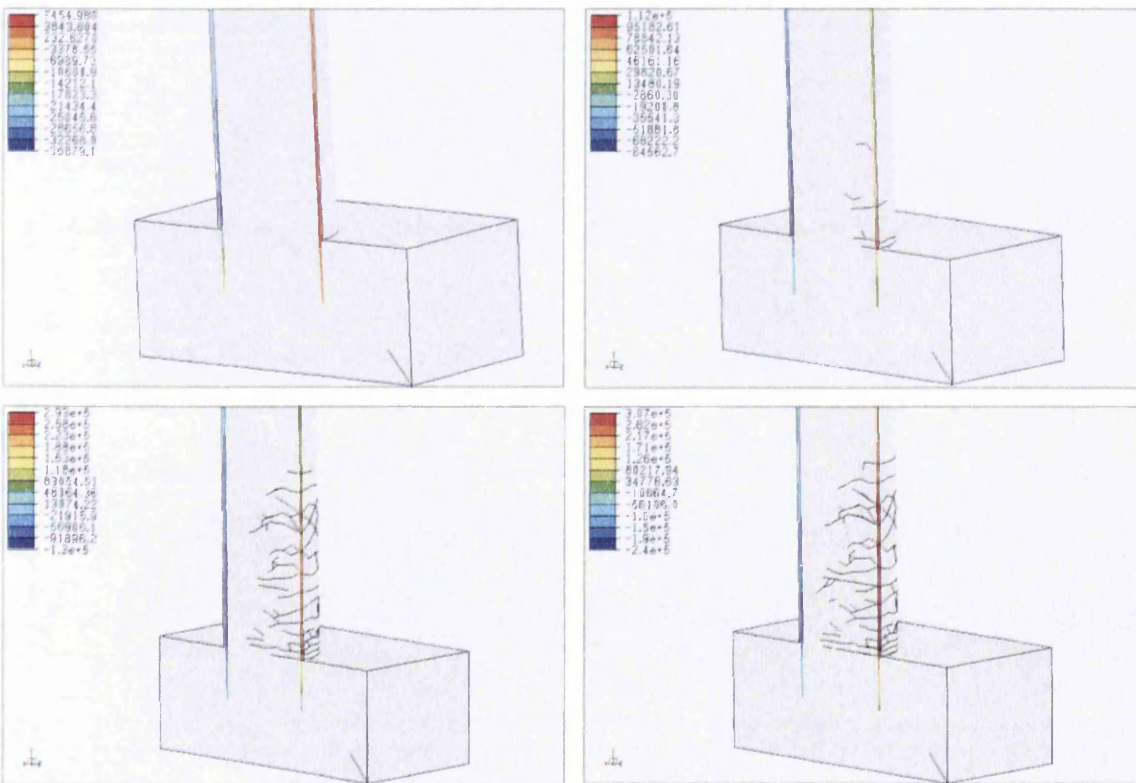
The states of damage caused by the same 4 applied loads but with a shorter duration of loading, case (B), were also captured in Figures 7.15, 7.16, 7.17 and 7.18.

It is obvious that cracks tend to grow densely in the long duration case more than in the short duration case, even though both loading cases have the same peak magnitudes.

As the structure is symmetrically modelled and loaded, the pictures show an obvious growth of cracks inside the column core itself, especially with the lower rate of the dynamic loading. Such cracks are obtained for a partial loading range, only 0.47 seconds, but more cracks could have accumulated if the rest of the loads of the record had been included.



Figures 7.11, 7.12, 7.13 and 7.14 Concrete fracture and steel tensile forces due to applied loads of 0.821, 1.208, 1.619 and 2.03 MN, respectively, for longer duration case (A)



Figures: 7.15, 7.16, 7.17 and 7.18 Concrete fracture and steel tensile forces due to applied loads of 0.821, 1.208, 1.619 and 2.03 MN, respectively, for shorter duration case (B)

Damage is the result of lateral displacements, and the maximum displacement in case (B) is approximately 20% of that in case (A) even though both are subjected to the same load value, but with different loading rates.

In respect of tensile stresses in the reinforcement bars, stresses are consequently less in case (B), and their ductility is less consumed than in case (A). However, bar tensile stresses in case (B) rise fast as loading rises, and then reach 86% of the tensile stresses in case (A). This shows that a huge part of the seismic energy is dissipated by the steel reinforcement bars, causing less damage to the concrete body. At displacement of 0.095m, the tensile stresses in case (B) reaches 475MPa, while a displacement of 0.102m, the tensile stresses in case (A) does not exceed 269MPa. This is because that less damage is found in case (B), and therefore, more concrete-steel bond exists in the context of the plastic hinge, while in case (A) more crack growth formation with less concrete-steel bond exists, and thus, less tensile stresses may be produced. This indicates that ductility is affected and the member does not follow the demand/capacity principle sufficiently in the nonlinear stage. Therefore, the SDC seismic design criterion based on this principle could fail due to a lack of ductility.

### 7.2.2.3 Conclusion

- The damage of quasi-brittle materials such as concrete is very sensitive to the rate of loading, and the inconsistency of loading rates in earthquake motion makes the damage pattern in such low-confinement RC columns unpredictable and difficult to generalize. Therefore, it is very much recommended to analyse each loading case independently for fracture simulations.
- At load 2.03MN, the bar tensile stresses reach 550MPa and 475MPa in the two non-linear analyses of long duration and short duration loads, respectively. This is because less displacement is reached in the short duration loading case, and therefore, less damage is found, while more displacement is reached in the longer duration loading case, and thus more crack growth is formed at the same loading.
- Lower loading rates have longer durations and lower frequencies, or relatively, acceleration pulses, are more vulnerable to damage than higher loading rates that have shorter durations and higher frequencies, or relatively, acceleration spikes.
- Base shear forces are more resisting when higher loading rates are applied, and less resisting when lower loading rates are applied. This indicates that less damage is



obtained with higher rates of loading, and more damage is obtained with lower rates of loading.

- Due to the severity of damage in both applied cases of loading rates, the structure top mass is deflecting towards an unstable position as the plastic hinge PH becomes severely fractured, but with different rates of crack growth, leading to total collapse.

## ( PART TWO )

### 7.3 MULTI-SCALE SEISMIC ANALYSIS

The global damage in (RC) reinforced concrete structures with performance-based seismic design PBSB is aimed to be relatively low after an earthquake, assuming that concrete cores and reinforcement bars of the structural members remain undamaged in the stressed zones. These assumptions need to be verified by using fracture analysis, which has become significantly important in non-linear dynamic solutions to RC skeleton structures subjected to earthquake strikes.

The Finite Element Method applications with fracture-based analysis are most suitable to analyse such stressed zones in a small-scale model. However, the Finite Element method associated with non-linearity, fracturing algorithm and simulating 3D RC members requires a huge number of 3D tetrahedral elements associated with 2D bar elements. Moreover, the mesh elements for the important zones such as at intensive stresses in the concrete cover and around the steel bar need to be substantially refined, especially for a 3D fracturing task so that the fracture mechanism wouldn't fail due to topological mesh errors. Such analysis performed for the global 3D RC structure will be excessively time consuming with a lot of computational capacity and processing time. Moreover, the analysis under long earthquake records will, obviously make the task unpractical to perform.

In this chapter, the (RRT) Relative-Response Technique is introduced, and used to re-produce the targeted RC members and joints out of their global context, and re-model them into a small-scale model with new constraints, loading vectors and boundary conditions.

Several restrictions and limitations concerning the set up of loading, constraints and meshing are considered when using this technique. In the proposed example, the global relative displacement response is obtained by a global-scale analysis using any dynamic solver that incorporates a non-linear algorithm. In this chapter, SeismoStruct is used to produce the

response of the global-scale analysis. Such a response becomes the applied loading record for the local-scale finite elements in their selected directions. To cut down the computational effort, only peak portions of the full record may be selected for the analysis, as this depends on the capacity and speed of the available computing system.

The small-scale model is built based on the (RRT) Relative Response Technique, which will be introduced herein.

### **7.3.1 Relative Response Technique RRT**

Two types of analysis are associated with this technique; the large-scale and small-scale analyses. The response vectors of the large-scale analysis are obtained analytically or experimentally, and utilized by the small-scale model as applied loading vectors. The response vectors can be static or changing with time in a dynamic mode. They may also be displacements, forces, accelerations, stresses or of any parametric quantity.

However, their values are computed for each joint independently relative to the other joint of the same member, which will be remodelled as a stationary joint in the small-scale model.

As an application to this technique, a relative displacement response between the two joints of a member, is obtained from the large-scale model, and is considered as a displacement load vector applied at one joint in the small-scale model, having the other joint constrained in the same working direction. For more than one member analysis, the joint connected to several members is the stationary joint, and should be fully constrained in the working directions of the other joints.

In the small-scale analysis, the relative displacement magnitudes of the same direction for the joints should be applied on their correspondent joints but in opposite directions, so that all displacements are relative to the stationary joint.

Figure 7.19 shows the sequence of steps performed by the RRT with large-scale via small-scale models. The large scale non-linear response is obtained by the global model, which is built by the SeismoStruct. This model and the relative response data are used as loading and constraints for the small-scale non-linear local model made by the Elfen. This analysis produces the fracture response for the required members.

Theoretically, both models employ non-linearity and dynamicity, therefore, there is no contrast in the method of analysis concerning the constitutive relation or the dynamic characteristics. However, the main difference is in terms of modelling formulation between the fibre element approach and the tetrahedral element approach. Theoretically, this should

not affect the final results even though differences are expected in the analyses before reaching the final points.

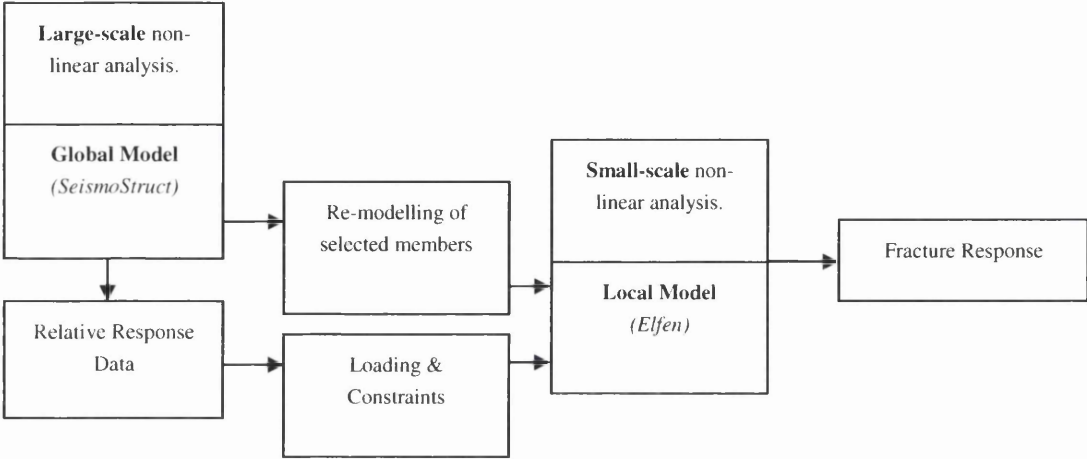


Figure 7.19 Flow-chart of the Relative Response Method

### 7.3.2 Set-up of Problem Modelling

As shown in Figure 7.20, the global structure consists of two RC frames with two bays and two floors height, and the earthquake loading is a ground acceleration applied at the base of the structure. The earthquake record is from the Loma Prieta earthquake, 1989, near fault Lexington Dam Record, with epicentral distance = 6.3 km and magnitude of 7.0 [9]. As shown in Figure 7.20, the seismic motion lasts for 40 seconds but the peak accelerations are clustered in the first 8 seconds with  $PGA = -6.73 \text{ m/s}^2$ .

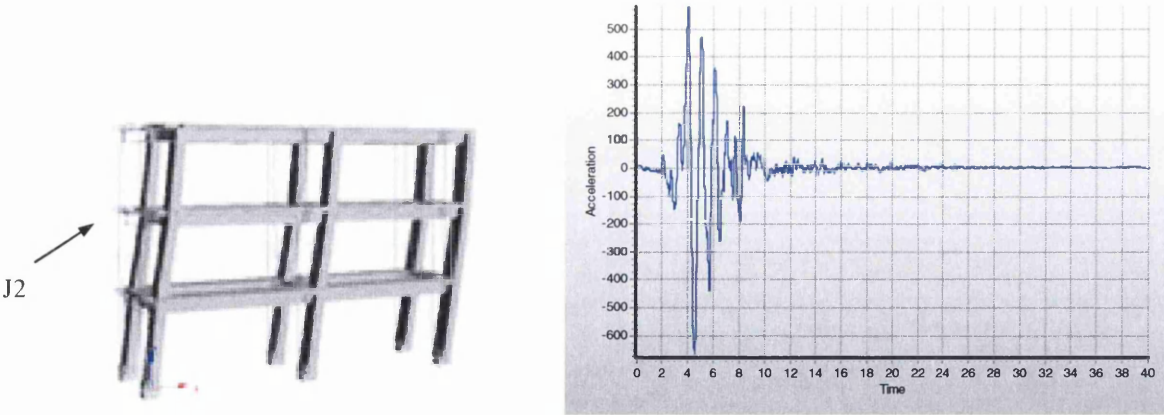
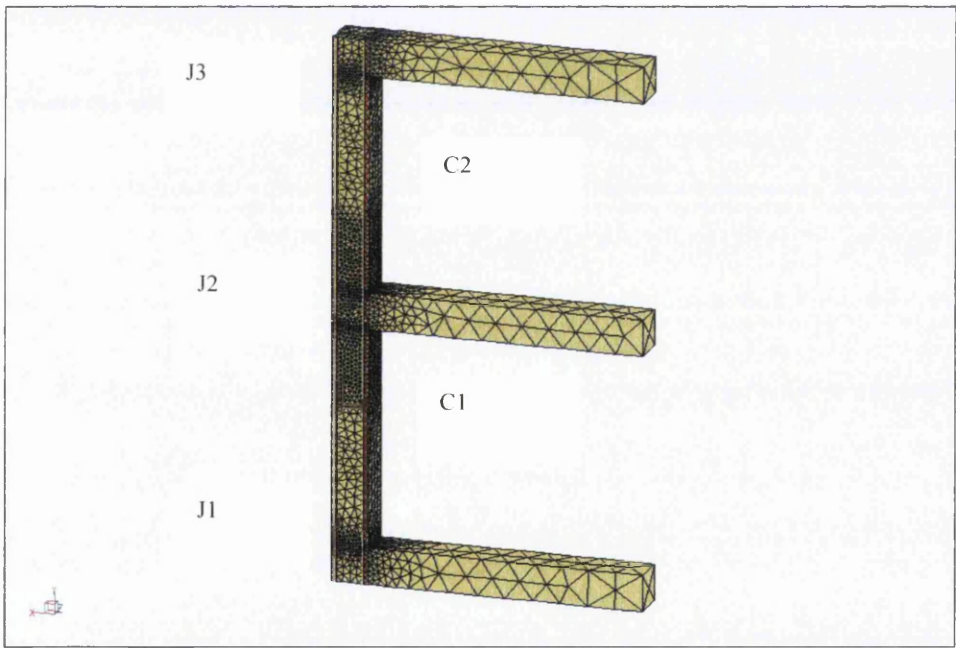


Figure 7.20 Large-scale non-linear analysis of RC frame structure subject to Lexington Dam Record

The analysis is performed by using the Seismostruct dynamic solver for the global structure, and the Explicit-Elfen DE/FE package to solve the local-scale model. Only 5 structural members are selected from the global structure to be re-modelled in the small-scale FE non-linear model analysis. They are namely; the 1st & 2nd floor level columns and associated beams. These members are re-modelled in the Elfen environment with new boundary conditions and loading applications.

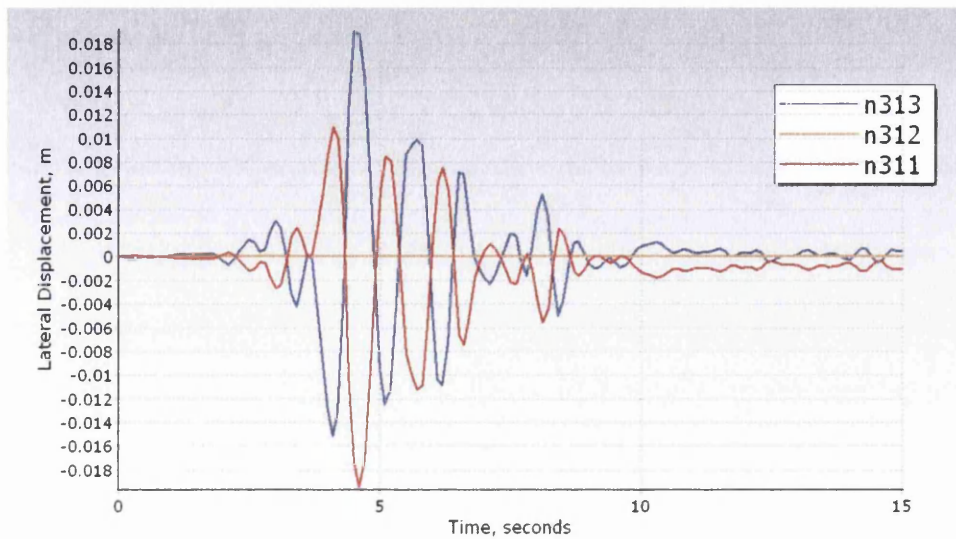
As shown in Figure 7.21, the first floor and second floor joints are labelled as J1, J2 and J3 respectively. Similarly, the first and second floor columns are labelled as C1 and C2.

The relative displacement responses obtained from the fibre element analysis by the SeismoStruct package are shown in Figure 7.22. They belong to the upper J3 and lower J1 joints; labelled as n313 and n311 respectively, and they are relative to the middle joint J2, or n312, which has no degree of freedom. These relative responses are used as loads applied on the C1 and C2 columns in the small-scale model.



**Figure 7.21 Small-scale FE model**

In order to lower the computational effort in the small-scale analysis for this particular example, the following assumptions have been considered to simulate the proposed example numerically:



**Figure 7.22** Displacement relative responses of joints J3(n313) & J1(n311), used as applied loads relative to the stationary joint J2(n312)

- Considering three degrees of freedoms only, lateral  $x$ , axial  $y$  and rotational  $\theta_z$  as active freedoms.
- Considering a Rigid Frame structure, in which a floor member is considered relatively much stiffer than columns, and consequently given one degree of freedom only, namely; the lateral motion  $x$ . The other freedoms, axial  $y$  and rotational  $\theta_z$  are considered very small, and numerically ignored.
- Considering a half symmetric 3D model, in which only the longitudinal half of the selected members is modelled, and the longitudinal  $xy$ -plane surface is constrained in the  $z$ ,  $\theta_x$  and  $\theta_y$  directions, but letting the lateral  $x$ -direction and axial  $y$ -direction free to move. This is possible since both geometry and loading on the structure are symmetric about the longitudinal  $xy$  plane.
- The lateral loads are applied as relative displacements on the upper and lower floors in opposite directions, while the middle floor beam is restricted with no allowable freedoms. This will produce the lateral relative motion in this local-scale structure equivalent to its corresponding motion in the global-scale when subjected to the ground acceleration motion at the base of the structure.
- When the applied displacement loading is directed in the lateral  $x$ -direction only, the loaded surface will not allow any rotational motion in the small-scale model to take place, thus applying additional unrealistic stresses to the associated members. However, this is acceptable in the proposed example, since the structural frame is assumed as a Rigid Frame structure, and its motion is lateral only.



In another configuration for the RRT, the relative response can also be assigned as forces and moments which are obtained from the dynamic solver, and then applied on the cross section of the column in the small-scale model. As shown in Figure 7.23, forces and moments have been applied in this example as axial stresses on the surface of the column cross section. However, stresses due to moments may unrealistically deform the loaded elements. Therefore, it is preferable to apply the forces and moments at positions where moments are minimum, or approximately equal to zero in that member, such as at the zero-moment inflection points at approximately the middle length of the member. However, moments can also be applied as rotational forces on the cross sectional area of the member, to avoid such unrealistic probable deformation. Explicit-Elfen v3.7 does not account for rotational forces loading or rotational restraints although the possibility of their input data is available.



Figure 7.23 half-member configurations of small-scale modelling

### 7.3.3 Discussion of Results

The targeted joint is the stationary joint J2, and the targeted members are the first and second floor columns. The fracture response for these targeted members is shown in Figures 7.24 and 7.25, where positions and intensities of the plastic hinges PH are determined and captured. Joint J2 is damaged at the upper and lower plastic hinges of columns C1 and C2, respectively. The zones near to the fractured elements are micro fractures, reaching up to 0.5 of the fracture state index, as can be seen in Figure 7.25.

The progress of the crack growth shows that the tension side is severely affected, and damage is mostly concentrated in the columns cover only, and very little penetrates to parts of the core. In this example, cracks start to grow as the stress in the longitudinal bars reaches between 200 and 250 MPa. In this example, the transverse reinforcements, stirrups, have no effect on the confinement of the concrete core, since the axial vertical load on the columns is

relatively small. This leads to less confinement, and thus, the principal stresses of the concrete become closer to the failure envelope, and concrete is more vulnerable to fail.

In this FE analysis the bond effect is not simulated since the 2D bar elements are fully conjugated with the 3D tetrahedral elements edges, and thus bond friction does not exist. This also affects the behaviour of the fracture mechanism and crack growth, as previously discussed.

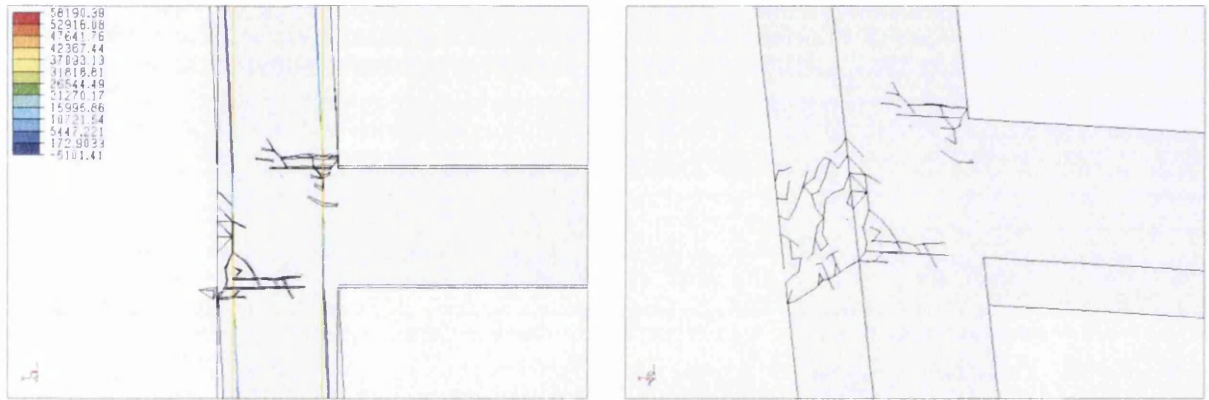


Figure 7.24 Displacement of column members relative to the stationary joint J2, showing cracks and reinforcement bars forces

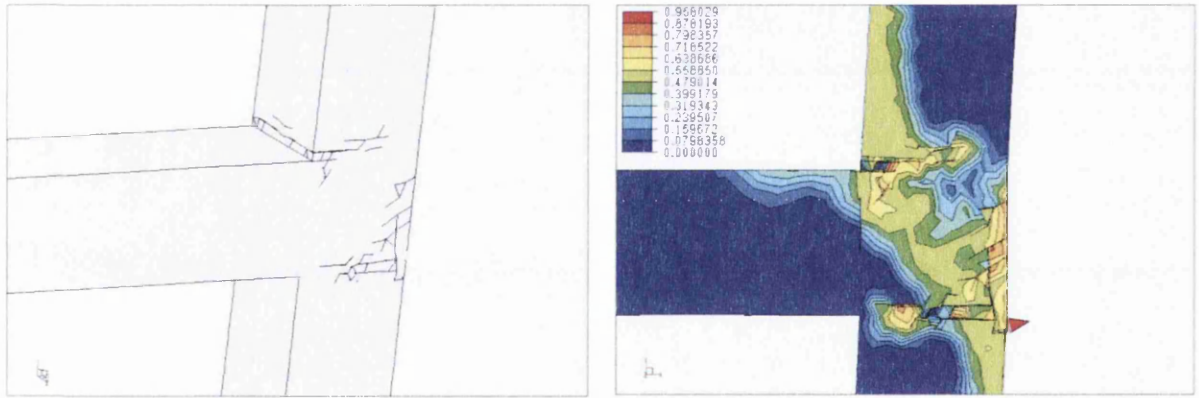


Figure 7.25 Crack growth and the fracture state indicator in stationary joint J2

### 7.3.4 Conclusion

- Damage in RC beam-column joints and plastic hinges need to be investigated in 3D small-scale models with a sufficient mesh refinement in order to obtain reliable results for the fracture analysis.
- The Relative Response Technique RRT is introduced in this chapter and used to re-model a part of the global structure into a small-scale model. This part should contain

the targeted joints and members for the proposed example, so that the fracture analysis can be performed with a computational capacity that's significantly less than performing the global model.

- A dynamic solver of non-linear analysis for the large-scale models are efficiently utilised to perform elasto-plastic analysis for RC members of skeleton frame structures, and provide a sufficient loading record for the small-scale model.
- Re-modelling of the loading and boundary conditions is performed for each case study independently, and is uniquely different for every targeted joint and corresponding members.
- The Relative Response Technique RRT can be extended via relative rotations and forces which are also obtained from the dynamic solver, and then applied on the members of the small-scale model.
- Further size-reduced models for the small-scale simulation can be made by modelling symmetric members in symmetric problems. Another possibility of size reduction is by applying the relative response RR at zero-moment inflection points, so that only half of the members are modelled. The validity of these modelling methods depends on the nature of the problem, its loading directions and boundary conditions.

## 7.4 REFERENCES

- [1] Rockfield Ltd. ELFEN Impact Modelling, Explicit User Manual. Rockfield Ltd, Swansea, 2008.
- [2] T. Ngo, P. Mendis, A. Gupta and J. Ramsay. Blast Loading and Blast Effects on Structures: An Overview. Int. EJSE Loading on Structures, Special Issue:76-91, 2007.
- [3] J.P. Singh. Characterization of ground motion for severity and damage potential. JP Singh & Associates, Richmond, California.1995.<http://nisee.berkeley.edu/lessons/singh.html>.
- [4] G.W. Housner, P.C. Jennings. Earthquake design criteria. EERI Monograph Series. Berkeley, CA: Earthquake Engineering Research Institute. 1982.
- [5] E. Cosenza, G. Manfredi. Damage indices and damage measures. Progressive Structural Engineering Mater.2000; 2: 50–59, John Wiley & Sons, Ltd.
- [6] J. Zhangh, Y. Huo, Evaluation effectiveness and optimum design of isolation devices for highway bridges using fragility function method. Journal of Engineering Structures,1648-1660, March 2009.



- [7] J. P. Singh. Directivity evidence from the August 6, 1979 Coyote Lake Earthquake Proceedings. Conference on earthquake hazards in the eastern San Francisco Bay area, Hayward, California. California Division of Mines and Geology. Special Publication 62, March 24-27.
- [8] Bibliography of SeismoStruct Earthquake engineering Software, SeismoStruct v5.2.2 Official release of 22/08/2011.
- [9] J. Sakai, S. A. Mahin. Analytical investigations of new methods for reducing residual displacements of reinforced concrete bridge columns. Pacific Earthquake Engineering Research Centre, PEER Report 2004/02, University of California, Berkeley.
- [10] M.C. Kunde, R.S. Jangid, Seismic behaviour of isolated bridges: A-state-of-the-art review, *Electronic Journal of Structural Engineering*, 3 (2003).
- [11] TA. T. Bere. Computational modelling of large-scale reinforced concrete structures subjected to dynamic loads. PhD Thesis, University of Wales, Swansea, 2004.

# Chapter 8

---

## Conclusions, Recommendations and Future work

---

### Contents

8.1	CONCLUSIONS.....	254
8.1.1	Chapters Conclusions.....	254
8.1.2	General Conclusions .....	256
8.1.2.1	The Damage Mechanism.....	256
8.1.2.2	The Seismic Design Criterion.....	256
8.2	RECOMMENDATIONS.....	257
8.2.1	Numerical Modelling .....	257
8.2.2	Alternative Systems .....	259
8.2.3	A Criticism on the Eurocode8, (part 2: Seismic Design on Bridges) .....	260
8.3	FUTURE WORK.....	262
8.4	REFERENCES .....	263

## 8.1 CONCLUSIONS

### 8.1.1 Chapters Conclusions

The following are concluding summaries of the main remarks in the chapters of this research:

1. There is a large variety of numerical models for simulating non-linear and damage behaviour of RC bridge columns under seismic loading. Selection of a specific numerical model depends on the range and quality of output results required for the analysis.
2. The fibre element method is an effective method for modelling RC framed structures under dynamic loading. It is still a powerful method even when applied with simplified assumptions such as linearization of the tangential stiffness, in which errors can be minimized by reducing the time-step interval to a relatively small value. The un-loading and re-loading non-linear material paths of constitutive relations can also be simplified by linearizing the constitutive relation. Such simplifications can be implemented, yet produce acceptable approximate results.
3. Energy dissipation of the RC bridge columns under dynamic loading is one of the useful representative measures for a global damage index, which is described by the damage state in a qualitative manner based on previous experimental and site observations. However, the local damage measure in this research is based on determination of the axial stress of concrete fibres after losing some of their strength during the plastic unloading and reloading cycles.
4. Damage can be controlled by using seismic isolation bearings which absorb dynamic shocks and partially dissipate the seismic energy. The performance of the isolated sub-structure/super-structure zones based on the yield energy curves is a useful method to evaluate and control the seismic performance of the RC column. Such evaluation methods help to design the mechanical properties of the isolation devices.
5. Despite of its excessive time and huge computational capacity, the combined DE/FE analysis using Elfen-Explicit application is a successful tool for investigating the plastic hinge zone for RC columns under dynamic loading.
6. Engineering assumptions must be taken to reduce the size and geometry of the problem. In contrast, the computational size of the problem needed to be increased by factorising the time-step by less than 0.6 as it is strongly recommended to obtain fracture propagation. Therefore, practical judgements must be made to run such problems on PC systems. Furthermore, users should be aware that reinforcement bar elements in such

problems are the most time consuming among all other parameters, even though they are not under fracturing mechanism, and follow a non-linear constitutive algorithm only.

7. The Elfen-Explicit code is best working with Model 19 for quasi-brittle 3D structures since it contains detailed properties for the material such as hardening, dilation and both tension and shear failure modes. It is also provided with the Rotating Crack Model which is more sophisticated than the Fixed Crack Model. However, the modelled fracture is due to the tensile mode only, Mode (I), and other modes such as shear, torsion and the compression are not included.
8. The interaction between the tetrahedrals and bar elements of the concrete and steel respectively is considered as full bond, with no possible frictional action between the two materials, and thus a damping ratio of 5% was implemented in the analysis to account for possible viscous damping due to particle frictions.
9. Due to the very low confinement around the concrete core in the proposed model, there is no contribution to preserve the integrity of the confined core during the dynamic action, and thus, cracks grow and spread densely, leading to a total collapse.
10. Ductility of the RC section is totally dependent on the reinforcement since concrete starts to fracture even before steel bars become plastically ductiled. Therefore, the overall ductility of the section is disrupted by the concrete cracks which cause less concrete/steel bond, and thus, the steel bars become vulnerable to large deformation or buckling. Therefore, the seismic demand/capacity principle is not sufficiently fulfilled.
11. The damage state for RC piers in the zone of a plastic hinge is unpredictable, mainly because of its sensitivity to the rate of loading. The rate of applied seismic loading could lead to an acceleration pulse, affecting the displacement response, and thus increasing the amount of damage. In an acceleration pulse, the relatively lower loading rates have longer durations with lower frequencies. In other words, longer-duration loading causes higher displacements, and consequently more damage, while shorter-duration loading causes less displacements. Thus different intensities of crack growth can be formed under the same loading magnitude.
12. This challenges the level of seismic performance of the structure. The effect of acceleration pulses with long durations in a seismic record may not be predicted if the demand was not determined through a full dynamic history analysis for the MDOF structure.
13. Plastic hinges need to be investigated in 3D small-scale discrete element modelling with a sufficient mesh refinement in order to obtain reliable results for the fracture analysis.

14. Techniques that are used to reduce the computational efforts are recommended, such as the Relative Response Technique, but more investigations are required to verify the accuracy of results for different problems with different loading rates.

## **8.1.2 General Conclusions**

### **8.1.2.1 The Damage Mechanism**

When viaducts supported by RC single piers are subjected to seismic loading, the seismic energy is dissipated, mainly, through the formation of plastic hinges in which part of the column base is partially or severely damaged. It should be noticed that the geometry of such structures supported by single piers lead to experiencing a flexural failure mode which is resisted by the ductility action of the single piers. Pure flexural mode permits crack growth to interfere with the concrete core, and the longitudinal reinforcement bars overburden dissipating the hysteretic energy independently, and not in association with the concrete material due to its lack of ductility. This, obviously leads to buckling of the longitudinal bars, and thus to a progressive collapse of the structure.

The severity of damage is related to the amount of energy dissipated during the inelastic stage, and in RC structures concrete starts to undergo the damaging process much earlier before the steel reinforcement tends to yield [1]. Therefore, as damage is related to the hysteretic energy and maximum ductility, the fracture energy could be released in some critical members during minor damage stages of the structure [1].

### **8.1.2.2 The Seismic Design Criterion**

A seismic performance-based design of a structure implies that the seismic capacity of a structural response should meet the seismic demand of that structure under the target ground motion excitations. However, when a shortage of seismic capacity exists, certain damage would occur as corresponding to that shortage. However this concept may not be valid for single RC columns, since severe damage could grow inside the column core much earlier before the steel reinforcement tends to yield, as mentioned earlier.

In terms of the seismic design criterion (SDC) of California Transportations (CALTRANS), the Demand/Capacity balance principle is assumed to occur with minor damage of cover spalling at the plastic hinge region. However, shaking table tests, especially under multi-directional load effect, prove severe crack growth inside the concrete core of RC columns

which are designed according to the demand/capacity principle, and consequent progressive collapse occurs as a result. The demand/capacity principle does not guarantee the exemption of the column core from being severely damaged, especially under strong ground motions or when experiencing acceleration pulses. Further damage could also occur due to the lack of core confinement when axial stresses of the transverse bars are relatively low.

## **8.2 RECOMMENDATIONS**

### **8.2.1 Numerical Modelling**

Numerical modelling using fibre elements and beam-column (bar) elements to solve non-linear RC structures are mainly based on a constitutive relationship for updating strength and ductility. Both strength degradation and ductility of the members are based on the parameters of stresses and strains. However, they have no connection with the damage evolution of the quasi-brittle material nor are they related to fracture energy release due to the stress drop during the crack growth, but they still give approximate analytical results in terms of the hysteresis and time history in terms of global behaviour of the structure, without describing the damage in the plastic hinges. A major drawback in such RC numerical models is that they are not capable of detecting core fracturing since the overall strength and ductility of the section is still functioning due to the steel bars' properties, i.e. they are not capable of detecting all stages of the progressive collapse for the structure, since they were designed to simulate the structure mainly based on its elastoplastic constitutive behaviour.

In one of their conclusions, S. Yavari et al. in 2009 [2] concluded that the overall-scale modelling using overall global equilibrium forces are not suitable for strong ground motion loading.

The commonly used damage descriptors such as damage indices and damage states for the expected damage are based mainly on the global parameters which are obtained from those numerical investigations, such as drift ratios and energetic computations. Such damage descriptors are practically approved for global scale assessment, but not accurate for small-scale investigations.

As a summary, the following drawbacks are listed below:

1- In fibre elements modelling, failed fibres (due to tension or compression) do not sustain further stresses, but due to steel strength and ductile limit the overall structure is capable of

withstanding further loading before steel collapses. In reality, the overall collapse of RC structures may have occurred much before the steel collapse limit.

2- In bar elements modelling, a failed element is due to the built-in elastoplastic hysteresis model of the combined RC section that is based on quasi-static loading tests, without considering the damage effect inside the core.

3- In bar elements modelling, a failed element is due to the built-in damage constitutive model of the combined RC section that is based on theoretical assumptions of the damage evolution theory which needs to be verified experimentally for different cross section geometries.

Furthermore, none of these numerical models are capable of predicting bar buckling which is the threshold of the progressive collapse of the structure.

The fracture due to multi-directional dynamic loading on the quasi-brittle material in 3D structures is a complex problem. If fracture-based small-scale FEM models are technically improved, they should be capable of simulating such problems more than fibre elements and bar-element models which are based on global damage concepts such as energy dissipation and the control of joints mechanism for the non-linear behaviour. More research is still needed for FE models to approximate the fracturing behaviour in RC structures from the following points of view:

- 1- Modelling of concrete as a heterogeneous material.
- 2- Simulating fracture due to compression and twisting, since multi-directional loading causes more damage than lateral loading.
- 3- Including bonding of rebars with concrete in the RC combined section.
- 4- Including refined damping values which are verified with shaking table tests.

In general, numerical methods using fibre elements and bar elements can predict the overall hysteretic behaviour, and produce hysteresis curves and approximate displacement responses, yet not indicating the collapse state of the column, regardless of the severe damage that's attained by the concrete core of the column. Such hysteresis cannot be reliable to investigate the behaviour of single piers without having investigated the crack growth in the concrete section by means of experimental testing or explicitly analytical crack modelling.

## 8.2.2 Alternative Systems

Alternative systems should be substituted for the monolithic system of single RC columns supporting box-girder bridges, since they are vulnerable to severe damage when subject to strong ground motion. However, existing bridges with monolithic structures of single RC columns are widely used even in seismically active regions.

Alternative systems can be based on many approaches, which are listed below:

1. Yielding energy dissipating devices such as seismic isolation bearings SIB's, which utilize rubber bearings (RB) or lead rubber bearings (LRB).
2. Sacrificial yielding braces, or buckling-resistant braces, which are specially designed members to deform plastically in a controlled manner during an extreme seismic event, keeping the main structural members to remain elastic.
3. Damping energy dissipating members such as the sacrificial damping braces which absorb dynamic shocks during the earthquake event and mitigate a large amount of the seismic energy.
4. The approach of weakened-column base which formulate the plastic hinge (PH) as being a zero-moment region, while the rest of the column body remains elastic.
5. Self-Another alternative system is designed to post-tensioning strands (tendons) or steel jackets to increase confinement of the columns.
6. Re-centring or self-centring techniques such as post-tensioning strands (tendons) which is based on applying axial compressive stresses on the column section to reduce the residual strains. In addition, other re-centring techniques such as steel plate jacketing are used to increase the section's confinement and reduce the damage growth. In these techniques, the lateral drifts are reduced to some extent as well as they do a perfect job in preventing residual deformations. However, the concrete core damage could still exist but with cracks being closed after the re-centring action. This is still a hazardous situation for the bridge columns that could lead to collapse at subsequent seismic actions, even with moderate ground motions. In fact, many of these techniques are still under research.
7. Another alternative is changing the design from single piers to multi-columns that support the bridge and strengthen it against the pure flexural mode of failure in order for the columns to behave in a less damaging manner.
8. Other structures with similar geometry as single piers, such as RC columns supporting elevated water tanks, should also fall under the same hazards of damage under seismic loading, and should also be considered.



### 8.2.3 A Criticism on the Eurocode8, (part 2: Seismic Design on Bridges)

Three important topics in the Eurocode8 regulations for the seismic design of bridges are given by EC8-2 [3], and specified in the observations listed below, and criticism remarks are then followed:

- There are two basic requirements of seismic design; the non-collapse requirement, and the minimization of damage requirement. In general, the bridge, according to EC8-2, ‘should retain its structural integrity and adequate residual resistance’. In particular, the resulting damage in some bridge components due to their contribution to energy dissipation is described by the EC8-2 as in the following points:
  1. For the whole structure, it should be damage-tolerant i.e. the structure can sustain emergency traffic actions, and allow performing inspections and repair easily.
  2. For secondary components and for parts that are intended to contribute to energy dissipation during the earthquake event, the damage should be minor with a high probability of occurrence.
  3. For non-critical structural components, such as deck movement points and abutment back-walls, a predictable mode of damage is expected to hit the details of such components, with the possibility of permanent repair.
- As a design criterion, the EC8-2 is imposing a (compliance criterion) in the non-linear analysis of ductile RC members, i.e. those members associated with a flexural mode of motion, that the plastic hinge rotation demands  $\theta_{p,E}$  should be lower than the design rotation capacities  $\theta_{p,d}$ , or:

$$\theta_{p,E} \leq \theta_{p,d}$$

- As a more specifying measure of capacity, the EC8-2 is defining the seismic deformation capacity of bridge piers as the maximum displacement of a structure capable of sustaining at least 5 full cycles of load-deflection hysteresis curves without initiation of failure of the confining reinforcement or drop exceeding 20% of the maximum resisting forces for RC ductile members.

## Criticism Remarks:

In respect to the above mentioned Eurocode8 regulations, the following are my criticism remarks introduced in correspondence with the aforementioned three points respectively;

- The flexural failure mode in case of single RC piers supporting viaducts, dissipate the hysteretic energy through initiated plastic hinge, which is likely to cause severe damages under strong ground motions, as was proved by several shaking table tests under transversal and multidirectional seismic excitations [4,5,6]. The damage is severe in the way that crack growth is damaging the concrete core leading to a total collapse, especially when longitudinal reinforcement bars buckle at the plastic hinge zone. Such damage is mainly attributed to the yield energy dissipation in the reinforcement bars only as ductile materials [7], while concrete is not dissipating any energy but rather become fully damaged as a brittle material under tensile and compressive stresses. Such a mechanism is likely to occur in this flexural mode of motion.
- Using the seismic design criterion SDC, the RC piers are designed according to the principle of demand/capacity balance [3,8], which is best functioning in cases where both steel reinforcement bars and concrete are working together in the best manner, so as to effectively exploit their workability limits of strength and ductility, respectively, and dissipate the seismic energy with the most minor or reparable damages possible. However, this mechanism does not apply in single RC piers subjected to strong ground motion, since pure flexural mode permits crack growth to interfere with the concrete core, leading to possible total collapse. Therefore, the principle of demand/capacity balance stated by the EC8-2 [3] may not be sufficient for single RC columns [9].
- The numerical methods based on non-linear behaviour of beam-column elements represent the overall dynamic, or quasi-static, response of severely damaged piers as hysteretic loops with degrading strength, showing no clear indication of the damage in the disintegrated sections. This is because they are not based on the theory of damage evolution and its effects on crack growth. The requirement of the EC8-2 concerning having sustained least 5 full cycles of the load-deflection hysteresis curves with limited degradation [3] may not be sufficient in this case. However, alternative numerical methods which simulate the fracture mechanism are significantly needed to investigate the suspected damage inside the concrete core of the column.

## 8.3 FUTURE WORK

The following project is chosen since it combines research work and practice together in the field of earthquake engineering and structural dynamics. Furthermore, it forms the basis for the infrastructure of bridges as it provides an engineering system for a proposed seismic evaluation program for the existing bridges.

One of the important objectives for the Department of Transportation in Libya is to establish a seismic evaluation system for the local motorway bridges and viaducts, which are needed to function properly during earthquake events, especially for those that exist in seismically active regions along the south coast of the Mediterranean, as can be seen in Figure 8.1, [10].

There are three parts of in this project associated with establishing this evaluation system; definition of parameters, modelling of the structure and construction of damage and fragility charts. The project parts can be summarised as follows:

1- Utilizing the technique of Ambient Vibrations, such as in [11,12], to define the dynamic characteristics and structural parameters of the bridge as a first step towards building an analytical model based on realistic structural parameters. A numerical model of free-vibration motion is used to calibrate the structural parameters of stiffness and mass for the bridge members, based on the realistic dynamic characteristics of frequencies, damping ratios and effective mode participation factors. For bridges that could experience seismic excitations, the technique of System Identification (SI), such as in [13,14,15], is more likely to be used to obtain more reliable information. In contrast to the ambient vibration technique, the SI requires permanent accelerometers to be previously installed along the bridge members using techniques similar to the field of Structure Health Monitoring (SHM).

2- Building the numerical model as based on the calibrated parameters. Selection of the model depends on the required output data. From the literature review, it was found that the moment-curvature damage model, built by S. Oller and A. H. Babat [16], is very suitable for the seismic evaluation project since it is based on the damage evolution theory of isotropic damage constitutive law. It is also provided with soil-structure interaction and formulated by using classical structural analysis which enables modelling the RC bridge structure easily as a whole. The model was partially funded and supported on a European governmental level; namely the European Commission, Environmental program RTD Project, the Spanish

Government (Ministerio de Educacio´n y Ciencia), and the Spanish Government (Ministerio de Fomento) [16], as was previously mentioned in Chapter 2.

3- Using the analytical methodology procedure made by Moschonas, Kappos et al. [17] to produce seismic fragility curves for different categories of classified bridge types. The procedure is based on defining the damage states which are obtained from the pushover analysis for the entire bridge [17]. The methodology has different definitions for damage states according to energy dissipation mechanism in each bridge, either with yielding piers or non-yielding walls [17]. The procedure was applied on the Greek motorway bridges in which 11 different classes of bridge types have been evaluated by fragility curves versus PGA measures [17].

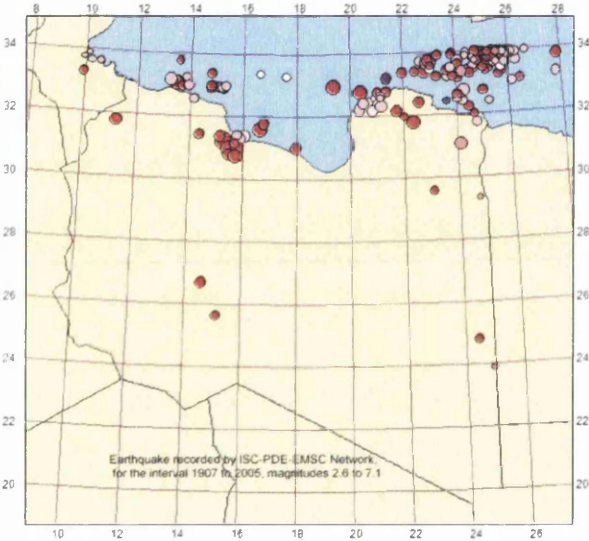


Figure 8.1 Earthquake intensities in Libya from 1907 to 2005, magnitudes from 2.6 to 7.1 [10]

### 8.4 REFERENCES

- [1] J. Faleiro, S. Oller , A.H. Barbat, Plastic–damage seismic model for reinforced concrete frames, *Computers and Structures* 86 (2008) 581–597.
- [2] S. Yavari, K. Elwood, C. Wu. Collapse of a nonductile concrete frame: Evaluation of analytical models. *Earthquake Engineering and Structural Dynamics*. 2009; 38:225–241.
- [3] European Committee for Standardisation. Eurocode 8: Design Provisions for Earthquake Resistance of Structures, Part 2: Seismic Design of Bridges. ENV1998-2, CEN, 1998.

- [4] H. Nishida, S. Unjoh. Dynamic Response Characteristic of Reinforced Concrete Column Subjected to Bilateral Earthquake Ground Motions. Proc. of 13th World Conference on Earthquake Engineering, Vancouver, Canada, 2004, CD-ROM No. 576.
- [5] J. Sakai, S. Unjoh. Earthquake simulation test of circular reinforced concrete bridge column under multidirectional seismic excitation. *Earthquake Engineering & Engineering Vibration* 1671-3664(2006)01-0103-08.
- [6] H. Jeong, J. Sakai, S. Mahin. Shaking Table Tests and Numerical Investigation of Self-Centring Reinforced Concrete Bridge Columns. PEER Report 2008/06, Pacific Earthquake Engineering Research Centre, College of Engineering, University of California, Berkeley. September 2008.
- [7] T. Eom, H. Park. Evaluation of energy dissipation of slender reinforced concrete members and its applications. *Engineering Structures* 32(2010) 2884-2893.
- [8] J. Sakai, S. Mahin. Analytical Investigations of New Methods for Reducing Residual Displacements of Reinforced Concrete Bridge Columns. PEER Report 2004/02, Pacific Earthquake Engineering Research Centre, College of Engineering, University of California, Berkeley. September 2004.
- [9] M. Benamer, Y. Feng, Seismic reliability in reinforced concrete bridge columns based on local and global damage approaches. International Conference on Computational Mechanics CM13, Durham, March 2013.
- [10] A. Elmelade. General information about seismicity & seismotectonics in Libya. Libyan Center for Remote Sensing & Space Science (LCRSSS), Libyan National Seismological Network (LNSN). IRIS Metadata Workshop, 2013, Kuwait.
- [11] M. Tsai, S. Wu, K. Chang, G. C. Lee. Shaking table tests of a scaled bridge model with rolling-type seismic isolation bearings, *Engineering Structures* 29 (2007) 694–702.
- [12] W. Ren, W. Zatar, I. E. Harik. Ambient vibration-based seismic evaluation of a continuous girder bridge, *Engineering Structures* 26 (2004) 631–640.
- [13] M. Chaudhary, M. Abe, Y. Fujino. Performance evaluation of base-isolated Yama-age' bridge with high damping rubber bearings using recorded seismic data. *Engineering Structures*, 23 (2001) 902–910.
- [14] S. Chao, C. Loh. Inelastic response analysis of reinforced concrete structures using modified force analogy method. *Earthquake Engineering and Structural Dynamics*: 36:1659–1683. 2007.

[15] S.J. Li, H. Yu, Y. Suzuki. Identification of non-linear hysteretic systems with slip. *Computers and Structures*, 82 (2004) 157-165.

[16] S. Oller, A. Barbat. Moment–curvature damage model for bridges subjected to seismic loads. *Computer Methods in Applied Mechanics and Engineering*, 195 (2006) 4490–4511.

[17] I.F. Moschonas, A. J. Kappos, P. Panetsos, V. Papdopoulos, T. Makarios, P. Thanopoulos. Seismic fragility curves for greek bridges: methodology and case studies. *Bull Earthquake Engineering* (2009) 7:439-468.

# APPENDICES

## Appendix [A]

This MatLab code applies fibre element modelling to perform non-linear dynamic analysis for a MDOF RC column using Newmark's method. It applies simplified constitutive modelling of the envelop curves for the concrete and steel fibres, and displacement-based formulation for solving the equation of motion. A complete list of the written code is in this Appendix [A].

```
clear all;
clc;
% ..... MDOF Algorithm .....
% ..... MDOF Algorithm .....Normal, More fibres.....
% ..... MDOF Algorithm .....with Reduced K .....
% .....with Damage approximation
% .....with uuu is moved below P(:,1)
% (((((( ... WITH Emerlyville Ground motion
% Problem in Seismo-Struct...)))))))))

% Econc & Esteel are Full values for ALL Fibres
% Mass is divided unto 2 nodes .....
% Lateral Load is accord to Mass values For ALL NODES...
% Initial axial Permanant load is provided.....
% Initial Strain is provided .....
% Damping is changing accord to kkk stiff Matrix
% STATIC run by multiplying c & m by 0.00001 in K-matrix
% No Top Mass ..... only Column .....

%.....Using the NewMark Method to solve a Dynamic problem with Non-Linear
%.....behaviour of (concrete + steel bars), Using the Fibre Element
%.....Method
%
% .....(I) PART ONE : Definitions .....
% .....(I) PART ONE : Definitions .....
% .....(I) PART ONE : Definitions .....

% .....(i) Defining constant parameters.....
DOF=18;

rest = 3; % Number of restrained nodes.....
elem = 5;

LP11 = 0 ; % Lateral Load point at node 32
LP10 = 0 ;
LP9 = 0;
LP8 = 0;
LP7 = 0;
LP6 = 17;
LP5 = 14;
LP4 = 11;
LP3 = 8;
LP2 = 5;
LP1 = 2;

LPX= 16; % Axial Load point at node 16
%LP2=29; LP3=26;
% .....
EDOF=6;
fibres=57; % fibres=29
width = 0.70; % .....

size = 800;

%size= 1500; % number of time-steps .(size of files)...% SHOULB BE
%55.....

L = 1.2; % Length of Element = Length of Fibres .....
bars1=5; bars2=2; bars3=0.5+0.5; % number of bars at fibre strip, bars3 is not included.
augmentation= 30000*10 ; % this is the TOP lateral load using the TOP MASS .....
augmentation2= 735 *10 * 0; % this is the Column lateral load using the COLUMN MASS....

%AXIAL = 19700 * -9.81 * 1; % Axial Load point at node
```

```

%AXIAL =-300000; % -5451000 ; % Axial Load point at node
AXIAL =-3; % to cancel axial load (Method 2)

%AXIALload= -8.23e6; %-21000.000; %-5.45100; % Axial load at Top node ....
%AXIALload= -3.00e5; %
AXIALload= -30000 *10 ; % *0.00001 ; % BY ZEEEEEEEEEEEEERRRRROOOOOOOOOO

massreduc =1;
accel=1; % 0 testing 0 uuu(:,1)
dt=0.01; % time step
%gr=-10; % -9.81 ; % gravity ground force

EC = 2.10e10; % = 21000 MPa = 2.10e10 Pa (N/m2)
ES = 1.75e11; % = 175000 MPa = 1.75e11 Pa (N/m2) .....NNNNNNNNNNNN
%AAA= 3.5; % this is reduce 0.002 since Fy is reduced by 3.5.....look line 433, or rais Deps by3.5 look line 577
AAA=1;
%BBB= 1.00005; % to enlarge Deps
BBB= 1 ;
Fy = 3.4e8 / AAA ; % N/m2 Steel Axial Strength .....Fy = 3.5e8 ;

FC = -4.2e7 ; %FC = -1.2e7 ; % N/m2 Concrete Axial Strength .....NNNNNNNNNNNN
BIGG = -43e7 ; % BIG Number.....

% .....(ii-a) Defining STRUCTURE parameters.....(time-step parameters)...
% .....

P=zeros(DOF,size); % External load
PP=zeros(DOF,size); % 'Computed' External load
Pcap=zeros(DOF,size); % (not needed) Cap External load
dP=zeros(DOF,size); % Nodal Increment of External load
DP=zeros(DOF,size); % Nodal Cap Increment of External load
DPred=zeros(DOF-rest,size); % definition of DPred.....

fs=zeros(DOF,size); % Nodal Restoring forces (axial, Shear and moment)
dfs=zeros(DOF,size); % Nodal Restoring Incremental forces (axial, Shear and moment)

u=zeros(DOF,size); % Nodal displacement
uu=zeros(DOF,size); % Nodal velocity
uuu=zeros(DOF,size); % Nodal acceleration

du=zeros(DOF,size); % Nodal displacement increment
dured= zeros(DOF-rest,size); % reduced du
duu=zeros(DOF,size); % Nodal velocity increment
duuu=zeros(DOF,size); % Nodal acceleration increment

kkk=zeros(DOF); % STRUCTURE stiffness matrix.....
kkkred=zeros(DOF); % STRUCTURE stiffness matrix.....
Axial=zeros(DOF-rest,1); % reduced initial Axial Forces
Initial=zeros(DOF-rest,1); % reduced initial displacement
uG=zeros(DOF-rest,1); % reduced Gravity displacement

% .....(ii-b) Defining ELEMENT parameters.....( ELment & time-step parameters)...

ddu=zeros(EDOF,elem); % ELEMENT displacement increment
k =zeros(EDOF); % ELEMENT stiffness matrix.....
km =zeros(EDOF,EDOF,elem); % ELEMENT stiffness matrix.....
kk =zeros(DOF,DOF,elem); % Global ditribution for stiffness terms of
% of one element ONLY.....

Econc =zeros(fibres,size); % Defined here, OUTside the time-step LOOP ...
Esteel=zeros(fibres,size); % Defined here, OUTside the time-step LOOP ...

%input data ....materials vectors....
%input data ....materials vectors....

% .....LUMPED Mass...w/LOCAL rotational mass.....

mv=[ 735 735 1058 ]; % diagonal elements ...
for ij=1:3:DOF
m(ij+0,ij+0)= mv(1);
m(ij+1,ij+1)= mv(2);
m(ij+2,ij+2)= mv(3);
end
% Except for .....
m(1,1)= 735/2; m(2,2)= 735/2; m(3,3)= 0.1;

m(DOF-2,DOF-2)= 30000 ; % HERE; ignoring the vertical mass effect.....
m(DOF-1,DOF-1)= 30000;
m(DOF,DOF)= 43200 ; % to be cancelled if using (Glabal) rotational Mass
%.....

% .....LUMPED Mass...w/LOCAL rotational mass.....

%mv=[ 735 735 4.14 ]; % diagonal elements ...
% for ij=1:3:DOF

```



```

% m(ij+0,ij+0)= mv(1);
% m(ij+1,ij+1)= mv(2);
% m(ij+2,ij+2)= mv(3);
end
% Except for :.....
m(1,1)= 735/2; m(2,2)= 735/2; m(3,3)= 4.14/2;

% m(DOF-2,DOF-2)= 30000 ; % HERE; ignoring the vertical mass effect.....
% m(DOF-1,DOF-1)= 30000;
% m(DOF,DOF)= 5630.14 ; % to be cancelled if using (Global) rotational Mass
% .....
% .....LUMPED Mass...w/GLOBAL rotational mass.....

% m(6,6)=1058.4; m(9,9)=4233.6; m(12,12)=9525.6; m(15,15)=16934.4;
% m(18,18)=1080000;

% .....

% .....forming CONSISTANT mass matrix m .....
% m=zeros(DOF);
% mv1= 735; % column mass
% mv2= 30000; % TOP mass
% m = Mass ( EDOF,DOF,elem,mv1,mv2,L); % consistant MASS
% .....

% ..... Geometry & Area Definitions for (Concrete & STEEL) fibres ....
% .....

% .....
% function (1) .....
% function (1) .....
y=zeros(fibres,1);
[y,Aconc,Asteel] = GeomHigh(L,fibres,width,bars1,bars2);
% .....
% ..... Same As (iv) 2.4.d Same As.....
% get Econcret & Esteel for every fibre .....
Econc =zeros(fibres,size); % Defined here, inside the time-step LOOP ....
Esteel=zeros(fibres,size); % Defined here, inside the time-step LOOP ....

for j = 1: fibres
    Econc(j,1:2) = EC; % CONSTANT since initial % to be corrected.....
    % if you put HIGH values, sigmak will not be correct .....
    Esteel(j,1:2) = ES ; % CONSTANT since initial % to be corrected.....
end

% for j = (fibres-1)/2 :fibres
% Econc(j,2) = EC ;
% Esteel(j,2) = ES ;
% end

% .....Same As (iv) 2.4.e Same As .....

% construct k- matrix... function (4) to get the stiffness matrix .....
% Convert k(i,j)from LOCAL to GLOBAL stiffness matrix

% step 1: construct element stiff matrix...
% ..... element loop .....(1) .....
shift = 0;
for e=1: elem
    i=1; % this is to calculate k for ONE iteration ONLY; the Initial Condition ONLY.
    k = elemstiffmatrix ( i,fibres,Econc,Aconc,Esteel,Asteel,y,L); % for the Initial Condition ONLY.
    km(:,e) = k;
    % if e==10
    % km(:,e) = k ;
% end

% step2: Transform element stiffness matrices to global coordinates NOT NEEDED)
% step3: Combine element stiffness matrices to form global stiffness matrix
for iii = 1:EDOF
    for jjj = 1:EDOF
        kk(iii+shift, jjj+shift, e) = km(iii, jjj, e);
    end
    end
    shift = shift + 3;
end
% ..end of element loop .....(1) .....
kkk = sum(kk,3) ;
fs2kinitial(:,i+1)= kkk(2,:);
hhh=kkk;
%step4: Set to Zeros Boundary Positions in global stiffness matrix with constraints ..
kkkred = kkk; % definition of Kred.....
kkkred(:,3)= []; kkkred(3,:) = [];
kkkred(:,2)= []; kkkred(2,:) = [];
kkkred(:,1)= []; kkkred(1,:) = [];

```

```

% .....end of constructing Global stiffness matrix.....
% .....end of constructing Global stiffness matrix.....

% .....Similar To...(iv) 2.4.f ..... Similar To....
% get initial displacement
Axial=zeros(DOF-rest,1); % defining all Ext. initial Loading=0
Gravred=zeros(DOF-rest,1); % define the reduced Gravity Load
Gravity=zeros(DOF,1); % define the Gravity Load
uGred=zeros(DOF-rest,1); % define the reduced Gravity Load
uG=zeros(DOF,1); % define the Gravity Load

%Axial(LP11-1-rest,1)=AXIALload; % defining the TOP Load as the Axial Forces (method 1, STATIC)
%Axial(LP10-1-rest,1)=AXIALload;
%Axial(LP9-1-rest,1)=AXIALload;
%Axial(LP8-1-rest,1)=AXIALload; ( NO NO NO Not needed )
%Axial(LP7-1-rest,1)=AXIALload;
%Axial(LP6-1-rest,1)=AXIALload;
Gravred(LP6-1-rest,1)=AXIALload; % Define the Gravity load
%Axial(LP5-1-rest,1)=AXIALload;
%Axial(LP4-1-rest,1)=AXIALload;
%Axial(LP3-1-rest,1)=AXIALload;
%Axial(LP2-1-rest,1)=AXIALload;

Initial(:,1) = inv(kkkred) * Axial(:,1); %determine the initial displacement

uGred(:,1) = inv(kkkred) * Gravred(:,1); % Define the displacement due to the Gravity

uG(1:rest,1) = 0; % definig uG for the whole structure...
uG(rest+1:DOF,1) = uGred(:,1); % definig uG for the whole structure...
%Gravity(1:rest,1) = 0; % definig Gravity Load for the whole structure...
%Gravity(rest+1:DOF,1) = Gravred(:,1); % definig Gravity Load for the whole structure...
Gravity(:,1) = kkk * uG(:,1); % Obtain the Permenant Gravity Load
% end of (iv) 2.4.f .....

%....forming Element damping matrix c.... LINEAR, so it is NOT updated....
c=zeros(DOF);
%c= 0.9198 * m + 0.0021 * kkk; % Reilay Damping % to be corrected.....
%c= 0.2198 * m + 0.0021 * kkk;
%c= 0.2138* m + 0.000000524 * kkk NOT WORKING; % Reilay Damping From Seismo_Struct
%c= 0.71807* m ; % Mass-Proportional Damping From Seismo_Struct
%c= 0.008912 * kkk ; % Stiffness-Proportional Damping From Seismo_Struct
% to be corrected.....

c1= 1.71807* m ;
c20= 20.71807* m ;
c= 1.71807* m ; % * 0.582048461; % this is to make c = m

hhh=zeros(DOF,DOF);
for q=1:DOF
    hhh(q,q) = kkk(q,q);
end
%c= 0.231* m + 0.000501 * hhh ; % calculated from Chopra Equation 11.4.10

% .....(iii) Defining NewMarrk (Constants) ....

gama = 0.5; beta=0.25; %the Average Acceleration Method...AAM.....-->(used)
%gama = 0.5; beta=0.166; %the Linear Acceleration Method...LAM.....(not used)
%beta=0.166;

a=zeros(DOF);
b=zeros(DOF);

a = (1/(beta*dt))* m + (gama/beta) * c ;
b = (1/(2*beta)) * m + dt*((gama/2*beta)-1)* c ;

Aa= gama/(beta*dt) ; Bb= gama/beta ; Cc= dt*(1-(gama/(2*beta)));
Dd= 1/(beta*dt*dt) ; Ee= 1/(beta*dt); Ff= 1/(2*beta) ;

%.....(iv) importing (the Lateral Direc only) of the External Load P .....

Pv=zeros(size,1); % defining (the lateral direction only)
% P & dP already defined ....

%load('extforce.txt') ; % Elcentro acceleration
%fid = fopen('extforce.txt') ; % opening the file
%CCC = textscan(fid, '%f %f '); % scanning the file
%fclose(fid); % closing the file

%load('Emeryville>Loading.txt') ; %
%load('cyclic_zigzag_full.txt') ; %
%fid = fopen('cyclic_zigzag_full.txt') ; % opening the file
load('cyclicz20.txt') ; %
fid = fopen('cyclicz20.txt') ; % opening the file
CCC = textscan(fid, '%f %f '); % scanning the file

```

```

fclose(fid);          % closing the file

time = CCC[1];      % this is for the 1st-column data file

Pv = CCC[2];       % this is for the 2ed-column data file

%.....now.....finding the increment of Ext loading .....

%plot(Pv,'*r'); ;hold on; grid on; % a hysteresis loop....
% P(LP11,1:size)=augmentation *Pv(1:size); % defining the Ext. Load as the lateral Force of the 2ed node)

% P(LP10,1:size)=augmentation2 *Pv(1:size);
% P(LP9,1:size)=augmentation2 *Pv(1:size);
% P(LP8,1:size)=augmentation2 *Pv(1:size);
% P(LP7,1:size)=augmentation2 *Pv(1:size);
P(LP6,1:size)=augmentation *Pv(1:size);

P(LP5,1:size)=augmentation2 *Pv(1:size);
P(LP4,1:size)=augmentation2 *Pv(1:size);
P(LP3,1:size)=augmentation2 *Pv(1:size); % can be cancelled when NOT compared with
% Ground Accel. Loaded problem

P(LP2,1:size)=augmentation2 *Pv(1:size);
P(LP1,1:size)=augmentation2 *Pv(1:size);

P(LPX,1)=AXIAL; % defining the Ext. Load as the Axial Forces(method 2,Dynamic)
P(LPX,2:size)= 0 ; %

dP(LPX,1)=AXIAL; % defining the Ext. Load as the Axial Forces(method 3,Dynamic)
dP(LPX,2:10:size)= 0 ; % P(LPX,2:size) is constant, therefore dP =approx 0
dP(LPX,6:10:size)= 0 ; % P(LPX,2:size) is constant, therefore dP =approx 0

for ijj=1 : size-1
% not needed P(LP,size+1)= 0; % this is to avoid error, and find a value dP(LP,size) which's not needed
% dP(LP11,ijj) = P(LP11,ijj+1) - P(LP11,ijj);
% dP(LPX,ijj) = this is a constant value..... its dP = 0; But
% duuu(:,1) is added to uuu(:,1) and DP is formed with the Initial
% Condition...
% dP(LP10,ijj) = P(LP10,ijj+1) - P(LP10,ijj);
% dP(LP9,ijj) = P(LP9,ijj+1) - P(LP9,ijj);
% dP(LP8,ijj) = P(LP8,ijj+1) - P(LP8,ijj);
% dP(LP7,ijj) = P(LP7,ijj+1) - P(LP7,ijj);
dP(LP6,ijj) = P(LP6,ijj+1) - P(LP6,ijj);
dP(LP5,ijj) = P(LP5,ijj+1) - P(LP5,ijj);
dP(LP4,ijj) = P(LP4,ijj+1) - P(LP4,ijj);
dP(LP3,ijj) = P(LP3,ijj+1) - P(LP3,ijj);
dP(LP2,ijj) = P(LP2,ijj+1) - P(LP2,ijj);
dP(LP1,ijj) = P(LP1,ijj+1) - P(LP1,ijj);

end
% .....(v) Defining NewMark (Initial) parameters.....

%P(1:3:DOF-2,1)= m(DOF-2,DOF-2)*gr; % initial External load = (Gravity loading of top mass ONLY)
%fs(28,1)=AXIAL; % initial Restoring forces (axial forces)
% uuu(:,1)= accel*inv(m)*( P(:,1)- (c* uu(:,1)) - fs(:,1) ); % initial acceleration

%uuu(1:rest,:)=0.0; % Boundary conditions
%uu(1:rest,:)=0.0; % Boundary conditions
% u(1:rest,:)=0.0; % Boundary conditions

% .....(II) PART TWO: Calculations for each time-step .....
% .....(II) PART TWO : Calculations for each time-step .....
% .....(II) PART TWO : Calculations for each time-step .....

% ,,,,,,,,,, VERY INITIAL DEFINITIONS for (FIBRES) ,,,,,,,,,,
% ,,,,,,,,,, (BEFORE) getting into time-step LOOP ....

% Number of fibres already defined (fibres = ....)

epsk=zeros(fibres,size+1,elem); % ,,,,,,,,,, size i+1 NO NO NO
%epsk(:, 1 ,:)= -0.0005 ; % Initial Strains.....

sigmak=zeros(fibres,size+1,elem); % ,,,,,,,,,,size i+1 NO NO NO

Damsig=zeros(fibres,size,elem); % .. effective stress
Damsigma=zeros(fibres,size,elem); % .. effective stress ..Re-defined..
Damage=zeros(fibres,size,elem); % ...the Damage ....

sigmakS=zeros(fibres,size+1,elem); % ,,,,,,,,,,size i+1 NO NO NO

Brush=ones(fibres,size+1,elem); % .... this is a sign (=1) for Linearity ....
Bru =ones(fibres,size+1,elem); % .... this is a sign (=1) for Linearity ....

Depsk =zeros(fibres,1); % Defined here, ALSO inside the time-step LOOP ....
Deps=zeros(fibres,size,elem);
% ,,,,,,,,,,
% ,,,,,,,,,,

```

```

% ....(A)..... Initial cond'ns for Concrete fibres....
%.....
% EC = already Defined = 21000 MPa = 2.1e10 Pa (N/m2)
crush=-0.008;
CRUSH = zeros(fibres,size,elem); % .....
Top = zeros(fibres,size,elem); % .....
Bottom= zeros(fibres,size,elem); % .....

%Top(:,,:)= -0.0005; % update all Top-values to be -0.002
Top(:,,:)= -0.002; % update all Top-values to be -0.002

Tx= zeros(fibres,size,elem); % .....
Bx= zeros(fibres,size,elem); % .....
Cx= zeros(fibres,size,elem); % .....

%.....
%.....(B)..... Initial cond'ns for STEEL fibres....
%.....
% ES = already Defined = 1.75e11 = 175000 MPa = 1.75e11 Pa (N/m2)
% Fy = already Defined = 3.5e8;
DiffS= Fy/ES; % is repeated later in the function...
TopS = zeros(fibres,size,elem); % .....
BottomS= zeros(fibres,size,elem); % .....
TopS(:,,:)= 0.002 / AAA ; % / AAA
BottomS(:,,:)= -0.002 / AAA ; % / AAA
Middle= zeros(fibres,size,elem); % .....
TSx= zeros(fibres,size,elem); % .....
BSx= zeros(fibres,size,elem); % .....
Mdx= zeros(fibres,size,elem); % .....

% .....(C).... Geometry & Area fibres Definitions ...Already Defined....
% .....
% .....end of VERY INITIAL DEFINITIONS for (FIBRES) .....
% .....

% ..starting MAJOR TIME-STEP LOOP.....
% ..starting MAJOR TIME-STEP LOOP.....
for i=1 : size-1
% ..starting MAJOR TIME-STEP LOOP.....
% ..starting MAJOR TIME-STEP LOOP.....

% .....changing c Damping .....((begin here)).....

%c= 0.2138* m + 0.00524 * kkk ; % Reilay Damping From Seismo_Struct
%c= 0.71807* m ; % Mass-Proportional Damping From Seismo_Struct
%c= 0.008912 * kkk ; % Stiffness-Proportional Damping From Seismo_Struct
% to be corrected.....
%c= 1.71807* m ;

for q=1:DOF
hhh(q,q) = kkk(q,q); % this is to make the kkk-matrix LATERAL??
end
%c= 0.231* m + 0.00501 * hhh ; % calculated from Chopra Equation 11.4.10

% .....(iii) Defining NewMarrk (Constants) ...
gama = 0.5; beta=0.25; %the Average Acceleration Method...AAM....->(used)
%gama = 0.5; beta=0.166; %the Linear Acceleration Method...LAM.....(not used)
%beta=0.166;

a=zeros(DOF);
b=zeros(DOF);

a = (1/(beta*dt))* m + (gama/beta) * c ;
b = (1/(2*beta)) * m + dt*((gama/2*beta)-1)* c ;

Aa= gama/(beta*dt) ; Bb= gama/beta ; Cc= dt*(1-(gama/(2*beta)));
Dd= 1/(beta*dt*dt) ; Ee= 1/(beta*dt); Ff= 1/(2*beta) ;

% .....end of ....changing c Damping .....end here.....

% .....(i) 2.1

DP(:,i) = dP(:,i) + a * uu(:,i) + b * uuu(:,i); % rest of DOF...
%DP(:,i) = dP(:,i)+0.00001* a * uu(:,i) +0.000001* b * uuu(:,i); % static
for j=1:DOF-rest
DPred(j,i) = DP(j+rest,i) ; % Boundary cond'n.....1st 3 DOF =0.0 restrained....
end

% .....(ii) 2.2
% get the Element stiffness matrix especially made for (THIS) time-step
% already obtained from (Previous) time-step or from
% initial codn's (k,kk,kkk)

% .....(iii) 2.3
K=zeros(DOF); % Defined here, inside the time-step LOOP ....
% Kred will be defined next step.....
K = kkk + Aa * c + Dd * m ;
%K = kkk + 0.000001* Aa * c + 0.00001* Dd * m ; % static

```

```

%step 4: Reduce global stiffness matrix with constraints
Kred = K; % definition of Kred.....
Kred(:,3) = []; Kred(3,:) = [];
Kred(:,2) = []; Kred(2,:) = [];
Kred(:,1) = []; Kred(1,:) = [];

% .....(iv) 2.4
% get Delta displacement from Cap stiff matrix.....

dured(:,i) = inv(Kred) * DPred(:,i) ;
% Also dured(:,i) = K \ DP(:,i) ;

%if i=1
% dured(:,1)= Initial(:,1); % this is to definee the Initial displacement
%end

du(1:rest,i) = 0; % definig du for the whole structure...
du(rest+1:DOF,i) = dured(:,i); % definig du for the whole structure...
% .....(iv) 2.4.a - 2.4.g >>>> FIBRES LEVEL <<<<<<

% get a (new Econc, Esteel)for the next time-step .....
% then get a (new k) for the next time-step .....
% .....
% .....

% .....(iv) 2.4.a
% get Delta strains & update the strains for NEXT time-step

% .....
% Convert du(...)from (GLOBAL) to LOCAL displacment increments
% Convert du(...)from (GLOBAL) to LOCAL displacment increments
% Convert du(...)from (GLOBAL) to LOCAL displacment increments

% element loop.....(2).....
jj=1;
for e=1 : elem

    ddu(1, e) = du(jj+0,i);
    ddu(2, e) = du(jj+1,i);
    ddu(3, e) = du(jj+2,i);
    ddu(4, e) = du(jj+3,i);
    ddu(5, e) = du(jj+4,i);
    ddu(6, e) = du(jj+5,i);

    jj=jj+3;
end
% end of element loop.....(2).....

% element loop.....(3).....
% element loop.....(3).....
for e=1 : elem

% function (2) .....get the Delta strains.....
Depsk =zeros(fibres,1); % Defined here, inside the time-step LOOP ....
%[ Depsk ] = Deltastrains( i,du,L,y,fibres); OR OR OR
Depsa = ( ddu(4,e)-ddu(1,e) ) / L ;

Dfai = ( ddu(6,e)-ddu(3,e) ) / L ;

for j=1 : fibres
%Depsk(j) = Depsk - ( Dfai * y(j) );
%Depsk(j,i,e) = Depsk(j);

Deps(j,i,e) = ( Depsa ) + ( BBB * Dfai ) * y(j) ; % To put the formal equation

Deltaa(j,i,e)= Depsa;
Deltaf(j,i,e)=Dfai;

end

% .....back to function (2).....
for j=1 : fibres
% epsk(j,i+1,e) = Depsk(j) + epsk(j,i,e); % future Uni-axial strains
%epsk(j,i+1,e) = Depsk(j)' + epsk(j,i,e); % future Uni-axial strains
% I claim Both are working (wih ' & without ')

epsk(j,i+1,e) = Deps(j,i,e) + epsk(j,i,e); % To put the formal equation

if e=1
    epseps1(j,i+1)=epsk(j,i+1,1);
    Depseps(j)= Depsk(j);

    Deltaepsa(j,i)= Deltaa(j,i,1);
    Deltafai(j,i)= Deltaf(j,i,1);
end
if e=2
    epseps2(j,i+1)=epsk(j,i+1,2);

```

```

Deltaepsa(j,i)= Deltaa(j,i,2);
Deltafai(j,i)= Deltaf(j,i,2);

end
if e==3
    epseps3(j,i+1)=epsk(j,i+1,3);
end
end
end

% .....(iv) 2.4.b
% get stresses from Concrete & Steel models.....
%if e==2
%Top(2,i,2)
%end

%for j=1:fibres
%if Top(j,i,e) < -0.002
%    Top(j,i,e)

%    end
%end
% function (3) ..... in a Function M-file.....
[ sigmak sigmakS Damsig Tx Bx Cx TxS BxS MdS Bru ] = GDstresses(
i,e,fibres,size,epsk,crush,EC,ES,Fy,Top,Bottom,CRUSH,TopS,BottomS,Middle,Brush );
for j=1 : fibres
    Top(j,i+1,e) =Tx(j,i+1,e); % ...up dating.....
    Bottom(j,i+1,e)=Bx(j,i+1,e); % ...up dating.....
    CRUSH(j,i+1,e) =Cx(j,i+1,e); % ...up dating.....

Brush(j,i+1,e) =Bru(j,i+1,e) ; % for the next iteration for the FUNCTION GDstresses..
% and also for section (iv) 2.4.d

TopS(j,i+1,e) =TxS(j,i+1,e); % ...up dating.....
BottomS(j,i+1,e)=BxS(j,i+1,e); % ...up dating.....
Middle(j,i+1,e) = MdS(j,i+1,e); % ...up dating.....
end

% ..... Damage PART .....
for j=1: fibres
Damsigma(j,i+1,e)= Damsig(j,i+1,e); % this is to Re-Define the parameter..
end
% .....end of Damage PART .....

%for j=1:fibres
%if Top(j,i+1,e) < -0.002
%    Top(j,i+1,e)

%end
%end
%Top(:,i+1,e) =TSx(:,i+1,e); % ...up dating.....
%BottomS(:,i+1,e)=BSx(:,i+1,e); % ...up dating.....
%Middle(:,i+1,e) =Mx(:,i+1,e); % ...up dating.....
% .....TSx BSx Mx.....to be added ....
%'Tx'
% Tx(:,i+1,e);
% .....(iv) 2.4.c
% get Delta stresses for every fibre.....
%Dsigmak =zeros(fibres,1); % Defined here, inside the time-step LOOP ....
%DsigmakS=zeros(fibres,1); % Defined here, inside the time-step LOOP ....

% .....(iv) 2.4.d
% get Econc & Esteel for every fibre .....
%Econc =zeros(fibres,size); % Defined here, inside the time-step LOOP ....
%Esteel=zeros(fibres,size); % Defined here, inside the time-step LOOP ....

for j = 1: fibres

    Econc(j,i+1) = sigmak(j,i+1,e) / epsk(j,i+1,e);
    Esteel(j,i+1) = sigmakS(j,i+1,e) / epsk(j,i+1,e);

% .....Exceptions for Econc & Esteel .....

% if strain is positive, (TENSION SIDE only), and HAS NOT BEEN PLASTIC YET (Brush=1 <200), then Econc = EC.....
% But if it had been Plastic ( Brush =200), then Econc MUST NOT = EC ...
%if epsk(j,i+1,e) > 0 && Brush(j,i+1,e) == 1
%    Econc(j,i+1) = EC ;
%end
%if Esteel(j,i+1) < 0
%    Esteel(j,i+1) = 0; % this is to cancel out the Esteel Negative (non-real) values...
%end

%Econc(j,1) = EC ; % CONSTANT since initial % to be corrected.....
% if you put HIGH values, eigmak will not be correct .....
%Esteel(j,1) = ES; % CONSTANT since initial % to be corrected.....

% .....end of.....Exceptions for Econc & Esteel .....

if e==1

```

```

EEE1(j,i+1)=Econc(j,i+1);
EES1(j,i+1)=Esteel(j,i+1);
sigsig1(j,i+1)= sigmak(j,i+1,1);
sigsigS1(j,i+1)= sigmakS(j,i+1,1);

end
if e==2
EEE2(j,i+1)=Econc(j,i+1);
EES2(j,i+1)=Esteel(j,i+1);
sigsig2(j,i+1)= sigmak(j,i+1,2);
sigsigS2(j,i+1)= sigmakS(j,i+1,2);
end
if e==3
EEE3(j,i+1)=Econc(j,i+1);
sigsig3(j,i+1)= sigmak(j,i+1,3);
sigsigS3(j,i+1)= sigmakS(j,i+1,3);

end

end

% .....(iv) 2.4.e

% construct k- matrix... function (4) to get the stiffness matrix .....
% Convert k(i,j)from LOCAL to GLOBAL stiffness matrix

% step 1: construct element stiff matrix...

k = elemstiffmatrix ( i, fibres,Econc,Aconc,Esteel,Asteel,y,L);
km(:,e) = k ;

end
% .....end of element loop....(3).....
% .....end of element loop....(3).....

% .....start of element loop....(4).....
% .....start of element loop....(4).....

shift = 0 ;
for e=1 : elem

% step2: Transform element stiffness matrices to global coordinates NOT NEEDED)
% step3: Combine element stiffness matrices to form global stiffness matrix

for ii = 1:EDOF
for jj = 1:EDOF
kk(ii+shift,jj+shift,e) = km(ii,jj,e);
end
end
shift = shift + 3;
end
% .....end of element loop....(4).....
% .....end of element loop....(4).....
kkk = sum(kk,3); % this is to sum the element matrices in ONE matrix

fs3k(:,i+1)= kkk(3,:); % Moment per unit rotation..
fs2k(:,i+1)= kkk(2,:); % Shear force per unit lateral displ
fs1k(:,i+1)= kkk(1,:); % Axial force per unit ROCKING displ

%step4: Set to Zeros Boundary Positions in global stiffness matrix with constraints ..
%kkk(1,:)= 0; kkk(:,1) = 0; NNNNOOOOOO
%kkk(2,:)= 0; kkk(:,2) = 0; NNNNOOOOOO
%kkk(3,:)= 0; kkk(:,3) = 0; NNNNOOOOOO
% .....end of constructing Global stiffness matrix.....
% .....end of constructing Global stiffness matrix.....

% .....(iv) 2.4.f
%
% get future displacement get u(1:6,i+1)
% already defined OUT side the loop....
u(:,i+1) = du(:,i) + u(:,i); % Displacement updating.....

% .....(iv) 2.4.g
% get fs
% already defined OUT side the loop....

dfs(:,i) = kkk * du(:,i) ; % GET future Restoring Incremental force
fs(:,i+1) = fs(:,i) + dfs(:,i) ;
fsl(:,i+1) = kkk * u(:,i+1) ; % not correct ...bad

% .....
% .....

% .....(v) ...2.5

duu(:,i) = Aa * du(:,i) - Bb * uu(:,i) + Cc * uuu(:,i) ;

```



```

% .....(vi) ....2.6
duuu(:,i) = Dd * du(:,i) - Ee * uu(:,i) - Ff * uuu(:,i) ;

% .....(vii) ....2.7
uu(:,i+1) = duu(:,i) + uu(:,i); % Velocity updating.....
uuu(:,i+1) = duuu(:,i) + uuu(:,i); % Acceleration updating.....

% PP(:,i)= kkk * u(:,i) + c * uu(:,i) + m * uuu(:,i);
% Pcap(:,i)= K * u(:,i);

% ..END OF MAJOR TIME-STEP LOOP.....
% ..END OF MAJOR TIME-STEP LOOP.....
end
% ..END OF MAJOR TIME-STEP LOOP.....
% ..END OF MAJOR TIME-STEP LOOP.....

% .....Adding the STATIC contribution of Gravity to
% ..... the DYNAMIC solution .....
for i=1: size
    uT(:,i)= u(:,i) + uG(:,1);
    fsT(:,i)= fs(:,i) + Gravity(:,1);
end

% .....

%plot(u(32,:),fs(5,:),'o-r'); hold on; grid on; % THE hysteresis loop....
%plot(epsk);grid on; %
%plot(sigmak);grid on; %

%plot(epseps1(1,:),sigsig1(1,:),'+-r');hold on; grid on;
%plot(epseps2(3,:),sigsigS2(3,:),'+-b');hold on; grid on;
%plot(epseps1(1,:),sigsigS1(1,:),'+-r');hold on; grid on;
%plot(time(i:1200),kk,'o-r');
% .....
% .....
%plot(u(17,1:721),-fs(2,1:721),'-r'); hold on; grid on; % THE hysteresis loop...
%plot(u(17,:),-fs(2,:),'-r'); hold on; grid on; %
%plot(epseps1(1,1:700),sigsig1(1,1:700),'-r'); hold on; grid on;
%plot(epseps1(1,1:700),sigsigS1(1,1:700),'-r'); hold on; grid on;
%plot(u(32,:),fs(32,:),'o-r'); hold on; grid on; % THE hysteresis loop...
%plot(u(32,:),V(1,:),'o-r'); hold on; grid on; % THE hysteresis loop...
%plot(u(32,:),PP(35,:),'o-r'); hold on; grid on; % THE hysteresis loop...
%plot(u(32,:),Pcap(26,:),'o-r'); hold on; grid on; % THE hysteresis loop...
% .....
% .....

```

## FUNCTIONS for the main code:

```

function [y,Aconc,Asteel] = GeomHigh(L,fibres,width, bars1,bars2)

% ..... function (1) to get arms distances y(j) and Area of each fibre A(j)...

for j=1 : fibres

    w= width/ (fibres-1) ;
    y(j)= -(((fibres-1)/2)- (j-1)) * w ; % neg. sign
    %y(j)= (((fibres-1)/2)- (j-1)) * w ; % POS sign

end
y;

for j=1 : fibres

    Aconc(j) = w * width;
    Asteel(j)= 0.0;
end

% ..... 57 fibres .....
Asteel(3)= 0.000245 * bars1 ; Asteel(54)= Asteel(3);
Asteel(4)= 0.000245 * bars1 ; Asteel(55)= Asteel(4);

Asteel(14)= 0.000245 * bars2 ; Asteel(43)= Asteel(14);
Asteel(15)= 0.000245 * bars2 ; Asteel(44)= Asteel(15);

Aconc(3)= Aconc(3)-Asteel(3); Aconc(54)= Aconc(54)-Asteel(54);
Aconc(4)= Aconc(4)-Asteel(4); Aconc(55)= Aconc(55)-Asteel(55);
Aconc(14)= Aconc(14)-Asteel(14); Aconc(43)= Aconc(43)-Asteel(43);
Aconc(15)= Aconc(15)-Asteel(15); Aconc(44)= Aconc(44)-Asteel(44);

```



```

% ..... 29 fibres .....
% Asteel(3)= 0.00049 * bars1 ; Asteel(27)= Asteel(3);
% Asteel(9)= 0.00049 * bars2 ; Asteel(21)= Asteel(9);

% Aconc(3)= Aconc(3)-Asteel(3); Aconc(27)= Aconc(27)-Asteel(27);
% Aconc(9)= Aconc(9)-Asteel(9); Aconc(21)= Aconc(21)-Asteel(21);

```

```

% .....
% .....
% .....
end

```

```

% .....

```

```

function k = elemstiffmatrix ( i,fibres,Econc,Aconc,Esteel,Asteel,y,L)

```

```

% function (4) to get the k matrix .....

```

```

EAT = zeros(fibres,1);
EGT = zeros(fibres,1);
EIT = zeros(fibres,1);
EA = 0.0;
EG = 0.0;
EI = 0.0;
% .....
EAT1 = zeros(fibres,1);
EGT1 = zeros(fibres,1);
EIT1 = zeros(fibres,1);
EA1 = 0.0;
EG1 = 0.0;
EI1 = 0.0;
% .....

```

```

for j=1 : fibres
EAT(j)= ( Econc(j,i+1)*Aconc(j) + Esteel(j,i+1)*Asteel(j) );
% if y(j) < 0
% y(j)=-1*y(j);
% end
EGT(j)= ( Econc(j,i+1)*Aconc(j)*y(j) + Esteel(j,i+1)*Asteel(j)*y(j) ); % could be NULLED to see the effect

EIT(j)= ( Econc(j,i+1)*Aconc(j)*y(j)*y(j) + Esteel(j,i+1)*Asteel(j)*y(j)*y(j) );
EA = EA + EAT(j);
EG = EG + EGT(j);
EI = EI + EIT(j);

```

```

% .....Constant E .....
E1=2.1e10;
Esl= 1.75e11;
EGT1(j)= ( E1*Aconc(j)*y(j) + Esl*Asteel(j)*y(j) ); % could be NULLED to see the effect

EIT1(j)= ( E1*Aconc(j)*y(j)*y(j) + Esl*Asteel(j)*y(j)*y(j) );
EA1 = EA1 + EAT1(j);
EG1 = EG1 + EGT1(j);
EI1 = EI1 + EIT1(j);
% .....Constant E .....

```

```

end
% get k matrix .....

```

```

k = (1/L) * [ EA 0 -EG -EA 0 EG
0 12*EI/(L*L) 6*EI/L 0 -12*EI/(L*L) 6*EI/L
-EG 6*EI/L 4*EI EG -6*EI/L 2*EI
-EA 0 EG EA 0 -EG
0 -12*EI/(L*L) -6*EI/L 0 12*EI/(L*L) -6*EI/L
EG 6*EI/L 2*EI -EG -6*EI/L 4*EI ];

```

```

k1 = (1/L) * [ EA1 0 -EG1 -EA1 0 EG1
0 12*EI1/(L*L) 6*EI1/L 0 -12*EI1/(L*L) 6*EI1/L
-EG1 6*EI1/L 4*EI1 EG1 -6*EI1/L 2*EI1
-EA1 0 EG1 EA1 0 -EG1
0 -12*EI1/(L*L) -6*EI1/L 0 12*EI1/(L*L) -6*EI1/L
EG1 6*EI1/L 2*EI1 -EG1 -6*EI1/L 4*EI1 ];

```

```

%k = 0.75* k1 + 0.25 * k ; cancelled ...
%k = 0.5* k1 + 0.5 * k ;

```

```

end
% .....

```

```

function Depsk = Deltastrains( i,du,L,y,fibres)
% HERE DISPL'S u(1,i+1)& u(1,i) ARE (IMPORTED) FROM 1ST PROGRAM (MAIN PROGRAM).....
% function (2 )to get the Delta Strains

```

```

Depsa = ( du(4,i)-du(1,i) ) / L;

```

```

Dfai = ( du(6,i)-du(3,i) ) / L;

for j=1 : fibres
  Depsk(j) = Depsa - y(j) * Dfai;
end

end

%
%
%
function [ sigmak sigmaks Damsig Tx Bx Cx TxS BxS MdS Bru] = GDstresses(
i,e,fibres,size,epsk,crush,EC,ES,Fy,Top,Bottom,CRUSH,TopS,BottomS,Middle, Brush )
% This fuction to get stressess & update the stressess for NEXT time-step
% get stressess from Concrete & Steel models.....
% function (3)

%
%
% ... This is the 2ed program to obtain the components of the Stiffness
% Matrix from the Fibres.....

%
% .....(i) give 0-values for sigmak sigmaks Tx Bx Cx TxS BxS MdS
% to avoid program termination when CRUSH(j,i,e)= 10

%
% THIS means if NONE of the following Loops is entered,
% because of CRUSH ==10,
% these 8 parameters are given a 0-value to PROCESS BACK to the
% Main Program. Otherwise, the Program is terminated...

for j=1 : fibres
if CRUSH(j,i,e)== 10
sigmak(j,i+1,e) = 0.0;
%'Tension'
Tx(j,i+1,e)=0 ; % ...up dating.....
Bx(j,i+1,e)=0; % ...up dating.....
Cx(j,i+1,e)=CRUSH(j,i,e); % ...up dating.....

Bru(j,i+1,e) = Brush(j,i,e) ; % for section (iv) 2.4.d
end
end

%
% .....give 0-values for Damsig
% to avoid program termination when envelope is not entered.....
% ..... Damage PART .....
Damsig(j,i+1,e) = 0 ;
% .....end of Damage PART .....

%
% .....(ii) obtain Delta of Uni-axial Fibre Strain &
% and Uni-axial Fibre Strains...

%
% .....MAJOR LOOP .....

for j=1 : fibres

%
% .....MAJOR LOOP .....

%
% ... (A) ...Tension .....
%.....
if epsk(j,i+1,e) > 0 ;
sigmak(j,i+1,e) = 0.0; % I CANCELLED THIS STEP TEMPORARILY TO SEE HAVE kkk=
%sum of E = higher value sothat I get better Hysteresis shape....
%sigmak(j,i+1,e) = epsk(j,i+1,e)* EC; % THIS IS ALSO TEMPORRILY
%'Tension'
Tx(j,i+1,e)=Top(j,i,e); % ...up dating.....
Bx(j,i+1,e)=Bottom(j,i,e); % ...up dating.....
Cx(j,i+1,e)=CRUSH(j,i,e); % ...up dating.....

Bru(j,i+1,e) = Brush(j,i,e) ; % for section (iv) 2.4.d
end

%
% ... (B) ...Linearity at (linear Loading), (Re-loading) and (Un-loading) ....
%.....
if epsk(j,i+1,e) >= Top(j,i,e) && epsk(j,i+1,e) <= Bottom(j,i,e) && CRUSH(j,i,e) < 10;

sigmak(j,i+1,e) = (epsk(j,i+1,e)- Bottom(j,i,e))* EC;
Top(j,i+1,e) = Top(j,i,e); % .....keep the same..update the Limits .... NNOO NNEEEEDD
Bottom(j,i+1,e)= Bottom(j,i,e); % .....keep the same..update the Limits ..... NNOO NNEEEEDD
%'Linearity'
Tx(j,i+1,e)=Top(j,i+1,e); % ...up dating.....
Bx(j,i+1,e)=Bottom(j,i+1,e); % ...up dating.....
Cx(j,i+1,e)=CRUSH(j,i+1,e); % ...up dating.....

Bru(j,i+1,e) = Brush(j,i,e) ; % for section (iv) 2.4.d

%
% if Top(j,i,e) < -0.002
% Top(j,i,e)
% e

```

```

%end

end

% ... (C) ... Non-linearly, (Envelope) .....
% .....
if epsk(j,i+1,e) < Top(j,i,e) && epsk(j,i+1,e) > crush && CRUSH(j,i,e) < 10;
% omitted && epsk(j,i+1,e) < epsk(j,i,e)

%sigmak(j,i+1,e) = (-6.7e09 * epsk(j,i+1,e) -1.30e07); % Temporary
%sigmak(j,i+1,e) = (-7.0e09 * epsk(j,i+1,e) -4.40e07); % Temporary
%sigmak(j,i+1,e) = (-7.0e09 * epsk(j,i+1,e) -5.60e07); % Temporary
%sigmak(j,i+1,e) = (-6.5e09 * epsk(j,i+1,e) -5.17e07); % Temporary

Top(j, i+1 ,e)= epsk(j,i+1,e); % .....update the LandMark point....
Diff(j,i+1,e)= sigmak(j,i+1,e) /EC;

Bottom(j, i+1 ,e)= Top(j,i+1,e)-Diff(j,i+1,e); % ..update the L/M point...

Tx(j, i+1 ,e)=Top(j,i+1,e); % ....up dating.....
Bx(j, i+1 ,e)=Bottom(j,i+1,e); % ....up dating.....
Cx(j,i+1,e)=CRUSH(j,i+1,e); % ....up dating.....

% ..... Damage PART .....
Damsig(j,i+1,e) = sigmak(j,i+1,e);
% .....end of Damage PART .....

% .....a sign for NON-Linearity .....
Brush(j, i:size+1 ,e) = 200 ; % this is to (prohibit) Econc from being EC in (iv) 2.4.d
Bru(j,i+1,e) = Brush(j,i,e) ; % for section (iv) 2.4.d
% .....end of a sign for NON-Linearity .....

%if Top(j,i+1,e) < -0.002
% Top(j,i+1,e)
% e
%end
%if e==2;
%if i>100;
%'Envelope.'
%i
%Bottom(2,i,2)
%epsk(2,i+1,2)
%Top(2,i,2)
% end;

end

% ... (D) ... Non-linear (Re/Un-loading) (Beyond the Bottom)..
% .....
if epsk(j,i+1,e) > Bottom(j,i,e) && epsk(j,i+1,e) < 0.00000003 && CRUSH(j,i,e) < 10
sigmak(j,i+1,e) = 0.0;

% Bottom(j,i+1,e)= epsk(j,i+1,e); % .....update the LandMark point..

%Top(j,i+1,e)= (-2100*Bottom(j,i+1,e)+5.60 )/(-2800);

Bottom(j,i+1,e)= Bottom(j,i,e) ; % .....keep the same previous LandMark point..
Top(j,i+1,e) = Top(j,i,e) ; % .....keep the same previous LandMark point..

Tx(j,i+1,e)=Top(j,i+1,e); % ....up dating.....
Bx(j,i+1,e)=Bottom(j,i+1,e); % ....up dating.....
Cx(j,i+1,e)=CRUSH(j,i+1,e); % ....up dating.....

Brush(j, i:size+1 ,e) = 200 ; % this is to (prohibit) Econc from being EC in (iv) 2.4.d
Bru(j,i+1,e) = Brush(j,i,e) ; % for section (iv) 2.4.d

end

% ... (E) ... Envelope crushing.....
% .....

% CRUSH(j,i:size+1,e)=0; % this is to define CRUSH = 0 if NOT Crushing..
% I don't think this is useful... it is already defined....

if epsk(j,i+1,e) <= crush
sigmak(j,i+1 : size+1,e) = 0.0;
CRUSH(j,i:size+1,e)=10; % this is to define CRUSH = 10 if Crushing..
%'CRUSH'
Tx(j,i+1,e)=Top(j,i+1,e); % ....up dating.....
Bx(j,i+1,e)=Bottom(j,i+1,e); % ....up dating.....
Cx(j,i+1,e)=CRUSH(j,i+1,e); % ....up dating.....

Brush(j, i:size+1 ,e) = 200 ; % this is to (prohibit) Econc from being EC in (iv) 2.4.d
Bru(j,i+1,e) = Brush(j,i,e) ; % for section (iv) 2.4.d
end

```

```

% .....END MAJOR LOOP .....

    for j=1 : fibres
    %if Top(j,i+1,e) < -0.002
        % Top(j,i+1,e)
        % e
    %end
    end
% .....END MAJOR LOOP .....

% '-----':
%plot(epsk,sigmak,'b-o');hold on; grid on;

% -----
% .....(iv) (Update) STEEL FIBRE STRESS .....
% for each (Fibre) & each (time-step) ...

% .....
% epskS(j,i+1,e) = epsk(j,i+1,e); % This is to know they are the same
% .....

% .....START MAJOR LOOP .....
for j = 1 : fibres
% .....START MAJOR LOOP .....

% ... (A) ...Linear Un/Re-loading ....
% .....
if epsk(j,i+1,e) <= TopS(j,i,e) && epsk(j,i+1,e) >= BottomS(j,i,e)
sigmakS(j,i+1,e) = (epsk(j,i+1,e)-Middle(j,i,e))* ES; % .....Modification Middle(j,i,e)

TopS(j,i+1,e) = TopS(j,i,e); % .....update the Limits
BottomS(j,i+1,e) = BottomS(j,i,e); % .....update the Limits

TxS(j,i+1,e)=TopS(j,i,e); % ....up dating.....
BxS(j,i+1,e)=BottomS(j,i,e); % ....up dating.....
MdS(j,i+1,e)=Middle(j,i,e); % ....up dating.....
end

% ... (B) ...Non-linearity, Top Envelope.....
% .....
if epsk(j,i+1,e) > TopS(j,i,e)

sigmakS(j,i+1,e) = Fy;
TopS(j,i+1,e) = epsk(j,i+1,e); % ...update the landmark point..
DiffS= Fy /ES;
BottomS(j,i+1,e)= epsk(j,i+1,e)- 2*DiffS; % ..update the L/M pt..
Middle(j,i+1,e)= (TopS(j,i+1,e)+BottomS(j,i+1,e))/2;

TxS(j,i+1,e)=TopS(j,i+1,e); % ....up dating.....Modification TopS(j,i+1,e);)
BxS(j,i+1,e)=BottomS(j,i+1,e); % ....up dating.....Modification BottomS(j,i+1,e);) ..
MdS(j,i+1,e)=Middle(j,i+1,e); % ....up dating.....Modification Middle(j,i+1,e);) .
end

% ... (C) ...Non-linearity, Bottom Envelope.....
% .....

if epsk(j,i+1,e) < BottomS(j,i,e)
sigmakS(j,i+1,e) = -Fy;
BottomS(j,i+1,e)= epsk(j,i+1,e); % ...update the landmark pt..
DiffS= Fy /ES;
TopS(j,i+1,e)= epsk(j,i+1,e) + 2*DiffS; % ..update the L/M pt..
Middle(j,i+1,e)= (TopS(j,i+1,e)+BottomS(j,i+1,e))/2;

TxS(j,i+1,e)=TopS(j,i+1,e); % ....up dating.....Modification TopS(j,i+1,e);)
BxS(j,i+1,e)=BottomS(j,i+1,e); % ....up dating.....Modification BottomS(j,i+1,e);) ..
MdS(j,i+1,e)=Middle(j,i+1,e); % ....up dating.....Modification Middle(j,i+1,e);)
end
% .....END MAJOR LOOP .....
end
% .....END MAJOR LOOP .....

%plot(epsk(:,:,2),sigmak(:,:,2),'b-o');hold on; grid on;

end

%%%%%%%%%%%%%%%%%%%%%%%%%%%%%%%%%%%%%%%%%%%%%%%%%%%%%%%%%%%%%%%%%%%%%%%%

```

## Appendix [B]

Sadeghi's method to produce energy-based damage curve is applied. The global damage is calculated for a RC bridge column structure exhibiting an oscillation movement due to a cyclic loading effect. The steps for calculating the global damage from a hysteresis curve are written in a MatLab program, and listed in this Appendix [B]:

```
clear all;
clc;
% .....Determining Damage from Area Under Hysteresis Loops...Sadeghi's Method.....
% .....Determining Damage from Area Under Hysteresis Loops...Sadeghi's Method.....
% .....From Selesmo-Struct .....
% .....POSITIVE side ONLY.....
% .....POSITIVE side ONLY.....
% .....POSITIVE side ONLY.....

% .....(i) ..... Definitions .....

size = 935; % 2000 for cv1.txt
dt =0.01;
loops = 10; % 150 for cv1.txt to be taken from the Hystersis graph (with + )

peak = zeros(loops,1);
kj = zeros(loops,1);
area = zeros(size,1); % very important to define the area ...
A = zeros(size,1);
aa = zeros(size,1);
Damage= zeros(size,1);
u = zeros(size,1);
displ = zeros(size,1);
fs = zeros(size,1);
displupdate = zeros(size,1);
% .....(ii) .....Importing Displacements & Base Shear forces .....

%for i=1: size
% u(i) = sin(i);
% fs(i) = 0.04*sin(i*0.01/sin(i));
%end
% .....
% asp6_Hysteresis
% asp3_Hysteresis
% aspl0_Hysteresis
% SAKAI_Hysteresis
% Hysteresis_Yakut

load('aspl0_Hysteresis.txt') ; % Loading a text file...
fid = fopen('aspl0_Hysteresis.txt'); % opening the file (cv1.txt)
CCC = textscan(fid, '%f %f '); % scanning the file
fclose(fid); % closing the file

u = CCC{1}; % this is for the 1st-column data file

fs = CCC{2}; % this is for the 2ed-column data file
%.....

% .....(iii).....Determining the Number of Vortices (Peaks).....

j=1;
for i=2 : size
    if u(i) > 0 && fs(i) > 0 % Only the positive quarter of the curves...
        if u(i) > u(i-1) && u(i) > u(i+1) % the re-treiving Peak displacement ...
            peak(j) = i; % find the peaks numbers .....
            j=j+1 ; % a counter for peaks ....
        end
    end
    counter=j;
end

for j=1: counter
    if j < counter
        j ;
    peak(j)
    end
end

% .....(iv) .....Determinig the area under each loop Curve .....

% ...First.....Determining area of the first Peak....
for i=2 : peak(1)

    if u(i) > 0 && fs(i) > 0 % Only the positive quarter of the curves...
```

```

        if u(i) > u(i-1) && u(i) < u(peak(1)) % Only displ before the 1st peak.....
            area(i) = fs(i)*( u(i)-u(i-1) ); % area for every slot...
            displ(i) = u(i); % this is to get the corresponding ONLY
        end
    end
end
ispl=displ;

% ....Second.....Determining area of All Peaks Except the first Peak....
j=2; % .....important to start with .....
for i=2 : size

    if u(i) > 0 && fs(i) > 0 % Only the positive quarter of the curves....
        if j < counter
            if u(i) > u(i-1) && u(i) > u(peak(j-1)) && u(i) < u(peak(j)) % Only displ between 2 peaks.....

                area(i) = fs(i)*( u(i)-u(i-1) ); % area for every slot...
                displ(i) = u(i); % this is to get the correspondings ONLY
            end

            if u(i)== u(peak(j)) % ..... to Update the Peak loop ...
                j=j+1;
            end
        end
    end
end

% .....(v).....accumulating area .....
ii=1;
for i=1 : size

    A(ii+1)= A(ii) + area(i); % total area
    ii=ii+1;
    aa=A(ii);
end

% ..... (v) .....damage index .....
for i=1 : size

    Damage(i) = ( A(i) / aa );
end

% .....(vi) ..... re-arranging displacements arrays to document
% .....forward displacements ONLY .....

Big = 0;
for i = 1 : size

    if displ(i) > Big
        Big = displ(i);
    end
    displupdate(i)= Big;

end

% .....(viii) ....Re-arranging time-step arrays to be time in seconds...

for i = 1 : size
    time(i) = i * dt;
end

% .....(vii) .....Plotting .....
%plot( time, Damage, 'x-b');hold on; grid on;

%plot( displupdate, 'x-b');hold on; grid on;
%plot( displupdate,Damage, 'x-r'); hold on; grid on;
%plot( displ, 'x-b'); hold on; grid on;
%plot( Damage, 'x-r'); hold on; grid on;

for i=2 : size
    if displupdate(i)== displupdate(i-1);
        Damage(i)= Damage(i-1);
    end
end

plot( displupdate,Damage, 'x-g'); hold on; grid on;

```

## Appendix [C]

Local damage curves are obtained using a MatLab programming code according to the local stress concept. The code is listed in this Appendix [C].

```
clear all;
clc;
% .....Determining LOCAL Damage from Stress Diagram Response of the Seismo-Struct
% .....Determining LOCAL Damage from Stress Diagram Response of the Seismo-Struct
% .....
% .....(i) ..... Definitions .....

size = 930; % 901
dt =0.01;

% strength for core
Elastic = -0.0040 ; % for core
Ultimate = -4.45e7 ; % for core ... Note, if Ultimate < some values in the stress,>> Damage will turn Negative

% strength for cover .....
Elastic = -0.002 ; % for cover, -0.002
Ultimate = -3.45e7 ; % for cover, -3.45e7 ..... Note, if Ultimate < some values in the stress,>> Damage will turn Negative

strain= zeros(size,1);
stress= zeros(size,1);
displ = zeros(size,1);
Damage= zeros(size,1);
%peak = zeros(size,1);

% .....(ii) .....Importing Stress-strain diagram .....
% asp6_core90
% asp6_core80
% asp6_core70
% asp6_core60
% asp6_cover

% asp3_core90
% asp3_core80
% asp3_core70
% asp3_core60
% asp3_cover

% asp10_core90
% asp10_core80
% asp10_core70
% asp10_core60
% asp10_cover

%stress_strain_core

%SAKAI_cover ??

%.....
load('asp6_core60.txt') ; % Loading a text file....
fid = fopen('asp6_core60.txt'); % opening the file
CCC = textscan(fid, '%f %f %f '); % scanning the file
fclose(fid); % closing the file

Time = CCC{1}; % this is for the 1st-column data file
strain = CCC{2}; % this is for the 2ed-column data file
stress = CCC{3}; % this is for the 3ed-column data file

%.....
% .....(ii) .....Importing Displacement diagram .....

%.....
% load('Displacement1.txt') ; % Loading a text file....
% fid = fopen('Displacement1.txt'); % opening the file
% CC = textscan(fid, '%f %f '); % scanning the file
% fclose(fid); % closing the file

%Time = CC{1}; % this is for the 1st-column data file
% displ = CC{2}; % this is for the 2ed-column data file

% .....(iii).....Determining the Vortices (iteration1 & peak(j) ).....
```

```

j=1;
for i=2 : size-1
    if strain(i) < Elastic % this is to go to the non-linear strains only
        stress;
        if stress(i-1) > stress(i) && stress(i+1) > stress(i) % scanning for the peak stresses..
            peak(j) = stress(i); % find the peak stress value..
            iteration1(j)=i; % find the peak stress (first) iteration...(iteration1)...

            j=j+1 ; % a counter for peaks ....
        end
        counter=j-1;
    end
end

for j=1: counter
    if j < counter
        j ;
    end
end

% .....(iv).....find the peak stress (first) iteration.... (iteration2).....
%iteration1(counter+1)= size;

for j=1 : counter-1

    for i= iteration1(j) : iteration1(j+1)
        if stress(i) < peak(j+1) % determining all stresses on the envelop only
            iteration2(j) = i ;
        end
    end
end

% .....(iv) .....Determinig the ALL Envelope stresses ....

diff= counter-j; % this is the difference between
for j=1 : counter-1

    % this is for the envelop stresses between iterations 1 & 2 for the
    % same j :
    for i=iteration1(j) : iteration2(j)
        envelop(i) = stress(i) ;
        station(j) = envelop(i); % recording the last envelop in the loop j.
    end

    % this is for the envelop stresses between iteration 2 of j &
    % iteration 1 of the next loop j+1 .... which has constant-values:
    for i=iteration2(j) : iteration1(j+1)
        envelop(i) = station(j); % defining the last envelop in loop j
        % as constant for ALL non-envelop stresses.
    end
end

% this is for the envelop stresses of the Last loop j=counter-1
for i=iteration1(counter) : size
    envelop(i) = station(counter-1);
end

% ..... Detetrminre the damage ....

for i=1 : size

    Damage(i) = 1 - (envelop(i) / Ultimate );
    if envelop(i) == 0
        Damage(i) = 0 ;
    end
end

% .....(vii) .....Plotting .....

plot( Time(1:size),Damage(1:size), 'x-g'); hold on; grid on;
%kj=u(peak(:));

%plot(u,fs,'x-b'); hold on ; grid on;

%plot( peak,'o-b' );
%plot( kj,'o-b' );

%plot(envelop);

```



## Appendix [D]

Definition of the dissipating yield energy for this purpose will require computing the accumulating dissipated yield energy in an ascending-order basis, i.e. the dissipating yield energy values must be summed up in an order that is corresponding to an ascending order of the displacement values. This has been performed by processing the output data attained from the dynamic analysis for the column, and have them written in a MatLab program as listed in this Appendix [D].

```
clear all;
clc;
% .....Determining Yield Energy from Area Under Hysteresis Loops
% .....Determining Yield Energy from Area Under Hysteresis Loops
% .....From Selesmo-Struct .....
% .....POSITIVE side ONLY.....
% .....POSITIVE side ONLY.....
% .....UPPER side ONLY.....
% .....UPPER side ONLY.....

% .....(i) ..... Definitions .....

iter = 10959; % SAKAI Experiment
%iter = 9627; % SAKAI Experiment
dt =0.005;

u = zeros(iter,1); % x-displacements....
fs = zeros(iter,1); % Base shear forces....
uu=zeros(iter,1); % updated x-displacement
udu=zeros(iter,1); % updated x-velocities,,,,,,this is to null un-required (negative) values..
fsu=zeros(iter,1); % updated Base shear forces,,,,,this is to null un-required (negative) values..

% .....(ii) .....Importing Displacements & Base Shear forces & Velocities, .....

for i=1: iter
    % u(i) = sin(i);
    % fs(i) = 0.04*sin(i*0.01/sin(i));
end
% .....
% asp6 Hysteresis
% asp3 Hysteresis
% aspl0 Hysteresis
% SAKAI_Hysteresis
% Hysteresis_Yakut

load('Sakai_Displ_Hystersis_rot.txt') ; % Loading a text file....
% load('Sakai_Displ_Hystersis_rot_isolation3.txt') ; % Loading
% a text file....
% the original Hysteresis is Given a flipped over Graph for a more convenient Hysteresis look ..
fid = fopen('Sakai_Displ_Hystersis_rot.txt'); % opening the file
% fid = fopen('Sakai_Displ_Hystersis_rot_isolation3.txt'); % opening the file
CCC = textscan(fid, '%f %f '); % scanning the file
fclose(fid); % closing the file
L=4.41;
u = CCC{1}/L; % 1st-column data file % Relative-rotation*column Hght= Relative-Displacement
n = CCC{1}/L; % 1st-column data file % Relative-rotation*column Hght= Relative-Displacement
fs = CCC{2}/L; % 2ed-column data file % BaseMoment/column Hght=BaseShear

% .....
% .....velocity to check the +ve and -ve quarters.....

load('Sakai_Velocity.txt') ; % Loading a text file....
%load('Sakai_Velocity_isolation3.txt') ; % Loading a text file....
fid = fopen('Sakai_Velocity.txt'); % opening the file
%fid = fopen('Sakai_Velocity_isolation3.txt'); % opening the file
CC = textscan(fid, '%f %f '); % scanning the file
fclose(fid); % closing the file

time = CC{1}; % this is for the 1st-column data file

ud = -CC{2}; % this is for the 2ed-column data file .... Given -ve sign since
%the original Hysteresis is Given a flipped over Graph for more a convenient Hysteresis look

% .....
```

```

% .....(iii-1) .....Sending Off all Un-Loading Displacements within the Positive
% Quarter ONLY.....

for i= 1: iter

    if u(i) > 0 && fs(i) > 0      % Only the positive quarter of the curves...
    if u(i+1) < u(i)             % Only the re-treiving UN-Loading displacements,,,
        u(i) = 0 ;              % this is sending displacements OFF.....
        udnloaded(i)=ud(i);      % this is the un-loaded velocity only
    end

    end

end

% .....(iii-2) ..... all re-Loading Displacements within the Positive
% Quarter ONLY.....

fsreloaded= zeros(iter,1);
udreloaded= zeros(iter,1);
for i= 1: iter

    if u(i) > 0 && fs(i) > 0      % Only the positive quarter of the curves...
    if u(i+1) > u(i)             % Only the re-Loading displacements,,,

        udreloaded(i) = ud(i);    % this is the RE-loaded velocity only in the first quarter..
        fsreloaded(i) = fs(i);    % this is the RE-Loaded forces matrix only in the first quarter ...
    end

    end

end

% .....(iv) .....Re-Ordering the Displacements in an Ascending Order ....

for jj= 1: iter

    small = 10 ; % the largest possible value for a via-duct lateral displacement...
    if u(jj) > 0 && fs(jj) > 0 % Only the positive quarter of the curves...

        for ii= 1: iter
            if u(ii) > 0 && fs(ii) > 0 % Only the positive quarter of the curves...

                if u(ii) < small
                    small = u(ii);
                    smalll(ii)= small;
                    q=ii;
                end

            end

        end

        uu(jj) = small; % this is the new re-ordered Displacement matrix, also uu(jj)= u(q)=small
        uorder(jj)=u(q); % this is the displ in order
        u(q) = 1000; % used values of old matrix must be sent off .....
        q; % this is the new ordering

        udu(jj) = ud(q); % this is the corresponding new re-ordered Velocity matrix..
        fsu(jj) = fs(q); % this is the corresponding new re-ordered Restoring and Yield forces matrix..

    end

end

% .....(v) .....the Nulled Updated Displacements uu need to be
% ..... re-written as the last value uu(i-1).....
% .....
for i=2 : iter
    if uu(i) == 0
        uu(i) = uu(i-1);
    end
end

% .....(vi) .....Yield Energy .....UUs.....
% .....
% .....Declaration of force & Energy components .....

UUs=zeros(iter,1);
countfs=zeros(iter,1); % accumulated Energy ...

% .....Energy components .....
% Numerical integration for stiffness force-velcity relation(k*u-vs-ud) to obtain Energy ...
% i.e. Linear or non-linear relations....

for i=2 : iter

    countfs(i) = countfs(i) + fsu(i) * udu(i) * dt; % re-ordered in an ascending displacement order
    %countfs(i) = countfs(i) + fsreloaded(i) * udreloaded(i) * dt; % not re-ordered

```

```

UUs(i) = UUs(i-1) + countfs(i);
% Choose either one (re-ordered, or Not re-ordered)to get what you want.....
end

%
% -----
%...declarations for Graphics .....
grid on;
% plot(n(1:10950),fs(1:10950),'m-'); % this is the Hysteresis

plot(uu,UUs,'m-');hold on;

% plot(uu(1:3950),UUs(1:3950),'m-*');hold on;
% plot(time(1:10959),UUs(1:10959),'m-');hold on;
% ylabel(' Kenitic & strain energy U = UK+ UUS1 , Damping and Yield UUS2');

%title('Accumulated Yield Energy Distribution ');

xlabel('x-Displacement (m)');
% xlabel('Time t (sec) ');
ylabel(' Accumulated Yield Energy (N.m) ');
grid on;

% -----End of Program -----

```